THE UNIVERSITY OF CHICAGO

ONTOGENY OF THE ANURAN UROSTYLE: THE DEVELOPMENTAL CONTEXT OF EVOLUTIONARY NOVELTY

A DISSERTATION SUBMITTED TO

THE FACULTY OF THE DIVISION OF THE BIOLOGICAL SCIENCES

AND THE PRITZKER SCHOOL OF MEDICINE

IN CANDIDACY FOR THE DEGREE OF

DOCTOR OF PHILOSOPHY

GRADUATE PROGRAM IN INTEGRATIVE BIOLOGY

BY

M.M. GAYANI SENEVIRATHNE

CHICAGO, ILLINOIS

AUGUST 2021

TABLE OF CONTENTS

LIST OF TABLES

LIST OF FIGURES

ACKNOWLEDGEMENTS

My dissertation would not be possible without the help of so many: your kindness and support helped me get here. Thank you.

My advisor, Neil Shubin, thank you for your patience, guidance, and advice throughout these years. When I was an undergraduate in Sri Lanka, reading your book *Your Inner Fish*, is the main reason behind my enthusiasm towards learning evo-devo. From fossils-to-genes, your excitement in the face of science and discoveries was contagious. From the very first day of meeting you in your office during my interview week at UChicago, I knew that this is where I wanted to be. You welcomed me to your lab with open arms, listened to my crazy experiments, and never failed to keep us motivated throughout these years. Year 2020 was particularly hard on all of us. You made sure to organize lab meeting every week; host lab happy hours on Sundays and to keep us sane even during lockdown. I am lucky to call you my mentor and my advisor. Thank you for everything.

My committee, Victoria Prince, Edwin Ferguson, and James Hanken, thank you for your continuous support throughout these five years. Jim, thank you for being the person who would always answer my amphibian and development questions. Your guidance for the past 7 years is something that I have always relied on. Vicky, thank you for being the most caring person I know –whenever I had a question regarding my experiments or when I wanted to talk about personal stuff, your door was always open. Chip, thank you for your broad knowledge in developmental biology and your honest opinion on most of the experiments.

Shubin Lab is where I grew up as a person for sure. It is my second home. Thank you for going beyond your way to help me in my work. Melvin, Igor, Tom, Nate, and Tetsuya: my labmates, who became my brothers, life-long friends, and people I would rely on whenever I

have a problem. Thank you for your patience; my lab days were filled with laughter because of you. Our lunches, afternoon coffee runs, lab spa days, crazy MBL summers, and lab-outings are some of my favorite memories.

Thank you for so many OBA faculty and staff, who took time from their busy schedules to talk about science and experiments, and specially, Audrey Aronowsky, for all your help with everything during my Ph.D. My friends (Stephanie Baumgart, Wei Liang, Noor Singh, Katie Whitlow, Samantha Gartner, Stephanie Sang, Kelsey Whitlow), thank you for sushi and ramen dinners, our lunches, gym outings, ice cream dates, and other countless memories. My days were filled with laughter because of you. Thank you.

To all my collaborators, past mentors, advisors, and colleagues -- thank you. Professor Meegaskumbura, my undergraduate mentor, the person who initially motivated and guided me to a path in evolutionary biology, I will always be grateful. Everyone at the Marine Biological Laboratory and the National Xenopus Resource Center (Marko Horb, Nikko-Ideen Shaidani, Marcin Wizla, Hilary Katz, Nipam Patel, Carrie Albertine), thank you for taking me under your wing every year when I visit Woods Hole, for letting me use the resources, and for teaching me new techniques. I will always remember those days.

Finally, my family, I love you and miss you. This is for all of you.

ABSTRACT

The urostyle, a composite skeletal structure formed at the onset of metamorphosis in frogs, is considered a structural novelty. Despite its evolutionary importance, major aspects of its development and evolution remain enigmatic. The urostyle forms by fusion of the mesoderm-derived coccyx with the endoderm- or superficial mesoderm-derived hypochord when the tadpoles metamorphose into frogs. Frog metamorphosis, where tissue coordination is mediated by thyroid hormone (TH), involves dramatic changes in locomotion. During this period, a remarkable transition from swimming using fins/tails (in tadpoles) to jumping, walking, digging, climbing, and swimming using limbs (in adults) occurs (an axial-driven to a limb-driven transition). Here, I focus on the ontogenetic and genetic underpinnings of development of the urostyle. Using a nearly complete developmental series from free-living larvae to metamorphs, I studied the ontogeny of the urostyle in *Xenopus tropicalis*, adapting clearing and staining techniques, histology, immunohistology, cell proliferation, and cell death (Chapter 2). Following documentation of morphological changes, I identified genes and gene-regulatory pathways responsible for formation of the urostyle (a structure that is conserved across all extant anurans) (Chapter 3), using RNA-seq and ATAC-seq approaches. Since formation of the urostyle coincides with metamorphosis, I also looked at the possible role of TH in controlling formation of this structure, both morphologically (Chapter 2) and genetically (Chapter 3), which helped me narrow down the genes directly regulated by TH. Finally, I tested the function of two candidate genes in development of the urostyle by using a functional assay (creating frameshift mutations and a conditional knockout system) (Appendix). Through my dissertation work, I highlight how the changes to an underlying ancestral gene regulatory network would eventually alter the phenotype and genotype, giving rise to evolutionary novelties.

CHAPTER 1

INTRODUCTION

1.1 – ABSTRACT

Amphibians are one of the most diverse group of vertebrates, and of these, anurans (frogs and toads) are the most speciose group. Anurans possess a unique body morphology, which we refer to as the frog morphotype. The urostyle, one such structure that is unique to the frog morphotype, is conserved across all species and is considered a structural novelty. It is a fused rod, composed of a paraxial mesoderm-derived coccyx and an endoderm or superficial mesoderm-derived hypochord. The ontogeny of the urostyle has received very little attention over the past few decades. Formed during metamorphic climax of a frog's life cycle, it hints at the possibility of being controlled by thyroid hormone. My dissertation work aims to address the missing link in literature regarding the evolution of the urostyle by looking at morphology, genetics, gene regulation, and thyroid-hormone control during its development.

1.2 – AMPHIBIAN DIVERSITY AND THE FROG MORPHOTYPE

Amphibians, an important group of extant vertebrates, are highly diverse in their body plans, reproductive behaviors, locomotion, and life history modes [1, 2]. Amphibians (total number of species ca. 7800; AmphibiaWeb 2018) comprise three orders: Caudata (salamanders – 710 species, have a well-developed tail, and paired, proportionate limbs), Gymnophiona (caecilians – 207, limbless with reduced eyes), and Anura (frogs – 6884, lack tails and have powerful hind limbs adapted for jumping). Frogs and toads have diversified across various habitats, occupying different ecological niches (trees, shrubs, rocky surfaces, aquatic habitats,

tree holes), and saltation (jumping) is considered the reason behind the evolutionary success of anurans [3].

The evolution of a saltatory mode of locomotion in anurans (frogs and toads) is derived, ancient and distinctive but evolutionarily, poorly understood. Even though various hypotheses have been proposed on the evolution of the saltatory mechanism, Jenkins and Shubin [4] interpreted that the "early establishment and persistence of hind limb and tarsal elongation, truncal shortening, and tibiofibular and radio-ulnar fusion" as evidence of saltation being the most primitive mode of terrestrial locomotion in anurans; all other locomotor modes in anurans (burrowing, walking, hopping) are considered to have evolved secondarily [4, 5].

In adult frogs, the vertebral column consists of presacral vertebrae (6–9), one sacral vertebra, undefinable caudal vertebrae, long hind limbs, and a urostyle, which is a composite structure, comprising of an ossified hypochord ventrally and a coccyx dorsally – these characters highlight the "frog morphotype" [1], and are considered key innovations for the saltatory lifestyle of an anuran. Adult frogs occupy different ecological niches (arboreal, aquatic, fossorial). Despite the secondarily evolved habitat preferences, the developmental patterns of the anuran postcranial skeleton show very little variation (e.g., [6, 7]). The shortened axial skeleton, radical transformation of the sacro-urostyle region, and ventral articulation of the posterolaterally oriented pelvic girdle are unique to frogs [1]. Despite the importance of these structures in understanding the evolutionary origin of this group and their locomotion, the anatomy of the caudopelvic region has received little attention, and the genetic basis of these morphologies remains obscure. Studying these will shed light in understanding evolution of the highly derived jumping morphotype in anurans, which is conserved across nearly 7000 species. The transformation of the sacrum (which supports the pelvic girdle) and the urostyle highlight the

frog morphotype among other vertebrates. The urostyle functions in transmitting thrust, from ilium to the sacrum, when jumping. All frogs jump, at least to some extent, but the articulation between the sacrum and urostyle defines how far/how well a frog can jump [1, 8]. In species where derived locomotory habits are seen – swimming, climbing, digging – the sacro-urostyle movement appears to be restricted. Nevertheless, the urostyle of frogs remains a conserved feature, an apparent key novelty of frogs that is unique to the clade.

1.3 – UROSTYLE – A UNIQUE STRUCTURE OF THE FROG MORPHOTYPE

The urostyle of adult anurans is a composite structure, present in all taxa regardless of the habitat they occupy, comprising an ossified hypochord (ventrally) and a coccyx (dorsally). Several hypotheses on the formation of the anuran urostyle have been put forward. Griffiths [9] proposed that the urostyle originates as a posterior outgrowth of the first postsacral intervertebral body, a proposal that was disputed later when it was observed that the hypochord forms ventral to the notochord (i.e., outside of the perichondral bone) [10]. Later, some authors discussed the possibility of urostyle formation by the fusion of a variable number of caudal vertebrae, and some even stated that the urostyle originates from a single cartilaginous rod (e.g., [11]). However, these hypotheses were challenged by the discovery that the urostyle forms from two individual units: hypochord and coccyx [8, 12].

Within vertebrates, the anuran urostyle is morphologically and developmentally distinct from structures found in all other vertebrates. The coccyx and the hypochord, which form at metamorphosis in anurans, fuse synostotically to form the urostyle. The anuran coccyx is formed from fused postcaudal vertebrae. Some lineages of vertebrates show modifications to the posterior end of the axial column (ancestral state is to have unfused caudal vertebrae, which

extends to the tip of the tail). These modifications to the vertebral column evolved with the loss of the tail in some vertebrate lineages – humans and apes (coccyx formed by the fusion of caudal vertebrae after birth), birds (pygostyle formed by the fusion of caudal vertebrae), and teleosts (ural plate, formed by the fusion of preural centra) [12]. The anuran coccyx is a result of postsacral vertebrae extending anteriorly (reaching the sacrum) and posteriorly (up to the junction where hypochord, pelvic girdle and coccyx fuse to form the "pelvic basket").

The embryonic hypochord is a thin rod-like structure that extends ventral to the notochord until the tip of the tail; it is seen in anamniotes (fish and amphibians) but not in amniotes [13-16]. However, an ossifying hypochord that forms independently from the axial column is only present in anurans. The source of cells contributing to the embryonic hypochord has been argued for decades. One set of studies implicated an endodermal origin of the hypochord. These experiments were done in zebrafish using cross sections viewed from a transmission electron microscope [15] and in amphibians using DiD injections, *VEGF in-situ* hybridization, and histological approaches [13, 14, 16, 17]. By contrast, another set of studies highlighted the possibility of the hypochord being derived from mesoderm or superficial mesoderm (in zebrafish using rhodamine dextran injections [18, 19]; in frogs using a scanning electron microscopy method [20]). This dilemma regarding the germ layer origin of hypochordal cells highlights the need for future experiments using a permanent cell-tracing method.

Typically, a frog attains its derived morphotype (including the urostyle) through a radical and rapid transformation during its life cycle. All frogs depend on an aquatic or moist habitat when laying eggs. The eggs, depending on their developmental mode, later hatch into tadpoles (in indirect developers) or froglets (in direct developers). Aquatic breeding characterized by an aquatic tadpole is considered to be basal (pleisiomorphic), a mode which a majority of anurans

possess [21, 22]. In direct developers, embryonic development occurs, where aquatic tadpole stages are absent and a fully formed froglet hatches from an egg [21, 22]. Metamorphosis is under hormonal control, and coordination between tissues and organs at the onset of metamorphosis is attained by thyroid hormone [23-25].

1.4 – FROG METAMORPHOSIS

Metamorphosis is classically defined as an abrupt postembryonic transformation of a larva into a juvenile, accompanied with an ecological transformation [26, 27]. Most animals undergo metamorphosis, but insects and amphibians are the most well-studied [25] examples. These two groups differ in mode of metamorphosis, mainly in that insects have an immobile, non-feeding stage and amphibians have an active larval stage (tadpole) during metamorphosis. Given the diversity, availability and often rapid metamorphosis, anurans (frogs and toads) are excellent model organisms for studying processes of metamorphosis and organogenesis. This stands true also when compared to caecilians, and salamanders who are slow to metamorphose and some are even characterized by paedomorphosis; this makes it difficult to ascertain some adult characters and evaluate their precise time of formation.

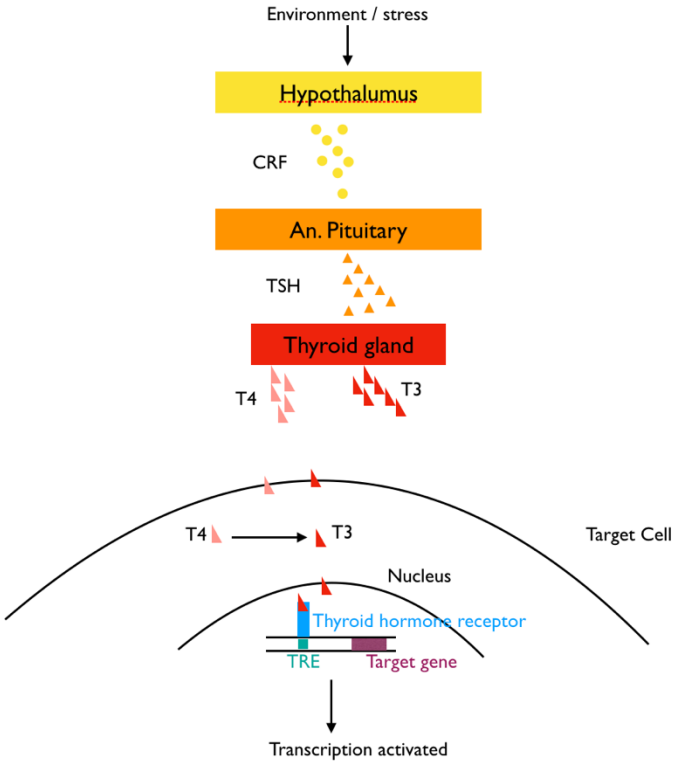

Figure 1.1. Thyroid hormone signaling pathway (redrawn and modified from Laudet, 2011).

The indirect-developing frogs go through an aquatic, free-swimming tadpole stage (unlike the direct developers, where the froglets directly hatch from the eggs) and later develop into a juvenile (froglet) with four limbs, adapted to limb-driven locomotory habits within 1–2 months depending on the species and extrinsic/intrinsic factors; the coordination among the tissues and organs is crucial during this period. Once the tadpole hatches from the egg, it undergoes three phases of development [24]: 1. Premetamorphosis – cell proliferation happens in the limb bud and brain; 2. Prometamorphosis – limb bud grows and differentiates; 3. Metamorphic climax – gill and tail resorption with dramatic remodeling of the skeleton and organs.

Changes happen in the tadpole during metamorphic climax, usually within 6–8 days [25]: the skin remodels acting as a barrier for dehydration while adjusting to its new terrestrial environment and at the same time functioning as a respiratory surface when it resorbs its gills; resorption of the gills subsequently enables development of well-functioning lungs, again to enable respiration in a terrestrial habitat; the simple intestine of the tadpole with a rudimentary stomach reduces in length (75%), forms new secretory glands adapting to the new feeding habits; the tail and notochord resorb, fore- and hind limbs form, enabling locomotion on land; the enzyme activity of the liver suddenly changes when the transformation occurs because the excretion of a tadpole shifts from ammonia to uric acid; and the cartilaginous skeleton of the tadpole ossifies and undergoes extensive remodeling [7]. Past studies have focused on the notochord, tail, skin, intestine, liver cells [25, 28-30], but so far, nothing is known about the genes involved in the dramatic remodeling of the urostyle.

1.5 – HORMONAL CONTROL OF METAMORPHOSIS

During frog metamorphosis, coordination between tissues is attained by a hormonal signal – mainly thyroid hormone (TH). A peak in TH can be seen in all vertebrates during their developmental transitions [27, 31-35]. The TH binds to thyroid hormone receptors (TRs), which are nuclear receptors. The TRs bind TH-response elements (TREs) located in the promotor region of the TH-response genes of the genome (Fig. 1); TREs control transcription. All vertebrates possess two isoforms of TRs – TRα and TRß, and their developmental expression profiles and tissue distributions differ from one another [23, 24]. In frogs, TRα is expressed in early stages, whereas TRß is expressed when dramatic metamorphic changes begin during metamorphic climax [27, 31-35]. A molecular cascade controls metamorphosis, where

increments of thyroid hormone coincide with changes in larval body form. The tadpole tissues/organs useful for the larval habits whither or get resorbed while tissues/new organs essential for the adult form *de novo*, and some tissues also undergo remodeling to facilitate this transition [27]. Environmental cues activate the hypothalamus to secrete cortico-releasing factors (CRFs), which bind to specific receptors on the anterior pituitary. This results in the anterior pituitary secreting thyroid stimulating hormone (TSH), which acts on the thyroid gland to release two forms of thyroid hormone – T4 and T3. Both T3 and T4 enter the target cells, where T4 would be transformed to T3 (via deiodinases), and ultimately, T3 would enter the cell nucleus. T3 binds to the thyroid hormone receptor (TRα or TRß) and forms a heterodimer with RXR (Retinoid X receptor), binding with the TRE, a region in that target gene's promoter, and subsequently transcription is activated. The TRs and RXRs are conserved across vertebrates, hence, studying frogs as a model organisms can also help us gain insights into vertebrate evolution and ancestral gene regulatory networks.

In frogs, embryogenesis takes about a week, followed by premetamorphosis, prometamorphosis, and metamorphic climax; thyroid hormone concentration is at its peak during the metamorphic climax (Fig. 2). Previous studies have found evidence for TRs controlling most of the events occurring at metamorphosis [27, 31-35], which include remodeling of the intestine, resorption of the tail and notochord, and structuring of the skin. Chromatin Immunoprecipitation (ChIP) experiments have revealed that TRs are bound to their corresponding TREs in an unliganded state [24], along with the respective corepressors; this is the baseline for the "dual-function" or the "gene-switching" phenomena discussed at the frog metamorphic climax [36, 37].

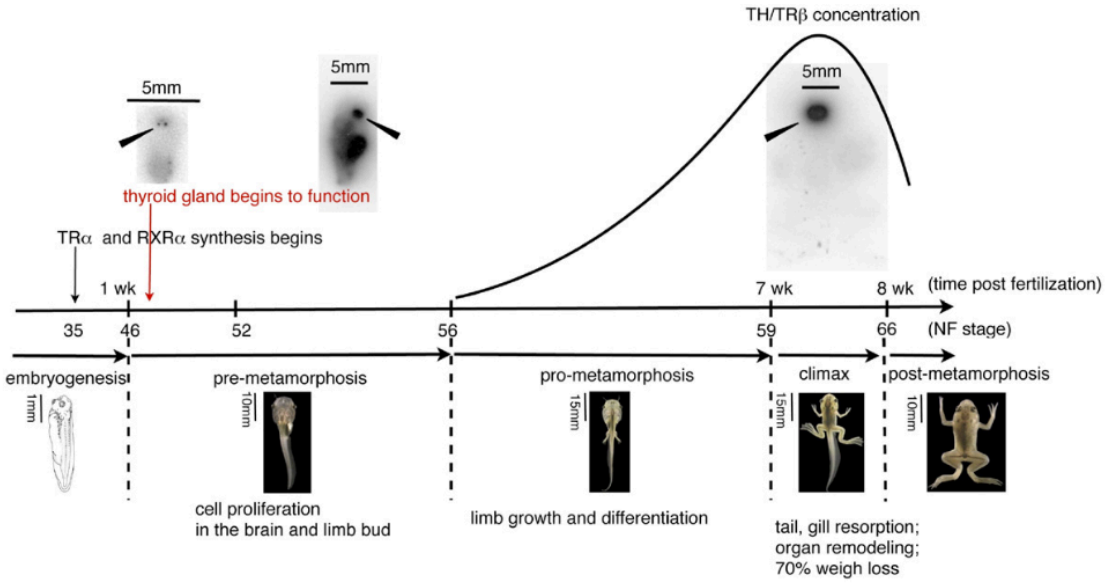

Figure 1.2. Three major transitional events in *Xenopus* development: pre-metamorphosis, pro-metamorphosis, and metamorphic climax. The line represents the thyroid hormone concentration, which coincides with TRß. Image adapted and modified from Brown & Cai (2007).

Gene-switching, which happens at the climax of amphibian metamorphosis (within 5-6 days), is when organs shut off "tadpole" genes and switch on/activate "frog" genes under the influence of TH [25]. A few well-studied examples of gene-switching occur within the tail fibroblasts, liver parenchymal cells, red blood cells, intestine, and the skin. The tadpole notochord is surrounded and supported by fibroblasts, and at the climax period, the fibroblasts switch from a growth program (synthesizes collagen and extracellular matrix) to expressing different proteolytic enzymes, which digest the notochord [25, 38, 39]. This switch in fibroblasts, from growth to digestion, is directly correlated with the rise in TH concentration [24]. Tadpole parenchymal cells in the liver express alcohol dehydrogenase (ALD) and Fetuin B when excreting ammonia, but they switch to express albumin, cytochrome p450, and carbonyl phosphate synthetase (CPS) during metamorphosis when excreting urea [25]. Further, at the

onset of metamorphosis, red blood cells expressing tadpole globin changes to adult globin [25, 40]. The tadpole skin (having only three layers and no dermis nor glands) remodels, replacing the tadpole epithelium by a germinative epithelium, and possesses two kinds of glands (mucous and granular) coinciding with the activity of TH [29]; tadpole keratin, expressed in all three tadpole skin layers, switches to adult keratin, which is restricted to the outermost two layers in the adult [25]. During the intestinal modification, TH controls apoptosis of most larval intestinal epithelial cells and concurrently adult epithelial cells form *de novo* through de-differentiation of some larval cells [41]. However, TH control of osteocyte-specific genes during skeletal development remains obscure.

1.6 – Developmental Basis Of Urostyle Formation

The presomitic mesoderm partitions into several segments called somites in vertebrates. A "clock and wavefront" mechanism controls the somite formation [42-48] – Notch and Wnt pathways represent "the clock," where an oscillating signal is generated, and FGFs creates a "wavefront" by provding a concentration gradient in the rostral-to-caudal direction. When somites mature, they give rise to three major compartments: the sclerotome (bones and cartilage in the axial skeleton), myotome (skeletal muscles), and the dermamyotome (dermis). Even though equivalent somites are formed at different anterior-posterior levels during early development, they will form different structures, and this specification is mainly because of the early *Hox* gene expression in the segmental plate mesoderm [42-48].

The anuran axial column, comprising of 7–9 postsacral vertebrae, is considerably truncated compared to the other vertebrate lineages. This truncation is driven by anteriorization of the *Hox* gene expression [49]. One of the examples of this anteriorized *Hox* gene expression in

anurans is the presacral-sacral transition zone markers – *Hoxc10* and *Hoxd10*; the expression terminates at somite 8 in anurans, but at somite 20 in chick, somite 25–27 in mouse, and somite 15–16 in salamanders [50]. Interestingly, the frog axial column has also refrained from being specified into different regions – in vertebrates, usually, the axial column would consist of cervical, lumbar, thoracic, sacral, and caudal. By contrast, in anurans, the axial column has one cervical vertebra (atlas), 5–7 presacral vertebrae (not differentiated into thoracic nor lumbar), one sacrum, and 1–2 postsacral vertebrae. The early stages of anurans develop roughly 40–50 somites, proceeding in an anterior-to-posterior direction, and they are formed in a similar manner as in other vertebrates [51, 52].

However, only the most rostral somites contribute to the anuran axial column. The somitic compartment responsible for bone – the sclerotome – is present in the ventromedial region of the somites in anurans [53], and the position of frog sclerotome differs and is reduced compared to amniotes [53]. However, the sclerotome in frogs is formed and segregated normally in both rostral and caudal somites (confirmed by observing gene expression patterns of the sclerotome markers, *Pax1*/9, *Uncx* – [54, 55]). It is speculated that chondrogenesis is prevented in the differentiated sclerotome in caudal segments because of the inability to form cartilage condensations (confirmed by the reported disrupted expression patterns of *Shh*, *Sox9*, and *Col2a1*) and is considered the reason why the anuran tail lacks ossifications [12]. The presacral vertebrae form in a typical manner after the sclerotome is differentiated. However, the developmental mechanisms behind the formation of the coccyx, which is initially formed as reduced postsacral vertebrae, is unknown.

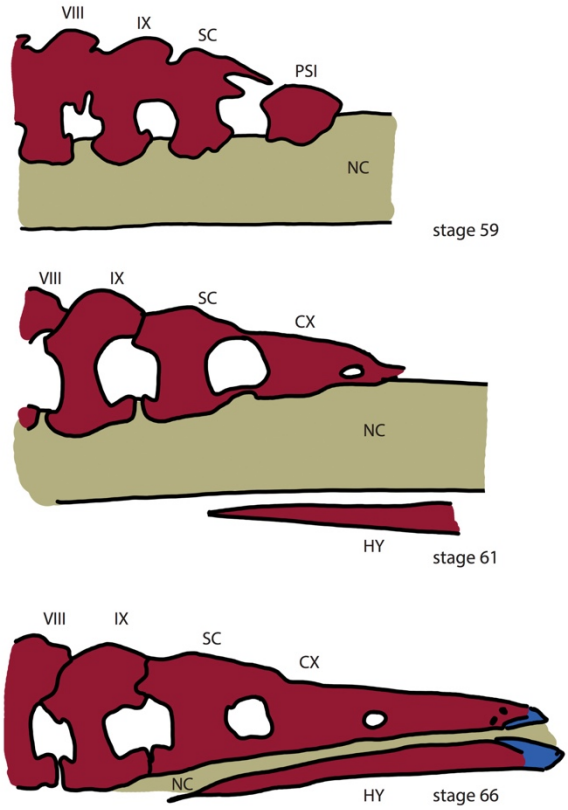

Figure 1.3. Illustrations of the urostyle formation at NF stages 59, 61 and 66. Blue denotes cartilage, red denotes bone, and brown denotes notochord. Abbreviations: SC: sacrum; CX, coccyx; NC, notochord; HY, hypochord.

The larval hypochord, which is present in embryonic stages of fish, amphibians, and lampreys (absent in amniotes), is involved in formation of the dorsal aorta [14, 16, 17]. Hypochordal cells express vascular endothelial growth factor (*VEGF*), which is a growth factor that mediates migration of angioblasts to the dorsal midline. It has been shown that early notochord plays an important role in hypochord formation: removal of the early notochord in *Xenopus* (at early neurula stage) disrupts hypochord development [14, 16, 17]; in zebrafish, *flh* and *ntl* mutants (which show mutations in early notochordal cell differentiation) also fail to develop the hypochord [56]. However, it is hypothesized that the hypochordal cells flatten against the notochord after contributing to their role in forming the dorsal aorta in early

embryonic stages of amphibians and fish. The hypochord arises independently from the vertebral column, and only in frogs it contributes to the adult skeleton, forming the urostyle, a morphological novelty of the frog radiation. However, the cells that contribute to adult hypochord formation remain to be understood, and it is important to recognize the genetic networks underlying this structure.

The coccyx and hypochord formation are suspended until frogs reach metamorphosis, where sclerotome-derived mesenchymal cells and embryonic hypochordal cells remain undifferentiated, and an external cue (i.e., thyroid hormone) could be activating the differentiation of cells.

1.7 – Questions Addressed In This Thesis

My thesis concentrates on the morphological, genetic, and evolutionary changes underlying an evolutionary novelty, the anuran urostyle. It focuses on the following: **Chapter 2** explores the embryology of the urostyle, and **Chapter 3** identifies genes and gene-regulatory pathways behind this structural innovation and its hormonal control. Finally, I also focus on functional aspects of the identified candidate genes (**Appendix A** and **Chapter 4**). The above-mentioned three approaches helped me study an evolutionary novelty in depth, and to understand the morphological, developmental, and genetic mechanisms behind the rapid transformation of the postcranial skeleton during aquatic-to-terrestrial transition of frogs.

In Chapter 2 I determined how chondrogenesis and osteogenesis reform the skeleton, aiding the transforming tadpole to adapt to a new habitat by observing bone and cartilage development and cell differentiation through a nearly complete developmental series using *Xenopus tropicalis* as the model organism. Remodeling of an organ requires changes to the

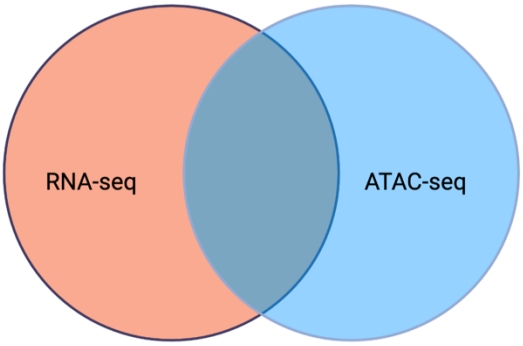

Figure 1.4. Candidate genes will be narrowed down based on the overlap between the RNA-seq and ATAC-seq analysis.

neurons, muscles and blood vessels surrounding the targeted tissue, and cell proliferation and apoptosis in most instances (e.g., studies done on the remodeling of the intestine, skin, liver during metamorphic climax; Buchholz 2017; Mukhi *et al*. 2010; Brown & Cai 2007). Using an immunohistochemistry approach, I studied cell proliferation and cell death (apoptosis), and remodeling of the muscles, neurons and vasculature at the urostyle-forming tissues. I used a microCT method to visualize 3D views of the vasculature and its changes in the newly forming frog body. My key findings and conclusions were as follows: first, I found that the coccyx and hypochord have two different developmental patterns. Second, I hypothesize that thyroid hormone directly affects hypochord formation and appears to have a secondary effect on the coccygeal portion of the urostyle. My results also suggest the ossifying hypochord plays a significant role in the evolution of the anuran body plan by occluding the dorsal aorta.

Chapter 3 focuses on the molecular underpinnings and gene-regulatory networks responsible for urostyle formation. Frog metamorphosis and the dramatic remodeling during this period are controlled by thyroid hormone. I also focused on the thyroid hormonal control that may underlie formation of the urostyle. To identify the molecular underpinnings responsible for

the formation of the urostyle at metamorphic climax, RNA-seq (a spatial transcriptomic approach) and ATAC-seq were carried out. The stages I used for these molecular genetic studies correlated with those that I used for the morphological studies (i.e., stage 57/58, stage 60/21, stage 65/66). The rationale for the stages selected for the RNA-seq approach is as follows: the

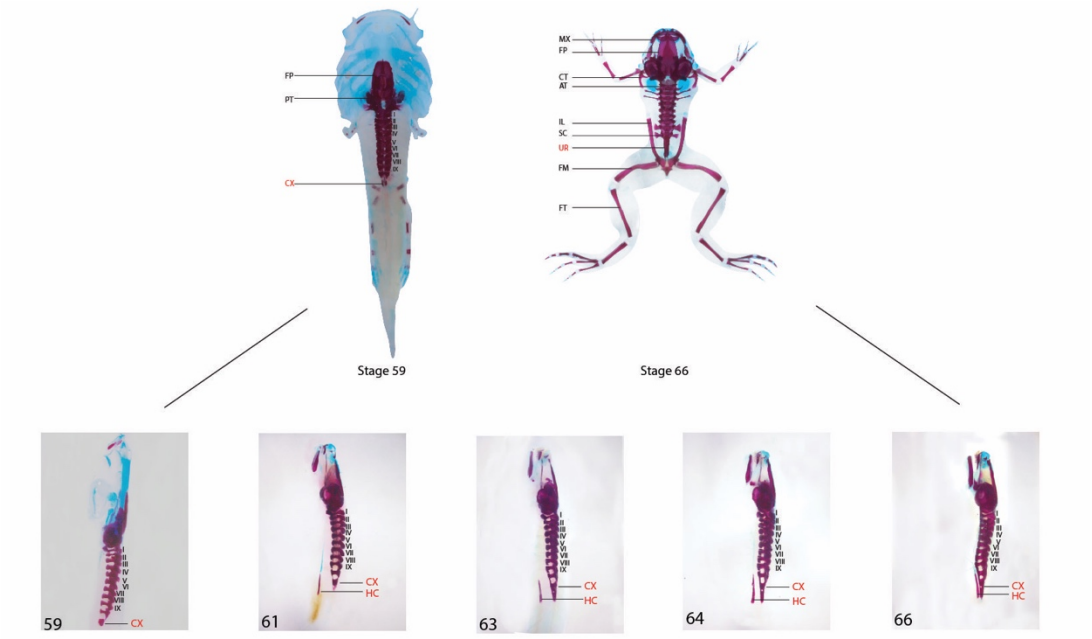

Figure 1.5. Skeletal development in *Xenopus tropicalis.*

tadpole axial skeleton (presacral vertebrae I–VII, sacrum) completes chondrification and ossification of the neural arches and centra before metamorphosis is initiated (within the first 20–30 days of the life cycle). The sclerotome-derived, mesenchyme cells remain undifferentiated at the site of coccyx formation (until it reaches stage 56/57). Hypochord, which develops ventral to the notochord, remains undifferentiated until the onset of metamorphic climax. Therefore, my objective was to identify the genes that become activated during the mesenchymal-chondrocyte transition, and to identify genes unique to the coccygeal and hypochordal tissues and to see if TH directly controls hypochord-specific genes.

Comparing the data gathered from the preceding experiment in a spatial and temporal manner helped me in identifying candidate genes responsible for the formation of the urostyle. The urostyle-responsive regulatory regions were then identified using an ATAC-seq approach. Comparing the ATAC-seq and RNA-seq results helped me narrow down the candidate genes effectively. My primary findings from the chapter were as follows: first, I found out that the coccyx and hypochord have two distinct gene expression patterns. Second, coccygeal genes are enriched with genes involved in neuronal remodeling and skeletal muscle development, whereas the hypochordal genes have high expression levels of T-box genes and genes involved in extracellular matrix organization. ATAC-seq data revealed that thousands of chromatin regions respond dynamically during development. Finally, we hypothesize that even though an ossifying hypochord is only present in anurans, it appears to resemble a congenital vertebral anomaly seen prenatally in humans.

Appendix: After identification of the candidate genes and targeted gene regulatory pathways, I concentrated on a functional assay to allow me to address effects on the urostyle when a targeted gene is disrupted. I targeted the candidate genes *TBXT*/*TBXT*.2, carried out a frameshift mutation approach using CRISPR/Cas9 on one-cell-stage tadpoles, and also a conditional knockout approach targeting the metamorphic tadpoles using a U6-promoter, gRNA and a heat-shock promoter.

My dissertation work lays the groundwork to study evolutionary novelties using an integrative approach and identifies questions that need scrutinization in the future.

CHAPTER 2
PHENOTYPIC CHANGES OF AN EVOLUTIONARY NOVELTY: THE ANURAN UROSTYLE

2.1 – ABSTRACT

Developmental novelties often underlie the evolutionary origins of key metazoan features. The anuran urostyle, which evolved nearly 200 MYA, is one such structure. It forms as the tail regresses during metamorphosis, when locomotion changes from an axial-driven mode in larvae to a limb-driven one in adult frogs. The urostyle comprises a coccyx and a hypochord. The coccyx forms by fusion of caudal vertebrae and have evolved repeatedly across vertebrates. However, the contribution of an ossifying hypochord to the coccyx in anurans is unique among vertebrates and remains a developmental enigma. Here, we focus on the developmental changes that lead to the anuran urostyle with an emphasis on understanding the ossifying hypochord. We find that the coccyx and hypochord have two different developmental patterns: first, the development of the coccyx initiates before metamorphic climax, whereas the ossifying hypochord undergoes rapid ossification and hypertrophy; second, we hypothesize that thyroid hormone directly affects hypochord formation and appears to have a secondary effect on the coccygeal portion of the urostyle. The embryonic hypochord is known to play a significant role in the positioning of the dorsal aorta (DA), but the reason for hypochordal ossification remains obscure. Our results suggest the role of an ossifying hypochord in rearrangement of the DA in the newly forming adult body by partially occluding the DA in the tail, which subsequently regresses due to this occlusion. We propose that the ossifying hypochord-induced loss of the tail during metamorphosis has enabled the evolution of the unique anuran *bauplan*.

Attributions

Results reported in this chapter have been published in the Proceedings of the National Sciences as "Senevirathne G, Baumgart S, Shubin N, Hanken J, Shubin NH**.** Ontogeny of the anuran urostyle: the developmental context of evolutionary novelty. Proceedings of the National Academy of Sciences (PNAS), Feb 2020, 117(6) 3034-3044". microCT scanning (Fig. 2.5 panel C and Figs 2.20 and 2.21) was performed by Stephanie Baumgart. Nathaniel Shubin helped with some of the histology work. The remainder of the figures and analyses were my own work. Neil Shubin and James Hanken contributed to editing the manuscript.

2.2 – INTRODUCTION

Vertebrate diversification is punctuated by the origin of structural and developmental novelties (e.g., [57-62]). The pronounced key innovation that distinguishes all anurans (frogs and toads), and enabled them to occupy new niches, is the evolution of saltatory locomotion (jumping). This innovation entails remarkable structural and developmental changes, which compose the anuran *bauplan*.

The anuran *bauplan*, conserved across the clade and characteristic of all adults, includes several features: loss of a tail, a shortened vertebral column, long hind limbs, radical transformation of the sacral region, and ventral articulation of the posterolaterally oriented pelvic girdle with a rod—the urostyle—lying between the paired ilia. The developmental processes underlying the emergence of the urostyle have received surprisingly little attention.

The urostyle is first observed in the fossil record in the early Jurassic and has remained a conserved feature for over 200 million years [4, 5]. It plays a major role in transmitting thrust

from the hind limbs to the axial column during limb-driven locomotion [4, 5]. The urostyle articulates with the posterior end of the sacrum and is a composite structure, comprising an ossified hypochord ventrally and a coccyx dorsally [8].

The developmental origin of the anuran urostyle has been a source of speculation for over a century. Griffiths [9] proposed that the urostyle originates as a posterior outgrowth of the first postsacral intervertebral body, but this claim was disputed later when it was observed that the hypochord forms ventral to the notochord (i.e., outside of the perichondral bone). Later, some authors suggested that the urostyle forms by the fusion of a variable number of caudal vertebrae, and some even stated that the urostyle originates from a single cartilaginous rod (e.g., [11]). However, these ideas waned with the discovery that the urostyle forms from two discrete units: coccyx and hypochord [8, 12].

The coccyx has a mesodermal origin and is derived from sclerotomal (paraxial mesoderm) cells [8, 12, 63]. The coccyx fuses with the ossified hypochord at the onset of metamorphosis. Forming independently from the vertebral column, an ossifying hypochord is only present in anurans. An embryonic hypochord (non-ossified), however, is seen in fishes, amphibians, and lampreys [13-16, 20, 56, 64-67], but absent in amniotes. It is a rod-like structure located ventral to the notochord. The source of the embryonic hypochord needs deeper scrutiny and is argued to be of endodermal origin (e.g., zebrafish: [15]; amphibians: [13-16, 67]) or derived from the superficial mesodermal layer (e.g., amphibians: [18, 20]; zebrafish: [18]). Compared to the coccyx, the hypochord arises from an independent cell population that is not derived from the paraxial mesoderm [12]. The embryonic hypochord, which is only present in anamniotes, secretes VEGF and patterns nearby blood vessels [14, 16]. Even though amniotes lack a hypochord, it has been shown that dorsal endoderm of amniotes has taken over the

function of the hypochord, where the dorsal endoderm forms close to blood vessels and secretes VEGF in a similar manner [68, 69].

In embryonic amphibians, the hypochord (non-ossified) lies flat over the notochord once its function of positioning the dorsal aorta is completed [13, 14], but it is retained in the postsacral region only in anurans [12]. Many questions still remain unanswered regarding the ossifying hypochord: how and why does this structure ossify only in anurans? What initiates its formation? What is the function of it?

Using an integrative approach, we show how the axial skeleton, cellular composition, neuromuscular system, spinal cord, and vasculature change during development of the urostyle, focusing on the ossifying hypochord. We discuss the novelty of this structure and compare it across the convergently evolved caudal fusions.

2.3 – Materials and Methods

Different stages of *Xenopus tropicalis* tadpoles were purchased from the National Xenopus Resource (NXR) at the Marine Biological Laboratory (MBL), Woods Hole, MA. A nearly complete developmental series was obtained and euthanized using 0.2% aqueous tricaine methanesulfonate (MS-222), and the specimens were fixed in different fixatives according to each experiment. Tadpoles were staged according to [70] Nieuwkoop and Faber (NF; 1956). Developmental stages were obtained post-hatching until the end of metamorphic climax.

2.3.1 – Staining for Cartilage and Bone

The tadpoles were cleared and stained for bone and cartilage following Hanken & Wassersug [71] and Klymkowsky & Hanken [72]. Euthanized stages were fixed in 4% neutral-

buffered formalin from overnight to four days (depending on the size of the tadpoles) and subsequently stored in 70% ethanol until they were processed for staining. Developmental stages were dehydrated in absolute ethanol and stained for cartilage using Alcian blue. Following cartilage staining, specimens were re-hydrated in a graded ethanol series (95%, 80%, 75%, 50%, 25%) and, finally, distilled water. Next, the muscles were digested in an enzyme solution (trypsin dissolved in 30% aqueous sodium borate). Subsequently, the bones were stained in alizarin red and de-stained in a solution of 1% KOH and 1% H_2O_2. The stained specimens were stored in glycerin and scored for bones/cartilage within 2–3 days of staining. Terminology for the bones, cartilage, and neuromuscular system follows Pugener & Magalia [8], Trueb [73], Duellman & Trueb [1], and Trueb & Hanken [7].

2.3.2 – Histology

Euthanized stages were fixed in Bouin fixative (picric acid + formaldehyde + acetic acid) for between 24 hours and 1 week. The specimens were decalcified using a decalcifying solution (0.5 M EDTA pH 7.0) for 30 min, washed in 1X PBS 3 times (20 min each), dehydrated in ethanol, and followed by three xylene washes. Subsequent paraffin washes were conducted at 70˚ C, and finally, tissues of interest were embedded in paraffin/paraplast molds. Paraffin-embedded specimens were sectioned at 10 μm using a rotatory microtome and mounted on to Fisherbrand Suprafrost microscope slides. Both sagittal and transverse sections were left overnight on a slide-heater at 35° C. The sections were stained as follows: initially, de-paraffinization was done in two xylene washes, sections were re-hydrated using an ethanol series and stained with Mayer haematoxylin (2 min) to visualize nuclei, and the slides were kept under running water for 20 min. Next, eosin stain was used to visualize cytoplasm and extracellular

matrix. Subsequently, dehydration was done in an ethanol series and, finally, in xylene. The slides were mounted in xylene-based DPX, sealed with a coverslip (no. 1 thickness), observed under a Zeiss Axio Imager 2 microscope and photographed using a Leica DFC 490 camera.

2.3.3 – Thyroid hormone and the urostyle development

Two experiments were conducted to visualize thyroid hormone (TH) involvement in urostyle development. Five stage-54 tadpoles were reared in 1 mM goitrogen methimazole (MMI; Sigma-Aldrich; 100 mg/L of aquarium water) [23, 74, 75] and another five stage-54 tadpoles as the control experiment in 0.1 MMR (1x MMR = 100 mM NaCl, 2 mM KCl, 1 mM $MgSO_4$, 2 mM $CaCl_2$, 5 mM HEPES, pH 7.4). The tadpoles were reared for two months and then stained for bone and cartilage (see above) to see the effect of TH on urostyle development. This experiment was repeated twice.

2.3.4 – PMA staining and CT scanning

Five tadpoles (NF stages 58, 59, 61, 64, 66) were dehydrated in 100% methanol, taken through a sucrose series, and left in 25% sucrose overnight or until the tadpoles sunk to the bottom. Finally, tadpoles were stained with 5% phosphomolybdic acid (PMA) dissolved in distilled water for 5−7 days. Tadpoles were washed in distilled water prior to scanning to get rid of excess stain. The specimens were scanned with the UChicago PaleoCT scanner (GE Phoenix v/tome/x 240kv/180kv scanner). The settings for close-scans of the urostyle area are as follows: at 70 kV, 220 μA, no filtration, 3× averaging, exposure time of 1000 ms per image, and a resolution of 6.3330 μm per slice (512 μm^3 per voxel). Whole bodies of tadpoles were scanned by using the following parameters: at 90 kVp, 190 μA, no filtration, 3×-averaging, exposure time

of 200 ms per image, and a resolution of 17.9820 μm per slice (512 μm^3 per voxel). Scanned images were analyzed and segmented using Amira 3D Software 6.0 (FEI) (Fig. 2.1B) and Materialize Mimics 22.0 segmentation software (Fig. 2.5C).

2.3.5 – Cell proliferation

Two tadpoles each from NF stages 55, 57, 61, and 63 were exposed to water containing 5-bromo-2-deoxyuridine (BrdU, Sigma-Aldrich), 1 mg/ml, for 72 hr to label the proliferating cells. The tadpoles were subsequently euthanized in MS-222 and fixed overnight in 4% PFA at 4^o C. The next day, the specimens were washed three times in ice-cold 1x PBS (15 min each) and transferred to 15% and 30% sucrose solutions. They were left overnight at 4^o C until they sunk to the bottom of the tube. The tadpoles were then placed in TissueTek O.C.T compound, flash frozen using liquid nitrogen, and sectioned at 20–25 μM using the Leica cryostat CM1900 and mounted on Fisherbrand SuperFrost Plus slides. Cryosections were rinsed three times in 1x PBS, permeabilized using 0.01% Triton/PBS solution, blocked in 2% skim milk solution, and incubated with the anti-BrdU (Sigma-Aldrich, mouse monoclonal; 2:1000 concentration) for 1 hr. The next day, the sections were washed three times in 0.25% Tween/PBS solution (10 min each), incubated in a solution of the secondary antibody (ThermoFisher, goat anti-mouse, Alexa Fluor 594, 2:1000), phalloidin – Alexa 488 (Invitrogen, 1:1000) and DAPI (Life technologies, 1:1000) for 1 hr. Finally, the cryosections were washed in 0.25% Tween/PBS solution, mounted in 50% glycerol, and visualized using a Zeiss 710 confocal microscope. The results were analyzed using Fiji image analysis software.

2.3.6 – Section-immunohistochemistry for cell death, neurons and muscle remodeling

Six tadpoles from each stage (57, 60, 64, 66) were fixed overnight in 4% PFA and frozen in TissueTek O.C.T using liquid nitrogen. The frozen samples were sectioned using a cryostat at 30 μM and were dried at room temperature for 30 min. Antibody staining was done as described in the preceding section: tissues were permeabilized in Triton/PBS, blocked in 2% skim milk solution, and incubated overnight in the primary antibody solution. To observe cell death by apoptosis, anti-Caspase-3 antibody (abcam ab13847, 2:1000) was used; for neurons, acetylated Tubulin (Sigma, mouse monoclonal, 2:1000) was used; for muscle fibers, Laminin antibody from DSHB (3H11, 4:100) and anti-MyHC from DSHB (MF20, 1:20) were used; for sarcomere proteins anti-titin, anti-myomesin, and anti-tropomyosin were used (Table S1). The next day, the tissues were washed in 0.25% Tween/PBS solution and incubated in the secondary antibody (mouse monoclonal, 2:1000) + Phalloidin (to visualize the extracellular matrix, 1:1000) + DAPI (nuclei, 1:1000). Finally, the slides were washed in 0.25% Tween/PBS and visualized under a Zeiss 710 confocal microscope. The results were analyzed using the Fiji image analysis software.

2.3.7 – Whole mount *in-situ* hybridization (WMISH) and whole-mount immunohistochemistry (WMIHC)

Whole mount *in-situ* hybridization for the sclerotome marker *Pax9* was done as previously described [76]. The primer sequences for the gene *Pax9* are as follows: Forward – AGT AGG AAC ACG TTT CAG TCG and Reverse – TTG GAT CCT AGA GAT GAC AGC. After the color developed, the tadpoles were fixed overnight in 4% PFA at 4^{o} C, transferred to 30% sucrose solution and flash frozen in OCT using liquid nitrogen. The tissues were sectioned using a Leica cryostat and mounted using 50% glycerol. The slides were photographed using a

Leica DFC 490 camera. For WMIHC, tadpoles at stages NF 58, 59, 61, 63 and 66 were euthanized in MS-222 and fixed overnight in Dent fixative (methanol:DMSO = 4:1) at room temperature. The staining was done as previously described [85, 90] with slight modifications. Tadpoles were washed in 1% PBTriton (1x Phosphate-buffered saline + 1% Triton) for 3 hr and transferred to 25% trypsin in PBS for 10 min. Next, they were transferred to pre-cooled acetone for 20 min. Specimens were washed in 1% PBTriton and blocked overnight at 4° C in a solution containing 1% PBTriton + 10% goat serum + 5% H_2O_2 + 1% DMSO). Blocking solution was replaced by the primary antibodies: for muscles 12-101 (from DSHB, 1:50) and nerves (acetylated tubulin: Sigma, 1:1000) and were left at 4° C for 3 d. The tadpoles were washed five times in 1% PBTriton (1 hr each) and transferred to the peroxidase-conjugated secondary antibody solution (Jackson labs 115-035-003, 1:1000) in 10% goat serum + 1% PBTriton. Finally, the specimens were washed in 1% PBTriton for 5 hr and subjected to DAB reaction.

2.3.8 – Data deposition

The CT scanned data of stage 59, 64 and 66 have been submitted to MorphoSource (doi:10.17602/M2/M97424, doi:10.17602/M2/M97371, doi:10.17602/M2/M97372), under the project name "Ontogeny of the Urostyle"(project number: P884).

2.4 – RESULTS

2.4.1 – Coccyx and hypochord develop during metamorphic climax

We stained cartilage and bone using Alcian blue and alizarin red, respectively. The majority of postcranial elements complete ossification before metamorphic climax. The presacral vertebrae are recognized as I–IX, where the first vertebra is called the atlas, the IX vertebra – is the

Antibody	Source	Identifier	Dilution
Anti-myomesin (mouse monoclonal)	DSHB	mMaC myomesin B4	1:20
Anti-titin (mouse monoclonal)	DSHB	9D10	1:20
Anti-MyHC (mouse monoclonal)	DSHB	MF20	1:20
Anti-tropomyosin (mouse monoclonal)	DSHB	CH1	1:20
Anti-Caspase3 (mouse monoclonal)	abcam	Abcam13847	1:1000
Anti-acetylated tubulin (mouse monoclonal)	Sigma	T7451	1:1000
Anti-laminin	DSHB	3H11	1:25
Antibody for skeletal muscles	DSHB	12-101	1:50

Table 2.1. Details of the antibodies used in the study.

sacrum. A typical vertebra has two prezygapophyses (at the rostral end), two postzygapophyses (at the caudal end) and two transverse processes. The first presacral, atlas (= cervical vertebra) is distinct in having cervical condyles, which are articulating surfaces with the occipital condyles, and bears only postzygapophyses.

The cartilaginous precursors of the neural arches of presacral I–VI were formed by stage 45 (Fig. 2.7). By stage 50, VII–IX neural arches also formed. By stage 54, base of the pedicels of

the presacrals start to ossify (starting from the part where they are attached to the lateral ends of each centrum); cartilaginous models for each presacral, sacrum and postsacral I (PSI; (contributes to the future urostyle), also form. All the neural arch pedicels of the presacrals and sacrum have ossified by stage 55 (Fig. 2.7). By stage 58 (before the metamorphic climax), the centra of presacrals and sacrum have fused medially and also with left and right neural arch pedicels corresponding to each vertebra; the PSI centrum is fused medially (Fig. 2.1A, C). When the metamorphic climax is initiated (stage 59), the neural arch pedicels of the PSI fuse together, forming the anterior-end of the cone-shaped coccyx. PSI is triangular shaped, reduced in width compared to the rest of the vertebrae (Fig. 2.1A–C). By stage 61, the neural pedicels of the PSII ossify, and subsequently extends in length with development. The hypochord ossification was initiated ventral to the notochord and PSII, as a slender ossifying stripe, ventral to the PSII (Fig. 2.1A–C). The hypochord extends in length anteriorly and posteriorly (Fig. 2.1C). By stage 63, transverse processes of presacrals II–VIII, sacrum and PSI, which are connected to the neural arches laterally start to ossify. The PSIII neural arches formed by stage 64, and PSII and PSIII extend in length both anteriorly and posteriorly (Fig. 2.1C).

Concomitantly, the hypochord also increased in length, and extended up to the anterior-most margin of the sacrum and the posterior-most margin of the PSIII, anteriorly and posteriorly. By stage 65 and 66, the notochord degenerates; PSII and PSIII fuse together and form two strips of ossifications losing the myomere boundaries. PSI fuses with the anterior margins of PSII (Fig. 2.1C). At the end of metamorphosis, coccyx (cone-shaped) fuses synostically with the hypochord (a cylindrical rod).

Coccygeal formation is initiated during prometamorphosis (stage 54), when cartilaginous postsacral vertebra I (PSI) forms (Fig. 2.7). PSI is triangular-shaped and narrower than other

presacral vertebrae (Fig. 2.1A–C). By stage 61, the neural pedicels of PSII are ossified, and PSII continues to extend in length anteroposteriorly. At this stage, hypochord ossification is also initiated ventral to the notochord and PSII appears as a slender ossifying stripe (Fig. 2.1A–C). By stage 63, the hypochord has extended in length anteroposteriorly (Fig. 2.1C). The PSIII neural arches form by stage 64, and PSII and PSIII extend anteroposteriorly (Fig. 2.1C). Concomitantly, the hypochord extends anteriorly to the anterior-most margin of the sacrum and posteriorly to the posterior-most margin of PSIII. By stages 65 and 66, notochordal degeneration has initiated and PSII and PSIII have fuse, forming two strips of ossifications, losing the myomere boundaries. PSI fusion with the anterior margins of PSII happens subsequently (Fig. 2.1C). At the end of metamorphosis, the cone-shaped coccyx has fused synostotically with the hypochord.

2.4.2 – Osteocyte-chondrocyte differentiation at the sites of urostyle development

The cells contributing to the coccyx have a paraxial mesodermal origin [12], and the embryonic hypochord is argued to be derived from the endoderm/superficial mesoderm [13-16, 20, 56, 65-67, 69]. However, not much is known about the ossifying hypochord. We conducted histology of sectioned tissues and focused on ossification patterns of the hypochord. The sclerotome in frogs is formed in both rostral and caudal somites [55] but only the rostral somites (somites 1–12 in *X. tropicalis*) contribute to the axial column [12, 77]; somites 9–12 contribute to the coccyx (= fused postsacral vertebrae I–III) [8, 12]. The bony coccyx forms from three ossification centers, which subsequently enlarge via endochondral ossification. Before metamorphosis, sclerotomal mesenchymal cells (MS) are present within the extracellular matrix (ECM) around the spinal cord, dorsal to the notochord (Fig. 2.2A–B), and sclerotome-derived mesenchymal cells are not observed ventral to the notochord (Fig. 2.12). The MSs aggregate and

form the neural arch condensations for PSI by stage 57; these eventually form immature chondrocytes (IC) (Fig. 2.2A– A’’). By stage 61, osteoblasts form and cover the mature chondrocytes of the PSI, and the neural arches fused medially (Fig. 2.2C’). MSs condense and form immature and mature chondrocytes, forming the neural arches of PSII (Fig. 2.2D–D’’). Osteoblasts arrange around the anterior- half of the PSII cartilaginous neural arch and secrete bone matrix (Fig. 2.2C–C’’). Cartilaginous matrix of PSII was deposited; perichondrium forms surrounding anterior- half of the PSII cartilaginous condensation. Subsequently, the MSs continue to condensate, extending posteriorly from each neural arch of PSII. By stage 64 PSIII also starts to ossify in a similar manner as PSII. PSII-III neural arches ossify first, then the cartilaginous matrix connecting the arches ossify, forming two longitudinal stripes; finally, the two strips of ossifications fuse medially (Fig. 2.2E–E’’) and also with the PSI anteriorly. Periosteum forms surrounding the coccyx (Fig. 2.2E’). At the onset of metamorphosis, the ventral connective tissue around the notochord grows by increasing the number of cell layers (Figs 2.2D, D’’, H, 2.9–2.11). The undifferentiated cells giving rise to the ossifying hypochord (here referred to as osteo-chondro progenitors) aggregated and formed cartilaginous condensations (Fig. 2.12), which were seen within the body region (Figs 2.9–2.11) but not in the tail (Figs 2.19–2.11). Hypertrophic chondrocytes were visible in the ventral portion of the hypochord; osteoblasts formed below the chondrocyte-layer and began forming the perichondrium (Fig. 2.2D, D’’, H, Figs 2.10, 2.11). Within two days into metamorphic climax, hypertrophic chondrocytes differentiated and deposited cartilaginous extracellular matrix (ECM); the perichondrium with developing mineralized ECM was observed subsequently. Hypochordal ossification was more rapid relative to that of the coccyx (Fig. 2.2B–B’’, D–D’’, F–F’’). Initial hypochordal chondrocytes accumulated along the midline of the tadpole body and formed a rod,

with more cells accumulating on lateral sides of the hypochord (Figs 2.9–2.11). Cells at the lateral-most margins of the hypochord are irregular in shape with numerous filopodia and appear to be migrating from the connective tissue around the notochord (Fig. 2.12). Future studies are needed using a cell-tracing method to validate if it is the endoderm-derived embryonic hypochordal cells that undergo a cell-fate change during metamorphosis or if it is mesodermal cells that undergo ossification.

2.4.3 – Thyroid hormonal control during the formation of the urostyle

Thyroid hormone (TH) peaks during metamorphic climax [23, 24, 32, 34, 35, 78-80]and controls many structural modifications that a tadpole undergoes during metamorphosis, including loss or remodeling of larval cartilage and *de novo* formation of bones [81-83]. To see if TH affects the formation of the urostyle, which also forms at metamorphic climax, we inhibited TH using methimazole in stage-54 tadpoles; methimazole inhibits thyroid gland function and prevents metamorphosis [84-86]. The axial column is partially developed by stage 54 (Fig. 2.7), making it an ideal stage to begin testing the effect of TH on urostyle formation. After two months, the control tadpoles metamorphosed normally, but the methimazole-treated tadpoles had not completed metamorphosis and had halted their development (Fig. 2.14). TH-inhibited tadpoles had incomplete development of the coccyx: the neural arches of PSI and PSII were developed (Fig. 2.14), but PSI and PSII remained unfused. The coccygeal morphology of the methimazole-treated tadpoles resembled a stage-61 tadpole in the control experiment. However, hypochord formation was disrupted entirely (Fig. 2.14). Partial coccygeal development and no hypochordal development (Fig. 2.14) suggests the possibility of coccyx and hypochord being controlled by two developmental triggers. Hence, we hypothesize that the larval hypochordal

cells (at myotome 8–12) undergo chondrogenesis and osteogenesis in the presence of TH and contribute to the ossifying hypochord during metamorphosis in anurans.

2.4.4 – Muscular remodeling near the urostyle

A tadpole body possesses myotomes (dorsalis trunci: DT) that undergo secondary myogenesis during metamorphosis [87-89]. Three muscles are connected to the urostyle in an adult frog: longissimus dorsi (LD), coccygeo-iliacus (CI), and coccygeo-sacralis (CS) [1, 4]. This muscle arrangement enables saltation in anurans [4]. We conducted whole-mount and section-immunohistochemistry to observe the change in muscular composition with respect to the coccyx/hypochord formation, tail and notochord degeneration, and change in muscle fiber width. Before metamorphosis, the tadpole body (Fig. 2.3A, D–D'') and tail (Fig. 2.15) possessed muscle fibers that were between 20 and 150 μm wide. With the onset of metamorphosis (stage 61, Fig. 2.16), the dorsal-most muscles (newly forming longissimus dorsi, LD) increased in the number of muscle fibers and decreased in fiber diameter (< 20 μm). LD was the first urostyle-associated muscle to form by stage 61 (Fig. 2.16). Most of the ventral muscle margins disappeared (Fig. 2.2E'), and only the lateral and dorsal-most muscles were apparent (Fig. 2.16). By stage 63, CI started to form (Fig. 2.3E–E"). At the end of metamorphosis, LD had increased in area (Fig. 2.3F–F'', Fig. 2.17) and in the number of muscle fibers; area of DT had decreased (Figs 2.17, 2.19) and the number of muscle fibers had decreased (Fig. 2.3F–F''). Ventrally, two muscles were evident: CS and CI (CI is the last muscle to form), which were attached to the developing urostyle (Fig. 2.3F–F''). The number of muscle fibers of CS and CI was reduced, and muscle fiber width had increased (> 100 μm) compared to the ventral larval muscles seen at

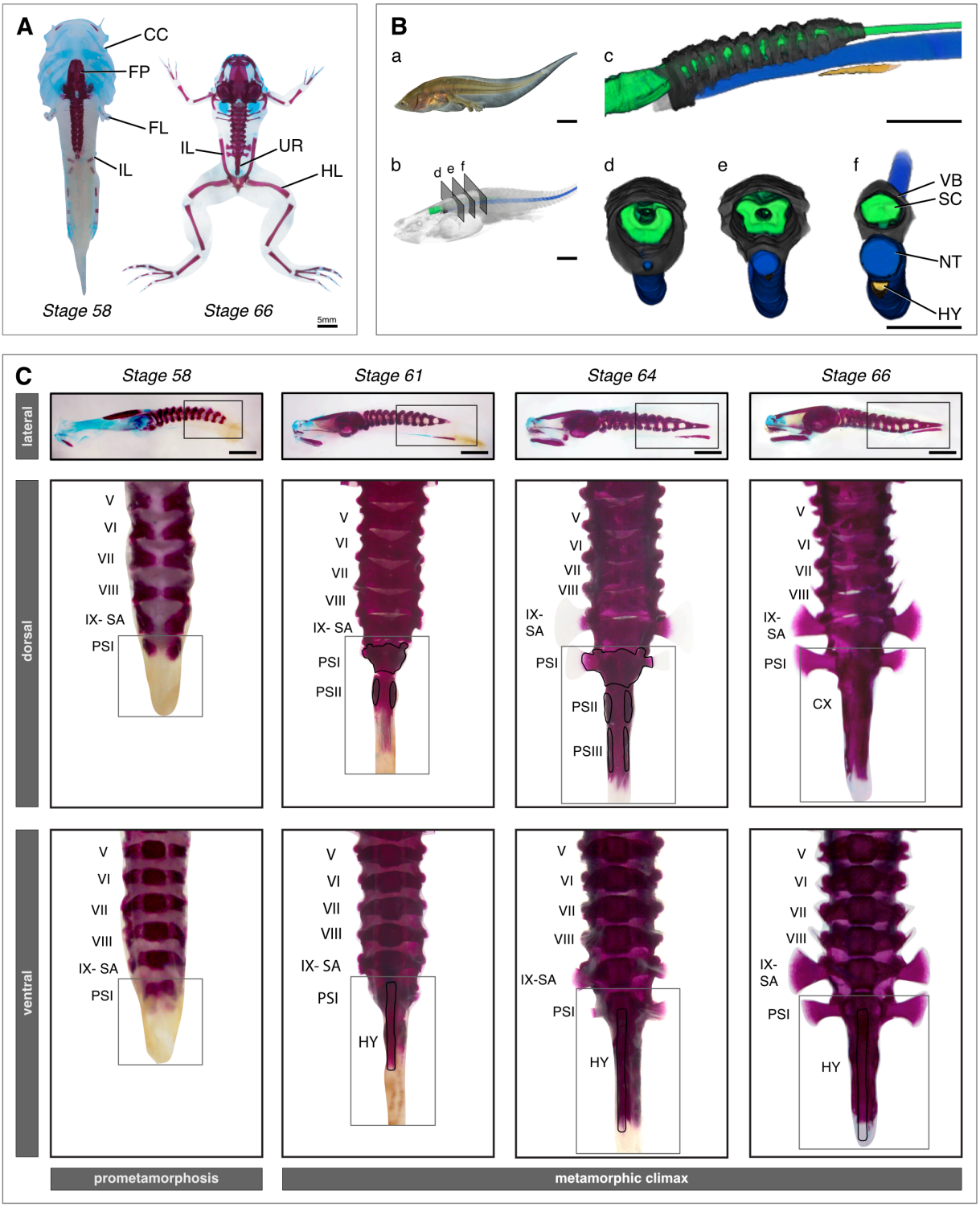

Figure 2.1. Bone and cartilage formation of the urostyle.

Fig. 2.1, continued. (A) Dramatic skeletal remodeling at metamorphic climax in *Xenopus tropicalis* visualized through cartilage and bone staining, using Alcian blue and alizarin red, respectively. Cartilage is depicted in blue; bone is depicted in red. The larval chondrocranium remodels and forms new cranial bones. The urostyle forms during metamorphic climax and lies between the two ilia. **(B)** CT-scanned tadpole of *Xenopus tropicalis*, NF stage 61 (metamorphic climax – day 2), highlighting axial skeleton formation at the rostral end of the tadpole body. The coccyx and the hypochord form mid-length of the body, and the tail resorbs completely during metamorphosis. Ba, photograph of a live NF-61 tadpole; Bb, CT-scanned tadpole after volume rendering; Bc–Bf, segmented tadpole highlighting the spinal cord, axial column, notochord, and hypochord. **(C)** Coccyx and hypochord formation at metamorphic climax in *Xenopus tropicalis*. The coccyx is initiated as two ossification centers, which extend posteriorly and anteriorly. The hypochord forms ventral to the notochord and fuses with the coccyx at the end of metamorphic climax. Dorsal and ventral views are higher- magnification images of the selected areas of the lateral view of each corresponding stage. The selected vertebrae are numbered from I to IX. Abbreviations: CC, chondrocranium; CX, coccyx; FP, frontoparietal; FL, forelimb; FM, femur; HY, hypochord; HL, hind limb; IL, ilium; NT, notochord; PS, postsacral; SA, sacrum; SC, spinal cord; UR, urostyle; VB, vertebrae. Scale bars denote 5 mm.

prometamorphosis and at the beginning of metamorphic climax. A close look at the sarcomere proteins of the muscles near the urostyle before, during, and at the end of metamorphic climax indicates that the muscle-sarcomeres are disorganized with the onset of metamorphosis (Fig. 2.18). Our findings suggest that the muscles near the developing urostyle may be undergoing "myofiber turnover" – a phenomenon that can be recognized by the large, larval myofibers degenerating and small muscle fibers forming and replacing the larval ones [90-93]. However, the change in myofiber width could also be due to re-shaping of the myofibers, corroborant with the posterolateral rotation of the pelvic girdle (Fig. 2.13). Future studies using a cell-lineage tracing method is needed to better understand these events.

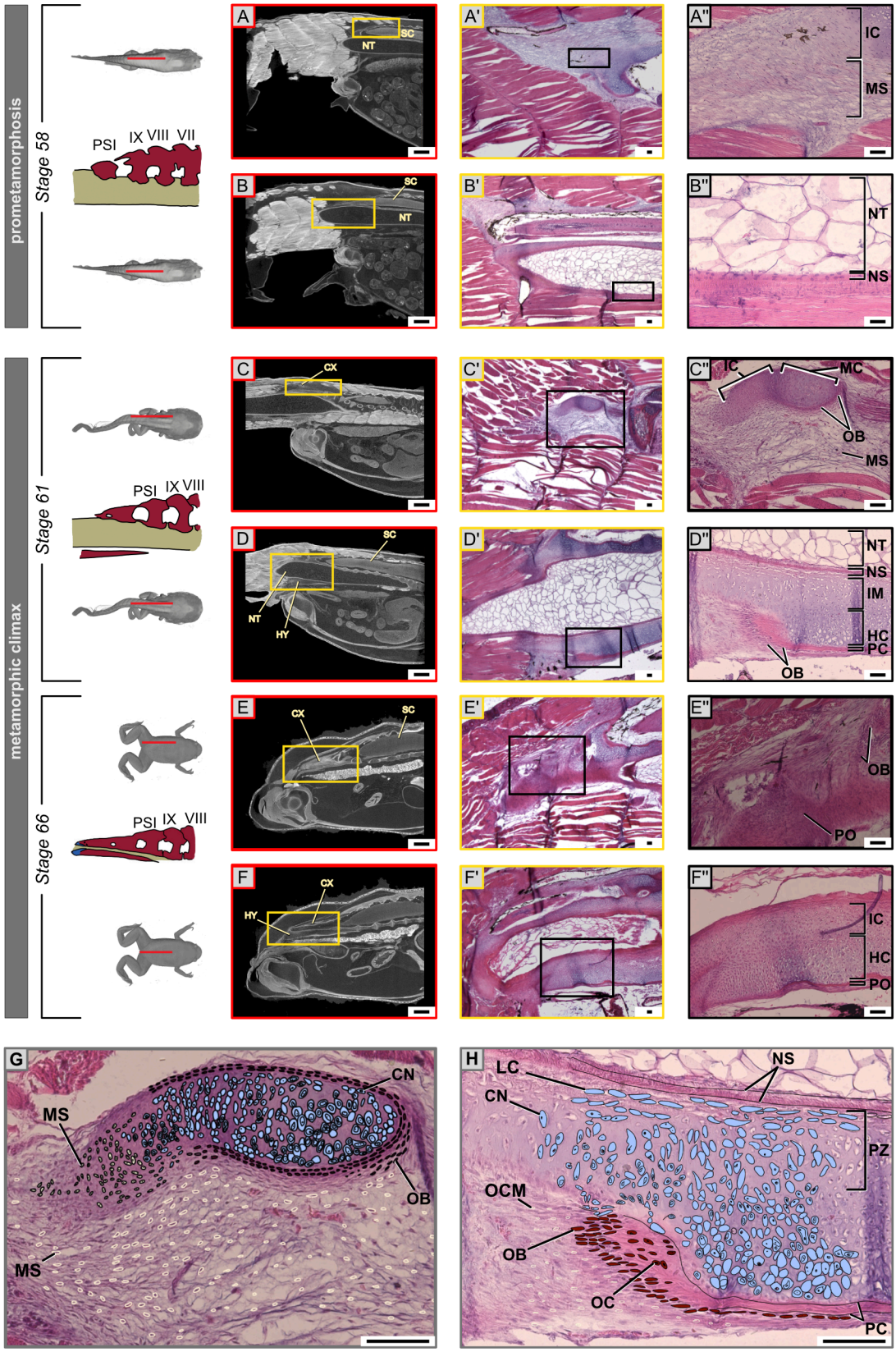

Figure 2.2. Chondrocyte-osteocyte differentiation during urostyle formation.

Fig. 2.2, continued. (A–H) Hematoxylin (stains nuclei purple) and eosin (stains cytoplasm and extracellular matrix pink) staining of histological sections (sagittal, **A'–F'**) and orthoslices (sagittal, **A–F**) of CT scans of *Xenopus tropicalis* at the site of urostyle formation. The upper row of each stage corresponds to a left parasagittal section. The lower row of each stage depicts a mid-sagittal section. Magnified cells in the last column (**A" –F"**) are cells of interest, which change during development. (**A', B', A", B"**) At stage 59, undifferentiated mesenchymal cells (scleroblasts) at the sites of the future coccyx aggregate to form mesenchymal condensations that form the rudimentary neural arches; osteo-chondro progenitors of the hypochord are present ventral to the notochordal sheath. (**C', D', C", D"**) Cartilaginous condensations are visible as immature chondrocytes and mature chondrocytes in the ossifying coccyx and hypochord; the perichondrium starts to form around the mature chondrocytes. (**E', F', E", F"**) The periosteum forms with the degeneration of the cartilaginous matrix, but, during hypochord ossification, hypertrophic chondrocytes degenerate and some de-differentiate into osteocytes. (**G, H**) Illustrations of ossification patterns of the coccyx and hypochord, highlighting the proliferating zone, growth zone and ossifying zones for the two tissue types. Abbreviations: CN, chondrocytes; CX, coccyx; ECM, extracellular matrix; HC, hypertrophic chondrocytes; HY, hypochord; IC, immature chondrocytes; LC, lacunae; MC, mature chondrocytes; MS, mesenchymal cells (scleroblasts); NS, notochordal sheath; NT, notochord; OB, osteoblasts; OC, osteocytes; OCM, osteo-chondro progenitors; PC, perichondrium; PO, periosteum; PZ, proliferating zone; SC, spinal cord. Scale bars denote 2 mm (**A–F**) and 100 μm.

2.4.5 – Remodeling of the spinal cord and peripheral nervous system (PNS) adjacent to the urostyle

The spinal cord and peripheral nervous system (PNS) differ between tadpoles and adults [94-96]. To see how innervation and the spinal cord change at the sites of the future urostyle, we conducted whole-mount and section immunohistochemistry. The spinal cord in transverse cross-sections across caudal myomeres XII-XIV appeared comparatively smaller than the presacral spinal cord (Fig. 2.15) but larger than the tail spinal cord (Fig. 2.15). At the end of metamorphosis, the spinal cord (referred to as the filum terminale in adults) is visible as fibrous tissue, and axons project outwards from the spinal foramina (Fig 4, See S1 Appendix, fig S9).

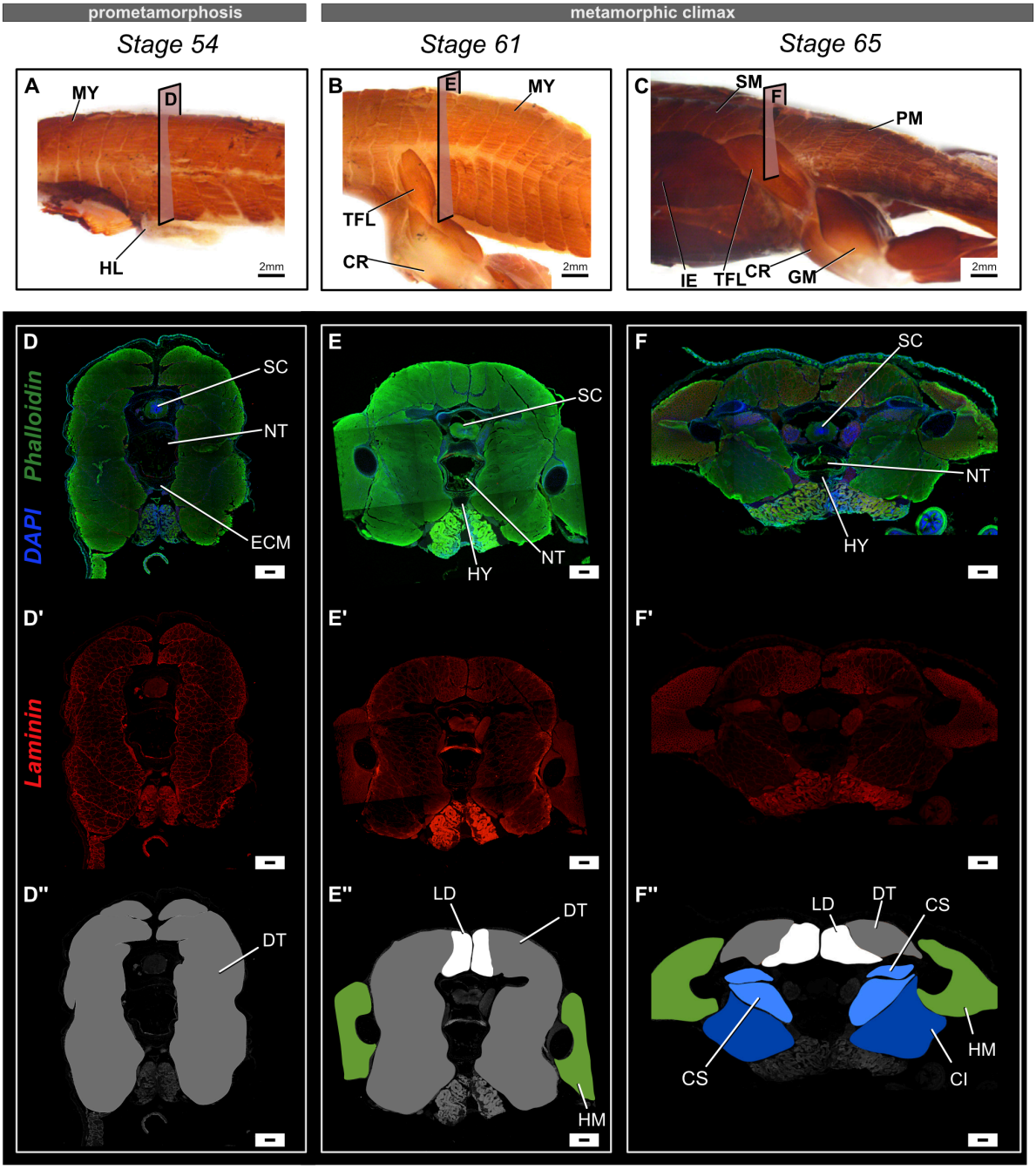

Figure 2.3. Changes in muscle composition near the urostyle before and after metamorphosis in *Xenopus tropicalis*. (**A–C**) Lateral views of whole-mount immuno-stained specimens for skeletal muscle marker 12-101 at stages 54 (**A**), 61 (**B**), and 65 (**C**). Before metamorphic climax, primary muscles are undifferentiated and referred to as dorsal trunci (DT). During metamorphic climax, the myomeres undergo secondary myogenesis and form new muscle types, which differ in muscle fiber width and are attached to the newly forming skeletal structures. The coccygeo- iliacus originates from the lateral surface of the urostyle; the

Fig. 2.3, continued. longissimus dorsi originates from the dorsal part of the urostyle and extends anteriorly; and the coccygeo-sacralis connects the sacrum and the coccyx. (**D–F and D'–F'**) Transverse cross-sections across the trunk myotome XII at prometamorphic and metamorphic stages, where phalloidin (green) stains the extracellular matrix, DAPI (blue) stains nuclei, and laminin (red) stains muscle fibers. (**D, D', D"**) Comparison of muscle fiber width shows that primary muscles have a constant width across the trunk body. (**E', F'**) Newly differentiating muscles (dorsal-most muscles) are smaller in fiber width. (**D", E", F"**) Illustrations of the transverse cross-sections of the respective stages highlighting the different types of primary and secondary muscles. Abbreviations: CI, coccygeo- iliacus; CR, cruralis; CS, coccygeo-sacralis; DT, dorsalis trunci; GM, gluteus magnus; HL, hind limb; HM, hind limb muscles; IE, iliacus externus; LD, longissimus dorsi; MY, myomeres; PM, primary muscles; SM, secondary muscles; TFL, tensor fasciae latae. Scale bars denote 2 mm (**A– C**) and 100 µm.

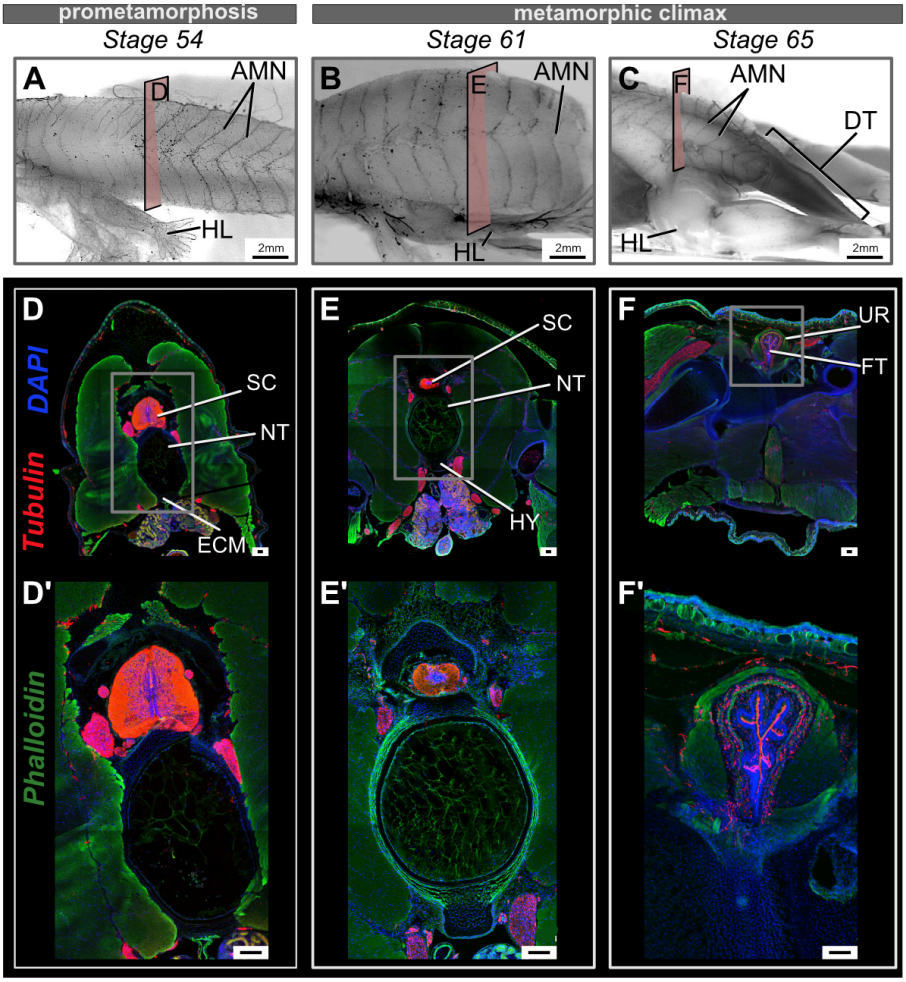

Figure 2.4. Changes in the spinal cord and innervation at the sites of urostyle formation during development.

Fig. 2.4, continued. (**A–C**) Lateral views of whole-mount immuno-stained tadpoles using acetylated tubulin, at stages 54 (**A**), 61 (**B**), and 66 (**C**). Before tail regression is initiated, the axial myomeres possess axial motor neurons (AMN), equally distributed, but AMNs degenerate with the regressing tail during metamorphic climax. (**D–F**) Transverse cross-sections across trunk myotome XII at prometamorphic and metamorphic stages, immuno-stained for acetylated tubulin (red), extracellular matrix (green), and nuclei (blue). (**D'–F'**) Magnified images of the spinal cord for each corresponding stage. (**D, D'**, **E, E'**) The spinal cord is recognizable as gray matter (in the middle) and white matter (surrounding the gray matter) in transverse cross-sections. (**F, F'**) The spinal cord changes shape with the fusion of the coccyx and hypochord and is referred to as the filum terminale. Abbreviations: AMN, axial motor neurons; DT, degenerating tail; ECM, extracellular matrix; FT, filum terminale; HL, hind limb; HY, hypochord; NT, notochord; SC, spinal cord; UR, urostyle. Scale bars denote 2 mm (**A–F**) and 100 μm.

The filum terminale had myelinated fibers running anteroposteriorly (Fig. 2.4F, F' and Fig. 2.15). When the tail started to degenerate the spinal nerves at the posterior-most end of the tail also degenerated (Fig 2.4C; Fig. 2.17). Spinal nerve X exited through the spinal nerve foramina of the urostyle, and the rest of the caudal spinal nerves degenerated concordant with the fusion of the coccyx and hypochord (Fig. 2.4C).

2.4.6 – Dorsal aorta and the ossifying hypochord

The embryonic hypochord (non-ossified) forms after 3–4 days in a developing embryo and helps position the dorsal aorta (DA) [13]. After DA is formed, the hypochord degenerates completely in fishes and salamanders [13, 14] but it ossifies at the mid-length of the tadpole-body in anurans and contributes to the axial column [12]. To see if the ossifying hypochord plays a role in major blood vessel re-organization during metamorphosis, we reconstructed the DA,

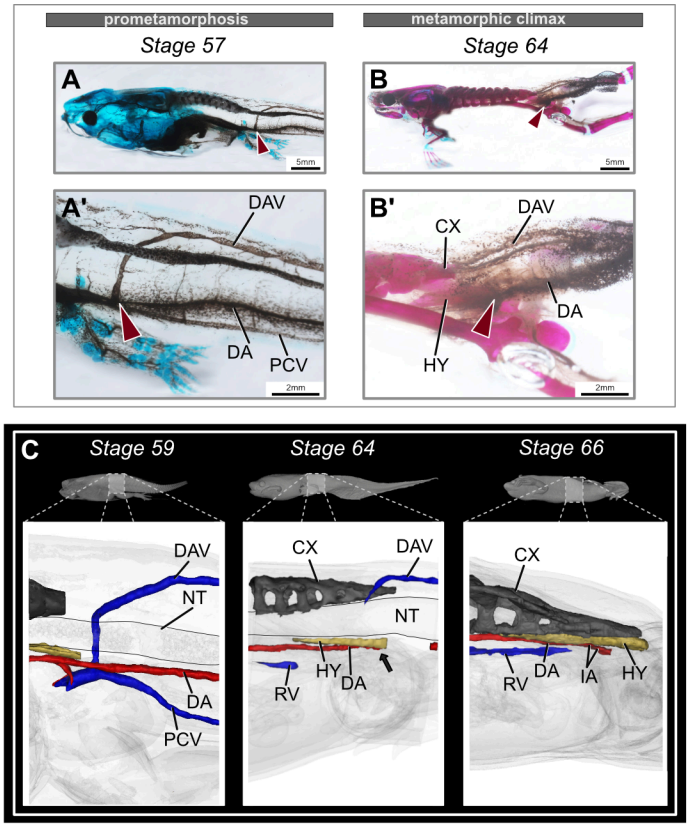

Figure 2.5. Rearrangement of the major blood vessels during metamorphosis.
(A, B) Comparison of the dorsal aorta and posterior veins in the tadpole tail during metamorphosis, lateral view. Before metamorphosis, the DA and PCV are present ventral to the notochord and the DAV is present dorsal to the spinal cord. The DAV then merges with the PCV. At the end of metamorphosis, stage-64 tadpoles lose the DA partially, along with PCV and DA. Red arrows point at the merging of DAV and PCV. (**A', B'**) Magnified images of the corresponding stage, highlighting the major blood vessels. **(C)** microCT-scanned tadpoles at prometamorphic and metamorphic climax stages. Black arrow points to the occlusion point of the DA at stage 64 (before the tail starts to regress). Stage 66 highlights the formation of new veins and rearrangement of the DA in the metamorphosed frog. Abbreviations: CX, coccyx; DA, dorsal aorta; DAV, dorsolateral anastomosing vessel; HY, hypochord; NT, notochord; PCV, posterior cardinal vein; RV, renal vein.

posterior cardinal vein (PCV), and dorsolateral anastomosing vessel (DAV) in metamorphosing tadpoles using microCT scans (Fig. 2.10). The DA was present ventral to the notochord along the trunk, the PCV was ventral to the DA before metamorphosis (Figure 2.5A, A', C; 2.9; 2.18), and the DAV was dorsal to the spinal cord; the DAV and PCV merged ventral to the PSI (myomere XI). At the onset of metamorphosis, the hypochord ossified dorsal to the DA (Figs 2.5C; 2.20). By stage 63, when the hypochord reached its maximum length, the DA was occluded at the posterior-most end of the hypochord (Figs 2.5C; 2.20). This occlusion could be a reason for the accelerated tail resorption within the next 2–3 days during metamorphic climax (Fig. 2.5B, B', C). Tail resorption is evident by the sudden pigmentation change (Fig. 2.5B, B') and is likely due to blood loss in the tail [49]. After partial occlusion of the DA, it was remodeled into two branches that form iliac arteries and enter the hind limbs (Fig. 2.5B, B', C; 2.21).

2.4.7 – Cell death and cell proliferation

Cell death and cell proliferation are two key processes of metamorphic climax [83]. To assess how these two phenomena affect bones, cartilage, neurons, and muscles at the site of the urostyle, we conducted cell proliferation (using anti-BrdU) and cell death (anti-caspase3 antibodies) immunohistochemistry on whole-mounts and sections. Before metamorphosis (e.g., stage 58), cells proliferate near the dorsal-most muscles (Fig. 2.6A, A', Fig. 2.22); no cell death was observed (Fig. 2.6D, D', stage 57). With the onset of metamorphic climax, dorsal-most and lateral muscles continued to divide (Fig. 2.6B'); innermost muscles surrounding the notochord and ventral-most muscles underwent apoptosis (Fig. 2.6E'). The lateral-most margin of the hypochord demarcated the proliferating chondrocyte zone (Fig. 2.6C, C', C'') with increased cell proliferation; no cell death by apoptosis was observed at the sites with mature hypertrophic

chondrocytes (Fig. 2.6G, G', G''). Usually, mature hypertrophic chondrocytes (HC) in an ossifying tissue undergo apoptosis [97-99]. However, the HCs within the hypochord survived, even when the hypochord was mineralized and vascularized at the end of metamorphosis. These results suggest that there is a possibility that the terminal chondrocytes de-differentiate into osteocytes. Such de-differentiation is a phenomenon commonly seen in rapidly ossifying bones [100-103]. By stage 63, dorsal-most and lateral muscles underwent apoptosis (Fig. 6F, F'). Once the hypochord ossification reaches its maximum length (by stage 63), the tail length reduction is initiated and can be observed by the presence of phagocytotic cells within the tail region (Fig. 6H, H', I, I'). With the fusion of coccyx and hypochord, the spinal cord also showed positive signal for cell apoptotic markers (Fig. 6G', G"), indicating the spinal cord only degenerates at the urostyle region.

2.5 – DISCUSSION

The anuran urostyle is a unique component of the vertebrate axial skeleton because it is formed from an ossifying hypochord, which contributes and fuses to the coccyx at the end of metamorphosis. In fishes, posterior-most centra fuse to form the ural, which supports the developing caudal fin [104-106]. Within the actinopterygian lineage, recently evolved teleosts have experienced a reduction in caudal elements with the evolution of homocercal tails (compared to the plesiomorphic state of having heterocercal tails) [107-109]. It has been hypothesized that having polyurals (more than two ural elements) is more primitive compared to the diural condition [107]; all individuals go through some fusion of the urals after they are formed as individual centra, and fish ural fusion progresses as a slow process [107-109]. Avian tails have also undergone considerable changes, from the plesiomorphic long tails of non-avian

dinosaurs to the short tails with a fused pygostyle of birds (the group Pygostylia; this includes modern birds) as an adaptation for flight [110-112]. During the embryonic period, pygostyle vertebrae chondrify, mineralize, and then fuse once the bird hatches [112]. Tail loss has also evolved convergently in mammals, including apes and humans. This loss has resulted in the evolution of the coccyx, commonly known as the tailbone. The coccyx is formed by fusion of 3–5 coccygeal vertebrae [113-115], which fuse completely with no visible sutures or partially with sutures still visible, and it attaches to the sacrum.

2.5.1 – Chronological events of how muscles, neurons, and vasculature change

Here, we offer a possible scenario and chronological events as to how the anuran urostyle develops and the order in which the neuromuscular skeleton, vasculature, and innervation change. Close to metamorphic climax: the PSI is formed, and MSs/chondrocytes forming the PSII are also aggregated; myomeres are made of large fibres and are referred to as DT, extends through out body and tail; spinal nerves extend up to the end of tail; DA, PCV, and DAV present. With the onset of metamorphosis, the hypochord ossifies. First thing to change are the muscle fibres: muscles undergo cell proliferation, starting from the dorsal-most and lateral areas (Fig. 2.6A',B', white arrows indicate newly forming muscles). At the same time, innermost muscles surrounding the notochord and ventral-most muscles (Fig. 2.6E') undergo apoptosis. Longismuss dorsi (LD) is the first muscle to form, which is connected to the coccyx. The spinal nerves are still intact and extend till the end of the tail; DA, PCV, and DAV present. By stage 63, the hypochord and coccyx has reached their maximum length posteriorly (up to mytome XIV). coccygeoiliacus (CI) starts to form (Fig. 2.3B), and, at the same time, the primary myomeres within the most lateral and most dorsal areas undergo apoptosis (Fig. 2.6F,F'). The CS is the last

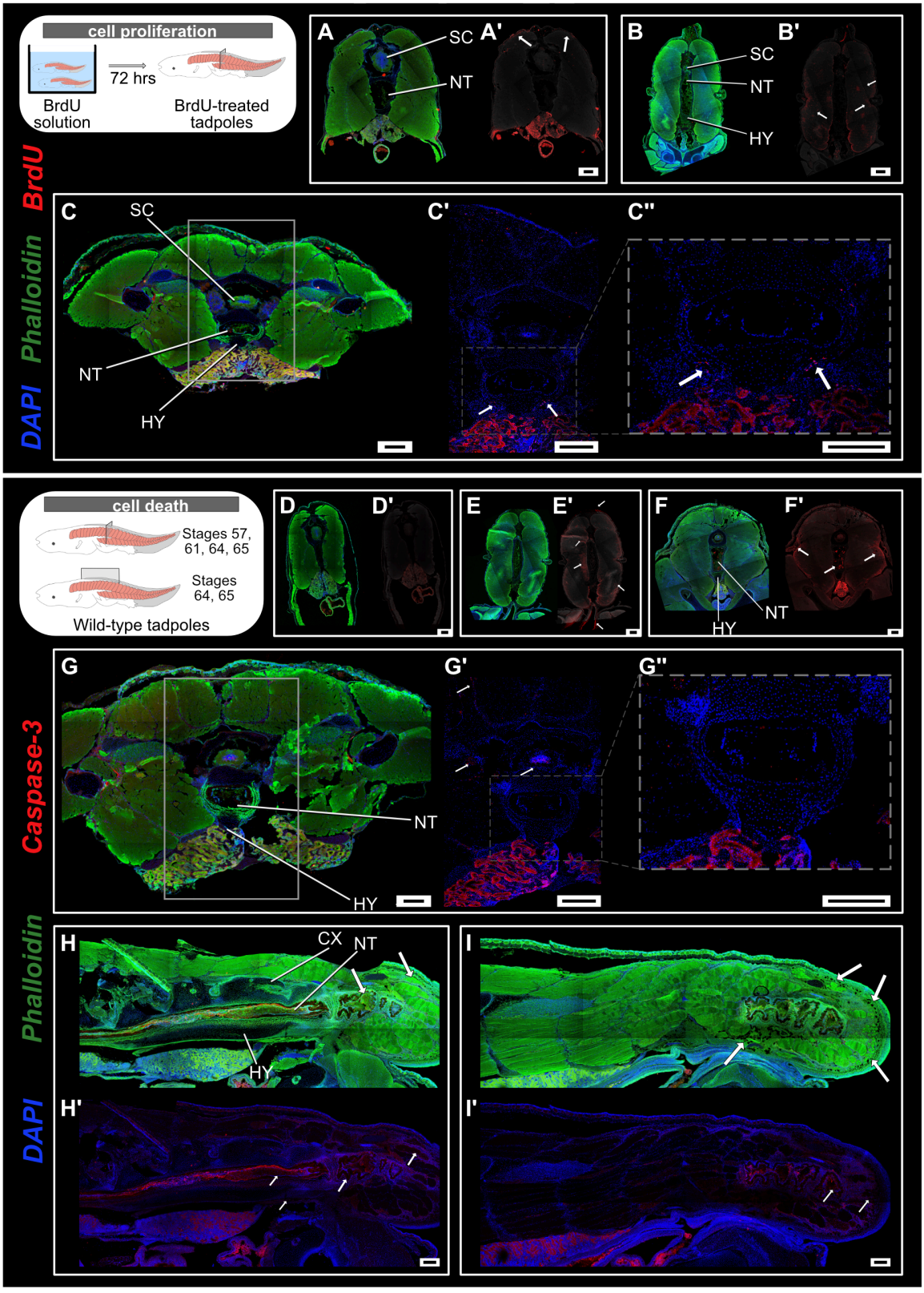

Figure 2.6. Cell death and cell proliferation at the site of urostyle formation. (A–C) Transverse sections across trunk myotome XII, immuno-stained for anti-BrdU (red) to observe

Fig. 2.6, continued. cell proliferation at stages 58 **(A, A')**, 61 **(B, B')**, and 64 **(C, C')**. **(A', B', C')** Anti-BrdU signal has been overlaid on a grey-scale background to highlight the proliferating cells. Muscle cells initiate proliferation prior to metamorphic climax, starting with the dorsal-most muscles (**A'**). With the initiation of metamorphosis, muscles along the lateral margins proliferate (**B'**). Lateral margins of the hypochordal rod demarcate the chondrocyte proliferating zone (**C, C', C"**). White arrows depict proliferating zones. (**D–I**) Transverse and sagittal cross-sections across the trunk myotomes, immuno-stained for anti-Caspase 3 (red) to observe cell apoptosis. There is no cell death at stage 57, before metamorphic climax (**D, D'**). With the initiation of metamorphic climax at stage 61 (**E, E'**), innermost muscles surrounding the notochord and ventral-most muscles undergo apoptosis ("suicide model"). Dorsal-most and lateral larval muscle fibers undergo cell death at stage 63 (**F, F'**). By stage 64, the coccyx and hypochord have reached the maximum length by extending up to the myotome and the spinal cord is degenerated (**G, G', G"**). Sagittal sections at stages 64 (**H, H'**) and 65 (**I, I'**) depict how the muscle cells are degenerated by phagocytosis ("murder model") with the reduction of the tail. Abbreviations: CX, coccyx; HY, hypochord; NT, notochord; SC, spinal cord. Scale bars denote 100 μm.

muscle to form, and the ventral-most muscles degenerate completely (Fig. 2.3F'', Fig. 2.6G,G',H,H''). With the DA occlusion, the tail regression happens rapidly, and the degenerating tail also loses its neurons. Neuron degeneration is last to happen within the urostyle region, and this concords with previous studies that looked at tail neuron degeneration ([56] Brown, 1946); during metamorphosis, neurons are the slowest to be absorbed ([56] Brown, 1946) (Fig. 2.4). Finally, when coccyx and hypochord fuses, the spinal cord changes its morphology, and forms the filum terminale (Fig. 2.4F,F'; Fig. 2.11), with the loss of tail.

2.5.2 – Coccyx vs. Hypochord

We found that coccyx and hypochord show two different developmental patterns. Firstly, the coccyx ossifies in a segmental and comparatively slow manner, whereas the hypochord ossifies as a single rod relatively quickly. Secondly, initiation of hypochordal ossification

appears to be mediated by thyroid hormone, whereas coccyx ossification is not; however, the postsacral vertebrae fusion was disrupted in methimazole-treated tadpoles (Fig. 2.18). Further studies using early and late developmental stages of tadpoles and comparative transcriptomics of the two tissue types are required to validate TH control of urostyle formation.

Previous studies have shown that removal of the embryonic spinal cord or notochord disrupts the morphology and regionalization of the vertebral column [102, 116, 117]. For example, removal of the notochord from *Ambystoma mexicanum* embryos resulted in a fused cartilaginous rod [116]. Even though cartilage was developed, the differentiation or regionalization was disrupted. Even in mice, removing the neural tube results in abnormally segmented ossifications around the notochord, and notochord removal results in unsegmented cartilaginous sheaths [102, 117, 118]. Studies have postulated that the notochord alone acts on the segmentation and notochord and spinal cord together influence the differentiation [117-122]. We hypothesize that the switch that happens within the notochord during metamorphic climax [83] to secrete proteolytic enzymes may have disrupted its inductive abilities and that this could be a reason why regionalization at the urostyle site is disrupted or has been lost.

2.5.3 – Ossifying hypochord and the anuran *bauplan*

Why does the hypochord ossify only in anurans? The tail, contributing to more than half of the tadpole's length, is composed of muscles, neurons, blood vessels, and a notochord and, hence, losing the tail rapidly is a developmental conundrum. It is suggested that the most vulnerable stage in terms of predation for a tadpole is when both its tail and four legs are present—the period leading up to metamorphic climax [123, 124]. Hence, a developing tadpole needs to lose its tail efficiently and quickly to assume its adult body form. Therefore, the tail

resorption process is completed within 2–3 days [74]—a remarkable evolutionarily favored transformation.

Tail loss has gained much attention over the past century mainly because of its importance in understanding the water-to-land transition. Previous work shows how increased TH at the beginning of metamorphic climax promotes autolysis of tail cells ("suicide model" [118, 119]; Fig. 6D', E', F'). However, the tail-length reduction, a result of cell phagocytosis ("murder model" [74, 125]; Fig. 6H, H', I, I'), initiates only after 3 days into metamorphic climax and is not directly controlled by TH. The trigger of the "murder model" was overlooked in previous studies.

We propose that rapid tail loss in anuran larvae is related to ossification of the hypochord in mid-length of the body. Our results show how ossification of the hypochord may promote tail loss by remodeling the dorsal aorta (DA): DA occlusion occurs ventral to the posterior-most part of the hypochord (Fig. 5 and See SI Appendix); subsequently, with the occlusion, the DA branches into two vessels ventral to the anterior-most margin of the hypochord, which enter the left and right hind limbs (Figs 2.5, 2.20, 2.21). This occlusion happens before the initiation of tail regression and posterolateral rotation of the pelvic girdle (Figs 2.5, 2.13, 2.20, 2.21). We propose that the low-pH environment resulting from the DA occlusion could be triggering the "murder model" in tadpoles.

The fossil record of anurans contains forms having a tail with a few caudal vertebrae, which is the plesiomorphic state (e.g., Triassic *Triadobatrachus massinoti* [126] and *Czatkobatrachus polonicus* [127]), followed by the sudden appearance of forms with a urostyle and no tail (*Prosalirus bitis* [4, 5]). However, intermediate fossils between these two states have not been discovered. Our study points towards an explanation for the evolution of tail loss in

anurans and the development of the urostyle: during the evolution of an anuran *bauplan*, hypochord ossification likely preceded loss of tail in salientians. This discovery of the developmental basis of the urostyle and the ossifying hypochord that unites all anurans will spur trait evolution, developmental and systematic studies in vertebrates. Future studies creating genetic knockouts in anurans, either by preventing the ossification of the hypochord or by generating tailless tadpoles, would help us better understand the significance of the ossified hypochord and tail resorption during metamorphosis, while reiterating the novelty of the urostyle.

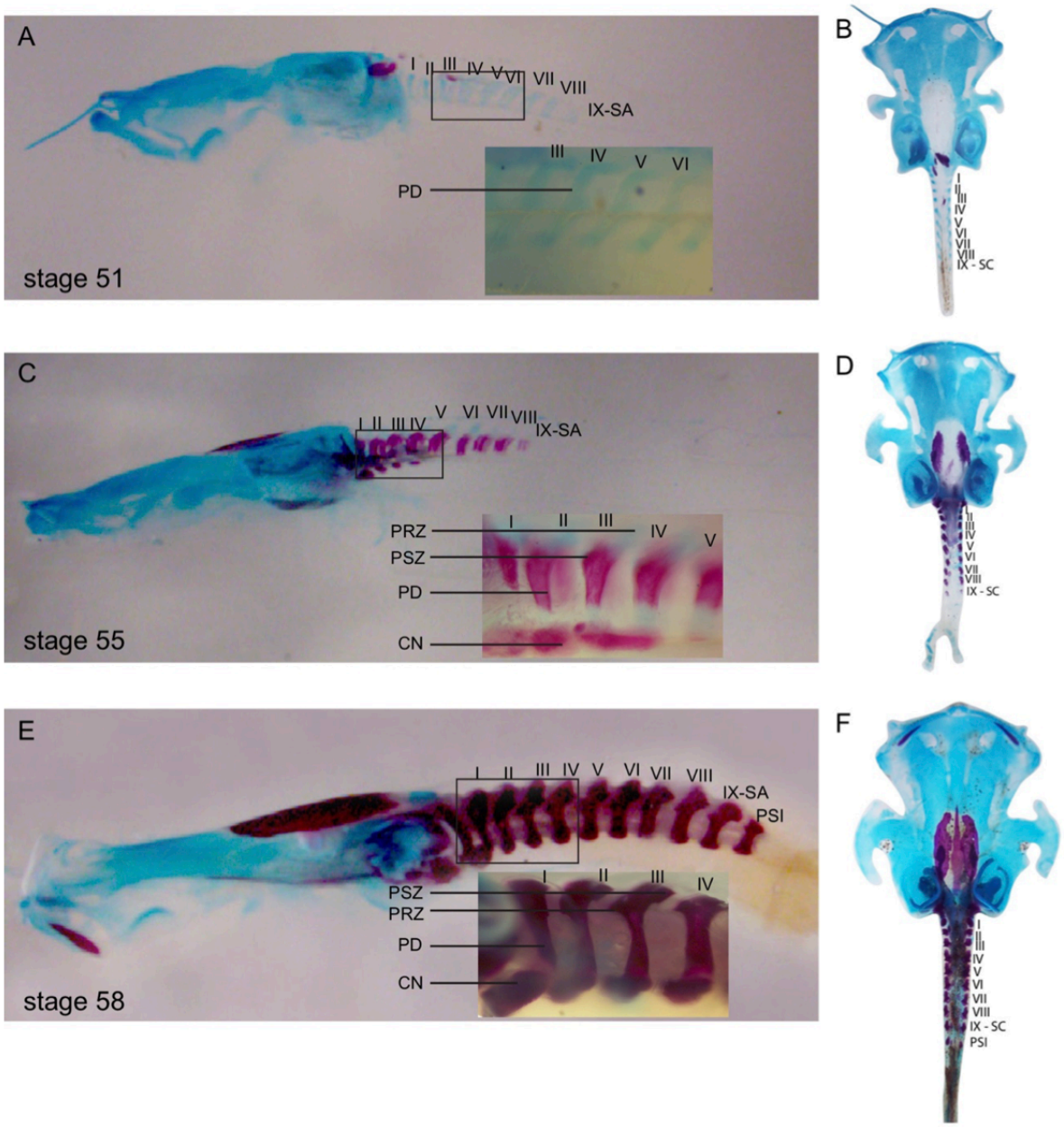

Figure 2.7. Axial skeletal formation in early postembryonic *Xenopus tropicalis* (NF stages 51, 55 and 58). Cartilaginous precursors of the vertebrae form by stage 51; the neural arch ossifies first; centra, prezygapophyses, and postzygapophyses ossify next. Presacral vertebrae I–VIII, the sacrum, and postsacral vertebrae I are formed prior to metamorphosis. Vertebrae

Fig. 2.7, continued. are numbered from I to IX. Abbreviations: CN, centrum; PD, pedicel; PRZ, prezygapophyses; PS, postsacral; PSZ, postzygapophyses; SA, sacrum.

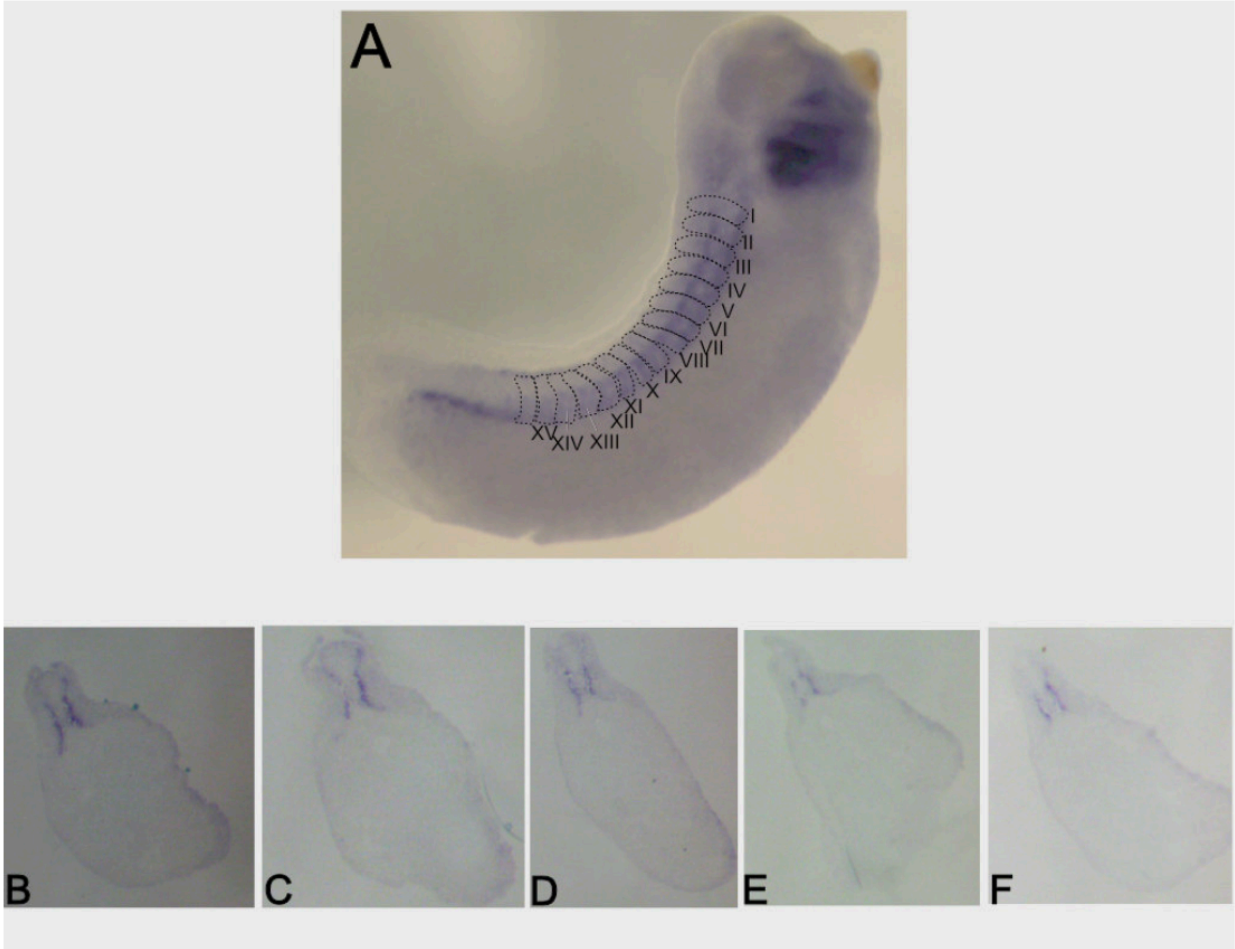

Figure 2.8. Pax9 expression in sclerotome-derived cells. Whole-mount in-situ hybridization and transverse cross-sections for *Pax9* at stage 27, showing that sclerotome-derived cells are around the spinal cord, across somites I–XIII. (A) Whole-mount in-situ hybridization embryo at stage 27. *Pax9* expression is seen in somites, anterior-to-posterior. Transverse cross sections across (B) somite III, (C) somite IV, (D) somite V, (E) somite VIII, (F) somite XI, and (G) somite XIII.

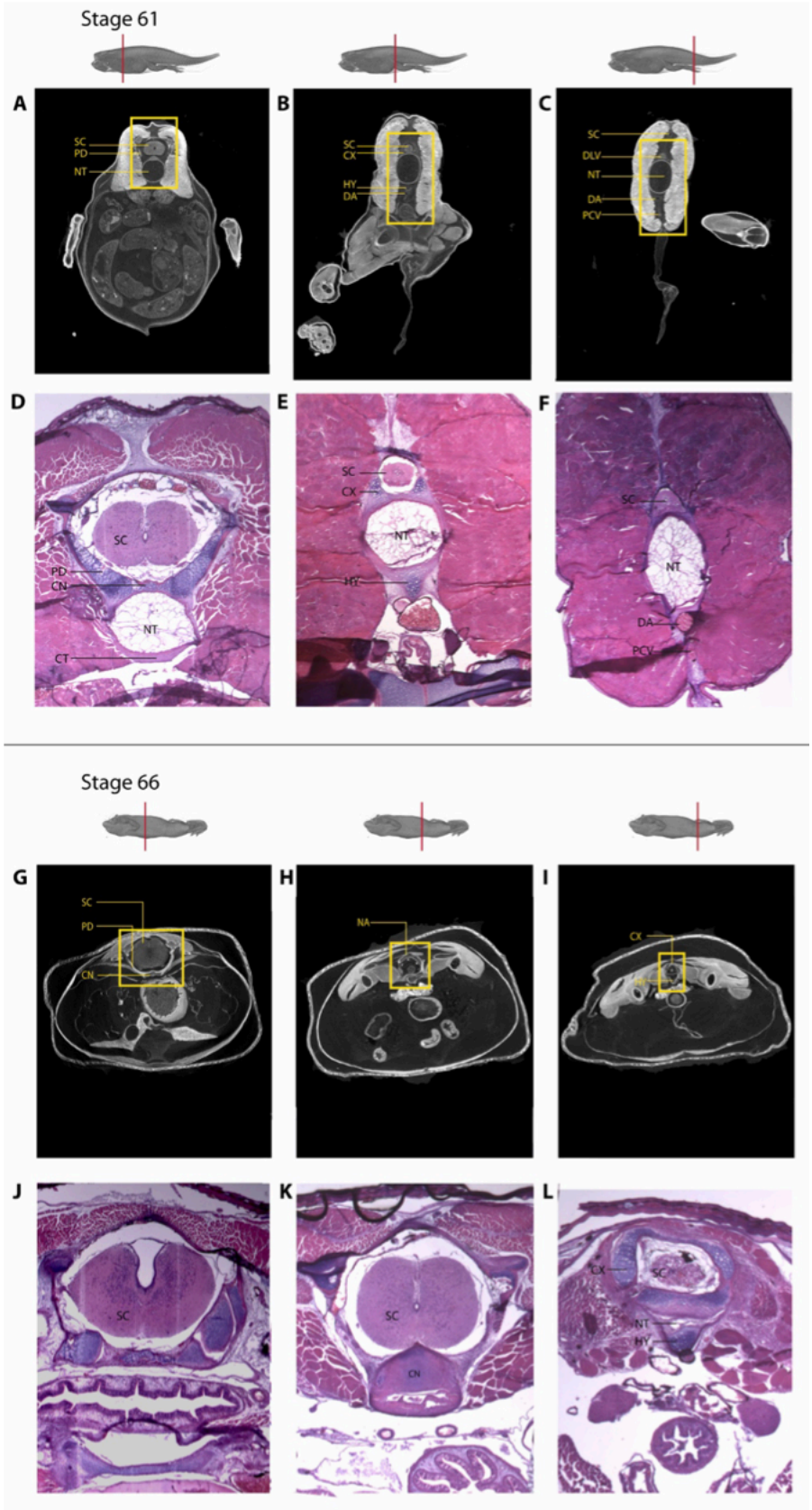

Figure 2.9. Ossification of the hypochord during metamorphosis.

Fig. 2.9, continued. Haematoxylin- and eosin-stained transverse histological sections and CT scans of *Xenopus tropicalis*, highlighting hypochord ossification as a midline structure, ventral to the notochord. Cross-sections across a presacral vertebra (A, D, G, J); across the sacrum-urostyle junction (B, E, H, K); and across a posterior part of the notochord (C, F, I, L). Histological sections depict the highlighted portions of the CT orthoslices. Abbreviations: CX, coccyx; DA, dorsal aorta; DLV, dorsal lateral anastomosing vein; NT, notochord; PCV, posterior cardinal vein; PD, pedicel; SC, spinal cord.

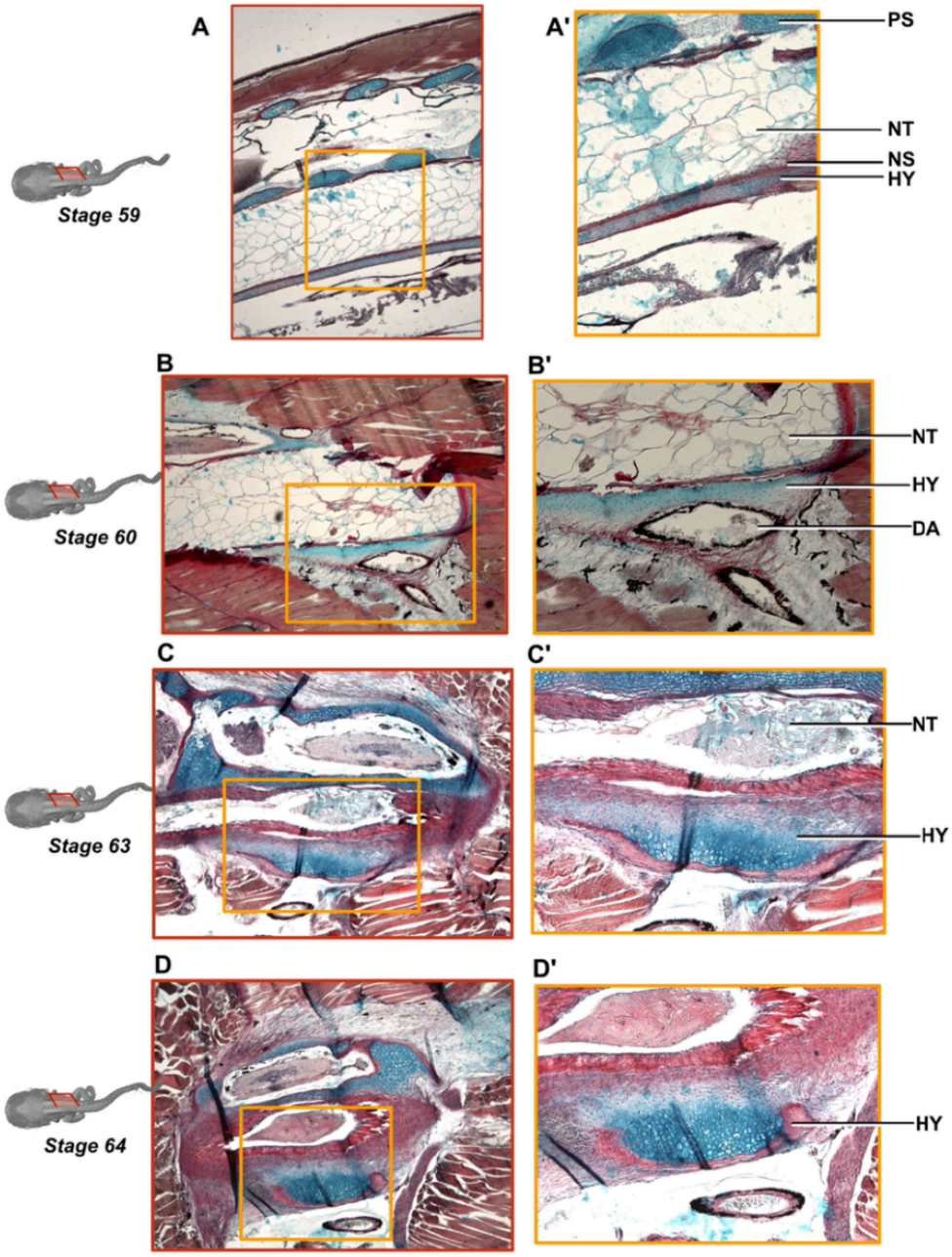

Figure 2.10. Hall-Brunt Quadruple (HBQ) stained sagittal sections of the ossifying hypochord.

Fig. 2.10, continued. This highlights cartilage (blue) and bone (red), focusing on the ossifying hypochord at stages 59, 60, 63 and 64. Hypochordal ossification is initiated ventral to the notochord and dorsal to dorsal aorta. Notochord degenerates with the fusion of coccyx and hypochord. Abbreviations: DA, dorsal aorta; HY, hypochord; NS, notochordal sheath; NT, notochord; PS, postsacral vertebra.

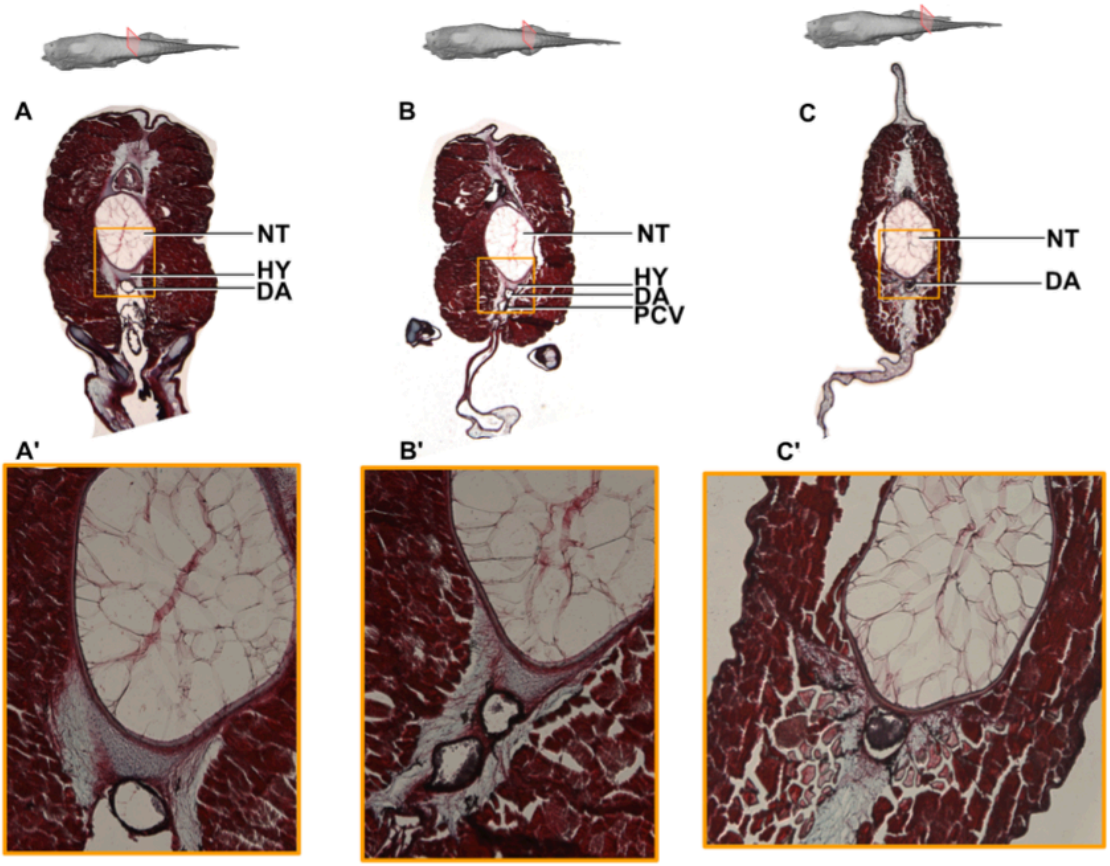

Figure 2.11. Hall-Brunt Quadruple (HBQ) stained transverse sections of the ossifying hypochord. HBQ-stained transverse cross sections, at stage 60, depicting the development of the hypochord. Cells aggregate ventral to the notochord and dorsal to the dorsal aorta (A, A', B, B'). No hypochordal cells are present in the tail region (C). Abbreviations: DA, dorsal aorta; HY, hypochord; PCV, posterior cardinal vein; NT, notochord.

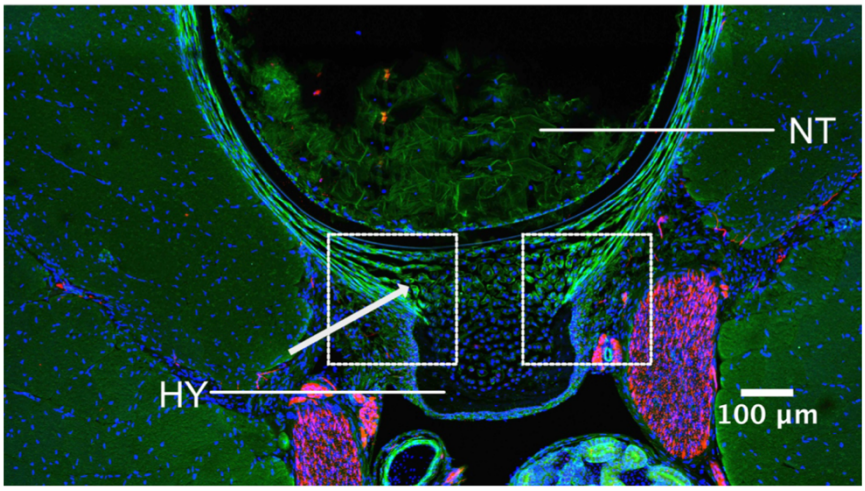

Figure 2.12. Migratory cells of the ossifying hypochord. A transverse cross-section across trunk myotome XII at stage 61, highlighting migrating cells during hypochord formation. White arrows point at the migrating cells with filopodia.

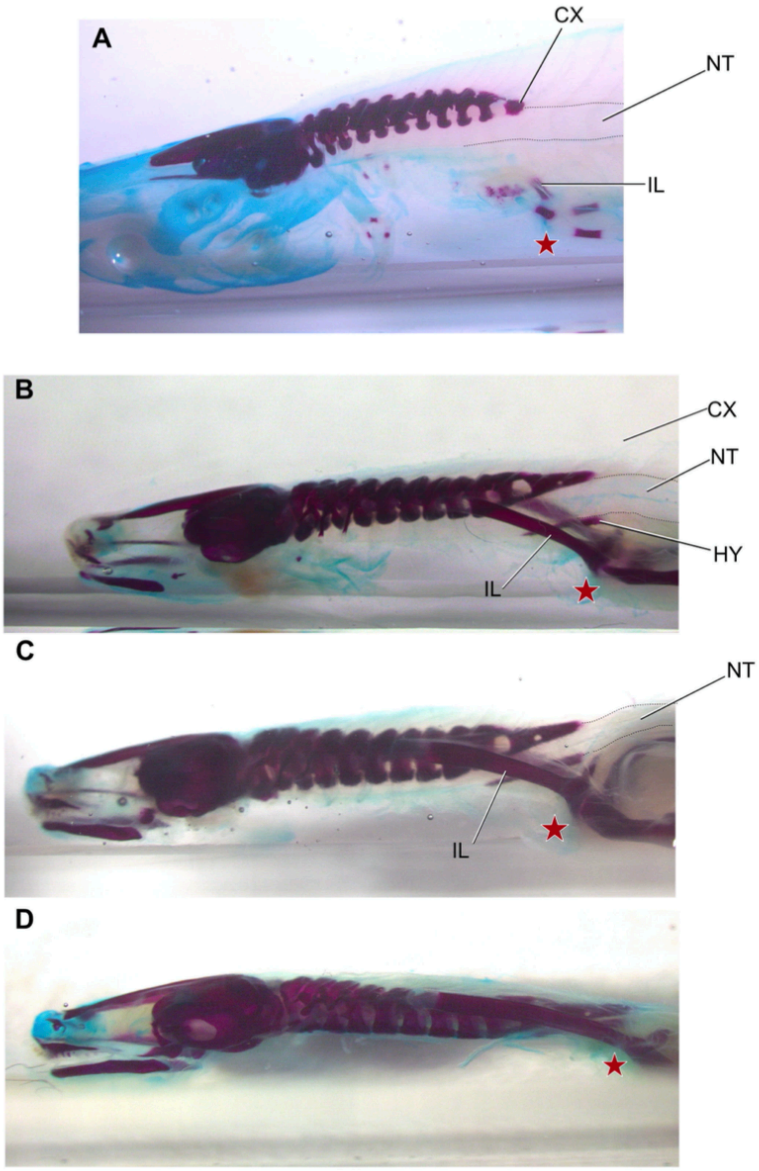

Figure 2.13. Posetorlateral rotation of the pelvic girdle. Bone- and cartilage-stained tadpoles, focusing on the posterolateral rotation of the pelvic girdle. Red stars demarcate the acetabulum. (A) stage 58, (B) stage 61, (C) stage 64, and (D) stage 66.

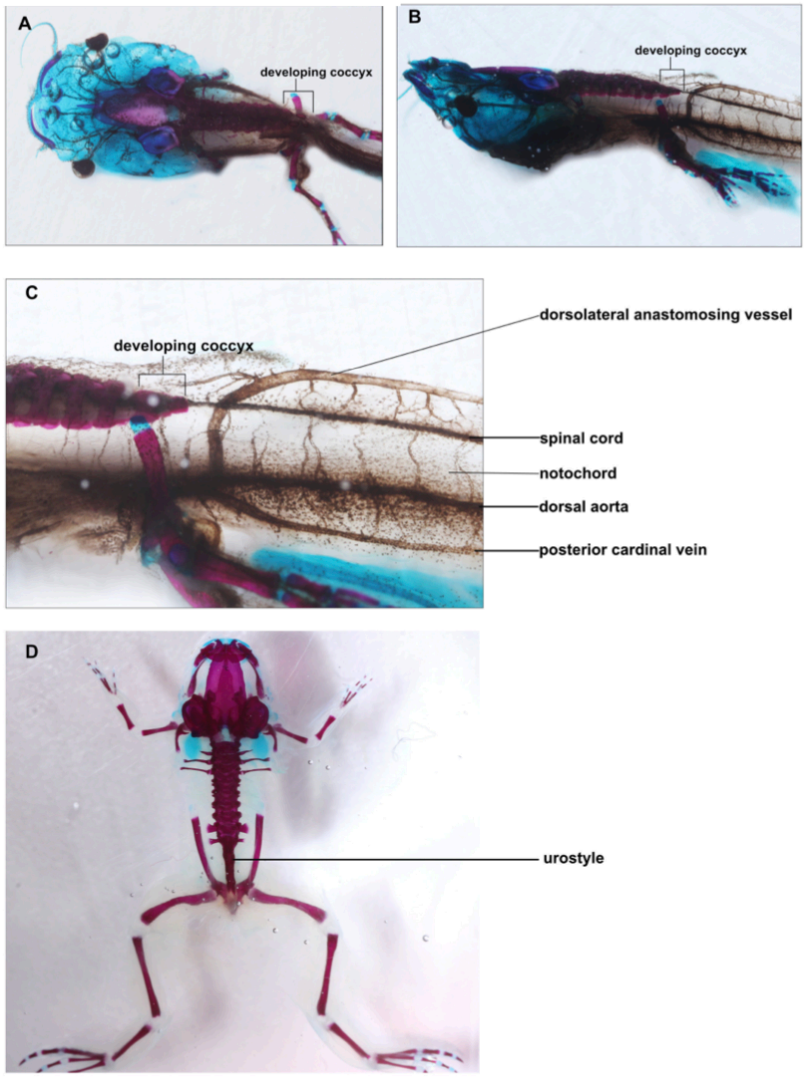

Figure 2.14. Urostyle development in Methimazole-treated tadpoles. Methimazole-treated stage-54 tadpoles (A, B, C), in which thyroid hormone production was prevented. The axial column ossifies, including the rudimentary neural arches of vertebrae X and XI, but formation of the hypochord is disrupted even after two months. Control tadpoles metamorphosed and had a urostyle (D).

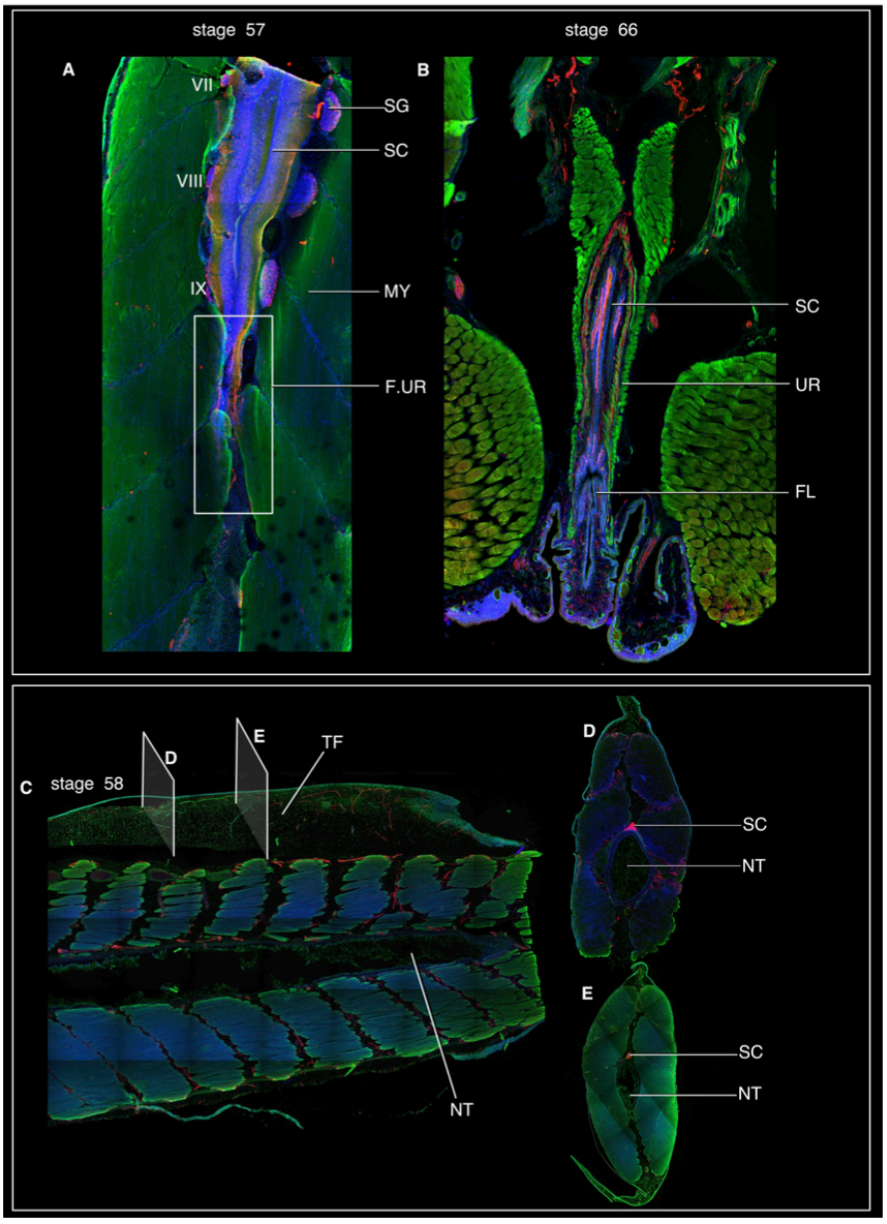

Figure 2.15. Sagittal sections of the spinal cord, before and after metamorphosis.

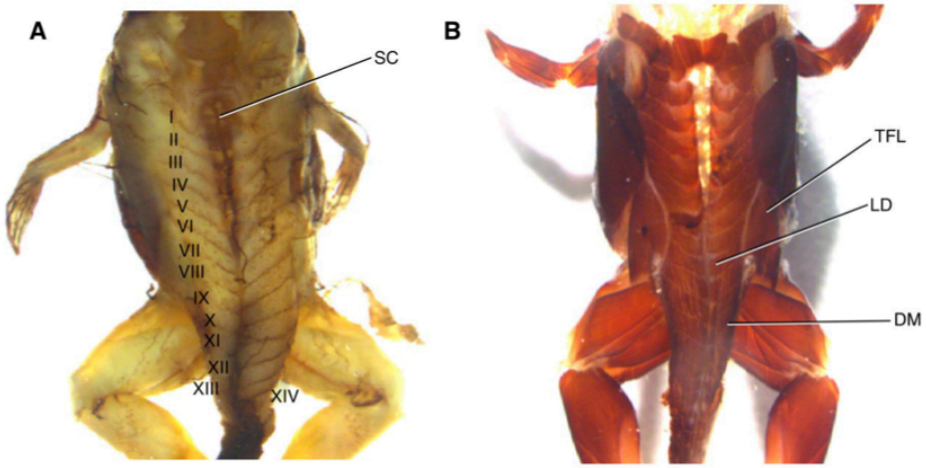

Figure 2.16. Transverse cross-sections across trunk myotome XII at stage 61 (beginning of metamorphic climax). Phalloidin (green) stains the extracellular matrix, DAPI (blue) stains nuclei, and laminin (red) stains muscle fibers.

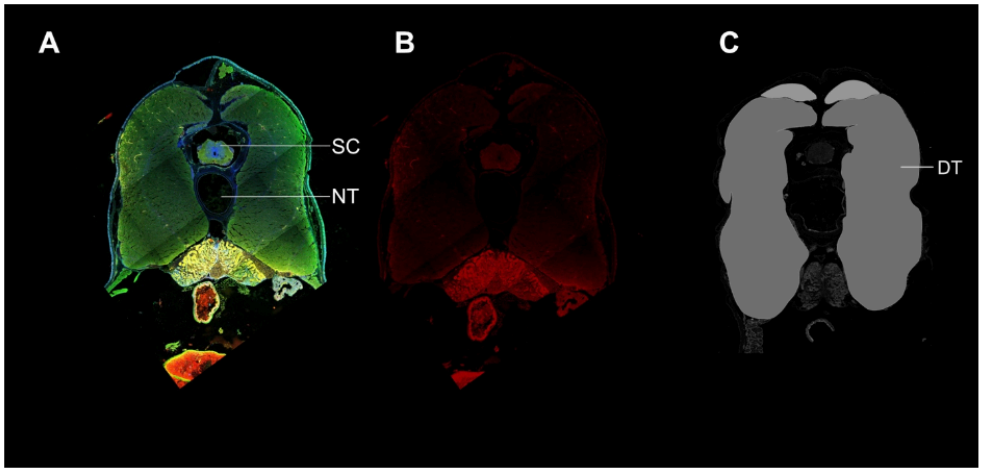

Figure 2.17. Dorsal views of whole-mount immuno-stained specimens for muscles (12-101 antibody) and neurons (acetylated tubulin), stage 65.

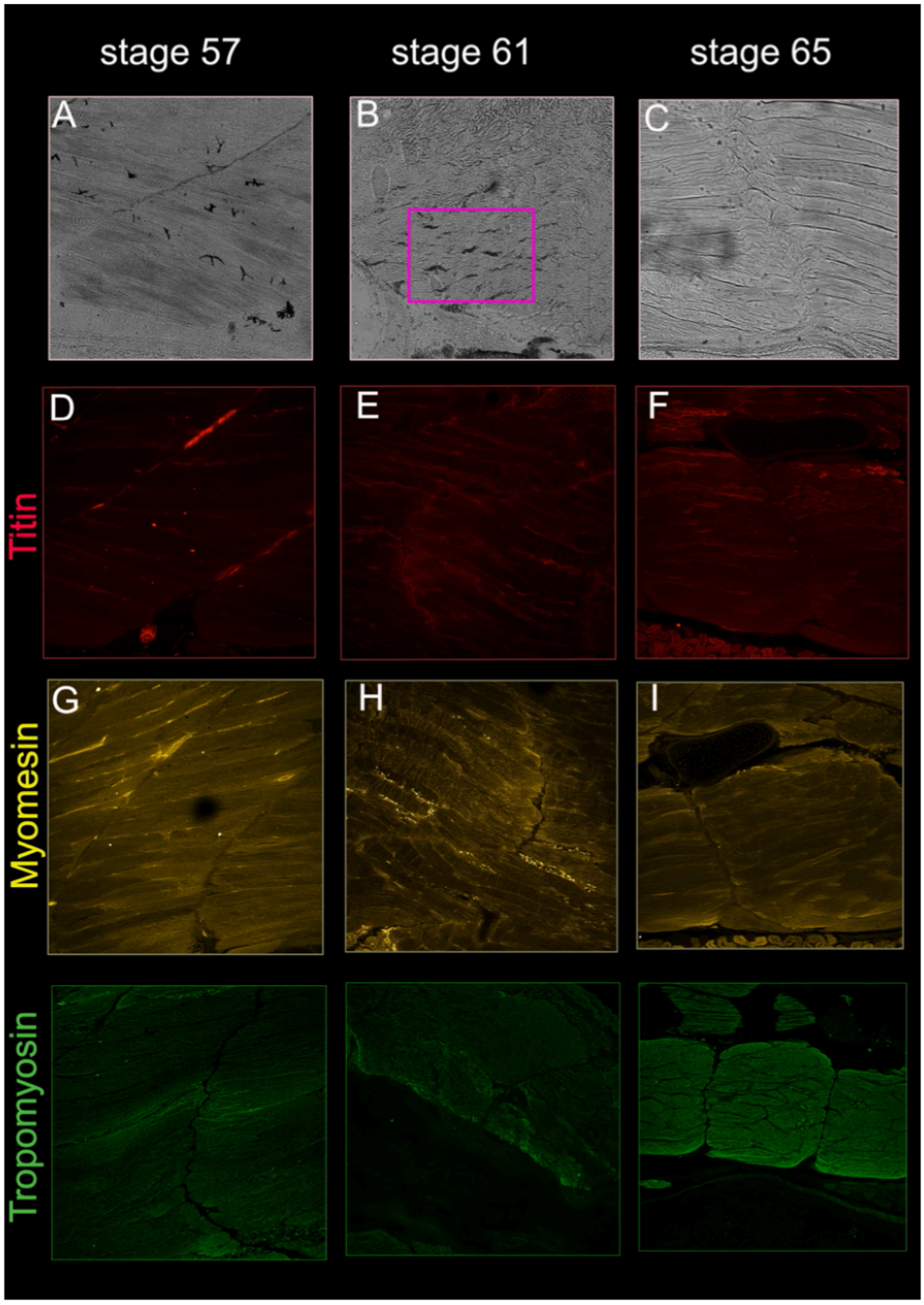

Figure 2.18. Sagittal cross sections across the developing urostyle to observe the sarcomere protein organization before metamorphosis (A, D, G), during metamorphic climax (B, E, H), and end of metamorphosis (C, F, I). Before metamorphosis, sarcomere proteins are distinguishable with a banded pattern; during metamorphosis the banded pattern of the sarcomeres become disorganized; and after

Fig. 2.18, continued. metamorphosis the banded pattern re-appear. A, B, C are bright-field photographs; titin is shown in red; myomesin in yellow, and tropomyosin in green.

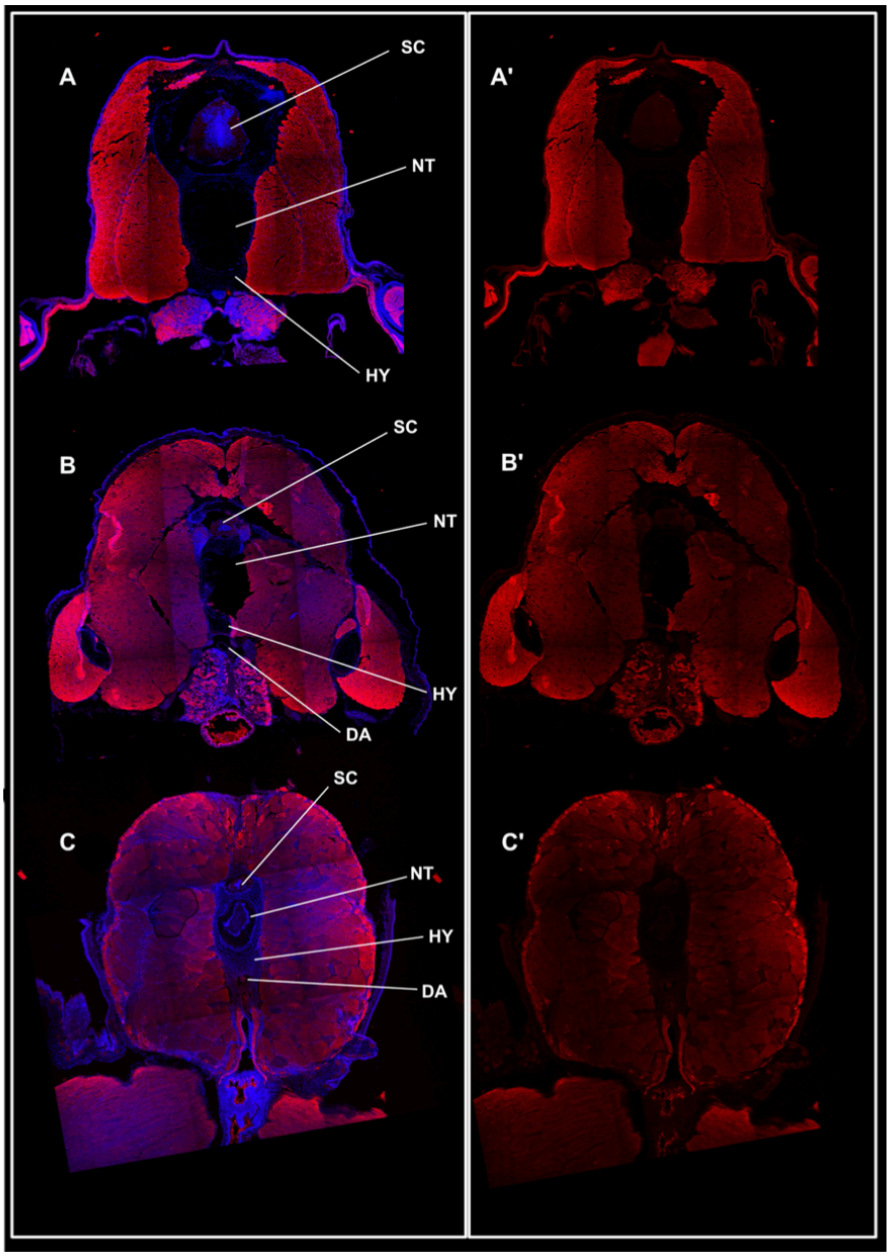

Figure 2.19. Transverse cross-sections across the urostyle, depicting skeletal muscle fibers (stained using an antibody for myosin) at stages 57 (A, A'), 61 (B, B'), and 65 (C, C'). Myosin is shown in red and DAPI (nuclei) in blue. Abbreviations: DA, dorsal aorta; HY, hypochord; NT, notochord; SC, spinal cord.

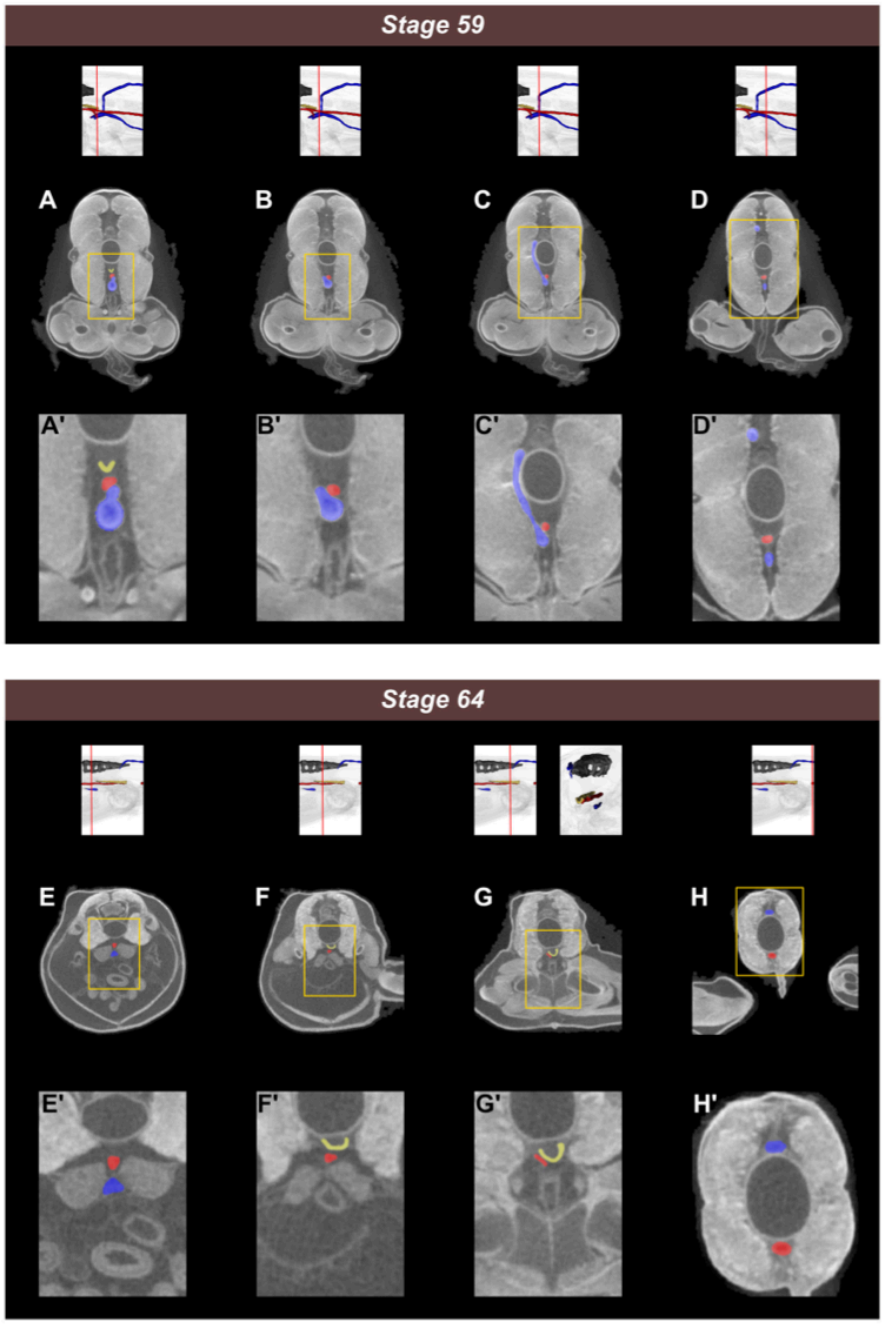

Figure 2.20. Transverse cross-sections of the CT-scanned tadpoles at stage 59 (A–D and A'–D'). The developing hypochord is shown in yellow; the dorsal aorta (DA) in red, and the posterior cardinal vein (PCV) in blue. With ossification of the hypochord between the notochord and DA the diameter of the DA is reduced, causing an occlusion at the posterior-most end of the hypochord (stage 64, E–H and E'–H').

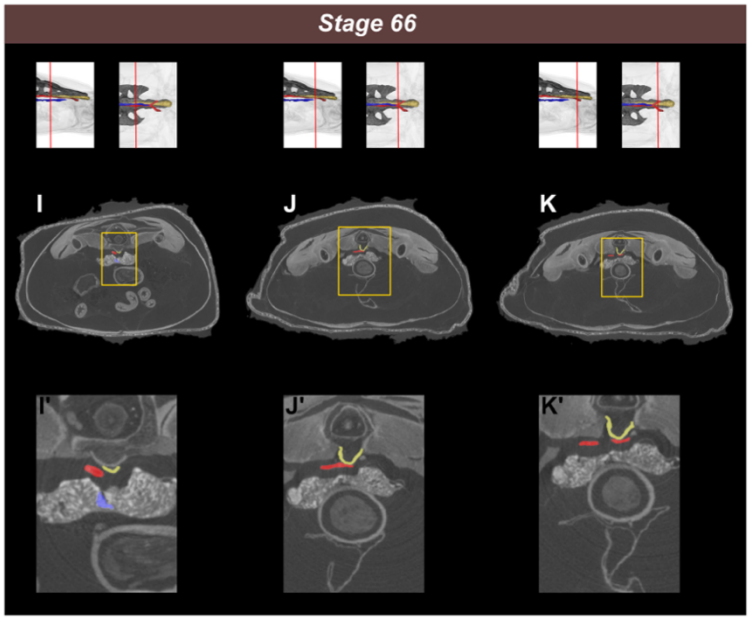

Figure 2.21. Transverse cross-sections of the CT-scanned tadpoles at stage 66; the dorsal aorta is red and the hypochord yellow.

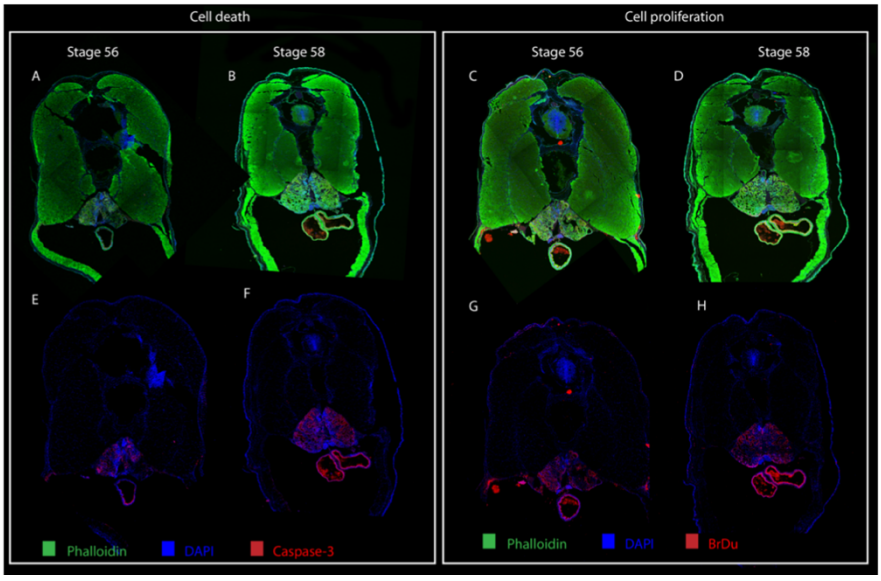

Figure 2.22. Cell death (A, B, E, F) and cell proliferation (C, D, G, H) during premetamorphic stages. Both processes are concentrated along the endoderm and the tadpole skin.

CHAPTER 3:
MOLECULAR BASIS OF THE UROSTYLE: GENES AND GENE REGULATION UNDERLYING AN EVOLUTIONARY NOVELTY

3.1 – ABSTRACT

Evolutionary novelties have facilitated successful inhabitation of ecological niches. These features are a result of changes to ancestral gene and gene regulatory pathways. One important novelty is the fused rod at the end of the vertebral column in frogs and toads, the urostyle. Unlike other such rods in other vertebrates it is composed of derivatives of the coccyx and an ossifying hypochord. The urostyle forms during the transformation of the tadpole-to-froglet metamorphosis, entailing substantial structural changes, especially to the skeleton. Despite being derived from different cell populations and having different cellular compositions during development, both coccyx and hypochord undergo endochondral ossification during metamorphosis. Previous studies have highlighted phenotypic changes during urostyle development, however, gene activity and gene regulation underlying this unique structure remain obscure. Our previous work allowed us to identify cells of interest during urostyle development. Here, I used Laser Capture Micro-dissection of these identified tissues and subjected them to RNA-seq and ATAC-seq analyses at three developmental stages in tadpoles of *Xenopus tropicalis* (prometamorphosis, beginning of metamorphic climax, and end of metamorphic climax). This revealed that the coccyx and hypochord have two different molecular signatures and genetic underpinnings. ATAC-seq data revealed that thousands of chromatin regions respond dynamically during metamorphosis, and potential regulatory regions were observed in proximity to candidate genes identified from RNA-seq. Immunohistochemical analyses show that neurons and muscles around the coccyx change dramatically, and coinciding with this, neuronal (*TUBB3*)

and muscle markers (*MYH3*) are upregulated in coccygeal tissues. The up-regulated genes in the hypochord include T-box genes (*TBXT*, *TBXT.2*, and *TBX1*), corticosteroid stress hormones (*CRCH.1*), and matrix metallopeptidases (*MMP1*, *MMP8*, *MMP13*). Even though an ossifying hypochord is only present in anurans, this ossification between the vertebral column and the notochord appears to resemble a congenital vertebral anomaly seen prenatally in humans, caused by an ectopic expression of the *TBXT*/*TBXT.2* gene. This work opens the way to functional studies that will allow to better elucidate anuran *bauplan* evolution.

3.2 – INTRODUCTION

Phenotypic and genotypic changes from an existing ancestral condition undergird the evolution of "key innovations" [128]. These evolutionary novelties could be either structural (new body plans or structures) or functional [129]. Functional novelties focus on novel functions (like flight, climbing, vision, digging), which have led to inhabitation of a diversity of ecological niches whereas the structural ones are considered to have no homologous structures in the ancestral lineages nor in the fossil record [129, 130]. Phenotypic changes that produce a structural novelty would reflect changes in the corresponding genotypic/gene regulatory networks [130-133].

Previous studies have highlighted that the anuran (frog and toad) urostyle, composed of a coccyx and a hypochord, is morphologically unique from the rest of the vertebrates because of the contribution of an ossifying hypochord, and is therefore considered a structural novelty [12, 67, 134-137]. The coccyx, which is derived from the paraxial mesoderm, gives rise to the caudal vertebrae [12, 54, 55], which subsequently undergo endochondral ossification and fuse together during metamorphosis [67]. The amphibian hypochord, thought to be derived from either

endoderm [13, 14, 16] or superficial mesoderm [20], is a thin embryonic rod, which degenerates in the rest of anamniotes during early embryonic development, but is retained only in frogs and undergoes endochondral ossification during the metamorphic climax [12, 67, 134-137].

The ossifying hypochord, an apomorphic structure in anurans, occludes the dorsal aorta and is hypothesized to aid in rapid tail resorption [67]. In Chapter 2 (see also Senevirathne et al. (2020)), I highlighted the phenotypic changes associated with the evolution of this structure in anurans and discussed how bones and cartilage, muscles, neurons form, and proposed how the hypochordal ossification has a role in the evolution of the anuran *bauplan*. Despite being derived from two different populations of cells, both coccyx and hypochord undergo endochondral ossification during metamorphosis. Undifferentiated mesenchymal cells of the coccyx and embryonic hypochordal cells chondrify and ossify when the tadpole locomotion changes from an axial-driven mode to a limb-driven one. Ossification of the hypochord is rapid, usually ranging from 6-8 days. Apart from the cartilage and bone formation, the neuro-muscular skeleton is also remodeled. The muscles near the future caudo-pelvic region of the tadpole are remodeled during metamorphosis. The primary myotomes (Dorsalis trunci) remodel to form three different types of muscles (Longissimus dorsi, Coccygeoiliacus, Coccygeosacralis), where all three attach to the coccyx. The axial motor neurons in the tail degenerate, and, at the same time, the spinal cord degenerates with the fusion of the coccyx and hypochord [67].

Embryonic hypochord in anamniotes is known to have a function in remodeling the dorsal aorta, and the hypochord degenerates (except in anurans) after serving its purpose. Surprisingly, in mature tadpoles, CT scanning data revealed a possible role of the ossifying hypochord in remodeling the dorsal aorta as well. As described in Chapter 2, the posterior-most end of the hypochord appears to occlude the dorsal aorta, which could aid the rapid tail loss by

cutting the blood supply to the tail [67]. Hence, we speculated that the ossifying hypochord has a role in the evolution of the anuran *bauplan*, and this could be a reason why it has been evolutionary favored in anurans for more than 200 million years [5, 131].

The phenotypic changes of the urostyle are well studied [67, 134, 136]; however, the molecular mechanisms underlying this unique structure have remained obscure to-date. In this part of my thesis, I investigate transcriptomic and gene regulatory networks in the developing urostyle by combining a RNA-seq and an ATAC-seq approach to study gene regulation.

Mesenchymal cells in vertebrates that undergo ossification have a significant transcriptomic signature (is there a general reference for this statement?). Vertebrate ossification can be either endochondral or intramembranous, and a compendium of genes, transcription factors, intrinsic and external cues control ossification. During this process mesenchymal cells initially condense and commit to form osteoprogenitors (genes like *SOX2*, *RUNX2* are involved in this). Next, the osteoprogenitors differentiate to form preosteoblasts and osteoblasts (BMPs, FGFs, TGFß, and Wntß/catenin are involved in this (e.g., [138-142] , and finally, mineralization and apoptosis of osteoblasts form mature osteocytes (e.g., [138-142].

Paraxial mesoderm-derived coccygeal cells are undifferentiated mesenchymal cells; they undergo chondrification and ossification prior to the initiation of the metamorphic climax [12, 67] and could be following a similar gene regulatory network as connective tissues and bones in vertebrates. However, when considering the ossifying hypochord, it initiates ossification at the onset of metamorphosis. The origin of amphibian hypochordal cells has been hypothesized to be from the endoderm [13, 14, 16], or the superficial mesoderm [20]. Regardless of which germ layer it is derived from, hypochord undergoes endochondral ossification only in anurans. But the genes and gene regulatory regions that control the development of this structural enigma remain

unknown. Here, I compare the gene expression patterns of coccygeal and hypochordal cells to identify similar/different pathways between the two tissue types, which are derived from two different cell populations. Our previous work established that Thyroid hormone (TH) directly controls hypochord ossification. Hence, using Methimazole as an inhibitor of TH, we also identified downstream targets of TH, by exposing tadpoles (both early and late) to Methimazole.

Through this work, I address the following questions: Why does the hypochord only ossify in anurans? Which genes are involved in this structural novelty? If this structure is an endoderm derivative, how does it acquire mesodermal (ossifying) properties? What are the similarities/differences between the hypochordal and coccygeal molecular pathways? Which genes switch on/off during metamorphosis? By identifying the underlying changes in the genes and gene regulatory networks, my study begins to shed light on the potential genotypic changes underlying a structural novelty.

3.3 – MATERIALS AND METHODS

Different stages of *Xenopus tropicalis* tadpoles were purchased from the National Xenopus Resource (NXR) at the Marine Biological Laboratory (MBL), Woods Hole, MA. Comparisons were made across three significant life-history stages to highlight the differences/similarities of genes and gene regulatory dynamics during metamorphosis. The developmental stages used for the experiments were as follows: before metamorphosis/prometamorphic stages (stage 56/57), at the beginning of the metamorphic climax (stage 60/61), and end of metamorphosis (stage 65/66). The tadpoles were euthanized using 0.2% aqueous tricaine methanesulfonate (MS-222), and the specimens were fixed in different fixatives or fresh tissues were taken according to each experiment. Tadpoles were

staged according to Nieuwkoop and Faber (NF). The code generated for the bioinformatics analyses are deposited in GitHub (https://github.com/GayaniSenevirathne/Senevirathne_et_al_RNAseq.git).

3.3.1 – RNA-seq using spatial transcriptomics and Laser microdissection (LCM)

Xenopus tropicalis tadpoles at prometamorphosis (stage 56), beginning of the metamorphic climax (stage 60/61) and end of metamorphosis (stage 65/66) were selected as the targeted stages for the RNA-seq experiment (stages were selected based on the significant phenotypic changes that were seen at each stage during the urostyle development based on Senevirathne *et al*., 2020). All forceps, scissors, surgical blades and lab benches were cleaned with RNAse away and 100% ethanol prior to any RNA sequencing experiment. Tadpoles were euthanized using MS-222. The region where the urostyle forms (demarcated by the tenth and fourteenth myotomes; Senevirathne *et al*., 2020) was dissected under a Leica L2 light microscope on ice-cold 1x DEPC-treated PBS; all the dissections were done on ice to prevent RNA degradation. The dissected tissue was immediately transferred to ice-cold OCT and flash frozen in liquid nitrogen and stored at -80ºC (for better RNA quality, the tissue blocks were processed the subsequent day). The frozen tissue blocks were sectioned using a Leica cryostat the next day.

To carry out a transcriptomic survey during urostyle development, I adapted a spatial transcriptomic approach (using Laser capture microdissections). The two targeted tissue types, coccyx and hypochord, from three individuals at each developmental stage (prometamorphosis, beginning of metamorphic climax, and end of metamorphosis) were dissected from frozen sections (Fig. 3.1A). The myotomic boundaries were used as a way of identifying the targeted

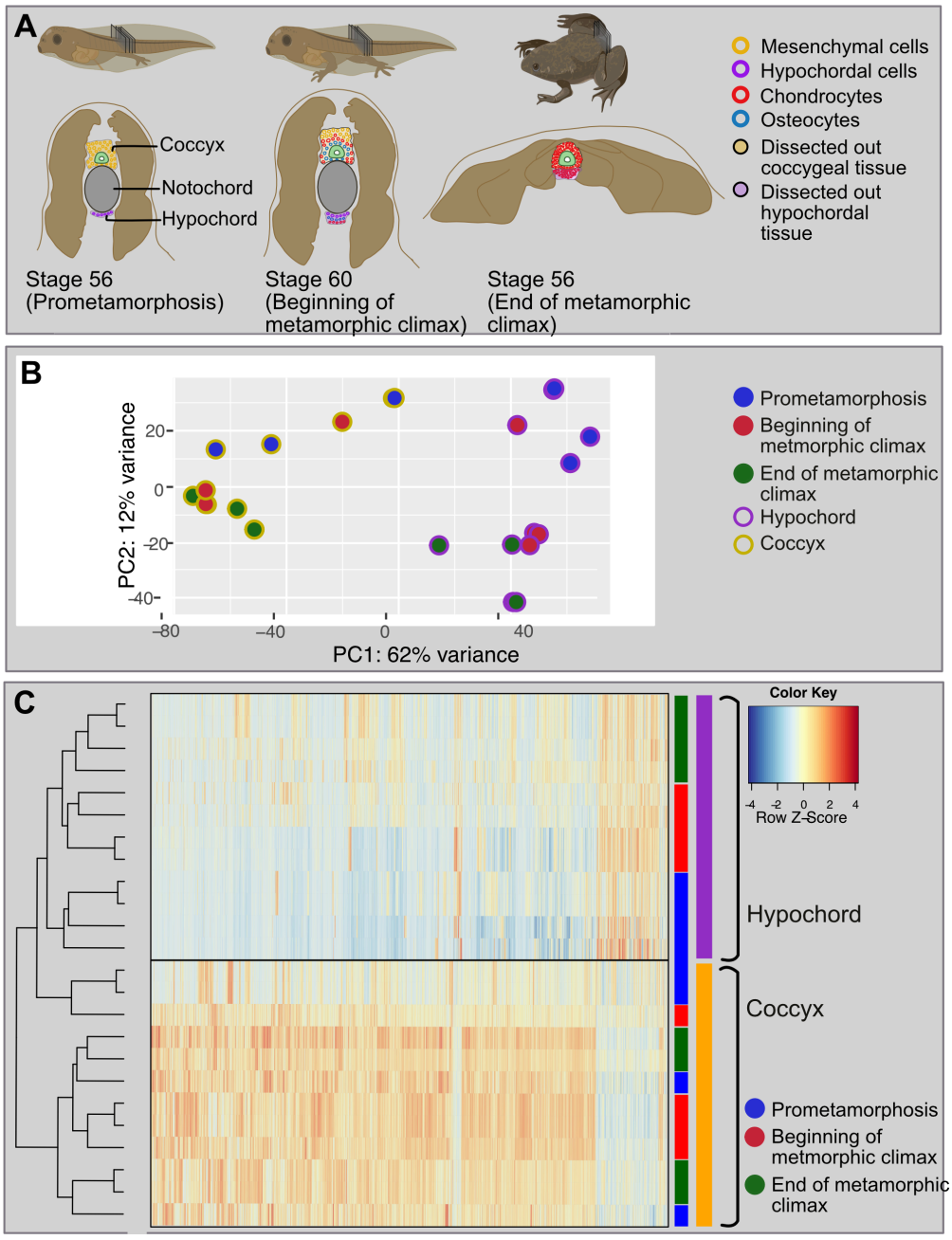

Figure 3.1. **Changes in transcriptomics during anuran urostyle development.** A. The experimental setup and the developmental stages used for Laser-capture microdissections. Ten sections of cryosections (16 mM each) were taken from three developmental stages (stage 56: prometamorphosis; stage 61: beginning of the metamorphic climax; stage 65: end of metamorphosis) and the coccygeal and hypochordal tissues were dissected out. B. Principal component analysis for the urostyle tissues (coccyx and hypochord) used for the transcriptomic assay (N=4 biological replicates per developmental stage). B. Principal component analysis of the log-normalized count data for all 24 samples. Each dot represents a tissue sample. C. Heatmap, highlighting the differentially expressed genes, compared between

Fig. 3.1, continued. three developmental stages and two tissue types. The heatmap highlights that the two tissue types possess two distinct sets of genes.

area to be dissected out. I used descriptions established in Chapter 2 (Senevirathne *et al*., (2020)) to identify cells of interest. Prometamorphic (stage 56) sections of coccyx had undifferentiated mesenchymal cells around the spinal cord, and the hypochord had embryonic hypochordal cells ventral to the notochord. The RNA-sequencing protocol followed a spatial transcriptomics method (Geo-seq; [143]). Prior to sectioning, the cryostat, brushes, adjacent benches/tabletops, blades, and pencils/pens were cleaned using RNAse away and 100% ethanol. The tissue blocks were left inside the cryostat for 20 minutes, allowing them to equilibrate at -20^{o} C (not doing this resulted in flaky sections or sections breaking when transferred onto the slides). The tissues were sectioned at 16 μM thickness on to PEN membrane 1.0 slides. Five–six sections were placed on each slide and were allowed to dry at room temperature for one minute before storing them at -80^{o}C for further processing (samples that were <1 month old were used for sectioning; the yield of RNA was high when the slides were sectioned on the same day).

On the day of the Laser capture microdissection step, slides were taken out of the freezer, thawed at room temperature for 2 minutes, and placed under an UV lamp for 2 minutes (UV helps the sections to adhere to the slide). Next, the slides were stained using Cresyl Violet to help visualize the cells. For this, slides were taken along an ethanol series, each wash was 30 seconds ~~each~~ (100% ethanol, 70% ethanol, Cresyl Violet in 70% ethanol, and were dehydrated in 70%, 90%, and 100% ethanol). Slides were allowed to dry completely before moving to the next steps (this step was important to avoid humidity affecting the RNA quality [144].

The dehydrated slides were processed via LCM with the following settings: aperture (10), speed (20) and energy (50). The hypochordal and coccygeal cells were identified (histological comparisons done in Senevirathne *et al*. [67] were used as a reference) using the x10 eye piece

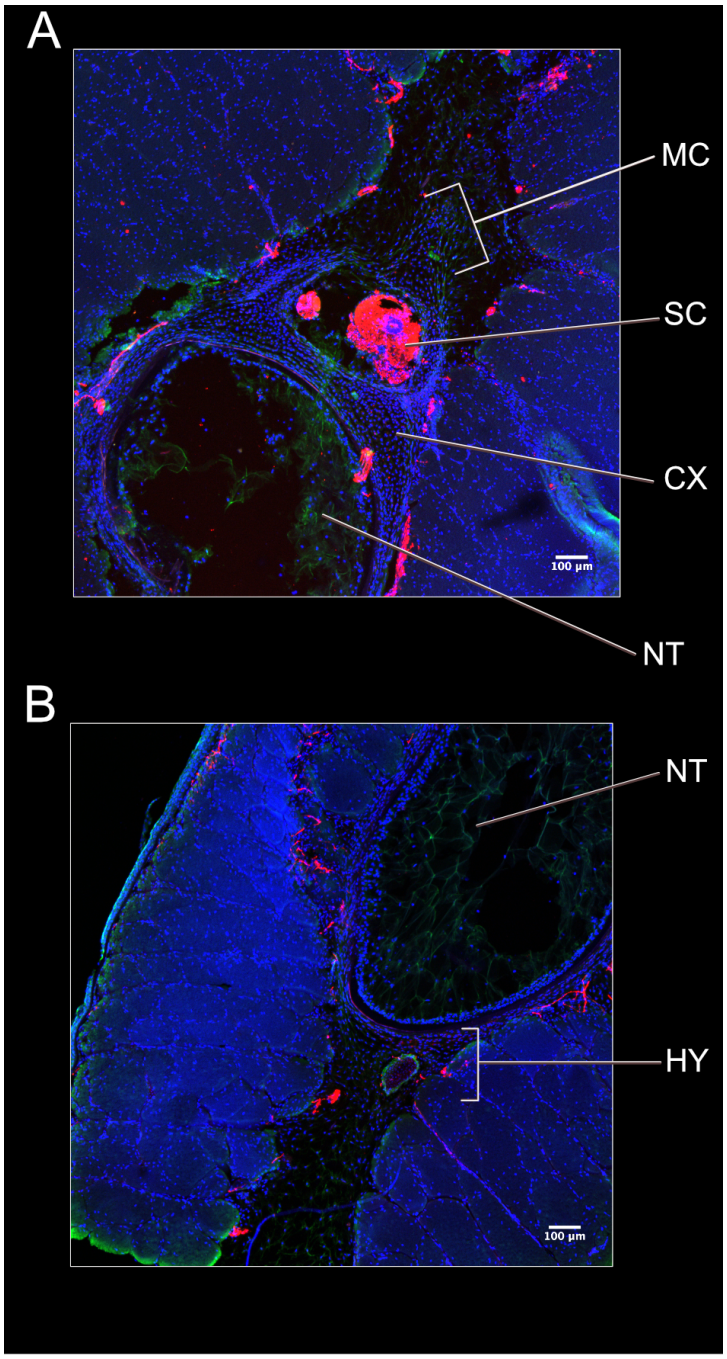

Figure 3.2. Comparison of the hypochordal and coccygeal sections before metamorphosis (stage 57). A. A transverse section across the coccyx, highlighting the aggregating mesenchymal cells around the spinal cord. B. A transverse section across the hypochord, highlighting the embryonic hypochordal cells ventral to the notochord and notochordal sheath. Nuclei stained in blue, using DAPI and neurons stained in red using acetylated tubulin.

and the dissections were done using the x20. Targeted cells were captured to an adhesive cap Eppendorf tube, with the cap consisting of 50 ul of the lysis buffer.

Once the cells from coccyx and hypochord were collected (~10,000 cells from 10 sections for each tissue type, 4 replicates were done for each stage, a total of 24 samples), 150ul of the lysis buffer was added to each tube and was left on ice for 20 minutes. RNA was extracted from the captured cells using the TAKARA NucleoSpin® RNA XS (Cat. No. 740902) kit with slight modifications (the filtration step was skipped). cDNA was generated using the SMART-Seq® v4 Ultra® Low Input RNA Kit for Sequencing (with the number of amplification cycles set to 18). cDNA was purified using Agencourt Ampure XP magnetic beads (Beckman Coulter) and were sequenced using the HiSeq PE100.

3.3.2 – Gene regulation and ATAC-seq

The same developmental stages that were used for the RNA-seq studies were taken, and the urostyle region was dissected out as a fresh chunk of tissue (morphological demarcations of the developing urostyle were decided based on Senevirathne et al. [67]). The OMNI-ATAC-seq protocol was used to identify open chromatin regions in the developing urostyle (two replicates from each developmental stage, coinciding with the RNA-seq and morphological studies, were selected).

The tadpoles were anesthetized in MS-222, dissected on ice-cold 1X PBS and were mechanically crushed using a pestle (cleaned using 100% ethanol prior to this step) to obtain a homogenized sample (all these steps were done on ice to prevent degradation of proteins). Once a homogenized sample was obtained, cells were counted using the BioRad Tc20 automated cell counter. All samples consisted of 75,000–100,000 cells. The subsequent steps followed the

OMNI-ATAC seq protocol [145, 146] with slight modifications using the Illumina Tagment DNA Enzyme and Buffer kit: cells were lysed in an ice-cold lysis buffer, followed by a transposition step using Tn5 Transposase, and DNA was purified using the Zymo DNA Clean and Concentrator. Purified DNA was amplified with 13 amplification cycles (the number of cycles were optimized by an additional qPCR step). Finally, the libraries were purified using the Zymo DNA Clean and Concentrator and were sequenced using the NovaSeq 2000 (100BP PE).

3.3.3 – Thyroid hormone and the urostyle development

In Chapter 2 [67] I implicated the involvement of TH in the development of the urostyle, especially having a direct impact on the ossification of the hypochord. To identify downstream targets of TH, which are directly affected during this process, two sets of experiments were conducted. 1. Early exposure where stage-54 tadpoles (prometamorphic) were reared in 1 mM goitrogen methimazole (a TH antagonist) (MMI; Sigma-Aldrich; 100 mg/L of aquarium water); 2. Late exposure where stage 57 (prometamorphic) tadpoles were reared in 1 mM MMI. Concurrently, another set of stage 54 and 57 tadpoles were reared using the same conditions in 0.1x MMR without adding methimazole as the control experiment (1x MMR = 100 mM NaCl, 2 mM KCl, 1 mM $MgSO_4$, 2 mM $CaCl_2$, 5 mM HEPES, pH 7.4). Tadpoles were reared for two months, and when the control tadpoles reached their metamorphic climax, RNA-seq (using spatial transcriptomics; Geo Seq) and ATAC-seq (following the OMNI ATAC protocol) were done for the methimazole-treated tadpoles following the same method described in the preceding sections.

3.3.4 – RNA-seq analyses

Three stages were targeted for all the next-generation sequencing steps – Before metamorphosis (stage 56/57), beginning of metamorphosis (stage 60/61), and end of metamorphosis (stage 65/66). RNA from two different regions, coccyx and the hypochord, was extracted from three individuals for each stage (18 samples). 9 samples were run per lane, using paired end 100 bp reads on a llumina HiSeq 2000, at the Genomic core at the University of Chicago.

Sequence quality was checked using FastQC (version 0.11.9). *Xenopus tropicalis* reference genome v. 9.1 (Xenopus_tropicalis_v9.1.dna.toplevel.fa.gz) and transcript annotations were downloaded from Ensembl (www. Ensembl.org). Adapter sequences were trimmed using Cutadapt (version 1.8.1). Trimmed sequences were mapped using two approaches to compare the differentially expressed genes: 1. Normal alignment using HTSeq v.0.13.5 [147] and Bowtie2 v.2.4.2 [148]; 2. Pseudoalignment using Kallisto v.0.46.0 [149] were used to assess differentially expressed genes across tissues and developmental time points. Counts for HTSeq2 and Bowtie2 alignment files were obtained using HTSeq-counts computed for the *Xenopus tropicalis* v.9 annotations. Kallisto counts were also used as a comparison method. The subsequent steps are for the aligned transcripts obtained from the HT-seq2 step. The differential gene expression between the two tissue types (coccyx and hypochord), three developmental stages, and three biological replicates, were analyzed using the DESeq2 [150] package (v.3.12) from Bioconductor. The dataset consisted of a total of 18 libraries (9 individuals, 3 replicates, 2 tissue types, 3 stages), differentially expressed genes were looked for either between stages (e.g., prometamorphosis *vs* beginning of metamorphic climax) or between the two tissue types (e.g.,

coccyx *vs* hypochord). A DESeq2 negative binomial generalized linear model was adapted, which has been highlighted in previous studies [150] as a robust method for identifying differentially expressed genes (DEGs). DESeq2 package was used in R to normalize the reads, and the reads were subjected to variance stabilizing transformation using the "vst" function. A principal component analysis (PCA) was carried out using the DESeq2 function "plotPCA" to observe the clustering of the 18 samples. Hypochord and coccyx show considerable differences in cellular composition and differentiation [67], and the gene expression profiles directly reflect this (Fig. 3.1.C). A False Discovery Rate (FDR) value of <0.05 was used as the statistical significance threshold. DEG comparisons were depicted in three ways: prometamorphosis *vs* beginning of metamorphic climax; beginning of metamorphic climax *vs* end of metamorphosis; coccyx *vs* hypochord. The results of the DEG experiments were visualized in three main ways: 1. heatmaps were generated from the lists (Appendices C, D and Tables 3.1 and 3.2) of significant genes using the normalized values. Differences in expression data were visualized using z-scores calculated for each gene (=each row); 2. Volcano plots were drawn highlighting the up/down regulatory genes in the DEGs. Here, log-transformed p-values (y-axis) were plotted against the log2 fold change (x-axis); 3. Narrowed down gene symbols of the DEGs were used for GO enrichment analysis. The reactome web-based analysis tool was used to determine the overrepresentation of Reactome pathways where the up/down regulatory gene lists (Appendices C,D,E and F), genes within the intersections of the Venn Diagrams (drawn using the package "VennDiagram") were given as inputs.

3.3.5 – ATAC-seq analyses

Adapter sequences were trimmed from the raw paired end 100-bp files using NGmerge [151] and the trimmed sequences were aligned to the *X. tropicalis* reference genome v. 9.1

(Xenopus_tropicalis_v9.1.dna.toplevel.fa.gz) using Bowtie2. Duplicated reads were removed from the subsequent analyses using Picard (http://broadinstitute.github.io/picard/). Peaks were called using MACS2 [152] (--nomodel --extsize 200 --shift -100 --nolambda) and Genrich (-e chrM -r -j). Two peak callers were used to compare the peaks, where Genrich's "j" command specifically signifies the ATAC-seq mode. Irreproducible discovery rate (IDR) <0.01 was used as the threshold to screen the replicate samples. Here, the IDR method compares ranked peak lists to identify overlapping peaks. Finally, the peak files were directly uploaded to Integrative Genomics Viewer (IGV) and were visualized along with their respective. bam and bam index files.

3.3.6 – HCR *in-situ* hybridization

Targeted urostyle tissues were fixed in 4% PFA, dehydrated in a methanol series, and stored at -20^{o} C until future use. On the day of sectioning, tissues were rehydrated using an ethanol series, rinsed in histosol, and subsequently, washed and mounted in paraffin. The microtome, brushes, bench/tabletops were cleaned using RNAse away and 100% ethanol and the tissue blocks were sectioned to obtain 12 μM-thickness paraffin sections. Paraffin sections can be stored at room temperature, indefinitely, until the day of staining.

For HCR *in-situ* hybridization [153] of paraffin sections (the protocol followed https://www.molecularinstruments.com/protocols with slight modifications), the sections were initially dewaxed using histosol, re-hydrated in ethanol, and treated with a Proteinase K/PBS solution to increase the tissues' permeability. Prehybridization step was followed by the addition of the targeted probe (1 μM probe/100 ul of hybridization buffer) and leaving the slides in a 37^{o} C incubator overnight. Next day, the slides were washed in the wash buffer and subjected to an

amplification buffer with hairpins overnight. On the third day, the slides were washed using dilution a series of SSCT, mounted using Fluoromount G + DAPI, and visualized using a Zeiss LSM 710 confocal microscope. The results were analyzed using Fiji image analysis software.

3.4 – RESULTS

3.4.1 – Disparity in gene expression profiles of Coccyx and Hypochord

At the beginning of metamorphic climax (stage 60/61) both hypochordal and coccygeal cells underwent chondrogenesis and osteogenesis (dissected cells at this stage included immature chondrocytes, mature chondrocytes, osteocytes, mesenchymal cells, and extracellular matrix) (Fig. 3.1.A and 3.2). At the end of metamorphosis, coccygeal and hypochordal cells completed ossification, and the majority of the cells consisted of osteocytes, osteoblasts, and mature chondrocytes. The two tissue types fuse at the end of metamorphosis, coinciding with the degeneration of the notochord. The total analysis consisted of 21458 genes, out of which 3286 genes exhibited considerable variation between the two tissue types across development (the FDR <0.05); both tissue types and the three timepoints were used as factors in the DESeq2 analysis where a binomial generalized linear model was implemented. Principal component analysis (PCA) revealed that the coccygeal and hypochordal samples generate two separate clusters (Fig. 3.3.B), and a heatmap showed the two tissue types possess two different gene expression profiles (Fig. 3.3.C). 3298 genes were differentially expressed between the urostyle and hypochord, whereas 1845, 385 and 3434 genes were differentially expressed between the prometamorphic *vs* beginning of metamorphic climax, beginning of metamorphic climax *vs* end of metamorphosis, and prometamorphosis *vs* end of metamorphosis, respectively. Among these

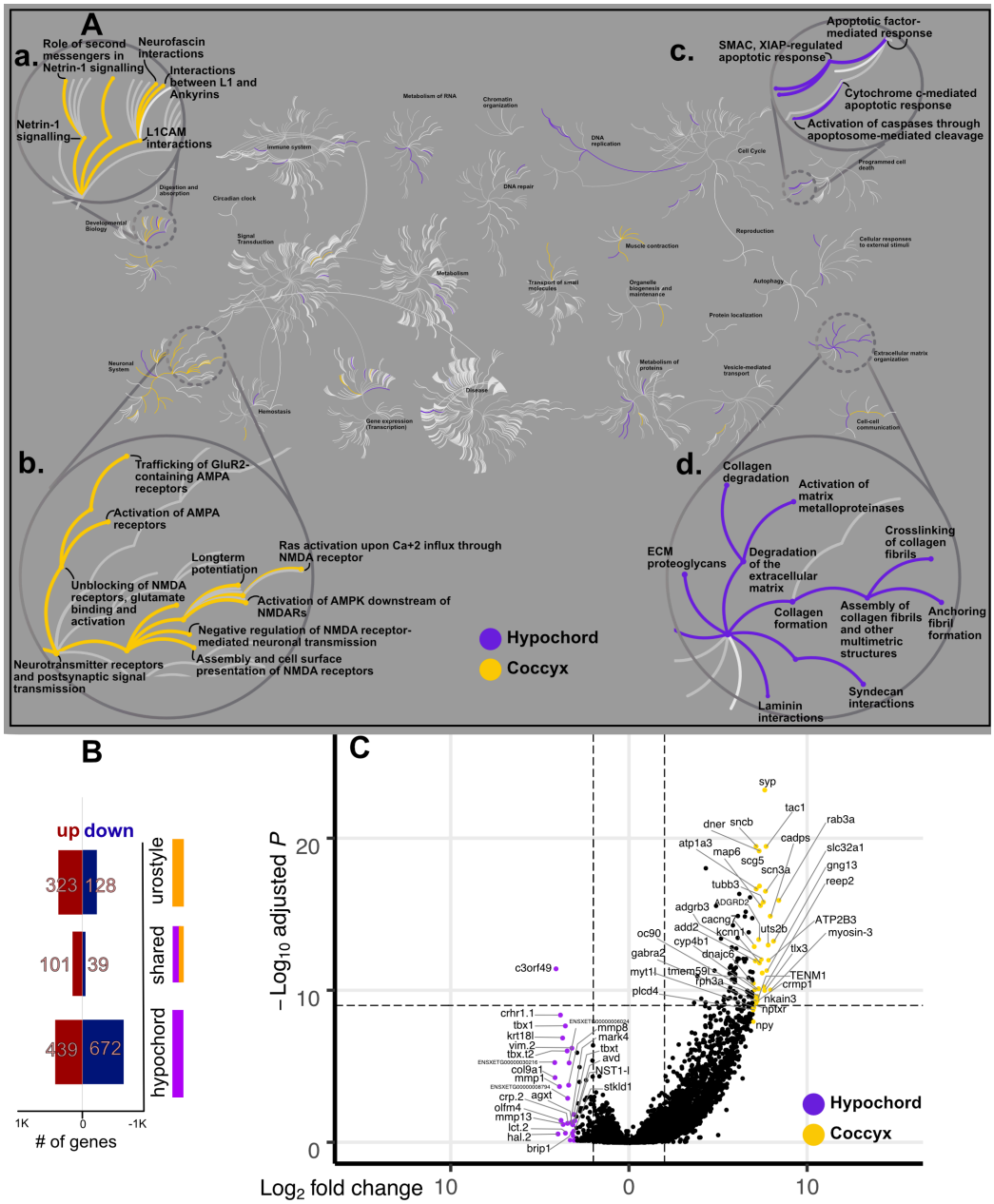

Figure 3.3. Comparative transcriptomic analysis of the two tissue types: coccyx and hypochord. A. A Reactome pathway analysis for up/down regulatory genes in coccyx vs hypochord; the central circles represent a top-level pathway, and the circles away from the center represents lower levels in each respective pathway. Zoomed-in sections of top-level pathways of Developmental Biology (Aa), Neuronal system (Ab), Programmed cell death (Ac), and Extracellular matrix organization (Ad) are shown. Overrepresented pathways ($P < 0.05$) are colored in yellow (coccyx) and purple (hypochord). Pathways that are not significant are shown in light gray lines. B. Most hypochordal genes are involved in organizing the extracellular matrix, whereas the majority of coccygeal genes are involved in neuronal

Fig 3.3, continued. remodeling and modifications. B. The total number of urostyle-responsive genes (FDR < 0.01) between hypochord and coccyx. C. Volcano plot showing differentially expressed genes across hypochord and coccyx during development (P < 0.05, FDR<0.01).

DEGs, 2828 genes were significantly upregulated and 470 were downregulated in the coccygeal region compared to hypochord. During coccygeal development, several modifications happen around the areas of interest. The coccyx develops dorsal to the notochord and around the spinal cord, initially as two ossification centers, which later fuse together during metamorphosis. Concomitantly, muscles and neurons around the coccyx remodel. Primary myotomes remodel into secondary muscles and attach to the coccygeal bone. The spinal cord degenerates and axons project outwards from the coccygeal spinal foramina [67]. These phenotypic changes are reflected in the underlying gene regulatory networks. The majority of the upregulated genes in the coccygeal tissue samples are involved in differentiation and development of the nervous system (e.g., *NEUROD6*, *PRDM12*, *COCH*, *APBA2*) [154, 155], or are genes that are expressed during skeletal muscle development (e.g., *ACTN2*) [156]. Apart from these, the rest of the upregulated genes within coccygeal tissues are directly involved in chondrocyte/osteocyte differentiation (e.g., *RUNX2*, *COL9A1*, *SOX8*) (Fig. 3.3) [157, 158].

Embryonic hypochordal cells are thought to have an endodermal [13, 14, 16, 67] or a superficial mesodermal origin [20]. Whether it is endoderm- or superficial mesoderm-derived, a cell population that is completely different from the sclerotomal cells (of the coccyx) forms the ossifying hypochord and contributes to the adult axial column. Hence, this unusual ossification of the hypochord, seen only in anurans (ranging from the

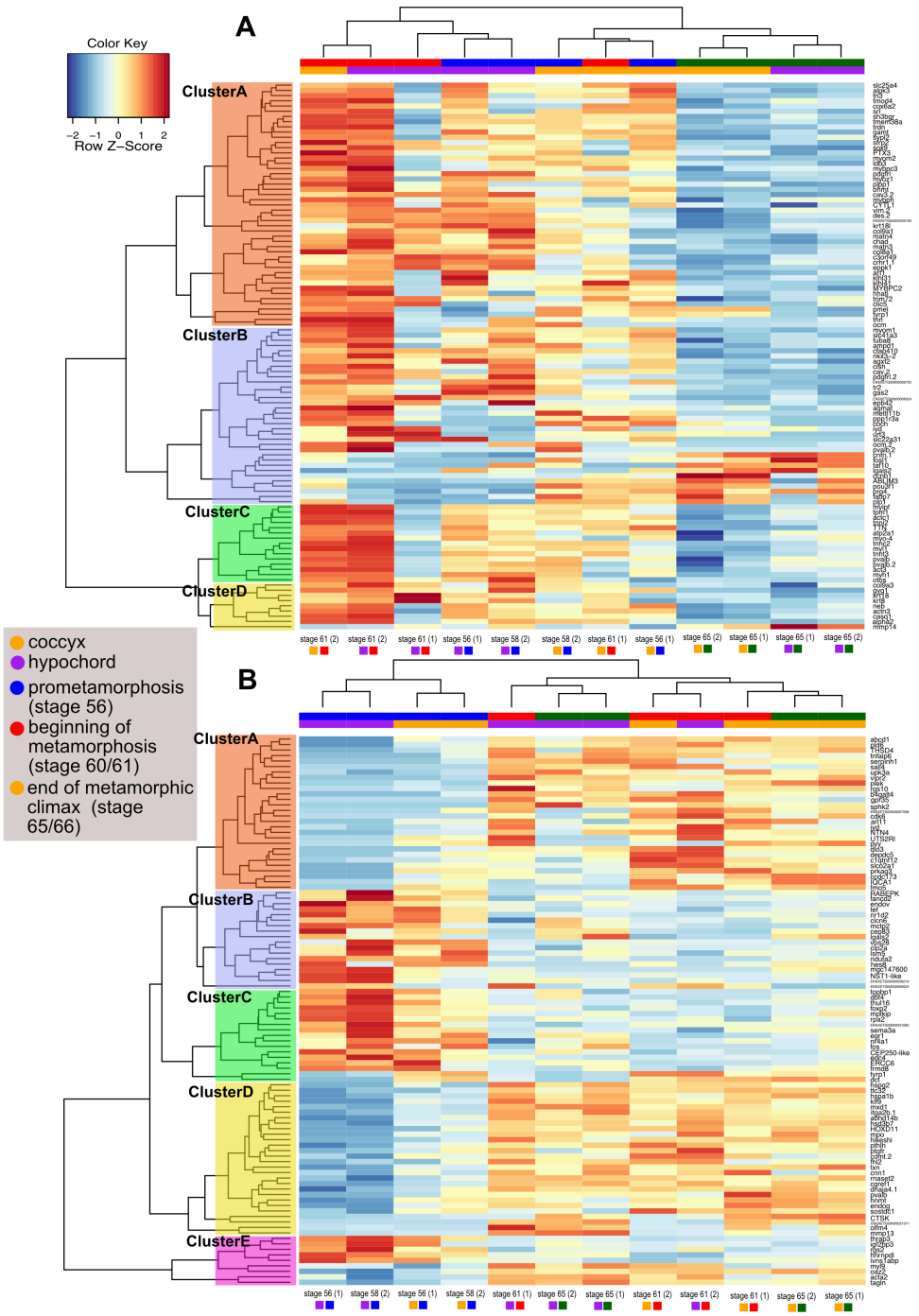

Figure 3.4: Differentially expressed genes across different time points during urostyle development. A. Heatmap showing before and beginning of metamorphosis vs end of metamorphosis, indicating that there is a set of genes (eg., *PTX3*, *SOX9*, *KRT18*) that switch off at the end of metamorphosis in both tissue types. B. Heatmap comparing before and beginning of metamorphosis, highlighting a set of genes (eg., *DIO3*, *HOXD11*, *PVALB*) that switch on during urostyle development. Purple: coccyx; Yellow: hypochord; Blue: before metamorphosis; Red: beginning of metamorphosis; Green: end of metamorphosis.

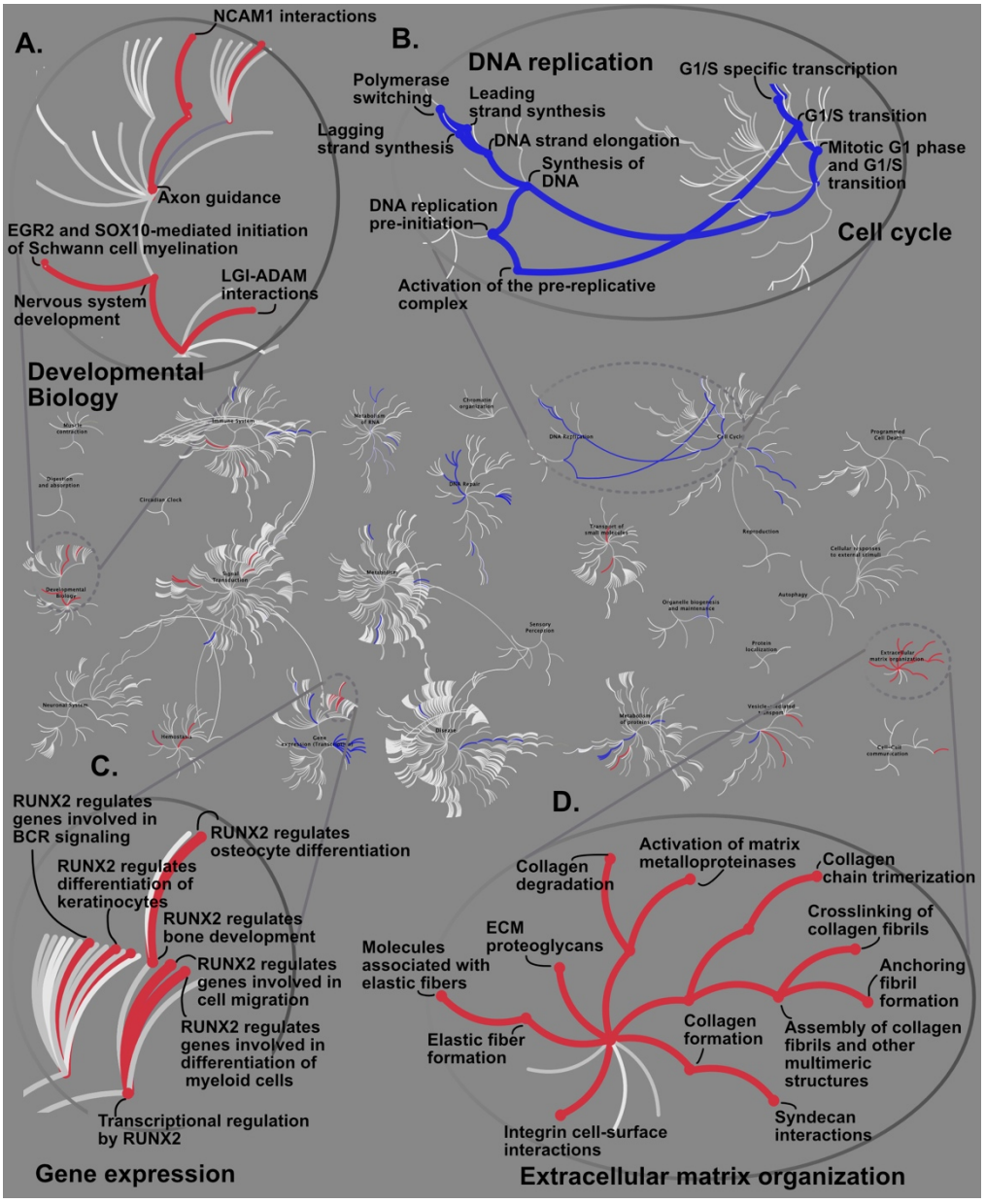

Figure 3.5. Reactome pathway analysis for up/down regulatory genes in two different time points: before metamorphosis (blue) and beginning of metamorphosis (red). The central circles represent a top-level pathway, and the circles away from the center represents lower levels in each respective pathway. Zoomed-in sections of top-level pathways of Developmental Biology (A), DNA replication and Cell cycle (B), Gene expression (C), and Extracellular matrix organization (D) are shown. Overrepresented pathways ($P < 0.05$) are colored in blue (prometamorphosis) and red (beginning of metamorphosis). Pathways that are not significant are shown in light gray lines.

myotome 10–14), is considered an apomorphic state, compared to the rest of the vertebrates. Embryonic hypochordal cells undergo chondrification and ossification as soon as the tadpole reaches its metamorphic climax. The transcriptomic assay between the two tissues revealed that hypochordal tissues express high concentrations of *TBX1*, *TBXT.1*, *TBXT.2*, and *HAND2* (Fig. 3.3.C). T-box genes are involved in early mesodermal patterning and their expression has not been recorded in adult tissues before (explained in detail in a subsequent section; 3.4.3). Here, we hypothesize three possible scenarios: if the hypochordal cells are of endodermal origin, the increased *TBXT*/*TBXT.2* could be initiating a cell-fate switch from endoderm-to-mesoderm (there are some instances where T-box genes have been recorded to enable a cell-fate switch e.g., [159]). To the best of our knowledge, there are no other studies looking into the possibility of an endoderm-derived tissue undergoing ossification. Secondly, if the hypochordal cells are superficial mesoderm derived, *TBXT* and *TBXT.2* could be activating the downstream targets involved in cellular matrix organization (seen by the up-regulated expression patterns of *MMP1*, *MMP8*; Fig. 3.3) and chondrification. Thirdly, another possibility is that the ossification of the hypochord could resemble an endothelial-to-mesenchymal transition (EMT). During EMT, the epithelial cells adapt a morphology similar to fibroblasts and acquire migratory properties (at the same time the epithelial cells lose adhesion to the surrounding extracellular matrix) [160]. Several studies hypothesize how Brachyury (TBXT/TBXT.2) plays a pivotal role in EMT, where overexpression of Brachyury would induce mesenchymal properties, and reduce epithelial properties, in the migrating epithelial cells [161, 162]. This phenomenon has led to abnormal ossifications in the vertebral column (i.e., vertebral column chordomas, where some are observed between the notochord and vertebral column) [163-165]. There are endothelial

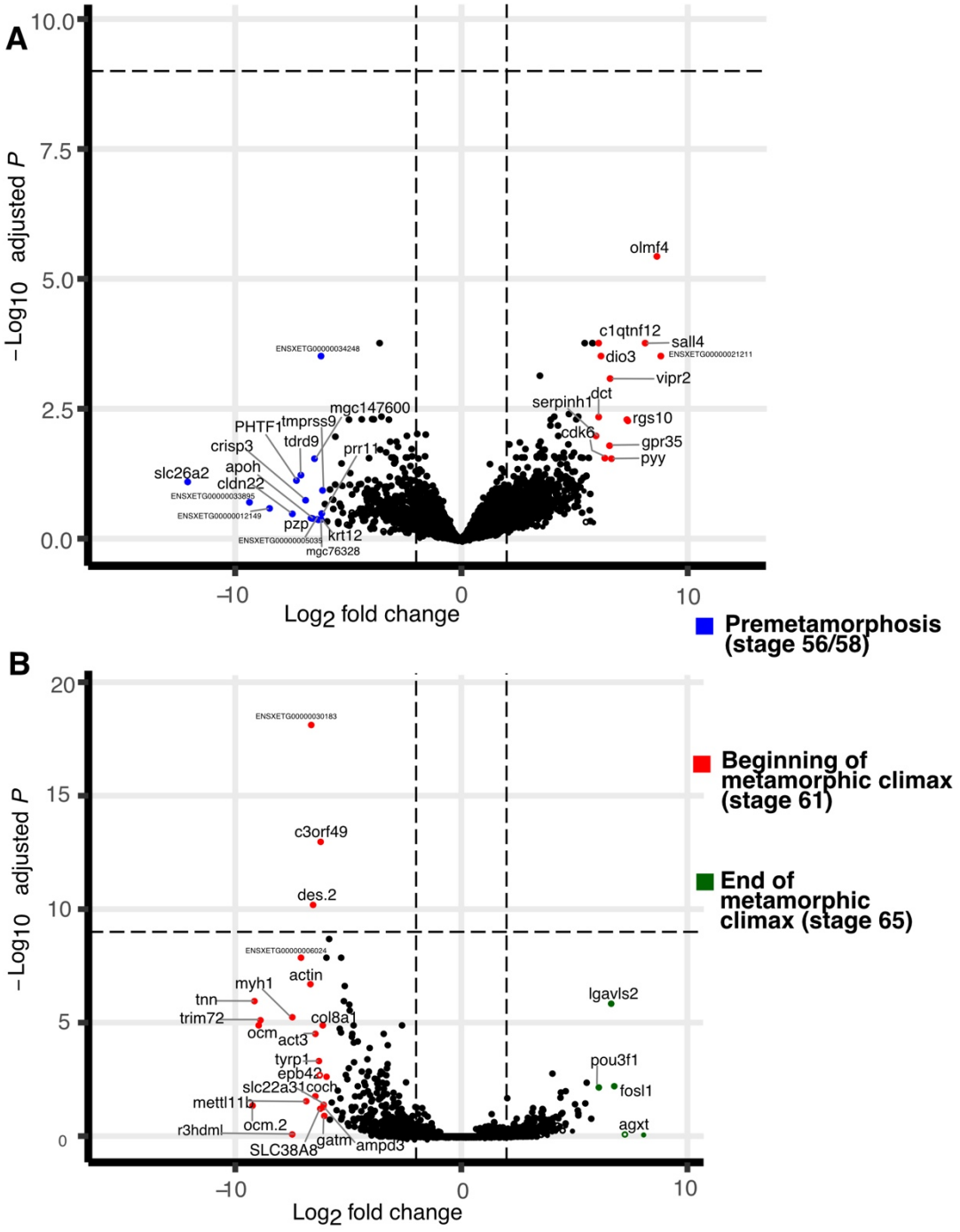

Figure 3.6. Volcano plot showing differentially expressed genes across three developmental time points, during the formation of the urostyle (P < 0.05, FDR<0.01).

cells lying between the embryonic hypochord and endoderm (where the dorsal aorta runs between these two tissues) [67]. Hence, the increased expression of *TBXT*/*TBXT.2* in

hypochordal cells could potentially lead to increased mesenchymal properties and eventually activate chondrifying and ossifying genes.

T-box genes have already been recorded as pivotal components in the differentiation of the posterior axial column [163, 164, 166-174], and seem to be playing a role in hypochordal ossification as well. However, all the three scenarios explained above, would require the activation of T-box genes at the onset of metamorphosis because of extrinsic/intrinsic signals, which could be either hormonal or environmental.

The pelvic region undergoes dramatic changes during metamorphosis, and this period is thought to represent the developmental stage that is most susceptible to predators. The underlying stress of the remodeling tissues and hormonal responses can also be seen by the increased expression of *CRCH.1* (corticosol steroid stress hormones), having a normal hormonal response to stress. Other than these genes, the hypochord also expresses significant concentrations of *VEGF* and *HAND2*. These two genes are involved in vascular development and can also be seen expressed in embryonic hypochord where *VEGF* plays a role in the formation of the hypochord (e.g., [14, 16, 17]). My previous work (Chapter 2) showed how the ossifying hypochord may also play a role in modifying the dorsal aorta by occluding it at the posterior-most end of the hypochord and remodeling it to form two branches, which enter the fore- and hind limbs respectively.

3.4.2 – Transcriptomic differences across different time points during urostyle development

The coccygeal and hypochordal tissues chondrify and ossify during development. At the end of metamorphosis, coinciding with the degenerating notochord, they fuse together to form the urostyle. I next delved into identifying genes that switch on/off during metamorphosis and

highlight DEGs that are expressed at each time point: before metamorphosis, beginning of metamorphic climax, and end of metamorphosis.

There are already studies done of metamorphic transcriptomes (e.g., [24, 38, 80, 175-178]), but none on the urostyle. Hence, I first looked into urostyle-responsive transcriptomes by comparing genes that are differentially expressed in the coccyx and hypochord at different time points: 1. Before metamorphosis vs beginning of metamorphosis (Figs 3.4.B, 3.5, 3.6) and before/beginning of metamorphosis vs end of metamorphosis (Figs 3.4.A). This analysis identified 5664 number of DEGs that fell within the thresholds of FDR< 0.01 (adjusted p-values <0.05 and log fold change of 1.5) and showed unique expression patterns that were significant at each time point.

I uncovered unique sets of genes that were up- and down-regulated across the three time points when the top 100-most significant genes across the hypochordal and coccygeal tissues were clustered. Through this step, I identified 4 unique clusters when the transcriptomes were compared between the three developmental time points (before and beginning of metamorphosis *vs* end of metamorphosis (Fig. 3.4)). Cluster A has 47 genes that were highly downregulated at the end of metamorphosis ("switched off") compared to the other two time points. This cluster includes genes involved in muscle contraction and M-band stabilization in fast skeletal muscles (e.g., *TRDN* and *MYOM2I*; [179, 180]), skeletal development (e.g., *SOX9* [181]), response to inflammation (*PTX3*; [182]), filament organizing genes (e.g., *KRT18.1* and *VIM.2*; [183, 184]), extracellular matrix organizing and connective tissue-strengthening (e.g., *COL9A1*, *COL8A1*, *CHAD*; [185, 186]), and stress regulation (*CRCH.1*; [187]). The other two gene clusters, B and C

(Fig. 3.4.A), comprise genes that are both down- and up-regulated at the end of metamorphosis. Cluster C also has 15 genes that are down-regulated at the end of metamorphosis, which include collagen markers (e.g., *COL9A3*), and skeletal muscle function genes (e.g., *MYL1* and *ACTN3*; [188, 189]). Genes that are up-regulated (10 genes) are

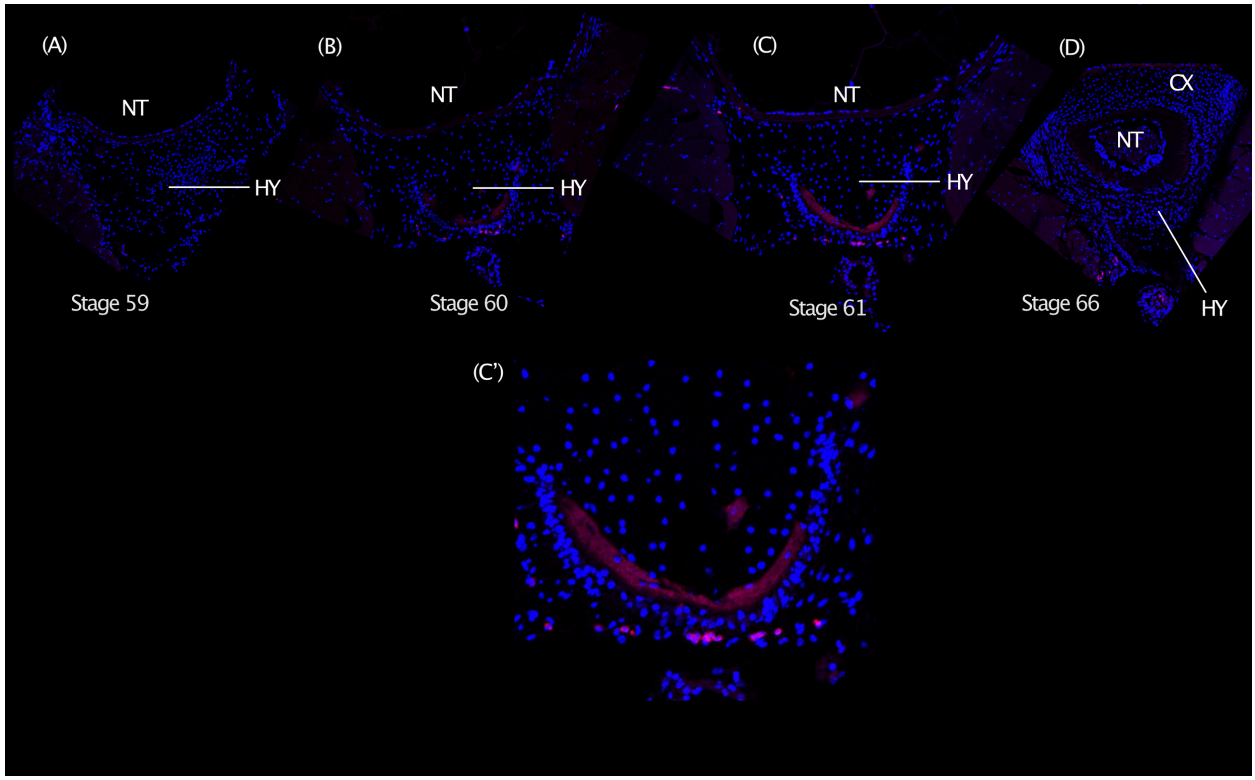

Figure 3.7. TBXT HCR in-situ hybridization on transverse sections of the urostyle. The periphery of the developing hypochord shows expression of TBXT (pink color), which is initiated once the hypochord starts to form and depletes when the hypochord fuses with the coccyx. Nuclei are stained using DAPI (blue). Abbreviations: CX, coccyx; HY, Hypochord; NT, notochord.

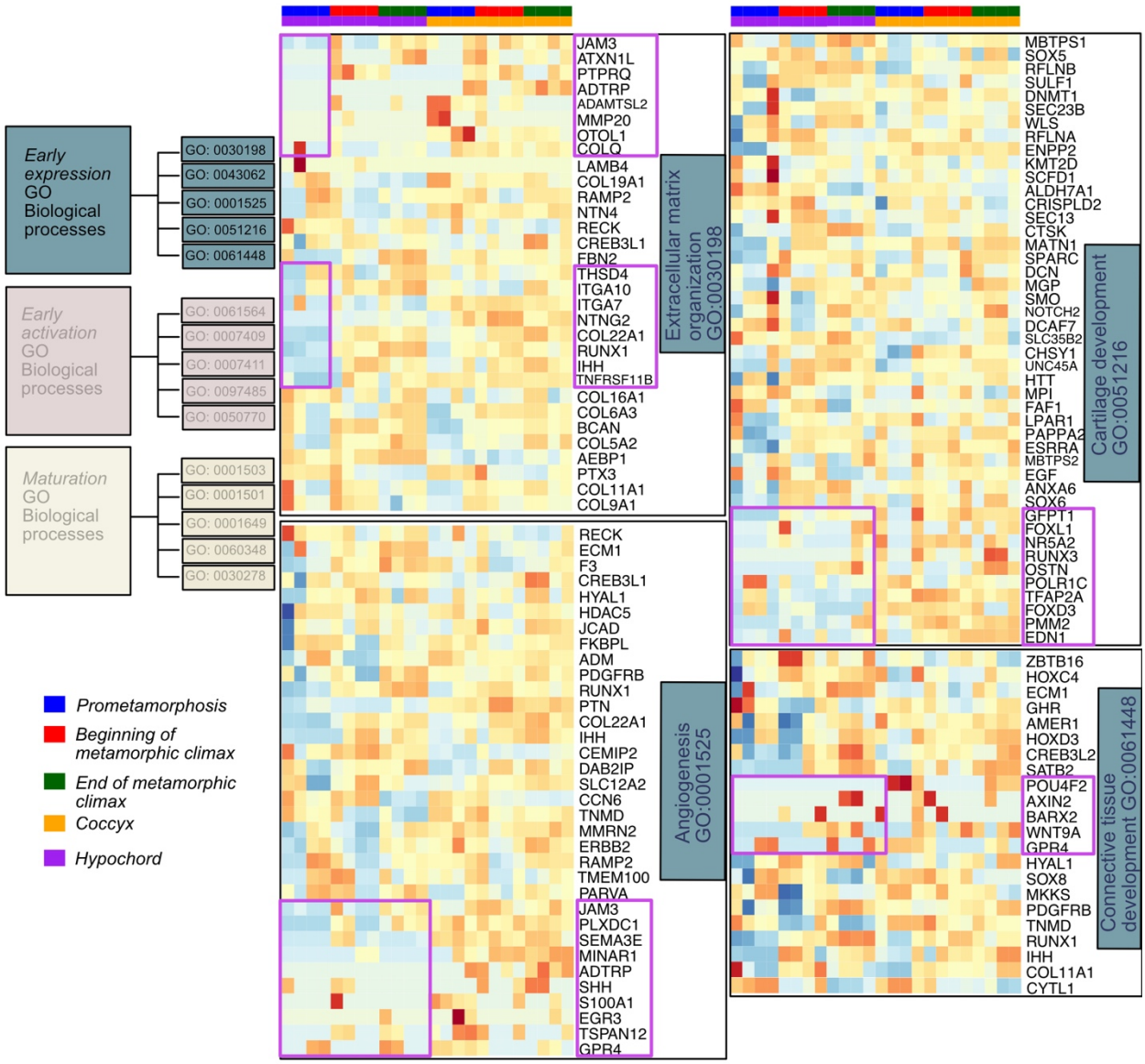

Figure 3.8. Heatmaps showing differentially expressed genes involved in GO functions belonging to the "Early expression cluster" of osteocyte differentiation. Significant genes of the osteocyte transcriptome are divided into three clusters [190]. This cluster includes the GO functions Extracellular matrix organization, Angiogenesis, Cartilage development, and Connective tissue development. Genes of interest that are differentially expressed between the coccyx and hypochord are highlighted in purple color.

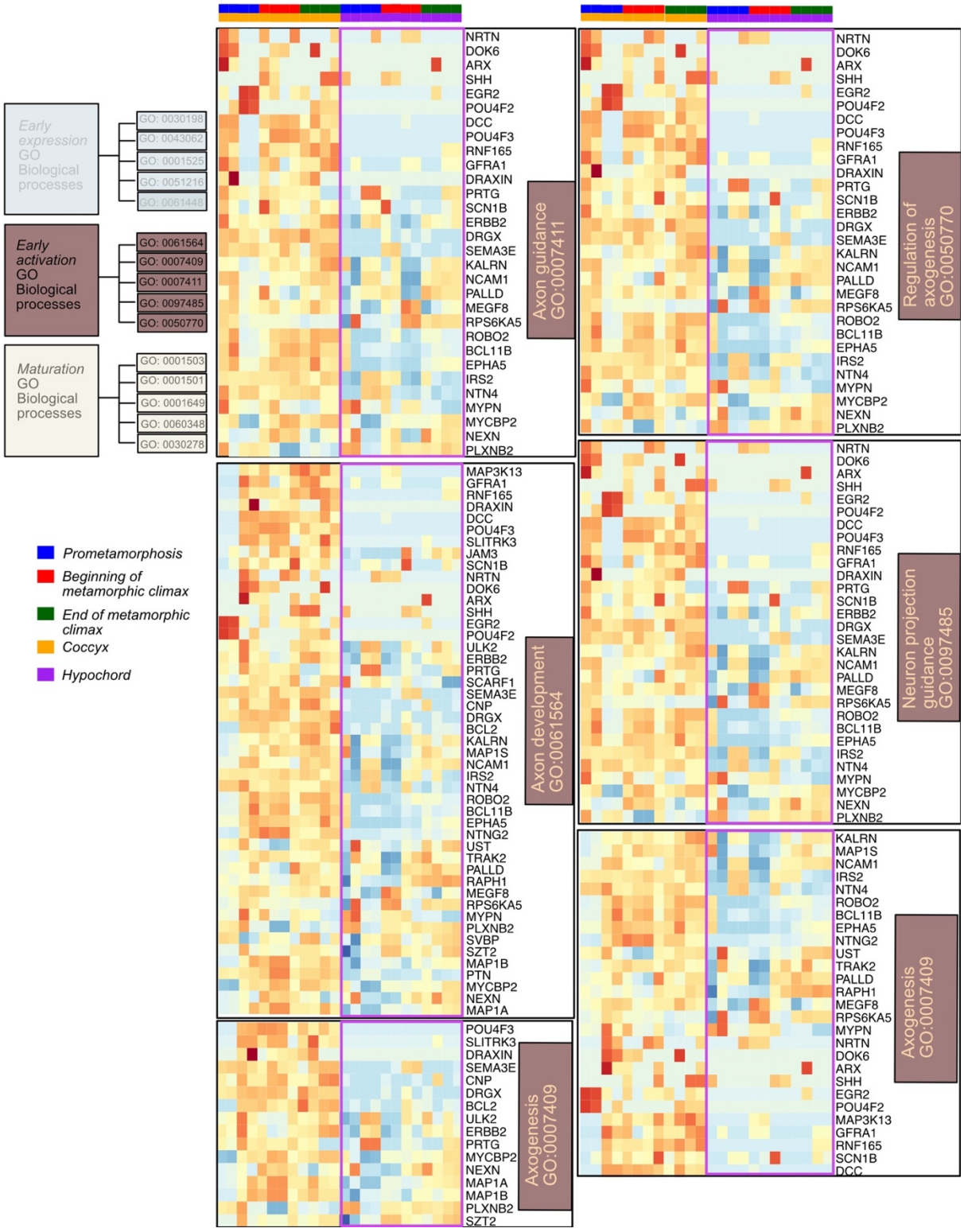

Figure 3.9. Heatmaps showing differentially expressed genes involved in GO functions

Fig. 3.9, continued. belonging to the "Early activation cluster" of osteocyte differentiation. Significant genes of the osteocyte transcriptome are divided into three clusters [190]. This cluster includes the GO functions Axon guidance, Axon development, Axogenesis, Regulation of axogenesis, and Neuron projection guidance. Genes of interest that are differentially expressed between the coccyx and hypochord are highlighted in purple color.

within Cluster B and are involved in mitosis (*CCNB1*; [191]), development of neurons (*POU3F1*; [192]) and maintenance of myelin sheath (*PLP1*; [193]). When before metamorphosis was compared with beginning/end of metamorphosis, clustering of the 100 top-most significant genes revealed metamorphic genes that were switched off before metamorphosis but were switched on during metamorphosis. Heatmap clustering revealed five main clusters (Fig. 3.4.B). Cluster A included 28 genes that were downregulated (switched off) before metamorphosis in both coccyx and hypochord, but as soon as metamorphosis was initiated, these genes were upregulated; they are involved in functions like collagen synthesis (*SERPINH1*; [194]), cell cycle (*CDK6*; [195]), and thyroid hormone inactivation (*DIO3*; [196]). Cluster B and C includes genes that are switched on prior to metamorphosis and are switched off at the onset of metamorphosis: *HES8*, *FOXP2*, *EGR1*, *HOXD11*, and *PVALB* are representative examples. Cluster D is enrichened with genes that are involved in blood sugar control (e.g., *THRAP3*, *IGF2BP3*; [197, 198]), which are down-regulated before metamorphosis but are up-regulated at the onset of metamorphosis. This part of the transcriptomic analysis identified DEGs that are specific to the three significant time points (before metamorphosis *vs* onset of metamorphosis *vs* end of metamorphic climax). I next explored the GO function of these significant genes during development. The DEGs and the corresponding P-values from the differential expression analyses were imported into a Reactome

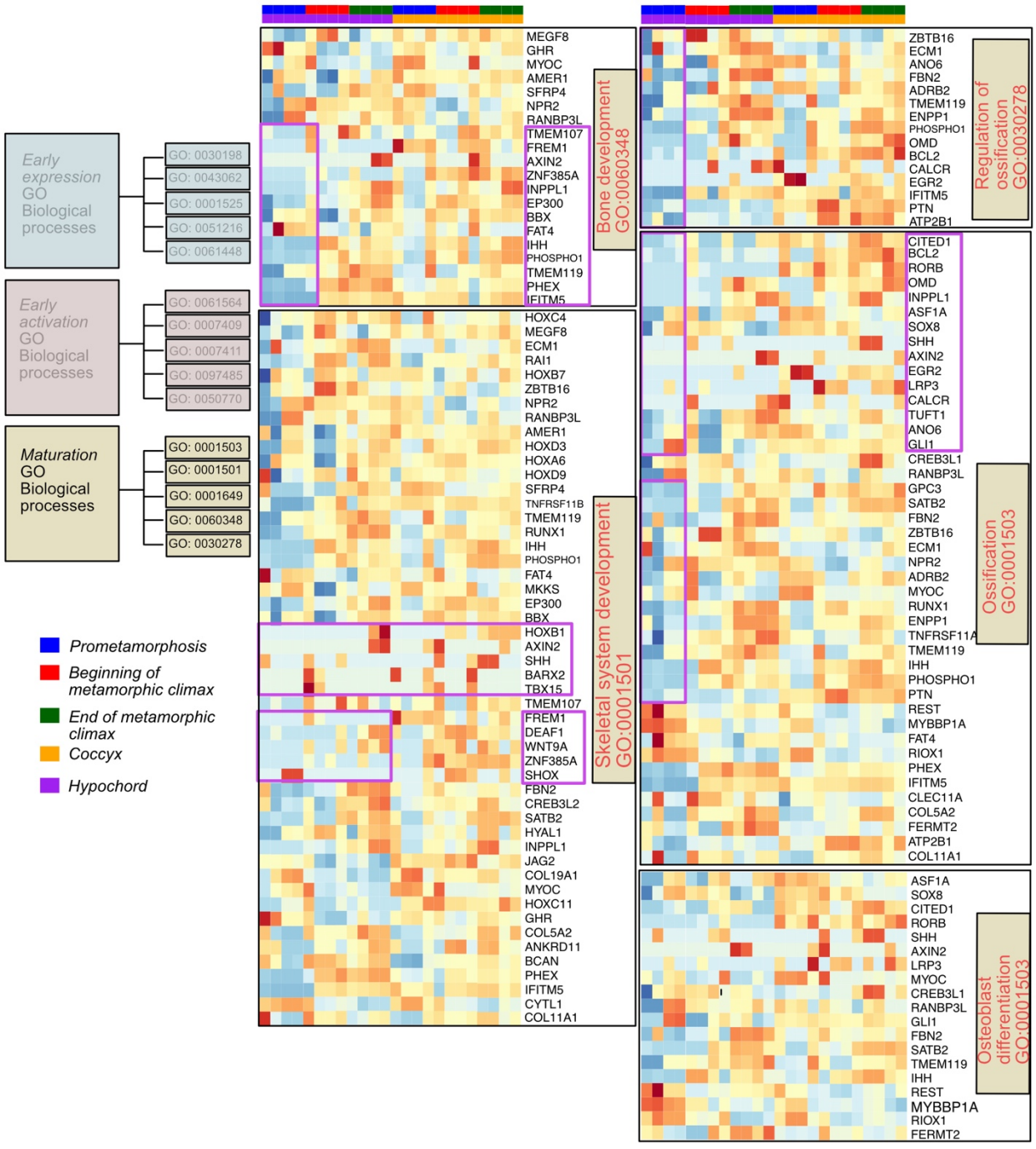

Figure 3.10. Heatmaps showing differentially expressed genes involved in GO functions belonging to the "Maturation cluster" of osteocyte differentiation. Significant genes of the osteocyte transcriptome are divided into three clusters [190]. This cluster includes the GO functions Bone development, Skeletal system development, Osteoblast differentiation,

Fig. 3.10, continued. Ossification, and Regulation of ossification. Genes of interest that are differentially expressed between the coccyx and hypochord are highlighted in purple color.

pathway browser to compare the functional aspect of these genes (Fig. 3.5). DEGs up regulated before metamorphosis were enriched for GO terms like "DNA replication and pre-initiation", "synthesis of DNA", "Polymerase switching", "G1/S transition" (Fig 3.5.B). Whereas the DEGs up regulated during metamorphosis include genes that function in "Collagen formation", "Cross linking of collagen fibrils", "*RUNX2* regulated bone development", and "Osteocyte differentiation" (Fig 3.5.C and D).

Morphological analyses highlighted that both urostyle and hypochord undergo endochondral ossification during development (Chapter 2) [67], and similar ossification patterns were reflected in the gene expression profiles as well. Though there were major differences in some transcriptomes (e.g., presence of T-box genes, *CRCH.1, MMP*s in hypochordal tissues at the onset of metamorphosis *vs* absent in the coccyx), there were similarities in genes that were involved in endochondral ossification: I show that genes that are involved in cartilage and bone formation, extracellular matrix organization, and thyroid hormone responsive elements are present in both tissues (Fig. 3.5), but differ temporally (coccyx starts ossifying after 1.5 months, whereas the hypochord initiates its ossification only at the onset of metamorphosis).

3.4.3 – Hypochord, metamorphosis and T-box genes

The ossifying hypochord in anurans is considered an apomorphic character among vertebrates. As there is no data on the genes that are expressed during hypochordal ossification, I used the DEGs identified by the coccyx *vs* hypochord comparisons (section 3.4.1) to scrutinize

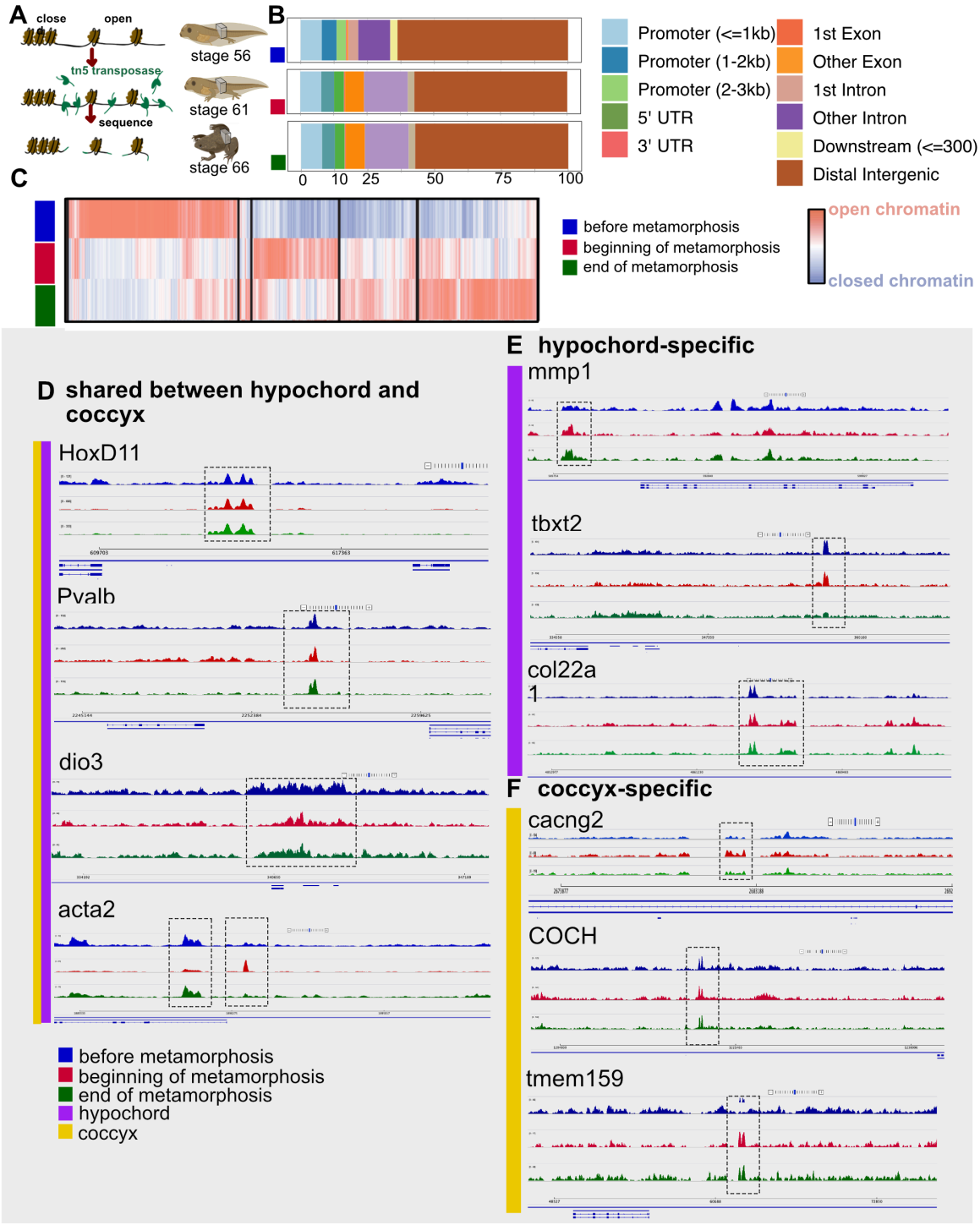

Figure 3.11. Urostyle-responsive regulatory regions. A. Schematic diagram showing the workflow for chromatin profiling experiment. B. Proportions of developing urostyle ATAC-seq peaks annotated to different genomic regions across development; majority of the peaks fall within the distal intergenic region and beginning (stage 61) and end of metamorphic

Fig. 3.11, continued. climatic (stage 65) peaks differ from the prometamorphic (stage 56) ATAC-seq peaks with respect to peaks falling within the exon regions that are not the first exon. C. Heatmap of ATAC-seq peaks showing open and closed chromatin regions during urostyle development across development. D. ATAC-seq urostyle profiles at stage 56 (blue), stage 61 (red), and stage 65 (green) at the loci of validated up-regulatory genes narrowed down from RNA-seq analyses.

this. This analysis identified 470 genes that were uniquely up-regulated only within the hypochordal tissues (they fell within the significant threshold of adjusted p-value <0.05 and FDR<0.01) (Appendix D). Compared to the coccyx, I identified DEGs that were only present in the hypochord (Table 3.2). Out of these, here, I will be focusing on the highly expressed T-box (*TBXT.1*, *TBXT.2*, *TBX1*) genes that are only seen in the hypochordal tissues in this section.

T-box genes have been implicated in early mesodermal patterning and, especially, *Brachyury*/*Xbra* is essential in early mesodermal formation [166, 167, 170, 172, 199], and Brachyury homologues across vertebrates induce the mesoderm [173, 200]. *Xenopus* has two paralogues of the gene *Brachyury*: *TBXT.1* (also known at *Xbra* or *T*) and *TBXT.2* (also known as *Xbra3* or *T2*). When *Brachyury* is knocked out, it causes loss of posterior mesoderm and failure to differentiate the notochord [168, 201]. *Brachyury* is also involved in controlling cell fate decisions while acting synergistically with the other transcription factors (like *Bix4*) and genes (*WNT11*) in the posterior mesoderm [202]. However, the expression of *TBXT*.1 and *TBXT*.2 in late developing tadpole structures has not been reported so far.

As described below, the temporal and spatial expression patterns of *TBXT.1* and *TBXT.2*, make them good candidate genes for regulating ossification only in hypochordal tissues. To study the potential role of *TBXT.1* and *TBXT.2* in hypochordal ossification further, I performed HCR in-situ hybridization to examine the temporal and spatial expression patterns. *TBXT.1*

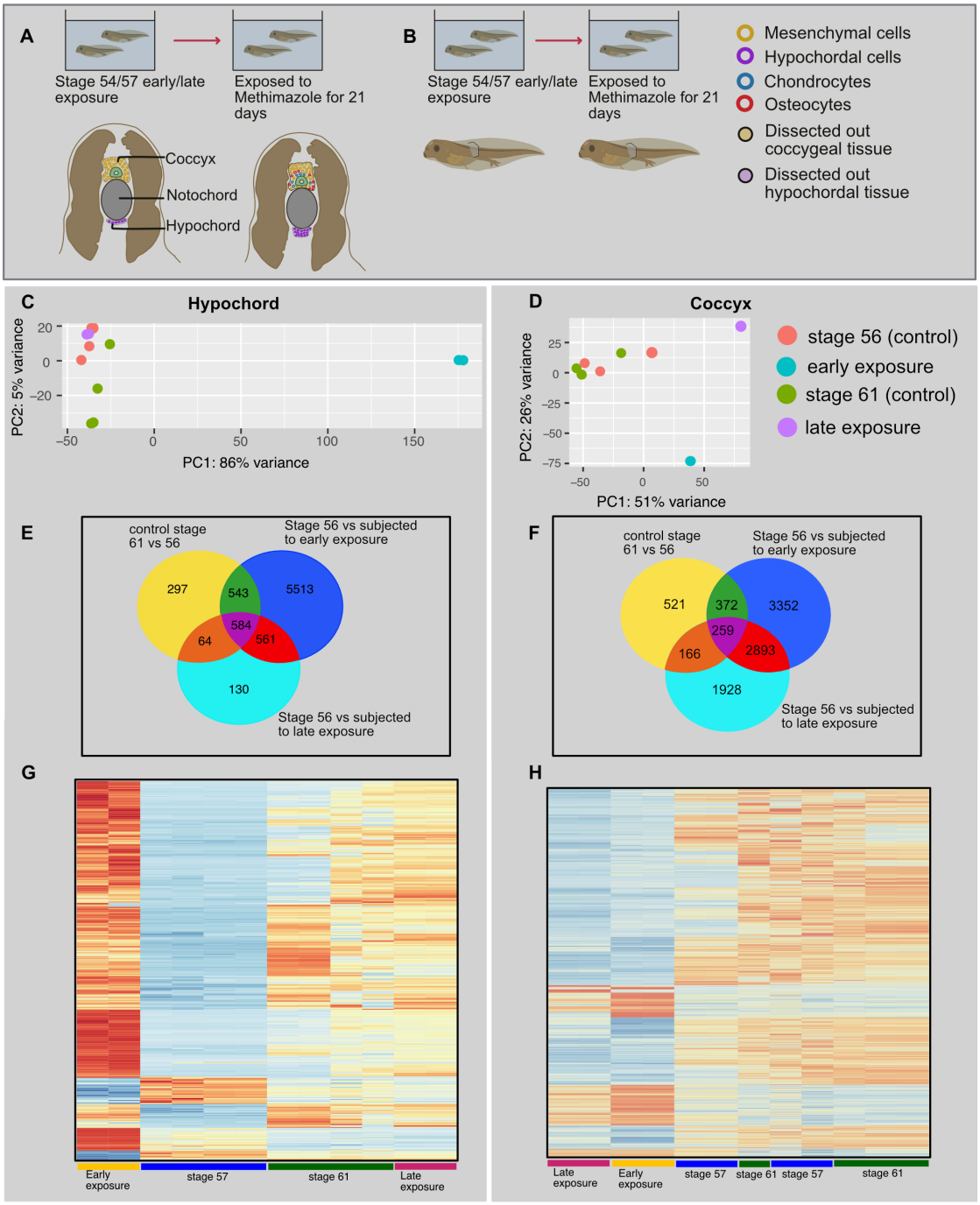

Figure 3.12. Transcriptomic comparisons between Methimazole-treated vs control tadpoles across development and coccyx and hypochord. A, B. Tadpoles were exposed to methimazole at two different developmental stages: stage 54 tadpoles (early exposure) and stage 57 (late exposure) for 21 days; they were subjected to Laser capture microdissection (for RNA-seq) and fresh tissue blocks for ATAC-seq. C,D. Principal component analysis (PCA) of the log-normalized count data for coccygeal and hypochordal samples (N=12 for each tissue

Fig. 3.12, continued. type) for control vs methimazole-treated samples. Each dot represents a sample. E,F. Venn Diagram showing differentially expressed gene-sets between control stage 56 vs 61; control stage 56 vs early exposure; control stage 56 vs late exposure for hypochord (E) and coccyx (F). G,H. Heatmaps, highlighting the differentially expressed genes, compared between hypochord (G) and coccyx (H) and three time points (control stage 56, control stage 61, early exposure, late exposure).

expression is exclusively concentrated along the ossifying hypochord at the onset of metamorphosis but is not evident in prometamorphic nor at the end of metamorphic climatic tadpoles (Fig. 3.7).

An ossifying hypochord is only normally present in anurans, however, interestingly, hypochord ossification between the caudal part of the vertebral column and notochord also appears as a congenital vertebral anomality seen prenatally in humans, caused by a mutation in the T (*TBXT*) gene [169, 203]. In humans with this abnormality, increased expression or duplications of the *TBXT* gene result in production of excess *Brachyury* [163, 165]. It has been hypothesized that this excess *Brachyury* causes residual cells ventral to the notochord to grow and ossify in humans and sometimes results in sacral agenesis in newly born babies (commonly to referred to as the "frog-like" syndrome). The observation of high levels of *TBXT*/*TBXT2* in ossifying hypochordal cells (which is ossified ventral to the notochord) and presence of two duplicated copies of the *TBXT* (*T* and *T2*/*TBXT* and *TBXT.2*) in anurans compared to normal humans and other vertebrates is thus tantalizing and needs further scrutiny. Previous studies have shown that *Brachyury* acts as a switch in posterior mesoderm specification during embryogenesis and is restricted to the anteroposterior axis [166, 167].

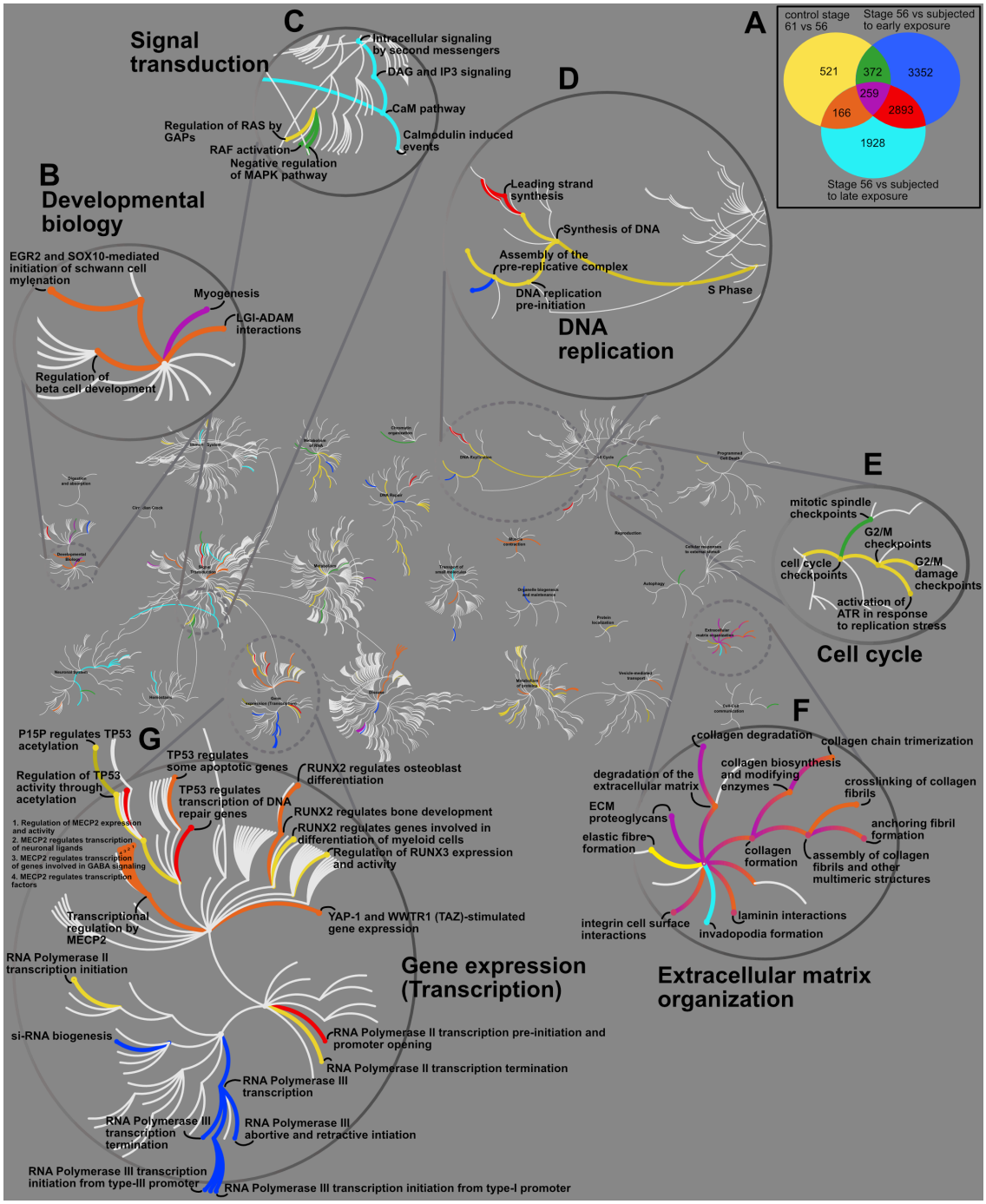

Figure 3.13. A Reactome pathway analysis for up/down regulatory genes in control vs methimazole-treated Coccygeal tissues. A. Venn Diagram showing differentially expressed gene-sets between control stage 56 vs 61; control stage 56 vs early exposure; control stage 56 vs late exposure for hypochord. (B-G) The central circles represent a top-level pathway, and the circles away from the center represents lower levels in each respective pathway. Zoomed-

Fig. 3.13, continued. in sections of top-level pathways highlight some of the differentially expressed pathways: Developmental Biology (B), Signal transduction (C), DNA replication (D), Cell cycle (E), Extracellular matrix organization (F), and Gene expression (G). Overrepresented pathways ($P < 0.05$) are colored, representing the intersections corresponding with the Venn Diagram's colors. Pathways that are not significant are shown in light gray lines.

Here, during hypochordal ossification, the onset of metamorphosis could be triggering ectopic expression of *TBXT*/*TBXT.2* in hypochordal cells, which could potentially express posterior mesodermal genes and subsequently activate down-stream targets of *TBXT*/*TBXT2*, which in turn initiates chondrification and ossification.

3.4.4 – Transcriptomic comparisons between coccyx + hypochord and other ossifying elements

Vertebrate ossification happens by distinct processes: endochondral (cartilaginous precursors used as a template) and intramembranous (direct ossification of the condensed mesenchymal cells) [204]. Even though coccyx and hypochord are derived from two different cell populations, they both undergo endochondral ossification [67]. During this process, mesenchymal cells condense (commit to form osteoprogenitors) and aggregate to form cartilaginous precursors during early development. Cartilaginous precursors expand and cells proliferate, next the extracellular matrix is synthesized, and finally, mineralization of the matrix occurs. These steps are similar to other bones in vertebrates, which undergo endochondral ossification as well [205]. However, to see if the transcriptomic profile during this process is conserved in the two bones that form the urostyle, I compared the spatial and temporal transcriptomic maps of the osteocytes (from published datasets of different skeletal tissues of different ages) with my current dataset.

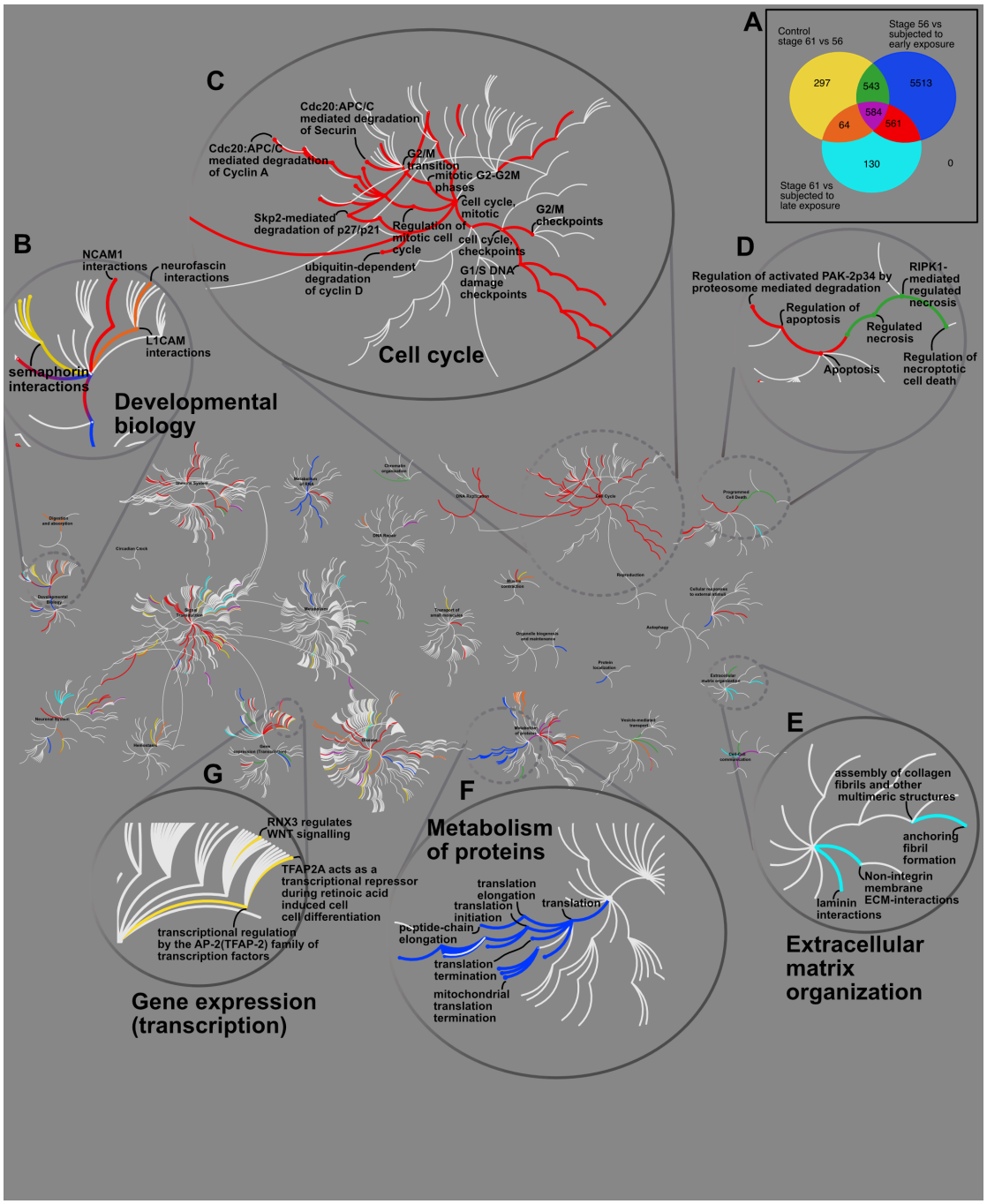

Figure 3.14. A Reactome pathway analysis for up/down regulatory genes in control vs methimazole-treated Hypochordal tissues. A. Venn Diagram showing differentially expressed gene-sets between control stage 56 vs 61; control stage 56 vs early exposure; control stage 56 vs late exposure for coccyx. (B-G) The central circles represent a top-level pathway, and the circles away from the center represents lower levels in each respective pathway. Zoomed-in sections of top-level pathways highlight some of the differentially expressed

Fig. 3.14, continued. pathways: Developmental Biology (B), Cell cycle (C), Programmed cell death (D), Extracellular matrix organization (E), Metabolism of proteins (F), and Gene expression (G). Overrepresented pathways ($P < 0.05$) are colored, representing the intersections corresponding with the Venn Diagram's colors. Pathways that are not significant are shown in light gray lines.

Youlten et al. [190] identified three clusters of GO functions during osteocyte development: 1. "An early expression cluster" (expressed in osteoprogenitors/osteoblast-like cells); 2. "An early activation cluster" (expressed in early osteocytes); 3. "A maturation cluster" (expressed in mature osteocytes). I compared the expression of the genes belonging to these GO functions with the coccygeal and hypochordal transcriptomics to see if the molecular underpinning of ossification is similar in the genes responsible for the formation of the urostyle as well.

Early expression cluster. —This included GO term functions "Extracellular matrix organization", "Angiogenesis", "Cartilage development", and "Connective tissue development" (Fig. 3.8). Out of the genes that are differentially expressed, there are some that are inactive before metamorphosis in the hypochord (e.g., *COL22A1*, *COL16A1*, *COL6A3*, *RUNX1*, *IHH*), but are highly expressed once the metamorphosis is initiated. High expression of these genes in the coccygeal cells even before the onset of metamorphosis corroborates our morphological studies, where I revealed that the post caudal vertebrae of the coccyx initiated mesenchymal cell aggregation early in development (1.5 months after embryogenesis) *vs* 2 months in hypochord. Apart from the differences in the temporal expression of genes within the "Early expression cluster", a few genes involved in cartilage development are not present in the hypochord compared to the coccyx (e.g, *FOXL1*, *RUNX3*, *FOXD3*, *PMM2*, *EDN1*).

Early activation cluster. —This cluster includes the GO terms "Axon guidance", "Axon development", "Axogenesis", "Regulation of axogenesis", and "Neuron projection guidance" (Fig. 3.9). While the coccyx DEGs act in a similar way to the rest of the long bones in

vertebrates within this cluster, hypochord shows a different pattern. Most of the genes (e.g., *NTRN*, *SLITRK3*, *POUF42*, *DCC*) that are discussed as essential regulators in guiding the axons in long bones are not expressed within the hypochord (Fig. 3.9).

Maturation cluster. —The GO term functions "Bone development", "Skeletal system development", "Regulation of ossification", "Ossification", "Osteoblast differentiation" are included in this cluster (Fig. 3.10). Maturation period in the hypochord happens once the metamorphosis is initiated and when the tadpole reaches the end of its metamorphic climax (Fig. 3.10). Within the hypochord, genes involved in ossification (e.g., *GPC3*, *TMEM19*, *IFITM5*, *COL11A1*, *PHOSPHO1*, *SOX8*) and osteoblast differentiation (e.g., *GLI1*, *FBN2*, *SATB2*) are highly expressed in tadpoles at the end of the metamorphic climatic and are inactive at prometamorphic stages. Comparatively, in the coccyx, since the ossification happens prior to the metamorphic climax, the majority of the genes are highly expressed even at the beginning of metamorphosis. A few genes (e.g., *TBX15*, *BARX2*, *SHH*, *AXIN2*) are not expressed in hypochord nor in the coccyx, compared to the other ossifying long bones in vertebrates.

This transcriptomic comparison led to three main findings: (1). Between the two tissue types, the coccyx's DEGs share similarities with the other bones' transcriptomics in vertebrates. (2). Hypochord undergoes its early activation period before metamorphosis, and a maturation period once metamorphosis is initiated. (3) Hypochordal DEGs lack an early activation period, which includes most of the axon developing genes.

3.4.5 – ATAC-seq and Urostyle-responsive gene regulation

During anuran metamorphosis, the larval body form undergoes dramatic remodeling within 6-8 days, and this is reflected in both morphological and gene expression patterns.

Therefore, it can be extrapolated that gene regulation changes over this same time period. To study the underlying changes in chromatin accessibility, I used an ATAC-seq approach using the same developmental stages and the same number of replicates as the RNA-seq work. The number of peaks varied between the three stages that I used: before metamorphosis (4563 peaks), beginning of metamorphosis (6805 peaks), and end of metamorphosis (6805 peaks). More than 50% of peaks were distributed in distal intergenic regions. The rest of the peaks were distributed along intronic, exons, and promoter regions. When comparing the three time points, the most significant change of peak distribution observed was the percentage of peaks that fell on the exon regions (other than the 1st exon): before metamorphosis the percentage was lower (<1%) when compared with the number of peaks that were seen at the beginning and at the end of metamorphosis (7–10%) (Fig. 3.11).

Next, I compared the ATAC-seq data with the RNA-seq data and observed that the majority of the peaks are located close to the up-regulated genes in the hypochord and coccyx that were identified from the transcriptomic data. The genes *TBXT* and *TBXT.2*, which are up regulated in the hypochord, have peaks located within the intronic regions before and at the beginning of metamorphosis, and the peak is lost at the end of metamorphosis. Other genes expressed in hypochordal tissues like *MMP1* and *COL22A1* have peaks downstream of the genes and are seen only once the metamorphosis is initiated. Genes that were upregulated in the coccyx, e.g., *HOXD11*, *PVALB*, *DIO3*, and *ACTA2* have ATAC-seq peaks closer to each gene and were present throughout development. This could be because the coccygeal ossification occurs early in development (after 1.5 months) compared to the hypochord. These results highlight urostyle-responsive regulatory regions during development and need further scrutinization using functional assays.

3.4.6 – Thyroid hormone and the development of the urostyle

Previous experiments [67] using Methimazole-treated tadpoles, showed that the hypochord's ossification was directly affected when TH secretion is disrupted, whereas the coccygeal postsacral vertebrae form but the fusion of them together is halted. Overall, formation of the urostyle is disrupted during development. To see which genes are directly affected when tadpoles are treated with Methimazole for 21 days, I used an experimental approach where I used early (stage 54) and late (stage 57) exposure stages and compared the results with the control tadpoles.

I used a spatial transcriptomic approach as the RNA-seq approach described under section 3.3.1. Coccygeal and hypochordal tissues were dissected out from frozen cryosections at three developmental time points: (1) Control tadpoles at prometamorphosis (stage 57); (2) Control tadpoles at the beginning of metamorphosis (stage 61); (3) Methimazole-exposed tadpoles after 21 days (for both late and early exposed stages). Control tadpoles underwent chondrification and ossification at the sites of urostyle. During both late and early exposures, hypochord underwent cell proliferation, with no chondrification nor ossification [67]. Hence, for the laser captured cells, only the proliferating cells were captured in treated tadpoles. Whereas the coccyx underwent chondrification and ossification and formed postsacral vertebrae but did not extend in length nor fuse with one another at the end of 21 days [67], and dissected out cells at this stage included immature chondrocytes, mature chondrocytes, osteocytes, mesenchymal cells, and extracellular matrix. The data matrix included 24 samples from the two tissue types: control stage 57 (4 replicates), control stage 61 (4 replicates), early exposure (2 replicates), late exposure (2 replicates). *Xenopus tropicalis* v.9 reference genome was downloaded from Ensembl and the same

methodology as before was used (Fig. 3.12.A). The transcriptomic analyses were conducted for the coccygeal and hypochordal tissues separately.

Hypochord. —The total analysis consisted of 16083 genes, out of which 7395 were significantly up/down-regulated between the control *vs* treated tadpoles. All three time points were used as factors in the DESeq2 analysis (binomial generalized linear model was implemented). When a PCA plot was drawn, all the samples, except the early exposed samples clustered together in PC space (Fig. 3.12.C). There were 7692 DEGs that were differentially regulated between control stage 57 *vs* stage 61(after 21 days) tadpoles, out of which 584 genes were not affected by TH (Fig 3.12.E). Looking at the functions of the genes that are directly affected by early/late exposure to Methimazole, 561 genes were mostly involved in the "Cell cycle." Genes involved in mitosis, G2/M transition, regulation of mitosis were directly down-regulated in the absence of TH Fig. 3.13). Majority of the genes were downregulated in early exposed tadpoles (i.e., 5513 genes): metabolism of proteins was halted; functions of the genes involved in translation initiation, elongation, and termination were disrupted (Fig. 3.13).

Coccyx. —The total analysis consisted of 16083 genes, and out of which 8970 genes were significantly differentially regulated between the control *vs* treated tadpoles. All three time points were used as factors in the DESeq2 analysis. When a PCA plot was drawn, all the samples were clustered together in PC space (Fig. 3.12.D). There are 9657 DEGs that are differentially regulated between control stage 57 *vs* stage 61 (after 21 days) tadpoles, out of which 259 genes were not affected by TH (Fig.3.12.F). Genes that are involved in the Cell Cycle, DNA replication, *RUNX2* regulated bone development, and Extracellular Matrix organization are not affected in the early/late exposed tadpoles during coccyx formation. Genes that were directly down-regulated in coccygeal tissues in treated tadpoles were involved in DNA repair and regulation of TP53 (Fig.

3.14). These observations again corroborate our morphological analysis: the coccygeal ossification is visible in treated tadpoles whereas the hypochordal ossification is completely disrupted.

3.5 – DISCUSSION

The anuran urostyle, composed of a coccyx and a hypochord, reflects how novel structures facilitate evolution of new body plans. In the previous chapter, I presented a morphological analysis of the ontogeny of the anuran urostyle using immunohistochemistry, histology, bone and cartilage staining, and microCT scanning. Through this, I identified cells of interest and the developmental stages to target for this follow up study. To elucidate how this structural novelty arose and its genetic underpinnings, I used a spatial transcriptomic (RNA-seq) and an ATAC-seq approach.

3.5.1 – T-box genes and the hypochord

The coccyx and hypochord have two distinct sets of differentially expressed genes. Hypochordal genes are active at the onset of metamorphosis, whereas the coccygeal DEGs are highly expressed even before metamorphosis. This analysis revealed a large set of genes (Tables 3.1 and 3.2 and Appendices C, D) that are uniquely up regulated in the hypochord and have not been reported before. One of the most significant groups of genes that is upregulated in the hypochord are the T-box genes (*TBXT* and *TBXT.2*). T-box genes have a 180-bp DNA binding domain that is highly conserved. Orthologues of the gene *Brachyury*, one of the highly expressed T-box genes in the hypochord, are present in all multicellular organisms [163]. *Brachyury* is important in posterior mesoderm development (initially expressed in the developing mesoderm but later restricted to the tail bud and notochord) [171]. While early mesoderm differentiation

patterning depends highly on *TBXT*/*TBXT.2*, a role for these genes in later developmental stages has not been previously reported or discussed. During metamorphosis, the tadpole body undergoes dramatic remodeling, including tail loss and development of new structures like the urostyle. The hypochord, thought to be of an endodermal or superficial mesoderm origin, undergoes ossification at the beginning of metamorphosis only in anurans. I hypothesize that presence of high levels of *TBXT*/*TBXT.2* causes the hypochordal cells to undergo ossification at the onset of metamorphosis. Such unusual ossification appears to also occur in response to a congenital vertebral column malformation (VCM) in humans that happens because of a *Brachyury* gene mutation in the intron 7 [169] and in the highly conserved T-box sequence [203]; these VCMs eventually lead to sacral agenesis ("frog-like") syndrome in babies. Apart from these mutations, *T*/*T2* genes also induce EMT in humans when over expressed in carcinoma cells [206], and it has also been recorded that duplications of the *Brachyury* gene cause vertebral column chordomas [164, 206]. Frogs have two paralogues of *Brachyury* genes, perhaps explaining the overexpression of *TBXT*/*TBXT.2* at the onset of metamorphosis, which could in turn allow the T genes to activate downstream targets that lead to chondrification and ossification. When *Brachyury* genes are highly expressed in human chordoma cells, matrix metalloproteinases (e.g., *MMP12*, *MMP13*, *MMP24*) [174] are also upregulated at the same time (which is also seen in hypochordal cells). However, to better understand the similarities between the human anomalies and the anuran urostyle requires well executed functional analyses of the *TBXT*/*TBXT.2*.

Establishment of a conditional knockout line, targeting *TBXT*/*TBXT.2* at late developmental stages, will allow us to evaluate the functional role of these genes in hypochord ossification. The hypochord could also be a model to study human vertebral chordomas and to

scrutinize upstream and downstream targets of Brachyury in tumor forming cells. Additionally, the ATAC-seq results also revealed an open chromatin region in proximity to the *TBXT*/*TBXT.2* genes at the onset of metamorphosis (Fig. 3.11.E). Knocking out this open-chromatin region (which could be a potential regulatory region) would also help us investigate the role of Brachyury in the ossification of the hypochord.

3.5.2 – Coccyx and hypochord *vs* other vertebrate bones

Coccyx and hypochord undergo endochondral ossification and shows an array of genes that are similar to the genes expressed in other long bones that undergo endochondral ossification in vertebrates (e.g., mesenchymal-to-chondrocytes involved genes like *BMP*s, *SOX9*; chondrocytes-to-osteoblasts/osteocytes was seen in highly expressed genes like *RUNX2*, Osterix, *IHH*). Apart from these similarities, when comparing the already published osteocyte transcriptomics [190], hypochord shows some considerable differences among the rest of the bones in vertebrates. Hypochordal cells express osteoprogenitor-specific genes before the metamorphic climax, and metamorphosis acts as a switch that activates osteogenesis (*vs* in coccyx osteogenesis is initiated prior to metamorphosis). Other than the temporal differences observed regarding ossification, the DEGs of the hypochord reveal that hypochordal cells lack the "early activation phase," which includes regulators needed in "Axogenesis" and "Axon development" in ossifying bones (Fig. 3.9). Vertebrate bones are innervated by sensory and sympathetic nerves during skeleton development [207], where the periosteum and bone marrow have the highest density of nerves whereas the mineralized matrix has very few [207-209]. During development, bone innervation and endochondral ossification happen simultaneously [207], and it is hypothesized that axon guidance regulates formation of the neuronal network,

which is subsequently required for the osteocyte network formation [190]. It is surprising that the ossifying hypochord lacks the genes needed for axon development (Fig. 3.9), and our results raises the possibility that the hypochordal development maybe disconnected from the neuronal signals. Future work is needed scrutinizing the innervation patterns within the hypochord during its development to better understand this.

3.5.3 – Thyroid hormone and the hypochord

Thyroid hormone directly regulates the development of the skeleton [79, 210, 211]. There are three thyroid hormone receptors (TRα1, TRβ1 and TRβ2), and these bind to genes that are directly controlled by the TH [210, 211]. Even though previous studies have focused on the genes that are direct targets of TH in chondrocytes, osteoblasts and osteoclasts (e.g., [212-217]), TH action in osteocytes has not been investigated. In the Methimazole-treated experiments, already recorded direct targets of TH were significantly down-regulated in the hypochordal tissues: e.g., *DIO3* (recorded to be present in all skeletal tissues, mostly in growth plate chondrocytes), *IHH*, *BMPs*, *MMP9*, *MMP13*, *WNT4*, Osteocalcin (expressed in chondrocytes and osteoblasts). Since hypochordal development directly coincides with the initiation of the metamorphosis (where we see a peak in the TH), the endochondral ossification is directly controlled by the TH. Apart from the already recorded direct targets of the TH, the T-box genes were also downregulated in the methimazole-treated tadpoles (Appendix E). This raises the possibility that the TH acts upstream of T-box genes, which could be eventually activating the subsequent gene regulatory network involved in ossification in the hypochord.

Our integrative approach, using morphological and molecular data sets (genes and gene regulation) on the development of the urostyle, scrutinizes the evolution of a novelty. The

underlying changes to the gene and gene regulatory networks have given rise to a structure, that is unique to frogs, and evolutionarily, this novel feature has been conserved for 200 million years. Future work targeting the candidate genes responsible for the development of the urostyle, together with functional assays, will shed light on the evolution of this structural enigma.

Table 3.1. Top 30 most up-regulated genes in the hypochord (when compared with the coccyx across three developmental time points).

ensembl_gene_id	baseMean	log2FoldChange	lfcSE	stat	pvalue	padj	External gene name
ENSXETG00000034242	35.8230417	24.7036175	2.85777385	8.64435705	5.41E-18	4.49E-16	fxyd2
ENSXETG00000006541	40.9652691	6.69967995	2.28452128	2.93264065	0.00336093	0.01972136	
ENSXETG00000012149	77.6250387	6.01600124	1.67977628	3.58143004	0.00034172	0.00275311	agxt
ENSXETG00000016908	24.8897042	4.6890795	1.11964801	4.1879943	2.81E-05	0.00030298	hand2
ENSXETG00000003243	1000.93714	4.35696557	0.69352363	6.28236065	3.33E-10	8.80E-09	crhr1.1
ENSXETG00000021898	67.3009209	4.31261345	0.87743561	4.91501984	8.88E-07	1.30E-05	
ENSXETG00000006540	1639.67141	4.23834629	0.659392	6.42765803	1.30E-10	3.69E-09	c3orf49
ENSXETG00000032045	7820.47401	4.21548727	0.97247174	4.33481726	1.46E-05	0.00016685	
ENSXETG00000006924	2.79000312	4.11156355	1.55038084	2.65197004	0.00800236	0.04026514	XB5798854 [provisional]
ENSXETG00000015388	11.6685248	4.09011045	1.25552208	3.25769694	0.0011232	0.0077883	asmt
ENSXETG00000023110	12.0474701	4.01455877	1.53929932	2.60804296	0.00910615	0.044697	dbh
ENSXETG00000014030	7.66185672	4.00034925	1.03403114	3.86869319	0.00010942	0.00100208	th
ENSXETG00000022198	232.76211	3.98664322	0.68791639	5.7952438	6.82E-09	1.46E-07	mmp1
ENSXETG00000020532	9090.35955	3.9083472	0.73493981	5.31791469	1.05E-07	1.82E-06	krt18.2
ENSXETG00000037291	898.061521	3.78499138	0.65947695	5.7393839	9.50E-09	1.98E-07	
ENSXETG00000039391	177.141617	3.75129699	0.32889885	11.405625	3.92E-30	2.21E-27	**tbx1**
ENSXETG00000012488	35.2761897	3.66551933	1.08253047	3.38606574	0.00070902	0.00524891	krt70
ENSXETG00000018715	3123.70349	3.56852113	0.99964484	3.56978899	0.00035727	0.00285254	olfm4
ENSXETG00000040960	11.8426493	3.56136467	1.31797523	2.70214841	0.0068893	0.03563579	
ENSXETG00000030601	139.407847	3.52217571	0.6876929	5.12172761	3.03E-07	4.84E-06	cpa6
ENSXETG00000022195	1097.50792	3.47078115	0.82224679	4.22109417	2.43E-05	0.00026554	mmp8
ENSXETG00000008017	10659.0702	3.45894498	0.82666242	4.18422913	2.86E-05	0.00030679	vim.2
ENSXETG00000026572	333.066855	3.38233236	0.62345359	5.42515496	5.79E-08	1.05E-06	**tbxt.2**
ENSXETG00000033563	35.7150317	3.38041089	0.96358317	3.50816721	0.00045121	0.00351704	
ENSXETG00000030183	15966.0621	3.32409705	0.60897153	5.45854264	4.80E-08	8.91E-07	eln2
ENSXETG00000040137	280.304367	3.28259008	0.70060179	4.68538638	2.79E-06	3.75E-05	

Table 3.1, continued.

ENSXETG00000024911	23.7124461	3.2749052	0.99315494	3.29747662	0.00097558	0.00687353	tgfa
ENSXETG00000007357	78.2794937	3.25941088	0.79907189	4.0789958	4.52E-05	0.00045903	tgm3l.1
ENSXETG00000023914	1336.13796	3.1864788	0.43957358	7.24902254	4.20E-13	1.69E-11	
ENSXETG00000006876	5653.20067	3.14180048	0.85457528	3.6764467	0.00023651	0.00198843	des.2

Table 3.2: Top 30 most up-regulated genes in the coccyx (when compared with the hypochord across three developmental time points).

ensembl_gene_id	baseMean	log2FoldChange	lfcSE	stat	pvalue	padj	External gene_name
ENSXETG00000036957	67.300658	-9.2314744	0.91539741	-10.084663	6.46E-24	1.41E-21	cldn3
ENSXETG00000025296	107.272902	-9.1704097	1.15360493	-7.9493503	1.87E-15	1.05E-13	**actn2**
ENSXETG00000023427	56.654877	-9.1599693	0.84252338	-10.872065	1.57E-27	6.50E-25	neurod6
ENSXETG00000001343	98.3298692	-9.1422797	0.74944351	-12.198757	3.16E-34	6.22E-31	prdm12
ENSXETG00000014163	298.956718	-9.049459	1.33599138	-6.7735908	1.26E-11	4.11E-10	**coch**
ENSXETG00000034240	93.2459233	-9.0191364	0.97623849	-9.238661	2.50E-20	2.87E-18	uts2b
ENSXETG00000031321	60.3744212	-8.9897459	0.83679614	-10.743054	6.39E-27	2.24E-24	cacng2
ENSXETG00000002052	51.4706447	-8.7651869	1.10629269	-7.923027	2.32E-15	1.29E-13	chodl
ENSXETG00000026873	76.9177596	-8.7109514	1.04632673	-8.3252689	8.41E-17	5.77E-15	trpm8
ENSXETG00000016503	56.4835353	-8.6749902	0.82948229	-10.458319	1.34E-25	3.85E-23	apba2
ENSXETG00000022933	79.7142449	-8.6133224	0.70922976	-12.144615	6.13E-34	9.66E-31	grin1
ENSXETG00000031473	466.644299	-8.5608363	0.76285713	-11.22207	3.18E-29	1.62E-26	
ENSXETG00000002106	39.9922769	-8.5049833	1.06936097	-7.9533324	1.82E-15	1.03E-13	cdh10
ENSXETG00000013277	74.956003	-8.4686481	0.806128	-10.505339	8.16E-26	2.43E-23	GRIK2
ENSXETG00000036319	72.3980829	-8.4252983	1.09170766	-7.7175407	1.19E-14	5.97E-13	
ENSXETG00000039335	34.1560441	-8.3935681	1.60913964	-5.2161838	1.83E-07	3.02E-06	btbd17
ENSXETG00000016588	172.249552	-8.3811753	0.67959205	-12.332657	6.04E-35	1.36E-31	acsl6
ENSXETG00000036131	77.7434483	-8.3704849	1.37996584	-6.0657189	1.31E-09	3.19E-08	
ENSXETG00000033877	107.395058	-8.3549404	0.90385167	-9.2437074	2.38E-20	2.76E-18	plppr1
ENSXETG00000017087	156.561404	-8.326654	0.94591353	-8.8027644	1.33E-18	1.20E-16	tnni1
ENSXETG00000031870	41.1106891	-8.300964	0.78337294	-10.59644	3.10E-26	9.57E-24	
ENSXETG00000032275	232.869845	-8.300314	0.85227831	-9.7389712	2.06E-22	3.52E-20	
ENSXETG00000035258	37.4481903	-8.287008	0.77089393	-10.749868	5.93E-27	2.13E-24	TAFA4
ENSXETG00000036709	605.540272	-8.2709612	0.6896834	-11.992403	3.89E-33	4.72E-30	hpcal4
ENSXETG00000013542	78.3873361	-8.2419078	0.83483847	-9.872458	5.48E-23	1.03E-20	kcnn1
ENSXETG00000004033	33.6003453	-8.2337066	0.8200789	-10.04014	1.02E-23	2.08E-21	ndst3
ENSXETG00000030987	29.495152	-8.1944553	0.97278238	-8.4237291	3.65E-17	2.62E-15	sp9
ENSXETG00000011460	207.379457	-8.1795343	0.94833645	-8.6251396	6.40E-18	5.23E-16	ADGRD2

Table 3.2, continued.

ENSXETG00000021651	53.6649194	-8.1579179	0.92988545	-8.7730353	1.74E-18	1.52E-16	nkain3
ENSXETG00000021737	71.570467	-8.1170733	0.75759771	-10.714226	8.73E-27	2.99E-24	astn2

CHAPTER 4

DISCUSSION

4.1 – HYPOTHESES FOR THE ORIGIN OF THE UROSTYLE

My dissertation focuses on the morphological and genetic underpinnings of the development of a structural novelty – the anuran urostyle. The urostyle is a composite of a paraxial mesoderm-derived coccyx and an endoderm or superficial mesoderm-derived hypochord. The coccyx is formed by fusion of post sacral vertebrae, and this fusion of vertebrae is convergently evolved in vertebrates with the loss of the tail [218-220]. The fusion of an ossifying hypochord with the coccyx makes the urostyle structurally unique within the rest of the vertebrates. The ossifying hypochord, an apomorphic structure in anurans, has received very little attention over the years and to date we do not know how the special features of the hypochord evolved in anurans nor its function. The germ layer derivation of the hypochord remains unresolved; it has been hypothesized to be derived from the endoderm or the superficial mesoderm [13-16, 20, 65, 66].

The second chapter of my thesis highlights the morphological changes (bone and cartilage, neurons, muscles, and blood vessel development) during urostyle formation. The coccyx and hypochord initiate chondrification and ossification at two different timepoints: post sacral vertebrae contributing to the coccyx begin ossification prior to metamorphosis whereas the hypochord ossifies at the onset of metamorphosis. Preventing the secretion of thyroid hormone (TH) revealed that ossification of the hypochord is controlled by TH. The results I report in chapter 2 allow me to hypothesize the following points regarding the evolution of the urostyle based on the experiments done in the second chapter: (1) the ossifying hypochord occludes the dorsal aorta during metamorphosis, and this process appears to aid in tail resorption during

tadpole metamorphosis. (2) the ossifying hypochord has evolved with the loss of tail and has been evolutionary favored for over 200 million years. However, tail loss in tadpoles is recorded to have a TH control to it (TH controls the autolysis of tail cells by triggering a "suicide model" [221]); our work proposed that the "murder model" of tail resorption (initiates after 3 days into the metamorphic climax) is triggered because of the low pH caused by the blood loss to the tail [66]. Future work is needed to see if the loss of tail is affected if hypochord ossification has been prevented (discussed in detail under the future directions 4.2.3 section).

The third chapter of my thesis explored the genetic underpinnings of the urostyle development. The coccyx and hypochord have two distinct gene expression patterns. However, since both structures undergo endochondral ossification, the coccyx and hypochord also share a subset of genes that are involved in chondrification and ossification. Out of the Differentially Expressed Genes (DEGs) in the hypochord *vs.* coccyx, T-box genes caught my attention. *TBXT* and *TBXT.2* are pivotal in early mesodermal patterning but neither expression nor function have previously been assessed in later stages, because the mesoderm patterning is already completed when a tadpole reaches its metamorphosis. I hypothesize that the *TBXT*/*TBXT.2* genes act upstream during hypochordal ossification in the presence of intrinsic/extrinsic factors and control the commitment of hypochordal cells to mesenchymal cells. The high expression levels of *TBXT* and *TBXT.2* in hypochordal cells subsequently activates the downstream targets involved in chondrification and extracellular matrix organization.

I propose the following scenario and highlight how changes at genotypic and phenotypic level give rise to evolutionary novelties: The fossil record of anurans contains plesiomorphic forms having a tail with a few caudal vertebrae (e.g., Triassic *Triadobatrachus massinoti* [222] and *Czatkobatrachus polonicus* [82]). These fossils are followed by the sudden appearance of

forms with a urostyle and no tail (*Prosalirus bitis* [5,6]). The stem anuran fossil *Triadobatrachus* is thought to have had an amphibious life: partly in land and partly in water, that walked and hopped along the woodlands and/or riparian forests with a very short tail bud [222]. This tail bud in *Triadobatrachus* is assumed to serve no function in locomotion and was lost with the reduction of the vertebral column as we see in the fossil *Prosalirus.* However, the lack of intermediate fossils raised the question when the hypochord evolved. My work focusing on the developmental basis of the urostyle implies that hypochord ossification likely preceded loss of tail in salientians. Through our anatomy and ontogeny work (Chapter 2; [67]), we depicted how the hypochordal ossification is initiated prior to the reduction of tail length in metamorphosing tadpoles (tail resorption happens at stage 63). Once the hypochord reaches its maximum length at stage 63, it occludes the dorsal aorta, which we hypothesize as the trigger for the initiation of tail length reduction. Hence, even though we lack evidence for when the hypochord appeared in the fossil record, my work highlights the possibility of this apomorphic structure evolving in anurans prior to the evolution of tail-less salientians.

The metamorphic climax is considered the most vulnerable stage of the anuran life cycle. The metamorphosing tadpole with a tail, fore- and hind limbs is the transition stage from a larval axial-driven locomotion to an adult limb-driven one. Hence, this period of 6-8 days of a tadpole's life cycle is considered the most susceptible to predators. Studies have shown how different factors affect the timing of metamorphosis, and evolutionarily, anurans have shown several adaptations to speed up this process (e.g., [223-226]).

Metamorphic climax is controlled by a compendium of extrinsic and intrinsic factors, including a peak in thyroid hormone at the onset of metamorphosis [23, 24, 80, 177, 178, 227]. Some of the processes that are directly controlled by TH are remodeling of the cranial skeleton,

degeneration of the notochord, remodeling of the liver and length reduction in gut [24]. My dissertation points out how a peak in TH could be controlling the ossification of the hypochord [66]. I hypothesize that TH could be acting upstream of the *TBXT*/*TBXT.2* gene expression in the hypochordal cells (i.e., changes occur at the genotypic level), which initiates downstream targets involved in chondrification and ossification in hypochordal tissues (i.e., changes at the phenotypic level). However, further studies focusing on the thyroid-hormone receptor elements are needed to confirm the role of TH in hypochordal ossification. We propose that this underlying genetic change within the ancestral gene regulatory network would have happened sometime during the upper Triassic and Lower Jurassic, giving rise to the ossifying hypochord in anurans. The hypochord reaches its maximum length by day 3 of the metamorphic climax (stage 63), which leads to the occlusion of the dorsal aorta. This blood loss to the tail creates a low pH within the tail, which potentially activates the "murder model" ([221]), leading to the rapid resorption (length reduction) due to cell phagocytosis. We hypothesize that this process has been evolutionary favored because it aids the metamorphosing tadpoles to transition from a larval locomotory mode-to-adult one within a shorter time period and at the same time, aids in the resorption of the tail, which is an impediment for movement in land.

This has been evolutionary favored for more than 200 million years and is seen in all extant anurans during their development. The rapid tail loss has enabled the unique body plan of anurans (i.e., changes in the adult body morphotype) and has been favored evolutionary and has been conserved across more than 8000 species of anurans. We propose that the underlying changes in the genetic network gave rise to the evolution of the anuran urostyle, and it is an evolutionary novelty that has enabled successful inhabitation of several ecological niches because of the unique anuran body plan.

4.2 – FUTURE DIRECTIONS

4.2.1 – Endoderm/Superficial mesoderm derivatives of the hypochord

The source of cells, which contribute to the adult hypochord in frogs, is still contentious and requires scrutiny. Frog-hypochord is thought to be either endoderm-derived ([13, 14]–confirmed through DiD labeling) or superficial mesoderm derived [20]. When gene expression patterns of the endoderm-specific genes were compared between the coccyx and hypochord, it showed that *DHX16*, *DUSP6*, *BMP4*, *GLP2R*, *BMP4*, *FOXI1*, *GLP2R*, and *COL12A1* are differentially expressed between the two tissue types. However, future work is needed to scrutinize the origin of cells that contribute to the ossifying hypochord, either by doing tissue-specific, Cre-mediated lineage tracing methods or by doing *in-situ* hybridization for endoderm-specific markers across development.

To begin to investigate the germ layer contribution of the ossifying hypochord, I conducted grafting and DiI-injection experiments. I grafted *CMV*:*GFP* (this line was obtained from the National Xenopus Resource/NXR) expressing tissues into wildtype embryos. I performed grafting at two developmental stages: stage 12 and stage 15, where I used different target tissues that contribute to the future paraxial mesoderm (Fig. 1 A–D). The grafted tadpoles were reared until they reached metamorphosis (i.e., when the urostyle starts to form), sectioned and stained using an anti-GFP antibody to visualize the source of cells that contribute to the ossifying hypochord. The survival rate of grafted tadpoles was as low as 10% in most instances. The experiments grafted different regions of the paraxial mesoderm, which would later give rise to the somites. Figure 1E depicts a grafted early stage (stage 26) tadpole. However, the grafted tadpoles did not show GFP signals at the sites of the ossifying urostyle (this was checked by

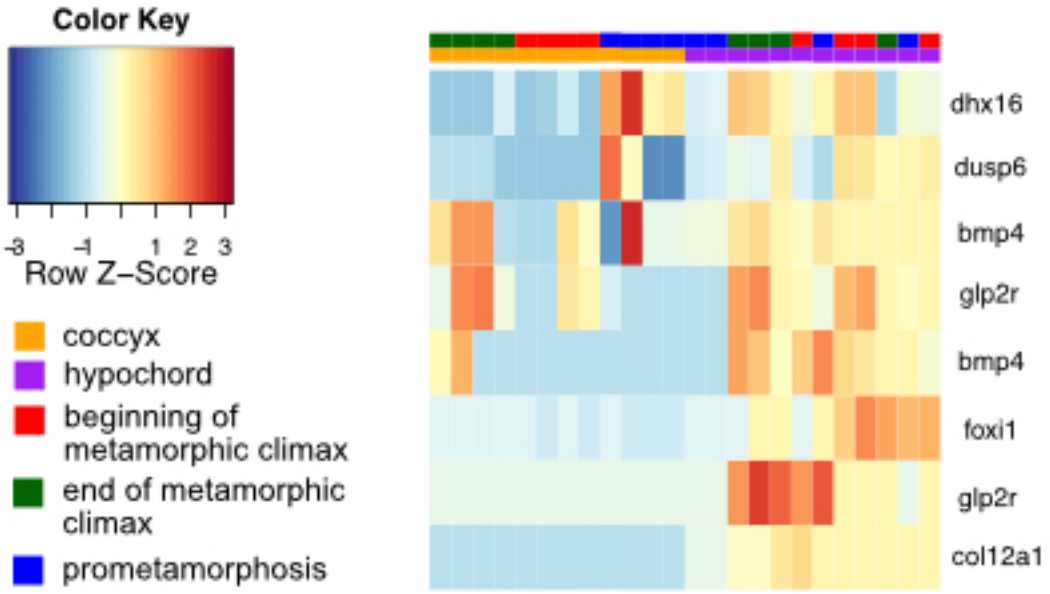

Figure 4.1. Heatmap showing differentially expressed genes involved in endodermal cell differentiation, compared across the hypochord and coccyx, during development.

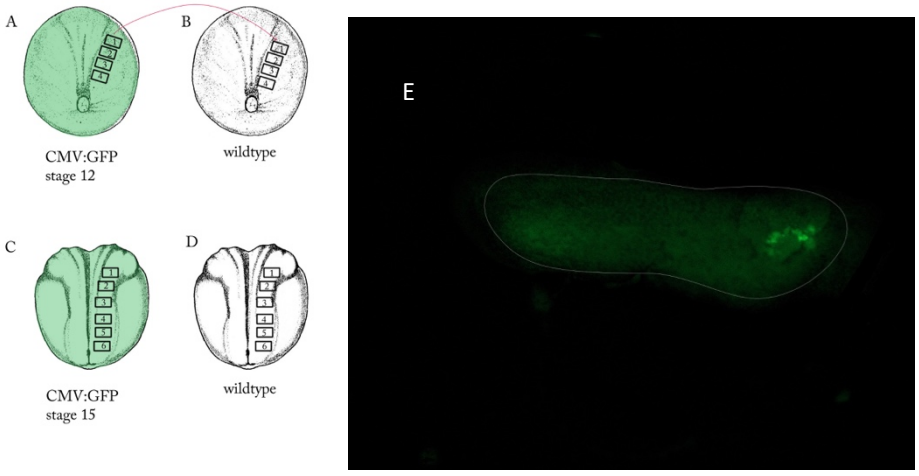

Figure 4.2. (A–D) Tissue grafted from CMV:GFP into wildtype embryos at stages 12 and 15. (E) A grafted tadpole after 7 days.

sectioning and staining using an anti-GFP antibody at different time points, mostly focusing on the stages when the hypochord starts to ossify).

For DiI injections, I conducted a similar set of experiments, where I injected DiI (CellTracker CM-DiI - an improved version, where fluorescence can be visualized for 2-3 months) into the paraxial mesoderm (injections were done, targeting the same tissues that have been highlighted in Fig. 4.1). The experimental approach was as follows: the two stages that were used for grafting as explained earlier, under "1" were used. DiI injections were done along the prospective mesoderm and the endoderm, injecting 10–15 embryos at each spatial point, as highlighted in Figure 4.1. The injected tadpoles were reared, and then frozen after 3 weeks, 4 weeks, 5 weeks, 6 weeks, 7 weeks, 8 weeks (Fig. 2 depicts a DiI injected tadpole, sectioned and stained). Tadpoles were frozen at different time points and sectioned using a cryostat (thickness of the sections were 10uM). The sections were permeabilized using Triton/PBS solution; DAPI was added in the final wash of PBS and mounted in a solution of 50% Glycerol/in PBS and observed under a confocal microscope (Fig. 4.2). Again, the DiI experiments also showed a similar observation as the grafted ones, where DiI did not last for 2 months and were not observed in the ossifying hypochord.

My experiments to analyze the germ layer derivative of the ossifying hypochord were not successful. Hence, to see if the adult hypochordal cells has an endoderm origin, future experiments can be done using a cell-tracing approach as discussed below (following [228]– which has given positive results in tracing skull bones in *Xenopus* and Axolotl). Lineage tracing using a specific promoter has proven to be useful in fate-mapping studies. However, in anurans, where the tadpole-body changes completely to accommodate an adult body form, using

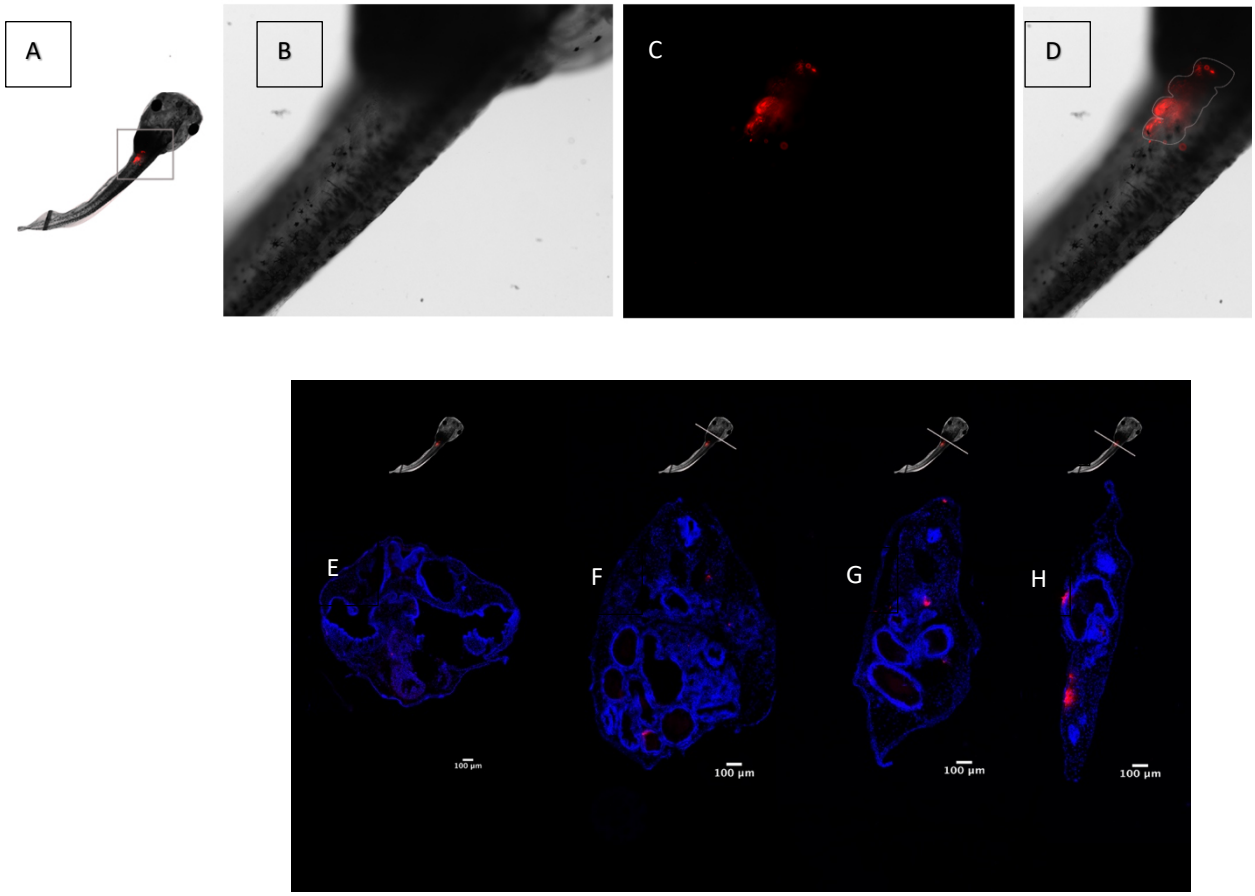

Figure 4.3. (A–D) DiI injected tadpole after 3 weeks. A, DiI visualized at 3-6 somites. B, Brightfield image of the tadpole. C, CellTracker DiI. D, Merged photograph of brightfield and DiI. (E–H) OCT-sectioned, DiI injected tadpole. E, A section across the head. F, A section across the anterior gut. G, A section across somite 4. H, A section across somite 6. The tadpole above each section corresponds with the anatomical placement of the tadpole. Red denotes DiI and blue denotes nuclei (stained with DAPI).

promoters has proven to be restricted as the tadpole ages [229]. Therefore, use of a stable transgenic line, which persists through metamorphosis is important when conducting cell lineage tracing studies. With this in mind, looking at the cells contributing to the adult hypochord using the transgenic line reported in Gross *et al*. [229], ROSA26:GFP which expresses Enhanced-GFP

(EGFP) under the control of the ROSA26 promoter would potentially yield positive results. The restriction enzyme-mediated integration (REMI) transgenesis, following Haeri and Knox [230] and Gross *et al*. [229] can be conducted, and the animals exhibiting GFP need to be reared through metamorphosis. GFP-expressing right trunk endoderm (and another set of experiments can be done with the mesoderm) of the transgenic donor embryo will be grafted onto a right trunk endoderm of a wildtype embryo. Left side would be left uninterrupted as the control (following [229]). The metamorphic climax stages will be the targeted stages and the same methodology for immunohistochemistry as in Chapter 2 (OCT-frozen sectioning) can be used with a polyclonal anti-GFP antibody to confirm the presence of trunk endoderm in the ossifying hypochord. These experiments will help us better understand the cell origin of the ossifying hypochord.

4.2.2 – Searching for potential enhancers and repressors during urostyle development

The transcriptomic and epigenomic analyses of the urostyle across developmental time points revealed candidate genes and potential gene regulatory regions that enabled us to understand molecular underpinnings of the urostyle. However, the current study does not identify enhancers or cis-regulatory elements (CREs), which are a main cause of morphological diversity. Future experiments can be done adapting a chromatin immunoprecipitation sequencing (ChIP-seq) using histone markers like H3K27ac and H3K4me3 to identify active enhancers and promoters [231]. A comprehensive study using the three developmental stages used in the current work (i.e., before metamorphosis, beginning of metamorphosis, and end of metamorphosis) would reveal temporal and urostyle-specific maps that would help us understand the conserved or modified CREs responsible for urostyle formation.

This above experiment will help us identify a set of CREs that are active during urostyle development in anurans; however, it is unclear if these enhancers/CREs that specify the urostyle in late developmental stages of frogs are the same ones that are responsible for early mesodermal patterning across vertebrates. Therefore, a comparison of the activity of enhancer orthologs in early and late developmental stages using STARR-seq [232] would help us better understand this. STARR-seq is a massively parallel reporter assay that will allow us to compare thousands of potential enhancers in the genome using a single experiment. The putative CRE sequences identified through ChIP-Seq and ATAC-seq for late and early developmental stages, can be cloned into reporter plasmids. If a late-enhancer element is present within the cloned region, its expression will be increased when transfected into one-cell staged embryos. Here, RNA production will be a direct qualitative readout of the putative CRE's ability to act as an enhancer/repressor. This will help in identifying conserved orthologous enhancer elements or novel enhancers responsible for the formation of the urostyle.

4.2.3 – Loss-of-function and gain-of-function experiments for T-box genes

There are records of ectopic expression of *TBXT*/*TBXT.2* in humans, causing abnormal ossifications ventral to the notochord in unborn babies [169, 203]. This usually happens during the last stages of gestation (this period is considered similar to a frog metamorphic climax because of the peak of thyroid hormone in both instances [203]). My RNA-seq results indicate that frog hypochordal tissues show an upregulation of *TBXT*/*TBXT.2* at the onset of metamorphosis when the hypochord starts to ossify. The ossification occurs at the mid-length of the body of a tadpole, and even in human babies, this ossification (when it happens ventral to the notochord) does not extend in an anterior-posterior manner across the vertebral column, but only

ossifies in some tissues ventral to the notochord [169, 203]. We hypothesized that in the presence of TH, *TBXT*/*TBXT.2* causes the tissue ventral to the notochord to ossify, and to test this hypothesis, I created a conditional knockout line using a heat-shock promoter (hsp) as described in detail in Appendix A. The expected outcome of this transgenic line is to observe a disruption in the hypochordal ossification, which would eventually disrupt/slow-down the resorption of the tail during the metamorphic climax. Future experiments could then be performed to evaluate the effects of *TBXT*/*TBXT.2* disruption in detail during formation of the hypochord by following a similar set of methods/experiments as described in Chapter 2, where the mutant *vs* wildtype tadpoles will be compared (using immunohistochemistry, bone and cartilage staining, *in situ* hybridization for *TBXT*/*TBXT.2*, and microCT scanning). Additionally, even if a significant phenotype is not visible, a real-time PCR step focusing on the *TBXT*/*TBXT.2* can be performed to evaluate whether the T-box gene expression is reduced in some-way. If the conditional knockout line yields a positive result, it would be an asset in future studies focusing on studying genes important in metamorphosis.

To bolster my hypothesis regarding the involvement of *TBXT*/*TBXT.2* in hypochord development, another set of experiments can be done focusing on the gain-of-function of *TBXT*/*TBXT.2* genes. Here, based on my RNA-seq and ATAC-seq results, we hypothesized that the TH acts upstream of *TBXT*/*TBXT.2* and the hypochord eventually undergoes ossification. To see if TH indeed acts as an activator if *TBXT*/*TBXT.2* in tissues ventral to the notochord, a gain-of-function experiments can be done using beads. My preliminary and published data suggest that the ossification of the hypochord is controlled as part by thyroid hormone. Hence, we hypothesize that thyroid hormone (T3) acts upstream of *TBXT*/*TBXT.2* and causes the hypochord to ossify. To see if hypochord ossifies prior to the metamorphic climax, T3-soaked beads can be

implanted before the tadpole reaches the metamorphic climax (stage 50-57) where the hypochord would normally ossify. At the same time, beads will also be implanted posterior to the normal ossification sites of the hypochord to see if *TBXT*/*TBXT.2* can be expressed ectopically. Real-time PCR assay targeting *TBXT*/*TBXT.2* would show if the expression has changed over time/tissues. Additionally, HCR-fluorescent in-situs or colorimetric in-situs can be done for *TBXT*/*TBXT.2* genes to verify the induced expression of the targeted genes.

My dissertation work delves into studying an evolutionary novelty in depth and focuses on identifying genetic and phenotypic changes that led to changes in adult body plans of frogs. Future work on functional assays and in identifying enhancers will help us better understand the evolution of this structural enigma that has been conserved for more than 200 million years.

APPENDIX A
FUNCTIONAL ASSAYS AND EVOLUTION OF THE UROSTYLE

A.1 – INTRODUCTION

Brachyury, belonging to the family T-box genes, has a conserved T-domain (a 180-bp DNA-binding domain). *Brachyury* is conserved across vertebrates [163, 233, 234] and is essential for axial mesoderm (trunk and tail) patterning. Homozygous mutants of the gene *Brachyury* have a striking phenotype and characterized by the absence of the tail, hence, *Brachyury* is also referred as "no-tail." Homozygous mice mutants for *Brachyury* exhibit several mesodermal defects and do not survive after gastrulation [202].

Anurans have two paralogs of the gene *Brachyury*, known as *Xbra* or *TBXT* and *Xbra3* or *TBXT.2*. Therefore, in order to see the effects of *Brachyury* in development, both genes need to be knocked out. Our study reveals that *Brachyury* exhibits a role in axial patterning in the late stages (in hypochordal ossification), not just in early-stage mesodermal patterning. To see if knocking out *Brachyury* affects the development of the hypochord, I created frame-shift mutations (by injecting targeted gRNAs at one-cell stage) and generated a conditional knockout line (using a heat-shock promoter and a targeted gRNA).

A.2 – Materials And Methods

A.2.1 – Creating mutants using a frame-shift mutation (CRISPR/Cas 9 injections)

Different gRNAs targeting the exon 1 and 2 of *TBXT* and *TBXT.2* were designed using CHOPCHOP. gRNA was synthesized using the MEGAshortscript kit (catalog number: AM1354; ThermoFisher) and RNA was purified using the Zymo RNA purification kit. To identify the gRNA mixture that creates a frameshift mutation effectively, I injected eight different mixtures (e.g., gRNA 1 for *TBXT* exon 1 + gRNA 1 for *TBXT.2* exon 1; gRNA 2 for *TBXT* exon 1 + gRNA 2 for *TBXT.2* exon 2). The injection solution consisted of 500 pg of each gRNA, 1% Texas red 1 ul, 2 ug of Cas9 protein, and water up to 10 ul. I injected ~2 nl of the injection solution into one cell. Injected embryos were flash frozen after 48 h and was subjected to DNA extractions. The tissues were lysed in a lysis solution, followed by a Proteinase-K treatment. DNA was purified using a column purification method (SIGMA). Finally, 250–300 bp of the exon 1 and exon 2 of TBXT and TBXT.2 were amplified using the following PCR primers (TBXT_exon1_F: GAGGAATGAGTGTAAGTGCCAC and TBXT_exon1_R: GGTGACGATCATCTCATTGGTG; TBXT_exon1_F: ACAGGCACAGCTGAGAGTT TBXT_exon1_R: TCCAAAGGTCTGTGTCTTCTAAA; TBXT2_exon1_exon2_F: GAAGGCAATCTCCCACAGAG and TBXT2_exon1_exon2_R: ATTTGGATCACCATGCCTTC). Subsequently, the samples were sent out for sequencing and the obtained injected sequences were compared with the wildtype ones.

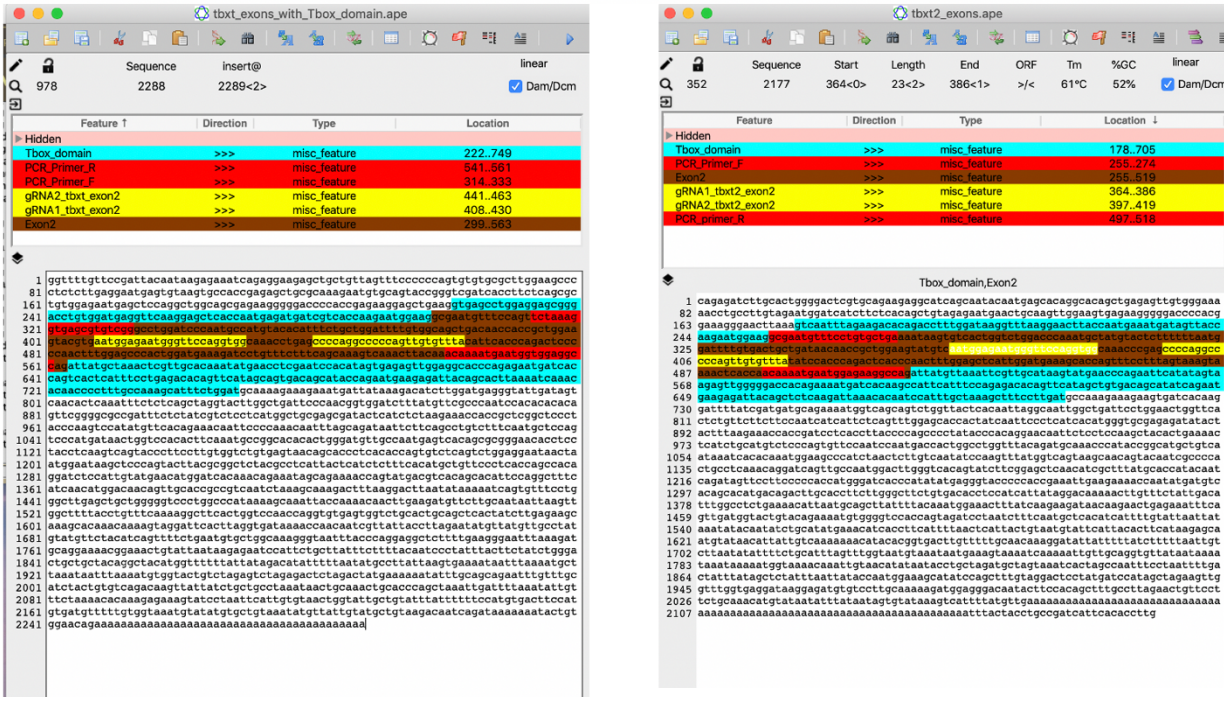

Figure A.1. The TBXT and TBXT.2 sequences of Xenopus tropicalis, highlighting the T-box domain (in blue), PCR primers used for sequencing (in red), targeted gRNAs (in yellow), and the targeted Exon 2 (in brown).

A.2.2 – Creating a conditional knockout line using a heat-shock promoter

One-cell-stage injections resulted in early mesodermal defects and the injected embryos/larvae did not survive for more than 2 weeks (Results section). Therefore, to target metamorphic stage tadpoles, we developed a plasmid that contains a sgRNA, which targets TBXT and TBXT.2 at the same time, a heat-shock promoter, a U6 promoter, Cas9 protein, and a transgenic marker. For the sgRNA that targets both TBXT and TBXT.2, we used the exon 2, which also involves in T-box domain (Fig. A.1). We selected two gRNAs, of which the second gRNA gave 100% positive results and created mutations in exon 2 of both *TBXT* and *TBXT.2* (TAAACACAACTGGGGGCCTGGGG, GC content = 55%).

I checked for mutations as the first section (A.2.1), where gRNAs were individually injected into one-cell stages, and DNA was extracted, sequenced and mapped with the wildtype ones to compare. For this conditional knockout system, we are combining the inducible CRISPR-based knockout approach by Ablain et al. [235] with the pTransgenesis system (a recombination cloning method based on Gateway cloning) that has effectively used in *Xenopus tropicalis* [236]. This will create a tissue-specific targeted knockout system. The final transgenic plasmid will be a

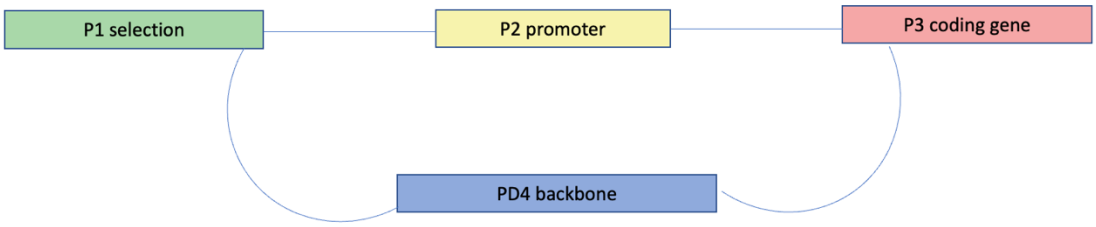

Figure A.2. The experimental setup, highlighting the donor vectors and the backbone plasmid following the pTransgenesis system.

combination of four plasmids (Fig. A.2). There are three entry vectors: (1) P1 containing the *X. tropicalis* U6 promoter and the sgRNA targeting both TBXT and TBXT.2; (2) P2 containing the heat-shock promoter; and (3) Cas9 protein and an EGF reporter construct. All three donor vectors will be recombined into a destination vector (P4). To construct the P1 construct, U6-sgRNA gene block from IDT was obtained (Fig. A.3.A, plasmid map), transformed, miniprepped, and digested using the necessary restriction enzymes (restriction enzyme used is shown in the map). The digested U6 plasmid was recombined with the donor p1 plasmid (Fig. A.3.B plasmid map; pDONR P4-P1R) using BP clonase. To construct the p3

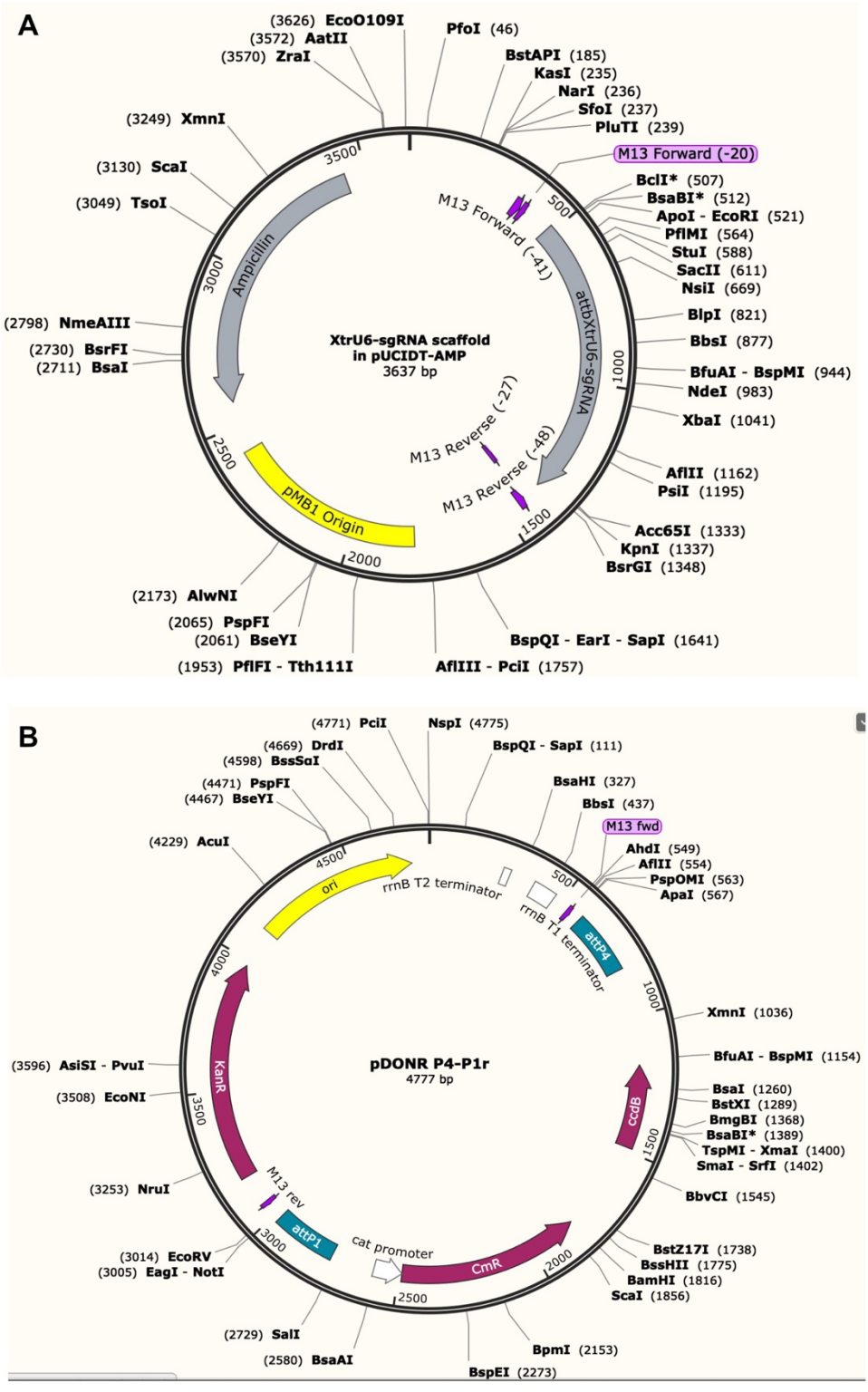

Figure A.3. The U6 construct plasmid and pDONR P4-P1R vector used to reconstruct

Fig. A.3, continued. the P1 of the recombination step.

construct, Cas9 plasmid was obtained from Addgene (Fig. A.4.A, plasmid map), transformed, miniprepped, and digested using the necessary restriction enzymes. The digested U6 construct was recombined with the donor p3 plasmid (Fig. A.4.B) using BP clonase. All the final plasmids were confirmed using sequencing (the primers used for sequencing are given in Table A.1). Finally, the newly made p1, p3, p2 (p2 plasmid with the heat-shock promoter was already available at the NXR; Fig. A.5 for the plasmid map) were recombined with the PD4 backbone plasmid.

For one-cell-stage injections of the constructed final plasmid, the digestion reaction was loaded into the needle and 2 nl was injected, the embryos were left to rest for 30 min, and were transferred to clean 0.1% MMR solution. Once the tadpoles reached the stage of interest, the tadpoles (stage 56/57) were put in 37^{o} C water bath for 30 min, and then moved them again to 22^{o} C and were grown until they reached metamorphosis. Here, the hsp drove the Cas9 and U6 promoter drove a sgRNA for *TBXT*/*TBXT.2* where a pTransgenesis vector was used, as well as a reporter construct to aid in identification of transgenic tadpoles. This plasmid construct was injected into one-cell-stage embryos. The embryos were allowed to develop at 16°C until they reach the desired stage (stage 57). To activate the hsp, the tadpoles were transferred between a pre-cooled dish of 0.1 MMR at 16°C and a prewarmed container of 0.1 MMR at 34°C or 37°C. Tadpoles were treated 3 to 4 times for 30 min at 37°C with an interval of 30 min at 16°C. To check if hypochord development was affected, the tadpoles were scrutinized for morphological changes using a similar set of experiments as in Chapter 2.

A.3 – Results And Discussion

The one-cell-stage injections done using mixtures of the *TBXT* and *TBXT.2* genes resulted in *X. tropicalis* embryos with severe mesodermal defects (Fig. A.6). The mutant embryo posterior mesoderm (i.e., the number of somites) were reduced when compared with the wildtype ones (Fig. A.6). The discussion section (Chapter 4) includes additional analyses and future directions for the conditional knockout line.

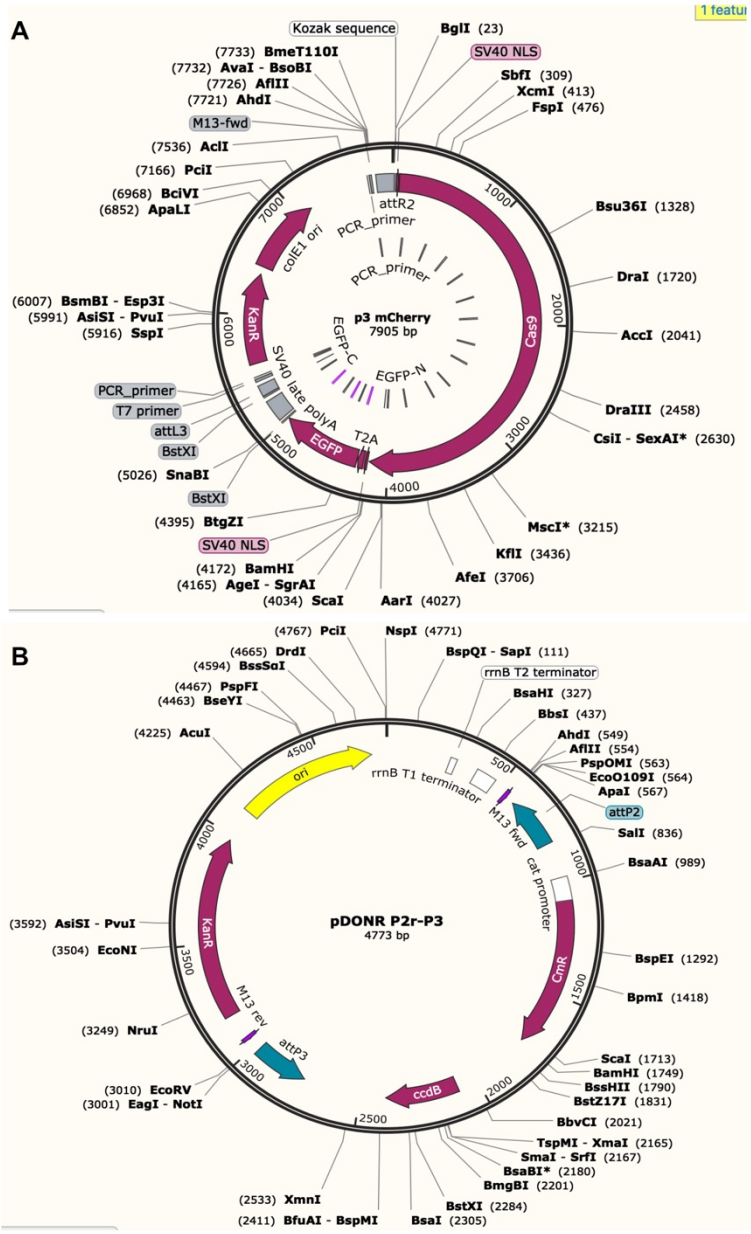

Figure A.4. The Cas9 construct plasmid and pDONR P2r-P3 vector used to reconstruct the P3 of the recombination step.

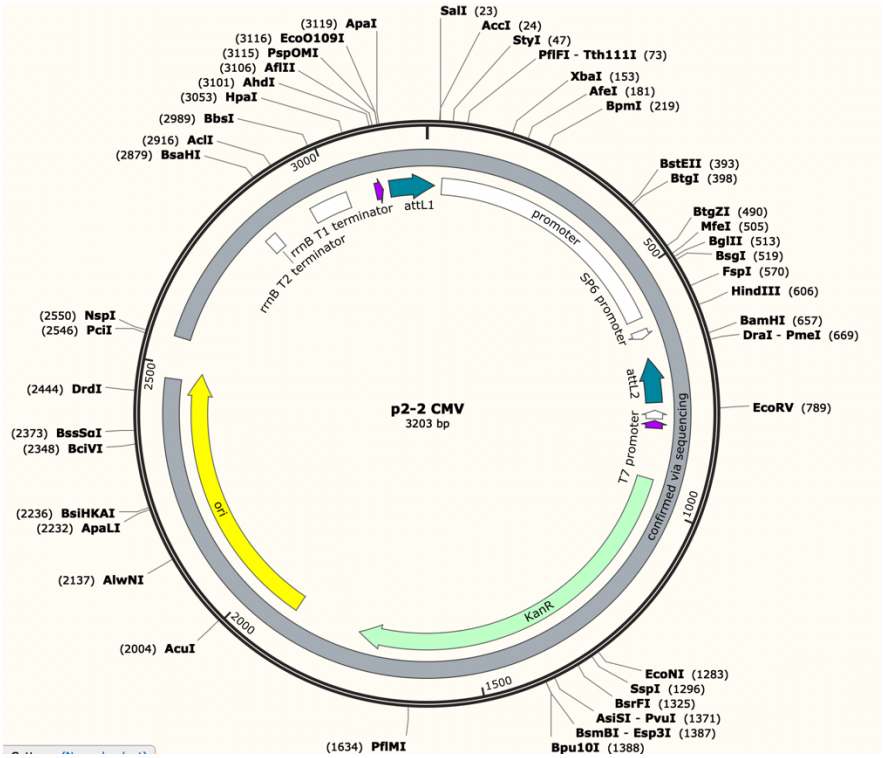

Figure A.5. The P2 plasmid with the heat-shock promoter.

Table A.1. Primers used to confirm the recombined plasmids.

Primers	Oligo sequence	Description
U6targetForSeq (U6 plasmid)	GGC TTT TGG GCT AAT GC	Forward cloning primer for sequencing to determine correct cloning of the sgRNA target into the plasmid.
U6targetRevSeq (U6 plasmid)	CGG TGC CAC TTT TTC AAG	Reverse cloning primer for sequencing to determine correct cloning of the sgRNA target into the plasmid.

Table. A.1, continued.

U6integrationForSeq (P1-U6 plasmid)	ACA GGG GTT CCA TCT GG	Forward cloning primer for sequencing to determine correct recombination of the gene block into the p1 plasmid
U6integrationRevSeq (P1-U6 plasmid)	GGC GAT GCA TAT TTT CCC	Reverse cloning primer for sequencing to determine correct recombination of the gene block into the p1 plasmid
attB2rCas9T2AGFPfor (Cas9 plasmid)	GAA TTG GGG ACA GCT TTC TTG TAC AAA GTG GAC GCC ACC ATG GCT TCT CCA CCT AAG	Forward cloning primer for the Cas9 cassette. Adds *attB2r* sequence at the 5' end.
attB3Cas9T2AGFPrev (P3 -Cas9 plasmid)	AAT TAG GGG ACA ACT TTG TAT AAT AAA GTT GGA GCT CCA CCG CGG TGG CGG CC	Reverse cloning primer for the Cas9 cassette. Adds *attb3* sequence at the 3' end.

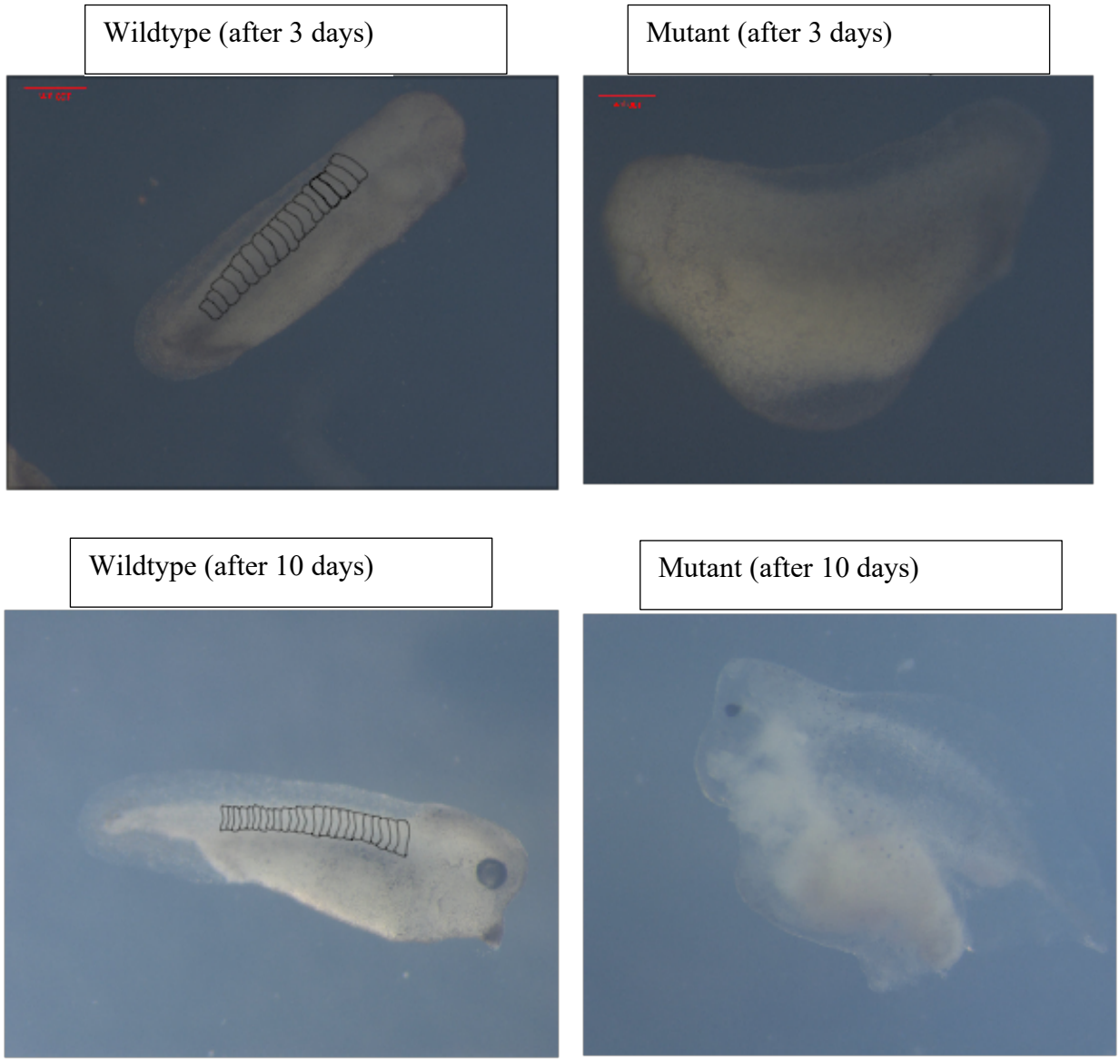

Figure A.6. Comparison between the CRISPR/Cas9 injected larvae vs wildtype ones.

Appendix B: Coccyx vs hypochord DEGs across time points.

ensembl_gene_id	baseMean	log2FoldChange	lfcSE	stat	pvalue	padj	External gene name
ENSXETG00000034242	35.8230417	24.7036175	2.85777385	8.64435705	5.41E-18	4.49E-16	fxyd2
ENSXETG00000006541	40.9652691	6.69967995	2.28452128	2.93264065	0.00336093	0.01972136	
ENSXETG00000012149	77.6250387	6.01600124	1.67977628	3.58143004	0.00034172	0.00275311	agxt
ENSXETG00000016908	24.8897042	4.6890795	1.11964801	4.1879943	2.81E-05	0.00030298	hand2
ENSXETG00000003243	1000.93714	4.35696557	0.69352363	6.28236065	3.33E-10	8.80E-09	crhr1.1
ENSXETG00000021898	67.3009209	4.31261345	0.87743561	4.91501984	8.88E-07	1.30E-05	
ENSXETG00000006540	1639.67141	4.23834629	0.659392	6.42765803	1.30E-10	3.69E-09	c3orf49
ENSXETG00000032045	7820.47401	4.21548727	0.97247174	4.33481726	1.46E-05	0.00016685	
ENSXETG00000006924	2.79000312	4.11156355	1.55038084	2.65197004	0.00800236	0.04026514	XB5798854 [provisional]
ENSXETG00000015388	11.6685248	4.09011045	1.25552208	3.25769694	0.0011232	0.0077883	asmt
ENSXETG00000023110	12.0474701	4.01455877	1.53929932	2.60804296	0.00910615	0.044697	dbh
ENSXETG00000014030	7.66185672	4.00034925	1.03403114	3.86869319	0.00010942	0.00100208	th
ENSXETG00000022198	232.76211	3.98664322	0.68791639	5.7952438	6.82E-09	1.46E-07	mmp1
ENSXETG00000020532	9090.35955	3.9083472	0.73493981	5.31791469	1.05E-07	1.82E-06	krt18.2
ENSXETG00000037291	898.061521	3.78499138	0.65947695	5.7393839	9.50E-09	1.98E-07	
ENSXETG00000039391	177.141617	3.75129699	0.32889885	11.405625	3.92E-30	2.21E-27	**tbx1**
ENSXETG00000012488	35.2761897	3.66551933	1.08253047	3.38606574	0.00070902	0.00524891	krt70
ENSXETG00000018715	3123.70349	3.56852113	0.99964484	3.56978899	0.00035727	0.00285254	olfm4
ENSXETG00000040960	11.8426493	3.56136467	1.31797523	2.70214841	0.0068893	0.03563579	
ENSXETG00000030601	139.407847	3.52217571	0.6876929	5.12172761	3.03E-07	4.84E-06	cpa6
ENSXETG00000022195	1097.50792	3.47078115	0.82224679	4.22109417	2.43E-05	0.00026554	mmp8
ENSXETG00000008017	10659.0702	3.45894498	0.82666242	4.18422913	2.86E-05	0.00030679	vim.2
ENSXETG00000026572	333.066855	3.38233236	0.62345359	5.42515496	5.79E-08	1.05E-06	**tbxt.2**
ENSXETG00000033563	35.7150317	3.38041089	0.96358317	3.50816721	0.00045121	0.00351704	
ENSXETG00000030183	15966.0621	3.32409705	0.60897153	5.45854264	4.80E-08	8.91E-07	eln2
ENSXETG00000040137	280.304367	3.28259008	0.70060179	4.68538638	2.79E-06	3.75E-05	
ENSXETG00000024911	23.7124461	3.2749052	0.99315494	3.29747662	0.00097558	0.00687353	tgfa
ENSXETG00000007357	78.2794937	3.25941088	0.79907189	4.0789958	4.52E-05	0.00045903	tgm3l.1
ENSXETG00000023914	1336.13796	3.1864788	0.43957358	7.24902254	4.20E-13	1.69E-11	
ENSXETG00000006876	5653.20067	3.14180048	0.85457528	3.6764467	0.00023651	0.00198843	des.2
ENSXETG00000034532	177.149052	3.10880602	0.91384769	3.40188638	0.00066922	0.00498236	
ENSXETG00000033506	176.31201	3.0595769	0.63406275	4.8253535	1.40E-06	1.97E-05	avd
ENSXETG00000037720	252.888083	2.96995458	0.94204919	3.1526534	0.00161794	0.01065621	crp.2
ENSXETG00000008794	375.712974	2.94264665	0.78836891	3.73257572	0.00018953	0.00163683	steap4.2

ENSXETG00000037411	129.539918	2.93172696	0.83278187	3.52040201	0.00043089	0.00337205	
ENSXETG00000026998	49.7619092	2.87777018	1.09183403	2.63572127	0.00839587	0.04176997	foxa2
ENSXETG00000012677	99.6672678	2.861932	0.67635257	4.23142029	2.32E-05	0.0002547	XB5886928 [provisional]
ENSXETG00000040567	5.55933856	2.8418085	1.01048368	2.81232498	0.00491848	0.02691694	
ENSXETG00000019408	550.007495	2.83236372	0.36626262	7.73314985	1.05E-14	5.39E-13	wnt11
ENSXETG00000008940	247.228156	2.78106429	0.64057243	4.34152982	1.41E-05	0.00016254	lamb3
ENSXETG00000033333	26.3191579	2.7760175	0.83953459	3.30661481	0.00094431	0.00671322	
ENSXETG00000010435	29.8341008	2.71120134	0.94495535	2.8691317	0.004116	0.02332698	prss23
ENSXETG00000003565	286.321505	2.70299096	0.39802322	6.79103841	1.11E-11	3.68E-10	foxf1
ENSXETG00000022637	53.367525	2.68545851	0.77700419	3.45616994	0.00054791	0.00415973	
ENSXETG00000030042	63.1396471	2.59199065	0.93034185	2.78606262	0.00533526	0.02873854	rab11fip4l
ENSXETG00000036739	934.826772	2.50474476	0.81102278	3.08837781	0.00201252	0.01272849	
ENSXETG00000007816	739.249361	2.50147813	0.41053062	6.09328033	1.11E-09	2.72E-08	itga11
ENSXETG00000033705	133.600631	2.48099748	0.71417391	3.47394024	0.00051288	0.00392972	
ENSXETG00000024588	1003.11683	2.45323061	0.6684761	3.66988529	0.00024266	0.00203542	g6pc.3
ENSXETG00000004424	68.8383378	2.4454972	0.78693378	3.10762768	0.00188595	0.01209298	scube2
ENSXETG00000041294	279.67972	2.44025074	0.61761683	3.95107555	7.78E-05	0.0007457	XB5886928
ENSXETG00000000543	1136.45309	2.42152603	0.5476019	4.42205558	9.78E-06	0.00011665	gldc
ENSXETG00000020288	39.599983	2.39232404	0.93376392	2.56202236	0.01040646	0.04995063	ntn3
ENSXETG00000036795	550.168926	2.3912307	0.73950378	3.23356115	0.00122257	0.00839606	dhfr
ENSXETG00000033310	23314.443	2.34711056	0.48899336	4.79988229	1.59E-06	2.23E-05	fap
ENSXETG00000009279	21732.3883	2.32262916	0.6587259	3.52594177	0.00042198	0.00332043	acta2
ENSXETG00000037243	274.54851	2.32094598	0.4411736	5.26084513	1.43E-07	2.43E-06	
ENSXETG00000012114	108.705226	2.29314967	0.58039935	3.95098591	7.78E-05	0.0007457	tnip2
ENSXETG00000038837	505.066735	2.2889188	0.61923786	3.6963483	0.00021872	0.00185638	EPPK1
ENSXETG00000008745	99.0645391	2.287567	0.85655433	2.67066189	0.00757019	0.03843869	fcgr1
ENSXETG00000020444	919.790828	2.27099877	0.57355476	3.95951519	7.51E-05	0.0007244	dsp
ENSXETG00000011276	29.9672319	2.26938277	0.84719725	2.6786947	0.00739097	0.03774762	slc22a31
ENSXETG00000030596	9911.92949	2.24880308	0.38901179	5.78080953	7.43E-09	1.58E-07	XB5852574
ENSXETG00000037790	512.255718	2.22030237	0.40633363	5.46423478	4.65E-08	8.66E-07	
ENSXETG00000008005	1033.37962	2.20633338	0.60881598	3.62397414	0.00029011	0.00238148	matn3
ENSXETG00000010510	1242.26959	2.20009077	0.26809154	8.20649079	2.28E-16	1.44E-14	tnfrsf10b
ENSXETG00000011779	2.50086359	2.17981892	0.81265026	2.68235798	0.00731052	0.03736092	glod5
ENSXETG00000023175	40.2393562	2.17082855	0.48647628	4.46235231	8.11E-06	9.82E-05	smyd2
ENSXETG00000024668	100.002371	2.15615151	0.6246584	3.45172902	0.00055701	0.00422676	lamc2
ENSXETG00000004086	66.839895	2.15493991	0.81617596	2.64028839	0.00828355	0.04128939	btg5.2
ENSXETG00000017676	94.2568145	2.10125645	0.69670475	3.01599273	0.00256139	0.01562312	adamts4
ENSXETG00000002874	198.16587	2.09893979	0.48108124	4.36296332	1.28E-05	0.00014892	b4galt3l2
ENSXETG00000038330	31.8649546	2.08566965	0.67775645	3.07731433	0.00208875	0.01315778	

ENSXETG00000021044	2168.33098	2.08062476	0.47741558	4.35809987	1.31E-05	0.00015182	spon2
ENSXETG00000023912	2908.71858	2.00878114	0.38944277	5.15809076	2.49E-07	4.03E-06	c1s
ENSXETG00000040019	292.762753	2.00721281	0.47708898	4.20720852	2.59E-05	0.00028026	foxf2
ENSXETG00000035911	33.4670318	1.98626941	0.72861409	2.7260925	0.0064089	0.03360304	SPATA48
ENSXETG00000019163	221.585317	1.97608089	0.42737489	4.62376456	3.77E-06	4.91E-05	itgb3
ENSXETG00000031974	386.465207	1.97003117	0.4473259	4.40401765	1.06E-05	0.00012564	
ENSXETG00000032698	2639.07402	1.96130876	0.26734324	7.33629461	2.20E-13	9.43E-12	AEBP1
ENSXETG00000024858	319.282609	1.96102353	0.53181893	3.68738945	0.00022657	0.00191675	cyp2a6.2
ENSXETG00000008198	60.5293394	1.95331882	0.58384209	3.34562866	0.00082096	0.00595453	antxr1
ENSXETG00000002733	705.024521	1.92222317	0.64724622	2.96984842	0.00297947	0.01780113	
ENSXETG00000000455	61.2538745	1.91306227	0.71683626	2.66875766	0.00761324	0.03861996	trim23
ENSXETG00000023497	392.836489	1.88407305	0.4683072	4.02315626	5.74E-05	0.00056886	pax1
ENSXETG00000002122	2996.68761	1.88221233	0.58765218	3.20293603	0.00136034	0.00921373	sod3
ENSXETG00000014465	1215.99664	1.88153717	0.53278864	3.53148889	0.00041323	0.00325481	poglut3
ENSXETG00000016402	1184.39495	1.87820613	0.3171642	5.92187305	3.18E-09	7.27E-08	myo1e.1
ENSXETG00000010700	32.3550032	1.87539954	0.71101906	2.63762203	0.00834896	0.04157597	
ENSXETG00000004104	7587.37454	1.87504715	0.40404794	4.64065508	3.47E-06	4.55E-05	cthrc1
ENSXETG00000041285	270.976337	1.86440149	0.38731568	4.81364837	1.48E-06	2.09E-05	
ENSXETG00000021851	273.920665	1.85053341	0.47737616	3.87646801	0.00010598	0.00097685	mmp19
ENSXETG00000000233	4983.99697	1.82548451	0.33367288	5.47088074	4.48E-08	8.38E-07	myh9
ENSXETG00000000152	273.042295	1.81701345	0.50532034	3.59576552	0.00032344	0.0026169	kcnk6
ENSXETG00000038800	114.530918	1.81083974	0.38655291	4.68458435	2.81E-06	3.75E-05	B3GNT9
ENSXETG00000037074	32.6929457	1.79808558	0.57998809	3.10021119	0.00193383	0.0123347	
ENSXETG00000015448	498.703058	1.79734525	0.53375509	3.36735946	0.00075892	0.00556112	serpine1
ENSXETG00000009523	47.0719026	1.79612824	0.66203996	2.71302088	0.00666729	0.03473824	htr2b
ENSXETG00000012973	1537.01486	1.79349649	0.35446394	5.05974317	4.20E-07	6.59E-06	anpep
ENSXETG00000021227	30.303572	1.78855454	0.6953534	2.57215187	0.01010685	0.0487287	tulp2
ENSXETG00000041137	31.7149773	1.78332509	0.50936277	3.50109038	0.00046336	0.00360108	
ENSXETG00000039768	32.0415077	1.78326424	0.64729625	2.75494294	0.00587024	0.03113082	
ENSXETG00000040738	2745.01249	1.77717582	0.35894318	4.95113407	7.38E-07	1.10E-05	G0S2
ENSXETG00000027407	815.138076	1.76911482	0.46462891	3.8075866	0.00014033	0.00124886	steap4.1
ENSXETG00000025867	117.977086	1.76431263	0.474624	3.71728491	0.00020138	0.001724	foxa1
ENSXETG00000000644	23.3295677	1.75117111	0.62415751	2.80565575	0.00502143	0.0273661	clec4e
ENSXETG00000002645	460.185794	1.73373777	0.44168544	3.92527717	8.66E-05	0.00081612	cryl1
ENSXETG00000037195	672.202888	1.72194254	0.44639607	3.85743208	0.00011458	0.00104271	mafb
ENSXETG00000033367	768.993589	1.71937836	0.3088219	5.56754027	2.58E-08	5.04E-07	CEMIP2
ENSXETG00000001223	569.693985	1.71759805	0.36755271	4.67306589	2.97E-06	3.95E-05	emilin1
ENSXETG00000006338	1611.00174	1.68046783	0.62139313	2.70435533	0.00684371	0.0354232	thbs3
ENSXETG00000023296	391.259732	1.6743266	0.29758258	5.62642678	1.84E-08	3.66E-07	smpdl3a

ENSXETG00000021098	4412.65352	1.67402526	0.38547957	4.34270812	1.41E-05	0.00016179	etnppl
ENSXETG00000000038	237.335214	1.66106671	0.6336324	2.62149901	0.0087544	0.04328047	arf6.2
ENSXETG00000018296	354.76613	1.65458131	0.49719878	3.32780646	0.00087533	0.00627948	fam20a
ENSXETG00000010042	786.976084	1.65057601	0.25167626	6.55833019	5.44E-11	1.65E-09	gusb
ENSXETG00000019908	1543.56416	1.64984574	0.43139828	3.82441426	0.00013108	0.0011752	BCAN
ENSXETG00000032066	52.5008004	1.64866493	0.44247747	3.72598614	0.00019455	0.00167013	sfmbt1
ENSXETG00000037381	68.5373543	1.64326144	0.6034158	2.72326553	0.00646401	0.03379079	
ENSXETG00000013887	90.0897287	1.62959745	0.51098464	3.18913199	0.00142701	0.00957882	ttll4
ENSXETG00000001613	381.812939	1.59584826	0.34722033	4.59606801	4.31E-06	5.52E-05	emilin2
ENSXETG00000003828	248.009319	1.59420846	0.39078006	4.07955426	4.51E-05	0.00045823	gfpt2
ENSXETG00000025090	1483.425	1.57615708	0.52109773	3.02468613	0.00248891	0.01525778	cyp3a4.2
ENSXETG00000006890	202.40774	1.57167792	0.41201552	3.81460856	0.0001364	0.00121801	wbp2nl
ENSXETG00000000758	427.276103	1.55639875	0.31377549	4.96023053	7.04E-07	1.05E-05	pcsk5
ENSXETG00000020454	6630.55546	1.54312805	0.50488985	3.05636577	0.00224038	0.01398439	krt8.1
ENSXETG00000008703	7103.87078	1.53719939	0.59925344	2.56519079	0.01031191	0.04956572	mmp9.1
ENSXETG00000019007	1491.04782	1.52411449	0.28624658	5.32448099	1.01E-07	1.77E-06	pold2
ENSXETG00000032514	146.164326	1.52031346	0.53840476	2.82373704	0.00474673	0.02620428	nfkbiz
ENSXETG00000038176	102.018497	1.5074761	0.41550089	3.62809353	0.00028552	0.00235046	
ENSXETG00000039322	2267.3674	1.49491654	0.30327864	4.92918507	8.26E-07	1.22E-05	clic4
ENSXETG00000013529	32.7844683	1.47456206	0.47522334	3.10288227	0.00191646	0.01223878	zfyve27
ENSXETG00000008826	2796.22946	1.47366181	0.38368978	3.84076382	0.00012265	0.0011059	pdlim1
ENSXETG00000014759	309.667438	1.47269251	0.5173769	2.84645971	0.00442083	0.02470806	pid1
ENSXETG00000040991	20.1686426	1.45940079	0.512554	2.84731126	0.00440902	0.02467706	
ENSXETG00000005217	168.465065	1.45428356	0.3065061	4.74471331	2.09E-06	2.86E-05	edem1
ENSXETG00000040958	151.97924	1.45073389	0.46380468	3.12789837	0.00176061	0.01138186	
ENSXETG00000009229	772.92292	1.42884788	0.31395773	4.55108355	5.34E-06	6.73E-05	metrnl
ENSXETG00000017909	133.001654	1.42745805	0.52202987	2.73443747	0.0062487	0.03289436	slc39a9
ENSXETG00000003135	40.1215882	1.42375095	0.52844886	2.69420763	0.00705562	0.03634105	ccn3
ENSXETG00000037748	526.8993	1.42055318	0.24056026	5.90518642	3.52E-09	7.97E-08	
ENSXETG00000033027	66.3408539	1.41889984	0.52466504	2.70439181	0.00684295	0.0354232	
ENSXETG00000000380	3651.47331	1.41858934	0.37373742	3.79568448	0.00014724	0.00130444	glul
ENSXETG00000030496	1800.99219	1.41381137	0.50119263	2.82089416	0.004789	0.02637297	SCARA5
ENSXETG00000033667	165.187444	1.39679713	0.34075275	4.09915143	4.15E-05	0.00042577	
ENSXETG00000011949	761.834336	1.38052984	0.29933409	4.61200331	3.99E-06	5.16E-05	antxrl
ENSXETG00000023966	74.473845	1.38004097	0.47490987	2.90590078	0.00366198	0.02114154	sfrpx
ENSXETG00000027626	272.29107	1.37755695	0.32267402	4.26919079	1.96E-05	0.00021836	
ENSXETG00000004699	184.45405	1.37296548	0.32183212	4.26609215	1.99E-05	0.00022126	bcar1
ENSXETG00000012929	114.39346	1.37201891	0.5037626	2.72354259	0.00645859	0.03377366	ccne1
ENSXETG00000024861	1912.43169	1.36740406	0.35181076	3.8867602	0.00010159	0.00093856	loxl1

ENSXETG00000007556	4149.17998	1.35574895	0.35217232	3.84967495	0.00011827	0.00107011	cd44
ENSXETG00000000804	1270.41848	1.34716365	0.34826529	3.86821108	0.00010964	0.00100348	nfil3
ENSXETG00000012036	46.8108416	1.34712959	0.47074695	2.86168524	0.00421395	0.02373699	coq10b
ENSXETG00000018487	1071.36443	1.34135292	0.29000686	4.62524553	3.74E-06	4.88E-05	cdc42ep3
ENSXETG00000039828	6128.85053	1.3371136	0.34035338	3.92860381	8.54E-05	0.00080636	cebpd
ENSXETG00000037225	106.484726	1.33353998	0.42587012	3.13133024	0.00174016	0.01128207	zfp2
ENSXETG00000032988	211.470339	1.33273934	0.46545349	2.86331365	0.00419235	0.02366427	RRP15
ENSXETG00000004376	101.033126	1.32986532	0.4359534	3.05047585	0.00228479	0.01418298	col8a2
ENSXETG00000004411	1733.59576	1.32799367	0.43524343	3.05115157	0.00227965	0.01415667	hsd17b6
ENSXETG00000019780	333.36321	1.32773103	0.29219848	4.54393542	5.52E-06	6.93E-05	rassf10
ENSXETG00000002807	250.261404	1.32564535	0.27762358	4.77497385	1.80E-06	2.50E-05	meis3
ENSXETG00000024632	1516.58496	1.32116881	0.46493078	2.84164625	0.00448813	0.02503977	socs3
ENSXETG00000035220	716.147355	1.31670281	0.27800749	4.73621345	2.18E-06	2.97E-05	hyal2
ENSXETG00000007332	555.427191	1.31513978	0.36781958	3.57550235	0.00034956	0.00280089	rassf1
ENSXETG00000034678	748.318401	1.31191647	0.40439616	3.24413685	0.00117807	0.00813297	gmfg
ENSXETG00000017928	246.225514	1.31075114	0.39221631	3.34190883	0.00083204	0.00601552	hpse
ENSXETG00000000689	1393.85566	1.30655016	0.34621438	3.77381826	0.00016077	0.00140848	pdgfrl
ENSXETG00000005906	386.056134	1.30617841	0.44453743	2.93828669	0.00330032	0.01940906	kiaa1217
ENSXETG00000038056	1177.30843	1.30179571	0.26237754	4.96153643	6.99E-07	1.05E-05	sh3pxd2b
ENSXETG00000001952	296.523442	1.29974441	0.44799395	2.90125437	0.00371672	0.02137928	polr1a
ENSXETG00000030953	1408.95188	1.2995208	0.36687518	3.54213333	0.0003969	0.00313565	FILIP1L
ENSXETG00000019257	283.512245	1.29549679	0.29777803	4.35054525	1.36E-05	0.00015669	rab34
ENSXETG00000036302	1990.16348	1.29515573	0.22945281	5.64454065	1.66E-08	3.31E-07	
ENSXETG00000017323	344.743904	1.29502261	0.30862772	4.19606702	2.72E-05	0.00029339	tgm2
ENSXETG00000015336	300.995384	1.2929573	0.39549229	3.26923513	0.00107839	0.00749072	hmgcl
ENSXETG00000025630	915.28058	1.29258289	0.26945764	4.79697991	1.61E-06	2.25E-05	twist1
ENSXETG00000018761	766.306083	1.28669209	0.19220065	6.69452503	2.16E-11	6.88E-10	prss16
ENSXETG00000018160	760.642506	1.28373686	0.35254482	3.64134373	0.00027122	0.0022451	net1
ENSXETG00000021893	180.782371	1.28186223	0.49883703	2.56970144	0.01017862	0.04902971	angptl4
ENSXETG00000005810	110.999299	1.28079815	0.47931788	2.67212678	0.00753722	0.03830831	pla2g15
ENSXETG00000011438	69.3554396	1.2738135	0.38829918	3.28049493	0.00103625	0.00723311	ccnk
ENSXETG00000011560	314.357409	1.26690991	0.31506924	4.02105233	5.79E-05	0.00057324	foxp2
ENSXETG00000025010	456.14978	1.26431024	0.30610464	4.13032038	3.62E-05	0.00037695	tgif1
ENSXETG00000023338	391.984636	1.26408514	0.47957422	2.63584881	0.00839271	0.04176745	pdgfrl.2
ENSXETG00000026298	142.409864	1.2577437	0.4315415	2.91453707	0.00356217	0.02067131	pitpnb
ENSXETG00000008945	596.119077	1.25228901	0.25207982	4.96782726	6.77E-07	1.02E-05	dhcr7
ENSXETG00000003194	1746.20373	1.25090636	0.29626042	4.2223202	2.42E-05	0.00026447	myo1d
ENSXETG00000034066	153.241826	1.24099598	0.34737949	3.57245037	0.00035366	0.00283087	synj2
ENSXETG00000022669	12084.8004	1.235692	0.32428185	3.81054938	0.00013866	0.00123678	mmp14

ENSXETG00000007336	1641.9879	1.22944053	0.25101341	4.89790787	9.69E-07	1.41E-05	lama4
ENSXETG00000005430	182.635818	1.22464788	0.36683503	3.33841584	0.00084258	0.00607495	slc12a4
ENSXETG00000031472	1350.05355	1.2240577	0.4426414	2.76534841	0.0056862	0.03029758	TENM3
ENSXETG00000013630	906.274839	1.22259179	0.3368782	3.62918044	0.00028432	0.0023425	cyyr1
ENSXETG00000015465	167.94694	1.22163295	0.41995581	2.90895592	0.00362638	0.02096675	cln5
ENSXETG00000032633	326.379537	1.22024102	0.30108563	4.05280393	5.06E-05	0.00050869	
ENSXETG00000041119	1601.94851	1.21844041	0.30995839	3.93098063	8.46E-05	0.00080098	
ENSXETG00000008736	14913.5628	1.20840754	0.38474265	3.14082033	0.00168475	0.01101801	tpm4
ENSXETG00000023522	198.735712	1.20834175	0.41468782	2.91385877	0.00356991	0.02070865	
ENSXETG00000013144	225.313701	1.20549905	0.41171934	2.92796311	0.00341191	0.01993144	dnajb4
ENSXETG00000040858	275.058707	1.20474988	0.3679334	3.2743694	0.00105898	0.00737217	
ENSXETG00000012239	406.64438	1.20387498	0.33278994	3.61752215	0.00029744	0.00243022	abcc3
ENSXETG00000016838	2103.22555	1.20045643	0.43423902	2.76450611	0.0057009	0.03035539	hspa5
ENSXETG00000023618	6713.653	1.19652743	0.29128139	4.10780595	3.99E-05	0.00041228	cald1
ENSXETG00000021236	120637.805	1.19192636	0.2786859	4.27695244	1.89E-05	0.00021179	fth1.1
ENSXETG00000017309	4053.2528	1.18994503	0.30399396	3.91437056	9.06E-05	0.00084934	vasn
ENSXETG00000027581	5028.53936	1.18992538	0.2896563	4.10805968	3.99E-05	0.0004121	ctsv
ENSXETG00000017088	1641.46557	1.18630388	0.39153197	3.02990296	0.00244632	0.0150435	csrp1
ENSXETG00000035558	2165.78264	1.18123636	0.36518905	3.23458868	0.00121818	0.00837685	ctsk
ENSXETG00000000078	465.98805	1.17863573	0.43677037	2.69852494	0.00696475	0.03595527	cish
ENSXETG00000010536	1664.17	1.17328681	0.43822929	2.67733546	0.00742103	0.03782683	bmp1
ENSXETG00000022804	635.103812	1.17174522	0.21512587	5.44678902	5.13E-08	9.47E-07	wdr45b
ENSXETG00000025974	482.871987	1.16980791	0.27605557	4.23758129	2.26E-05	0.00024798	b3gnt5
ENSXETG00000038597	383.570388	1.16565126	0.42130041	2.76679358	0.00566106	0.03018401	
ENSXETG00000014132	81.10299	1.16415402	0.40003569	2.91012537	0.00361284	0.02091915	setd4
ENSXETG00000010892	137.768698	1.16096693	0.25843109	4.49236559	7.04E-06	8.65E-05	slc35b2
ENSXETG00000026099	1334.35342	1.15669333	0.36923583	3.13266818	0.00173225	0.01124002	herpud1
ENSXETG00000009770	2247.39928	1.15605377	0.28567673	4.04672007	5.19E-05	0.0005201	msn
ENSXETG00000027353	344.765304	1.15316395	0.29567958	3.90004597	9.62E-05	0.00089587	hoxb2
ENSXETG00000002137	1816.79611	1.15011704	0.34185615	3.36433044	0.0007673	0.00561698	scara3
ENSXETG00000007240	4772.42256	1.14857562	0.38950753	2.94878922	0.00319021	0.01888842	pdlim7
ENSXETG00000035532	76.8314719	1.14618345	0.41932681	2.73338937	0.00626862	0.03298821	
ENSXETG00000014260	1115.76188	1.14492758	0.2780751	4.11733227	3.83E-05	0.00039769	niban2
ENSXETG00000010329	393.180101	1.14347925	0.26086306	4.38344634	1.17E-05	0.00013709	decr2
ENSXETG00000014268	14672.6137	1.14234274	0.23804387	4.79887485	1.60E-06	2.24E-05	flna
ENSXETG00000026716	3531.51288	1.14209908	0.25806547	4.42561762	9.62E-06	0.00011509	itgb1
ENSXETG00000020597	224.784338	1.14055614	0.41654157	2.73815679	0.00617846	0.03255725	efemp2
ENSXETG00000001769	2986.57772	1.13563257	0.27819737	4.08211103	4.46E-05	0.0004538	hes4
ENSXETG00000039890	295.401759	1.13381519	0.27303836	4.15258577	3.29E-05	0.00034565	CMTM4

ENSXETG00000035467	6165.78823	1.13333218	0.34914581	3.246014	0.00117033	0.00808662	sdc2
ENSXETG00000020206	10242.3491	1.13134053	0.33356626	3.39165152	0.00069473	0.00516004	timp2
ENSXETG00000036283	366.546423	1.13050874	0.42750693	2.64442199	0.00818306	0.0409049	
ENSXETG00000005937	4587.78536	1.13039415	0.37397157	3.02267407	0.00250552	0.01534765	amt
ENSXETG00000001299	217.467511	1.12946665	0.24239988	4.65951812	3.17E-06	4.19E-05	iqgap1
ENSXETG00000013638	363.700466	1.12623707	0.328408	3.4293838	0.00060495	0.00454248	adamts5
ENSXETG00000018791	984.669393	1.1252616	0.36861691	3.05265864	0.00226824	0.01410245	tgfb1i1
ENSXETG00000026160	454.370905	1.11983362	0.23935862	4.67847631	2.89E-06	3.86E-05	
ENSXETG00000000040	656.022725	1.11980374	0.35735636	3.13357716	0.0017269	0.01121833	actn4
ENSXETG00000021661	2539.84146	1.11834141	0.40401135	2.76809405	0.00563852	0.03009437	ptbp1
ENSXETG00000000663	820.765055	1.11080961	0.31806829	3.49236198	0.00047877	0.00370623	tram2
ENSXETG00000036112	575.347774	1.10706852	0.18713057	5.91602165	3.30E-09	7.50E-08	TEAD2
ENSXETG00000003737	2196.24765	1.08961173	0.32331529	3.3701213	0.00075135	0.00552077	cpn1
ENSXETG00000020940	7380.69313	1.08930989	0.35462984	3.07168141	0.00212857	0.01335763	arpc3
ENSXETG00000006965	235.059417	1.08662657	0.37863965	2.86981718	0.00410709	0.02328485	pxdn
ENSXETG00000015289	14500.1663	1.08018601	0.21552759	5.01182242	5.39E-07	8.27E-06	anxa2
ENSXETG00000003677	2312.78264	1.07830936	0.29654796	3.63620562	0.00027668	0.00228434	pls3
ENSXETG00000007198	371.219858	1.07577465	0.32640971	3.2957802	0.00098149	0.00690899	nudt22
ENSXETG00000001812	11906.9753	1.0751069	0.27153464	3.95937296	7.51E-05	0.0007244	postn
ENSXETG00000004172	3128.78583	1.07424339	0.21502843	4.99582029	5.86E-07	8.91E-06	gnpda1
ENSXETG00000003512	1412.23737	1.07096303	0.38571632	2.77655618	0.00549381	0.02951193	pdia6
ENSXETG00000006439	244.506086	1.07052103	0.33245729	3.22002571	0.00128179	0.00875542	enc1.2
ENSXETG00000004962	449.690193	1.06894466	0.4163077	2.5676793	0.01023818	0.0492865	grb10
ENSXETG00000033264	233.302669	1.06688871	0.23880142	4.46768158	7.91E-06	9.60E-05	
ENSXETG00000035556	419.141361	1.06611003	0.37479596	2.84450778	0.00444801	0.02484234	
ENSXETG00000001819	503.598335	1.06605289	0.33414594	3.19038104	0.00142085	0.00954157	exosc8
ENSXETG00000006191	215.030158	1.06478712	0.41120203	2.58945003	0.00961294	0.04674776	galnt4
ENSXETG00000027920	10982.2415	1.06388482	0.31104832	3.42032007	0.00062547	0.00468096	arpc2
ENSXETG00000019136	268.298204	1.0506727	0.3012767	3.48740119	0.00048774	0.00376776	ext1
ENSXETG00000039015	161.707665	1.05042566	0.33819351	3.10599	0.00189643	0.01214533	glod5
ENSXETG00000016987	1469.19997	1.04731017	0.34426748	3.04214089	0.00234902	0.01453588	zfp36l1
ENSXETG00000018036	665.431229	1.04694387	0.30526764	3.42959339	0.00060449	0.00454114	bnc2
ENSXETG00000010669	628.48735	1.03952464	0.15776115	6.58923089	4.42E-11	1.35E-09	scamp5.2
ENSXETG00000039670	7909.4539	1.03579687	0.39487972	2.62306931	0.00871415	0.04309833	CLEC11A
ENSXETG00000024006	510.945564	1.03057106	0.39032486	2.64029062	0.0082835	0.04128939	snai2
ENSXETG00000003603	14754.3651	1.02955059	0.27106571	3.79815867	0.00014578	0.00129222	col12a1
ENSXETG00000012532	144.224558	1.02823253	0.31125487	3.30350668	0.00095484	0.00676064	tsen54
ENSXETG00000014318	1984.0977	1.02632047	0.33167816	3.09432633	0.0019726	0.01253721	csrp2
ENSXETG00000041311	533.97168	1.02030531	0.36276278	2.81259643	0.00491433	0.02691694	

ENSXETG00000011748	1639.78708	1.01881528	0.26452112	3.85154613	0.00011737	0.00106379	ctsc
ENSXETG00000011464	788.061378	1.01840762	0.23026706	4.42272375	9.75E-06	0.00011646	nek6
ENSXETG00000024037	678.398737	1.01291644	0.29953589	3.38161956	0.0007206	0.00532459	bri3
ENSXETG00000038782	3310.01705	1.01064179	0.30667821	3.29544702	0.00098265	0.0069141	
ENSXETG00000010020	1565.67094	1.00775863	0.31444808	3.20484901	0.00135133	0.00916059	chka
ENSXETG00000016471	282.321333	1.00604898	0.37930958	2.65231626	0.00799416	0.04024145	casp7
ENSXETG00000003177	928.445487	1.00433678	0.313892	3.19962525	0.00137606	0.00929226	cd37
ENSXETG00000008785	687.705764	0.99888274	0.31822714	3.13889865	0.00169584	0.01106756	galk2
ENSXETG00000020281	273.598887	0.99807109	0.31387321	3.1798543	0.00147349	0.00983222	armc1
ENSXETG00000013295	1340.94307	0.99570934	0.38525147	2.58456986	0.00975006	0.04734153	npc2
ENSXETG00000024940	726.723003	0.99405911	0.30875793	3.21954192	0.00128396	0.00876415	ypel1
ENSXETG00000014608	353.524821	0.9932774	0.36901769	2.69167964	0.00710932	0.03653407	pck2
ENSXETG00000001856	314.916193	0.98634084	0.32165755	3.06643152	0.0021663	0.01357579	gli3
ENSXETG00000002042	379.467216	0.98578961	0.31732258	3.10658513	0.00189262	0.01213077	rnf113a
ENSXETG00000010450	132.036807	0.98428723	0.26107301	3.77016081	0.00016314	0.0014277	alg8
ENSXETG00000017162	2023.03629	0.98331036	0.23061305	4.26389737	2.01E-05	0.00022282	shmt2
ENSXETG00000013350	1817.9202	0.98267096	0.34834072	2.8210051	0.00478734	0.02637297	tfg
ENSXETG00000002419	352.90265	0.97798486	0.25957351	3.76766056	0.00016478	0.00143967	blzf1
ENSXETG00000018825	804.140617	0.97633066	0.28324909	3.44689783	0.00056706	0.00429068	cybrd1
ENSXETG00000003619	159.14516	0.97212184	0.28627649	3.39574458	0.00068442	0.00509069	gna14
ENSXETG00000037438	248.461987	0.97035505	0.25021575	3.87807346	0.00010529	0.00097099	ier5
ENSXETG00000000709	225.89005	0.9693825	0.2772516	3.49640002	0.00047158	0.00366137	prlr
ENSXETG00000021174	678.144873	0.96929411	0.30969784	3.12980587	0.00174922	0.01132215	acat2
ENSXETG00000021229	2394.10517	0.96605721	0.28625048	3.37486672	0.00073851	0.00544421	nucb1
ENSXETG00000021721	968.845174	0.96503843	0.22309527	4.32567863	1.52E-05	0.00017342	renbp
ENSXETG00000021660	1133.72876	0.96502851	0.18074646	5.33912822	9.34E-08	1.65E-06	scarf2
ENSXETG00000031309	360.870418	0.96468686	0.35480719	2.71890448	0.00654985	0.03418285	rab31
ENSXETG00000010653	312.534994	0.96397977	0.26993055	3.57121409	0.00035533	0.00283994	snx1
ENSXETG00000021481	272.853892	0.96051928	0.36863323	2.60562314	0.00917073	0.04495797	lrig3
ENSXETG00000022511	250.88855	0.95697836	0.31746681	3.01442021	0.00257471	0.01569826	mthfd1
ENSXETG00000007675	575.73907	0.95221699	0.24197849	3.9351307	8.32E-05	0.00078949	mlkl
ENSXETG00000008663	190.443155	0.95115283	0.26783769	3.55122841	0.00038344	0.00303992	flnb
ENSXETG00000017933	1814.09191	0.9506248	0.31851072	2.98459283	0.00283956	0.01706226	actn1
ENSXETG00000025513	187.702335	0.94014151	0.33319045	2.82163401	0.00477797	0.02633061	gnpnat1
ENSXETG00000011962	1929.65113	0.93851974	0.25992402	3.61074651	0.00030532	0.00248302	dact1
ENSXETG00000036865	5056.55093	0.93851786	0.26216625	3.57985766	0.00034378	0.00276728	
ENSXETG00000004670	700.378777	0.93367269	0.28578954	3.26699389	0.00108696	0.00754363	mvp
ENSXETG00000031617	301.859276	0.93166995	0.29138665	3.19736662	0.00138689	0.00934532	RHBDF1
ENSXETG00000011158	851.532937	0.93120552	0.26816301	3.47253531	0.00051557	0.00394268	pcdh18

ENSXETG00000023897	388.038125	0.92866906	0.23215015	4.00029482	6.33E-05	0.00062009	sord
ENSXETG00000024646	184.05017	0.9265111	0.27334293	3.38955579	0.00070006	0.00518986	smco4
ENSXETG00000011071	475.497608	0.92217008	0.15981278	5.770315	7.91E-09	1.67E-07	cipc
ENSXETG00000005075	2448.54432	0.92027774	0.2916696	3.15520626	0.00160385	0.01057224	hexb
ENSXETG00000018746	65.0649728	0.91833895	0.35214362	2.60785342	0.0091112	0.04470783	epha7
ENSXETG00000017411	298.824821	0.91824153	0.31550488	2.91038774	0.00360981	0.02090928	hmcn1
ENSXETG00000036288	64.4427029	0.91641696	0.31803544	2.88149319	0.00395796	0.02256108	
ENSXETG00000033169	692.153147	0.91282451	0.22134507	4.1239884	3.72E-05	0.00038713	ap1s3
ENSXETG00000024201	1705.00512	0.91037765	0.26416665	3.44622473	0.00056848	0.00429519	ipo7
ENSXETG00000027225	5528.67437	0.90966743	0.29215219	3.11367653	0.00184772	0.01188649	tagln2
ENSXETG00000003750	231.696068	0.9078314	0.32875976	2.76138238	0.00575572	0.03060593	rnf214
ENSXETG00000006741	684.642524	0.90654033	0.28056449	3.23112993	0.00123302	0.00846043	lman2
ENSXETG00000010791	180.434354	0.903821	0.3309335	2.73112569	0.00631184	0.03317136	socs6
ENSXETG00000012301	949.81375	0.89997382	0.24880435	3.61719489	0.00029781	0.00243204	cfl2
ENSXETG00000005675	1068.89588	0.89730916	0.33762391	2.6577181	0.00786717	0.03965284	rgs2
ENSXETG00000041079	268.482091	0.89594328	0.21552101	4.15710415	3.22E-05	0.00034047	cebpb
ENSXETG00000010703	152.718205	0.89583559	0.30843212	2.90448215	0.00367861	0.02120077	pak1
ENSXETG00000023695	337.982243	0.89572936	0.31094063	2.88070868	0.00396782	0.02259249	cdk12
ENSXETG00000016954	547.612118	0.89494283	0.17498426	5.11441893	3.15E-07	5.03E-06	c19orf47
ENSXETG00000021947	149.701771	0.89046206	0.30865453	2.88497974	0.00391439	0.02233707	scrn2
ENSXETG00000020057	577.123792	0.88875603	0.29245888	3.03890933	0.00237436	0.01464098	utp6
ENSXETG00000015941	214.678623	0.87175606	0.28332818	3.076842	0.00209206	0.01316812	rnf130
ENSXETG00000009170	254.290251	0.86917123	0.32801821	2.64976517	0.00805477	0.04040461	cep97
ENSXETG00000004794	2625.47344	0.86671701	0.27550191	3.14595651	0.00165545	0.01085788	txnrd3
ENSXETG00000017980	288.656893	0.86033854	0.21652801	3.97333603	7.09E-05	0.00068614	chmp3
ENSXETG00000019015	284.089865	0.85722626	0.23955029	3.57848137	0.0003456	0.00277564	tcf7l1
ENSXETG00000009237	344.45385	0.85445577	0.20571098	4.15367119	3.27E-05	0.0003447	usp44
ENSXETG00000004542	1097.40578	0.85205247	0.23933389	3.5600995	0.00037071	0.00294943	bambi
ENSXETG00000012824	660.492741	0.84163756	0.26200948	3.21224091	0.00131704	0.00895893	tbc1d16
ENSXETG00000034997	144.41942	0.84084217	0.29523775	2.84801714	0.00439926	0.0246399	
ENSXETG00000007430	86.8341664	0.84051154	0.23873886	3.52063148	0.00043052	0.00337205	nfs1
ENSXETG00000001447	105.573077	0.83724072	0.32283982	2.59336262	0.00950425	0.04628848	thumpd3
ENSXETG00000012433	305.531713	0.83616873	0.27471534	3.04376424	0.00233638	0.01446904	ears2
ENSXETG00000012046	772.299193	0.83238137	0.29022148	2.86809015	0.00412958	0.02337869	cpvl
ENSXETG00000024732	245.479832	0.83076054	0.27629487	3.00678964	0.00264022	0.01602332	ARHGAP31
ENSXETG00000007092	108.910812	0.82792511	0.27909051	2.96651116	0.00301199	0.01797503	tiprl
ENSXETG00000017985	2814.01627	0.82578162	0.20656394	3.9977047	6.40E-05	0.00062652	anxa3
ENSXETG00000011119	2999.12356	0.82376674	0.29318637	2.80970338	0.00495872	0.02710211	mxra8
ENSXETG00000021235	2643.65493	0.82022502	0.20596529	3.98234591	6.82E-05	0.00066389	mgc76132

ENSXETG00000027311	999.522785	0.81793037	0.23539101	3.47477315	0.00051129	0.00391944	hebp1
ENSXETG00000040672	316.800619	0.81680084	0.30414028	2.68560563	0.00723985	0.03706822	
ENSXETG00000035460	183.711398	0.81679493	0.29979341	2.72452595	0.00643939	0.0337068	
ENSXETG00000024869	649.664278	0.81506598	0.31621218	2.577592	0.00994914	0.04811549	sptssa
ENSXETG00000037711	513.573695	0.81376785	0.29339789	2.77359818	0.00554401	0.02971452	cnih4
ENSXETG00000014001	2652.55734	0.80630217	0.19225975	4.1938167	2.74E-05	0.00029592	actr2
ENSXETG00000000151	440.273102	0.80590322	0.25855342	3.11696991	0.0018272	0.01178336	yif1b
ENSXETG00000021035	439.385784	0.80434399	0.25952398	3.09930506	0.00193975	0.01235749	pdgfra
ENSXETG00000003238	176.629549	0.80395509	0.27825725	2.88925117	0.0038616	0.02209574	cdc27
ENSXETG00000008245	15181.7652	0.80358182	0.22818123	3.52168241	0.00042882	0.00336416	ccn2
ENSXETG00000022429	494.786697	0.80225421	0.28604287	2.80466424	0.0050369	0.02743145	rflnb
ENSXETG00000020089	1112.56556	0.80152571	0.26711131	3.00071799	0.00269344	0.01630234	rnf13
ENSXETG00000014368	2040.654	0.80004999	0.1982696	4.03516215	5.46E-05	0.00054361	zfand5
ENSXETG00000033044	863.403414	0.79679623	0.29239731	2.72504636	0.00642925	0.03367609	gal3st4.6
ENSXETG00000000777	3286.72231	0.79372018	0.26008975	3.05171655	0.00227537	0.01413563	rrbp1
ENSXETG00000020607	2068.07992	0.79278339	0.19426267	4.08098676	4.48E-05	0.00045571	ddx39a
ENSXETG00000009545	1214.09817	0.79210539	0.262127	3.02183828	0.00251245	0.01537813	ebna1bp2
ENSXETG00000006219	6791.33476	0.79121425	0.15637614	5.05968643	4.20E-07	6.59E-06	sat1
ENSXETG00000022926	276.5685	0.79033145	0.29977393	2.6364249	0.00837847	0.04170977	hspbp1
ENSXETG00000015291	1490.07545	0.78911182	0.17363472	4.54466605	5.50E-06	6.91E-05	actr3
ENSXETG00000010248	310.782264	0.78832085	0.25490841	3.0925651	0.00198435	0.01258563	prkd1
ENSXETG00000012856	25960.0379	0.78807991	0.26190417	3.00903914	0.00262075	0.01593584	rpl9
ENSXETG00000034888	1639.10673	0.78013808	0.2083288	3.7447443	0.00018058	0.00156464	hnrnpa0
ENSXETG00000036083	385.894159	0.77845912	0.20872386	3.72961255	0.00019177	0.00164987	med11
ENSXETG00000011270	179.624418	0.7780198	0.24568786	3.16670027	0.00154179	0.01020587	rae1
ENSXETG00000030391	520.809879	0.77397193	0.18785016	4.12015583	3.79E-05	0.00039337	AP3B1
ENSXETG00000022441	314.253938	0.77387375	0.29523021	2.62125525	0.00876066	0.04329784	ttc19
ENSXETG00000035652	546.867301	0.77002637	0.26547941	2.90051263	0.00372553	0.02140651	
ENSXETG00000015541	319.614095	0.76765167	0.22083167	3.47618462	0.0005086	0.00390077	fut11
ENSXETG00000006458	317.251326	0.76711012	0.29233685	2.62406236	0.00868879	0.04302129	dnajc3
ENSXETG00000029991	371.244938	0.76636519	0.28178281	2.71970169	0.00653408	0.03412316	acp7
ENSXETG00000007107	486.906803	0.75901703	0.20526129	3.69780897	0.00021747	0.00184955	prmt9
ENSXETG00000006318	538.841661	0.75855206	0.27060758	2.80314418	0.0050607	0.02753254	exosc10
ENSXETG00000004630	684.121829	0.75271431	0.2787049	2.70075739	0.00691818	0.03574997	dcxr
ENSXETG00000008602	827.452701	0.75140413	0.28881281	2.60169947	0.00927631	0.04539085	snx7
ENSXETG00000027478	7471.85926	0.75045999	0.25773329	2.91176978	0.00359387	0.02083231	anxa1.1
ENSXETG00000017719	117.668781	0.74731886	0.26372942	2.83365751	0.00460186	0.02556572	pde7b
ENSXETG00000016951	415.271888	0.74586099	0.27773018	2.68555977	0.00724084	0.03706822	cry1
ENSXETG00000031263	795.260355	0.74362579	0.23119195	3.21648654	0.00129771	0.00884269	traf7

ENSXETG00000019813	6122.59134	0.7374495	0.24483909	3.01197614	0.00259553	0.01580075	gsn
ENSXETG00000023673	291.739023	0.7355584	0.2515672	2.92390428	0.00345671	0.02013349	mapkapk2
ENSXETG00000000559	340.316229	0.73247986	0.20272317	3.6132025	0.00030244	0.00246541	rcbtb2
ENSXETG00000023676	715.147053	0.72786868	0.25930852	2.80696015	0.00500114	0.02728384	acox2
ENSXETG00000027249	3180.7778	0.72732173	0.2788309	2.6084689	0.00909483	0.04465532	mgc75753
ENSXETG00000008250	2087.72861	0.72607062	0.2828291	2.56717087	0.01025321	0.04934376	copb2
ENSXETG00000032294	165.896031	0.7249257	0.22997413	3.15220547	0.00162042	0.01066574	MGC145260
ENSXETG00000018552	1009.55493	0.72475978	0.19691195	3.6806287	0.00023266	0.00196303	psmd3
ENSXETG00000005597	1130.54616	0.72374816	0.25564466	2.83107087	0.00463924	0.02574617	man2b1
ENSXETG00000032680	278.017625	0.72321157	0.2324966	3.11063296	0.00186687	0.01198034	CEP63
ENSXETG00000035249	704.616307	0.72132418	0.25836472	2.79188349	0.00524022	0.02835261	MYBBP1A
ENSXETG00000010068	404.837315	0.71393707	0.22268754	3.20600363	0.00134592	0.00912784	sumf2
ENSXETG00000025105	664.583466	0.71301836	0.21682368	3.28847082	0.00100733	0.00705312	ruvbl2
ENSXETG00000018375	1088.90027	0.71036999	0.23505498	3.02214393	0.00250991	0.01536858	anxa11
ENSXETG00000008431	1414.19669	0.70964072	0.21141388	3.35664199	0.00078895	0.00575038	ltbp3
ENSXETG00000039509	425.329824	0.70736632	0.20866751	3.38992073	0.00069913	0.00518593	zfand3
ENSXETG00000001888	616.579992	0.69993292	0.18765819	3.72982877	0.00019161	0.00164935	appl2
ENSXETG00000001281	759.83266	0.69880239	0.18767916	3.72338819	0.00019657	0.00168558	gaa
ENSXETG00000006404	1951.42898	0.69836236	0.23072036	3.02687791	0.00247094	0.0151771	septin11
ENSXETG00000017911	371.094422	0.6935806	0.2420837	2.86504458	0.00416951	0.02357932	hspg2
ENSXETG00000031315	509.394381	0.69350216	0.26611071	2.60606634	0.00915887	0.04491381	
ENSXETG00000037152	422.472386	0.6931892	0.25131845	2.75821055	0.00581188	0.03085246	mob1a
ENSXETG00000019874	201.063577	0.68838911	0.23748398	2.89867592	0.00374742	0.02150877	znf276
ENSXETG00000032118	680.65319	0.68817242	0.24252233	2.8375631	0.00454594	0.02532644	tnfrsf1a
ENSXETG00000014266	3738.20087	0.68490633	0.22442647	3.05180719	0.00227468	0.01413563	psmc4
ENSXETG00000027641	80892.841	0.68085692	0.23515687	2.89533074	0.00378759	0.02169983	actg1
ENSXETG00000003055	238.650817	0.67752078	0.26233415	2.58266331	0.00980409	0.04757461	mvb12a
ENSXETG00000016900	320.645692	0.67704274	0.17378562	3.8958502	9.79E-05	0.0009083	naa15
ENSXETG00000002064	659.290721	0.67385591	0.24896112	2.70667131	0.00679615	0.03523491	ruvbl1
ENSXETG00000018368	444.475171	0.67132267	0.23146176	2.90036111	0.00372733	0.02140905	pelo
ENSXETG00000018997	1130.65308	0.66868926	0.1698507	3.93692384	8.25E-05	0.00078503	ogdh
ENSXETG00000024947	884.664297	0.66797892	0.25111769	2.66002331	0.00781352	0.03939506	tssc4
ENSXETG00000018839	705.627588	0.66607003	0.19199764	3.46915729	0.00052209	0.00398871	gorasp2
ENSXETG00000011707	815.536474	0.66486966	0.23537801	2.82468889	0.00473265	0.02614489	pum3
ENSXETG00000023674	567.043782	0.65627598	0.23706011	2.76839482	0.00563332	0.03007795	tada3
ENSXETG00000012766	825.712359	0.65522627	0.17500194	3.74410872	0.00018104	0.00156775	eif5
ENSXETG00000002770	252.530688	0.65286093	0.21699859	3.00859519	0.00262459	0.01595299	wbp11
ENSXETG00000023735	778.227858	0.65262425	0.23643698	2.76024609	0.00577578	0.03069188	psmg1
ENSXETG00000023561	1862.20115	0.65071264	0.23137912	2.81232222	0.00491852	0.02691694	cndp2

ENSXETG00000020788	284.680049	0.645528	0.2406092	2.68288998	0.0072989	0.03731364	med30
ENSXETG00000031596	2569.37261	0.64491198	0.21592453	2.98674714	0.00281963	0.01696189	fkbp2
ENSXETG00000037051	816.278721	0.63996056	0.21148793	3.02599093	0.0024782	0.01520984	SNRPA1
ENSXETG00000014258	758.025458	0.63239811	0.23522523	2.68847906	0.00717783	0.03680216	gosr2
ENSXETG00000008654	988.5015	0.63112168	0.2433648	2.59331543	0.00950555	0.04628848	arf4
ENSXETG00000008840	458.20296	0.62914546	0.23164859	2.71594766	0.00660864	0.03445541	fzd2
ENSXETG00000036372	3137.9399	0.62779183	0.21609823	2.9051225	0.00367109	0.02117092	
ENSXETG00000038971	401.21755	0.62514979	0.18996773	3.29082098	0.00099895	0.00700379	
ENSXETG00000038650	874.673781	0.62164911	0.22329143	2.78402582	0.00536888	0.02887212	REST
ENSXETG00000022057	397.671071	0.61755577	0.22034766	2.80264275	0.00506858	0.02756332	trpm7
ENSXETG00000018474	2618.61392	0.61466011	0.21546614	2.85269933	0.00433496	0.02432284	gars1
ENSXETG00000024088	968.017731	0.61217367	0.21579504	2.83682922	0.0045564	0.02536679	abcf1
ENSXETG00000008206	1862.44901	0.61012559	0.17174361	3.55253736	0.00038153	0.00302636	anxa4
ENSXETG00000011221	793.459336	0.60917256	0.17861879	3.41046189	0.00064853	0.00484201	eif2s1
ENSXETG00000011722	1322.2968	0.60129143	0.2023119	2.97210112	0.00295769	0.01768444	hnrnpk
ENSXETG00000004650	5259.52917	0.60091271	0.21348131	2.81482585	0.00488037	0.02677322	pdia3
ENSXETG00000040159	113.805995	0.59785333	0.23265073	2.56974624	0.0101773	0.04902971	snx17
ENSXETG00000007193	703.651845	0.59572871	0.17669646	3.37148082	0.00074765	0.00549872	ccdc22
ENSXETG00000013436	53637.724	0.59240916	0.17475752	3.38989231	0.0006992	0.00518593	ybx1
ENSXETG00000011010	428.992823	0.58800709	0.22449407	2.61925446	0.00881222	0.04345725	psme3ip1
ENSXETG00000026867	1431.4774	0.5755162	0.22270394	2.58422101	0.00975992	0.04737485	eif6
ENSXETG00000004144	498.712565	0.57162092	0.22045107	2.5929605	0.00951537	0.04631617	nipa2
ENSXETG00000023043	3808.55497	0.57089269	0.16953798	3.36734385	0.00075896	0.00556112	snd1
ENSXETG00000024453	840.113294	0.56642172	0.18280301	3.09853609	0.00194479	0.0123846	sympk
ENSXETG00000020686	1088.92068	0.55654086	0.20732231	2.68442346	0.0072655	0.03717908	nudc
ENSXETG00000012980	915.845852	0.55637062	0.18701151	2.97506087	0.0029293	0.01754714	mesd
ENSXETG00000016775	834.466675	0.55379923	0.2113661	2.62009483	0.00879053	0.04339103	fgfr1
ENSXETG00000022434	410.200447	0.55269918	0.21299163	2.5949338	0.00946091	0.04613659	plrg1
ENSXETG00000016744	1317.48099	0.53778267	0.17553853	3.06361605	0.00218679	0.01369331	prkcsh
ENSXETG00000009465	290.188666	0.52949631	0.16868608	3.13894491	0.00169557	0.01106756	cnnm3
ENSXETG00000017135	691.102379	0.52599295	0.16707925	3.14816445	0.00164299	0.01078517	fat1
ENSXETG00000002902	1038.43191	0.52285096	0.17106837	3.05638596	0.00224023	0.01398439	paf1
ENSXETG00000011623	485.215609	0.52042647	0.19283516	2.69881525	0.00695868	0.0359357	tyk2
ENSXETG00000036348	365.066087	0.51518874	0.18750804	2.74755548	0.00600413	0.03175543	
ENSXETG00000019265	864.152398	0.51452688	0.18465335	2.78644756	0.00532892	0.02872407	supt6h
ENSXETG00000026007	383.910947	0.51069701	0.18606124	2.7447792	0.00605516	0.03200383	slc25a24
ENSXETG00000014538	1057.46707	0.51009366	0.17733763	2.87639837	0.00402242	0.02284588	adss2
ENSXETG00000002496	1364.00487	0.49938307	0.18448457	2.70690968	0.00679127	0.03522121	neu1
ENSXETG00000010731	863.06565	0.49638386	0.17888378	2.77489594	0.00552194	0.02963271	rps6kb1

ENSXETG00000019575	566.025975	0.48078651	0.12277463	3.9160087	9.00E-05	0.00084409	tvp23b
ENSXETG00000000776	565.025306	0.47380078	0.16645196	2.84647165	0.00442067	0.02470806	snx5
ENSXETG00000012431	476.223509	0.46768494	0.17855196	2.61932116	0.0088105	0.04345725	cog7
ENSXETG00000007080	163.714906	0.44620073	0.17359139	2.57040823	0.01015787	0.04895971	fam76b
ENSXETG00000006620	1581.07617	0.42490072	0.15741065	2.69931375	0.00694826	0.03589367	mapre1
ENSXETG00000025300	3569.59466	0.41784223	0.15195217	2.74982732	0.00596267	0.03159973	srsf7
ENSXETG00000001291	372.872387	0.3531662	0.12044962	2.93206575	0.00336715	0.01973998	mbtd1

APPENDIX C: Hypochord vs coccyx DEGs across time points.

ensembl_gene_id	baseMean	log2FoldChange	lfcSE	stat	pvalue	padj	External gene_name
ENSXETG00000036957	67.300658	-9.2314744	0.91539741	-10.084663	6.46E-24	1.41E-21	cldn3
ENSXETG00000025296	107.272902	-9.1704097	1.15360493	-7.9493503	1.87E-15	1.05E-13	actn2
ENSXETG00000023427	56.654877	-9.1599693	0.84252338	-10.872065	1.57E-27	6.50E-25	neurod6
ENSXETG00000001343	98.3298692	-9.1422797	0.74944351	-12.198757	3.16E-34	6.22E-31	prdm12
ENSXETG00000014163	298.956718	-9.049459	1.33599138	-6.7735908	1.26E-11	4.11E-10	coch
ENSXETG00000034240	93.2459233	-9.0191364	0.97623849	-9.238661	2.50E-20	2.87E-18	uts2b
ENSXETG00000031321	60.3744212	-8.9897459	0.83679614	-10.743054	6.39E-27	2.24E-24	cacng2
ENSXETG00000002052	51.4706447	-8.7651869	1.10629269	-7.923027	2.32E-15	1.29E-13	chodl
ENSXETG00000026873	76.9177596	-8.7109514	1.04632673	-8.3252689	8.41E-17	5.77E-15	trpm8
ENSXETG00000016503	56.4835353	-8.6749902	0.82948229	-10.458319	1.34E-25	3.85E-23	apba2
ENSXETG00000022933	79.7142449	-8.6133224	0.70922976	-12.144615	6.13E-34	9.66E-31	grin1
ENSXETG00000031473	466.644299	-8.5608363	0.76285713	-11.22207	3.18E-29	1.62E-26	
ENSXETG00000002106	39.9922769	-8.5049833	1.06936097	-7.9533324	1.82E-15	1.03E-13	cdh10
ENSXETG00000013277	74.956003	-8.4686481	0.806128	-10.505339	8.16E-26	2.43E-23	GRIK2
ENSXETG00000036319	72.3980829	-8.4252983	1.09170766	-7.7175407	1.19E-14	5.97E-13	
ENSXETG00000039335	34.1560441	-8.3935681	1.60913964	-5.2161838	1.83E-07	3.02E-06	btbd17
ENSXETG00000016588	172.249552	-8.3811753	0.67959205	-12.332657	6.04E-35	1.36E-31	acsl6
ENSXETG00000036131	77.7434483	-8.3704849	1.37996584	-6.0657189	1.31E-09	3.19E-08	
ENSXETG00000033877	107.395058	-8.3549404	0.90385167	-9.2437074	2.38E-20	2.76E-18	plppr1
ENSXETG00000017087	156.561404	-8.326654	0.94591353	-8.8027644	1.33E-18	1.20E-16	tnni1
ENSXETG00000031870	41.1106891	-8.300964	0.78337294	-10.59644	3.10E-26	9.57E-24	
ENSXETG00000032275	232.869845	-8.300314	0.85227831	-9.7389712	2.06E-22	3.52E-20	
ENSXETG00000035258	37.4481903	-8.287008	0.77089393	-10.749868	5.93E-27	2.13E-24	TAFA4
ENSXETG00000036709	605.540272	-8.2709612	0.6896834	-11.992403	3.89E-33	4.72E-30	hpcal4
ENSXETG00000013542	78.3873361	-8.2419078	0.83483847	-9.872458	5.48E-23	1.03E-20	kcnn1
ENSXETG00000004033	33.6003453	-8.2337066	0.8200789	-10.04014	1.02E-23	2.08E-21	ndst3
ENSXETG00000030987	29.495152	-8.1944553	0.97278238	-8.4237291	3.65E-17	2.62E-15	sp9
ENSXETG00000011460	207.379457	-8.1795343	0.94833645	-8.6251396	6.40E-18	5.23E-16	ADGRD2
ENSXETG00000021651	53.6649194	-8.1579179	0.92988545	-8.7730353	1.74E-18	1.52E-16	nkain3
ENSXETG00000021737	71.570467	-8.1170733	0.75759771	-10.714226	8.73E-27	2.99E-24	astn2
ENSXETG00000040495	26.6718479	-8.1115161	0.87401481	-9.2807536	1.68E-20	1.99E-18	
ENSXETG00000011604	126.617492	-8.1097817	0.76996753	-10.532628	6.11E-26	1.85E-23	ppp2r2c
ENSXETG00000010546	45.4060364	-8.1063574	0.77650203	-10.439583	1.64E-25	4.52E-23	gfra2
ENSXETG00000001272	38.2647558	-8.1040933	0.76152977	-10.64186	1.90E-26	6.11E-24	pax8

ENSXETG00000008421	57.8891288	-8.1025405	1.02970946	-7.8687638	3.58E-15	1.97E-13	gabra2
ENSXETG00000005637	76.313616	-8.0937287	0.74492547	-10.865152	1.69E-27	6.83E-25	nrg3
ENSXETG00000011467	56.3789075	-8.071377	0.807625	-9.9939662	1.62E-23	3.23E-21	rph3a
ENSXETG00000014607	255.357189	-8.0487422	0.81186806	-9.9138549	3.62E-23	6.88E-21	calb1
ENSXETG00000034611	41.0671547	-8.0425818	0.88738611	-9.063227	1.27E-19	1.33E-17	RBFOX1
ENSXETG00000024458	43.1032182	-8.024764	0.79012616	-10.156307	3.11E-24	6.99E-22	zic3
ENSXETG00000001552	43.4042213	-8.0013014	1.11078068	-7.2033134	5.88E-13	2.29E-11	lingo2
ENSXETG00000008633	39.2990842	-7.9949643	0.96409777	-8.2926904	1.11E-16	7.39E-15	mcoln3
ENSXETG00000011683	430.351786	-7.9444144	0.84503283	-9.4013085	5.39E-21	6.96E-19	myl2
ENSXETG00000014328	33.9448812	-7.929918	0.7710728	-10.284266	8.30E-25	2.01E-22	ncan
ENSXETG00000003199	330.42169	-7.9289619	0.90057817	-8.8043017	1.32E-18	1.19E-16	tnnt1
ENSXETG00000018917	134.339382	-7.9160407	0.76941812	-10.288347	7.95E-25	1.96E-22	gabbr2
ENSXETG00000018386	53.8065499	-7.9157884	0.71893029	-11.010509	3.40E-28	1.53E-25	pou4f1.2
ENSXETG00000021492	43.3336524	-7.8967211	0.87828865	-8.9910317	2.45E-19	2.49E-17	lrfn5
ENSXETG00000022614	102.634303	-7.8938476	0.67507297	-11.693325	1.38E-31	1.09E-28	epcam
ENSXETG00000006349	32.1510427	-7.8932107	0.76522731	-10.314858	6.04E-25	1.51E-22	onecut1
ENSXETG00000036577	76.399271	-7.8891	0.91969747	-8.5779294	9.66E-18	7.81E-16	
ENSXETG00000011196	165.809871	-7.8846674	0.68680413	-11.480227	1.66E-30	1.09E-27	tmem59l
ENSXETG00000015711	88.3249725	-7.8822613	0.66064909	-11.931086	8.15E-33	8.56E-30	grm7
ENSXETG00000022063	41.3174959	-7.8776765	0.71180846	-11.06713	1.81E-28	8.65E-26	galnt14
ENSXETG00000013830	182.098119	-7.8742175	0.71374133	-11.032313	2.67E-28	1.24E-25	plcd4
ENSXETG00000001966	45.724763	-7.8691161	0.95680603	-8.2243588	1.96E-16	1.26E-14	glra1
ENSXETG00000011804	113.679239	-7.8617247	0.95191814	-8.2588244	1.47E-16	9.54E-15	grik1
ENSXETG00000032850	41.7142476	-7.8376136	0.82132437	-9.5426531	1.39E-21	2.07E-19	lrrn3
ENSXETG00000004192	23.370467	-7.8356702	0.77800582	-10.07148	7.39E-24	1.57E-21	kcnk18
ENSXETG00000005275	38.3276107	-7.8271805	1.00043288	-7.8237938	5.13E-15	2.76E-13	myom3
ENSXETG00000032143	25.506157	-7.8268368	1.02736	-7.6183975	2.57E-14	1.24E-12	
ENSXETG00000014530	34.5764471	-7.8260127	0.92545493	-8.4563953	2.76E-17	2.06E-15	mlc1
ENSXETG00000031266	24.2936504	-7.8201172	1.06969848	-7.3105808	2.66E-13	1.12E-11	CCDC106
ENSXETG00000021153	192.601587	-7.7876194	0.8251954	-9.4373034	3.82E-21	5.11E-19	grp
ENSXETG00000037436	29.833324	-7.7829343	0.9108328	-8.5448551	1.29E-17	1.01E-15	NECAB2
ENSXETG00000037882	41.329665	-7.7813343	1.56574823	-4.9697225	6.70E-07	1.01E-05	
ENSXETG00000002027	27.7142327	-7.7795976	1.06643936	-7.2949273	2.99E-13	1.25E-11	kcnc4
ENSXETG00000010125	29.8641234	-7.7695221	1.00393295	-7.7390846	1.00E-14	5.16E-13	tmprss13
ENSXETG00000005309	84.8048845	-7.7673463	0.70697235	-10.986775	4.42E-28	1.88E-25	lrfn1.1
ENSXETG00000010874	28.5789208	-7.7612439	0.81806666	-9.4873001	2.37E-21	3.28E-19	cntnap4
ENSXETG00000033774	80.8137619	-7.751616	0.88219192	-8.7867683	1.54E-18	1.37E-16	
ENSXETG00000041159	27.1609795	-7.7448099	0.87469993	-8.8542478	8.43E-19	8.05E-17	PIRT
ENSXETG00000004157	35.8330883	-7.737896	1.66208621	-4.6555323	3.23E-06	4.27E-05	oca2

ENSXETG00000037936	34.8987384	-7.7036858	0.79326817	-9.711326	2.70E-22	4.52E-20	TMEM200C
ENSXETG00000034937	1731.92335	-7.7030321	0.82378117	-9.3508232	8.70E-21	1.07E-18	
ENSXETG00000032005	24.2841616	-7.6996367	1.00615022	-7.6525717	1.97E-14	9.70E-13	GRXCR2
ENSXETG00000012238	31.2900924	-7.6736134	0.86937165	-8.8266203	1.08E-18	1.00E-16	cdh18
ENSXETG00000013082	41.4248954	-7.6626621	1.06028751	-7.2269663	4.94E-13	1.95E-11	nppb
ENSXETG00000015475	375.659616	-7.6359537	0.85587589	-8.9218003	4.59E-19	4.49E-17	zic4
ENSXETG00000007311	60.2223392	-7.6305545	0.86905666	-8.7802727	1.63E-18	1.44E-16	camkv
ENSXETG00000001296	20.9526233	-7.6206552	1.12004849	-6.8038619	1.02E-11	3.38E-10	ca10
ENSXETG00000003290	22.8983247	-7.6179561	0.8385755	-9.084401	1.04E-19	1.12E-17	gbx2.1
ENSXETG00000005518	101.996199	-7.617337	0.62721309	-12.144736	6.12E-34	9.66E-31	mtus2
ENSXETG00000013880	79.2548428	-7.6162731	0.73060803	-10.424568	1.92E-25	5.20E-23	reep2
ENSXETG00000002648	37.4234656	-7.6151562	0.77480197	-9.8285194	8.49E-23	1.54E-20	myo16
ENSXETG00000014601	82.3519393	-7.6038934	0.71464329	-10.640124	1.94E-26	6.11E-24	necab1
ENSXETG00000000190	280.577888	-7.5968892	0.75238457	-10.097083	5.69E-24	1.26E-21	tusc3
ENSXETG00000021820	35.9169616	-7.5931196	0.90975487	-8.3463358	7.04E-17	4.91E-15	pcyt1b
ENSXETG00000008423	39.7204148	-7.59262	1.01968633	-7.446035	9.62E-14	4.41E-12	cnih2
ENSXETG00000014206	33.4961523	-7.5809973	1.02752283	-7.3779356	1.61E-13	7.06E-12	pax2
ENSXETG00000012527	202.08389	-7.5540173	0.50062332	-15.089224	1.91E-51	3.01E-47	nmnat2
ENSXETG00000011749	150.157978	-7.5306397	0.53765899	-14.00635	1.43E-44	1.12E-40	adgrb3
ENSXETG00000025552	58.393956	-7.5283248	0.7796939	-9.6554876	4.66E-22	7.49E-20	trarg1
ENSXETG00000026517	22.1055839	-7.5235355	1.06372013	-7.0728524	1.52E-12	5.62E-11	gad2
ENSXETG00000019150	60.8554438	-7.519457	0.70464159	-10.671322	1.39E-26	4.55E-24	adgrb1
ENSXETG00000007969	36.028683	-7.5105109	1.20008641	-6.2583084	3.89E-10	1.02E-08	cyb5r1
ENSXETG00000021158	47.6355804	-7.5021673	0.65409431	-11.46955	1.88E-30	1.18E-27	pnoc
ENSXETG00000039048	46.6243062	-7.5013135	0.76173625	-9.8476519	7.02E-23	1.29E-20	cdk5r2
ENSXETG00000017780	188.515776	-7.4999708	0.8107431	-9.2507365	2.23E-20	2.60E-18	fez1
ENSXETG00000037805	49.2597361	-7.4867884	0.98488039	-7.6017234	2.92E-14	1.40E-12	
ENSXETG00000012950	25.8424207	-7.4821312	0.98606574	-7.5878624	3.25E-14	1.54E-12	cbln1
ENSXETG00000031391	55.8100111	-7.4772683	0.94074159	-7.9482701	1.89E-15	1.06E-13	
ENSXETG00000036810	134.884266	-7.4772056	0.79544214	-9.4000622	5.45E-21	6.99E-19	gpm6a
ENSXETG00000041393	66.4380644	-7.473479	0.71255598	-10.488269	9.78E-26	2.85E-23	cacnb3
ENSXETG00000020429	902.84034	-7.4688541	0.6929462	-10.778404	4.35E-27	1.60E-24	krt61
ENSXETG00000031739	262.281657	-7.4674918	0.62513075	-11.945488	6.85E-33	7.72E-30	ANO4
ENSXETG00000037146	82.5802944	-7.457029	0.62737606	-11.886059	1.40E-32	1.22E-29	mab21l2
ENSXETG00000002998	17.9893277	-7.4520973	0.96259748	-7.7416547	9.81E-15	5.07E-13	erich3
ENSXETG00000031348	29.0496559	-7.4504007	1.0831447	-6.8784906	6.05E-12	2.06E-10	hes6.2
ENSXETG00000037502	40.8086404	-7.4480637	0.72067427	-10.334855	4.90E-25	1.27E-22	ARMH4
ENSXETG00000010109	27.9340363	-7.4446255	0.91647297	-8.123126	4.54E-16	2.78E-14	galnt17
ENSXETG00000009478	360.402204	-7.4362336	0.56836594	-13.083531	4.09E-39	1.85E-35	ina

ENSXETG00000025405	39.2971894	-7.4329839	0.83775127	-8.8725427	7.15E-19	6.87E-17	INSYN2B
ENSXETG00000038446	4042.97087	-7.4218263	0.67010094	-11.075684	1.65E-28	8.11E-26	
ENSXETG00000001502	169.939675	-7.398894	0.61555256	-12.019922	2.79E-33	3.67E-30	cyfip2
ENSXETG00000003508	30.2799503	-7.3955615	0.81566278	-9.0669351	1.22E-19	1.29E-17	kcnf1
ENSXETG00000012196	27.7606574	-7.3915755	0.97426283	-7.5868393	3.28E-14	1.55E-12	slc26a4.3
ENSXETG00000037070	8779.09503	-7.3799733	0.76068089	-9.7017993	2.96E-22	4.86E-20	
ENSXETG00000028976	20.7081667	-7.3770866	0.83581184	-8.8262529	1.08E-18	1.00E-16	xtr-mir-9a-1
ENSXETG00000035593	23.6716827	-7.3680896	0.70852574	-10.399184	2.50E-25	6.68E-23	
ENSXETG00000010044	219.013553	-7.3598867	0.6376869	-11.541537	8.15E-31	5.58E-28	cacng7
ENSXETG00000002703	15.7720085	-7.3504043	0.83344248	-8.81933	1.15E-18	1.06E-16	pcdhgc4
ENSXETG00000041083	91.7939975	-7.3400372	0.74418324	-9.8632122	6.01E-23	1.11E-20	nppc
ENSXETG00000004012	24.7097144	-7.3383101	0.64905743	-11.306103	1.22E-29	6.65E-27	mogat2.1
ENSXETG00000003242	1240.16196	-7.3299364	0.72049917	-10.173414	2.61E-24	5.95E-22	myl4
ENSXETG00000016861	362.363835	-7.3134721	0.59010858	-12.393435	2.84E-35	7.45E-32	cbln2
ENSXETG00000019933	292.06157	-7.3014511	0.75693549	-9.6460679	5.11E-22	8.13E-20	c1qtnf4
ENSXETG00000024035	20.1417235	-7.2917073	0.90200106	-8.0839232	6.27E-16	3.79E-14	nptx2
ENSXETG00000022354	79.3714965	-7.2819845	0.87875841	-8.2866741	1.16E-16	7.74E-15	nos1
ENSXETG00000015086	155.610466	-7.2785844	0.67169348	-10.83617	2.32E-27	8.92E-25	lamp5
ENSXETG00000002168	14.5966775	-7.2769162	1.02878015	-7.0733443	1.51E-12	5.61E-11	epha10
ENSXETG00000023020	17.631651	-7.2715158	1.08130535	-6.7247571	1.76E-11	5.63E-10	ephx4
ENSXETG00000018182	135.088552	-7.2640942	0.6251994	-11.618844	3.31E-31	2.48E-28	ocln
ENSXETG00000011970	18.1204484	-7.2555961	0.75458559	-9.6153389	6.89E-22	1.07E-19	dtx4
ENSXETG00000039626	18.0742177	-7.2520383	1.48080936	-4.8973477	9.71E-07	1.42E-05	NXPH1
ENSXETG00000036701	14.6424443	-7.2511101	1.05841585	-6.8509085	7.34E-12	2.48E-10	neurod2
ENSXETG00000024787	20.5709988	-7.2407917	1.14983852	-6.2972248	3.03E-10	8.14E-09	htr2c
ENSXETG00000033967	67.130937	-7.2301837	0.99641122	-7.2562247	3.98E-13	1.62E-11	slc18a3
ENSXETG00000035236	15.3541111	-7.2091723	1.37765291	-5.232938	1.67E-07	2.78E-06	RGS8
ENSXETG00000027906	14.0179035	-7.2037059	1.3230767	-5.4446624	5.19E-08	9.57E-07	vip
ENSXETG00000014758	32.5489645	-7.202365	0.82526698	-8.7273151	2.61E-18	2.22E-16	dner
ENSXETG00000040461	16.6924229	-7.1934951	0.97479822	-7.3794709	1.59E-13	7.00E-12	
ENSXETG00000034866	694.556602	-7.1801296	0.61824089	-11.613806	3.51E-31	2.51E-28	cplx1
ENSXETG00000018003	16.439926	-7.1561446	1.13725309	-6.292482	3.12E-10	8.32E-09	
ENSXETG00000027998	46.1159706	-7.1482102	0.91812475	-7.7856633	6.93E-15	3.67E-13	prss8
ENSXETG00000020390	25.1656685	-7.1452727	0.76339937	-9.3598095	7.99E-21	9.91E-19	dnajc6
ENSXETG00000021372	37.2316086	-7.1349495	0.73847368	-9.6617518	4.38E-22	7.12E-20	slc6a15
ENSXETG00000038746	20.1492159	-7.1325799	0.97278051	-7.3321574	2.26E-13	9.70E-12	pou3f2
ENSXETG00000015025	64.8236198	-7.1325118	0.68311652	-10.441135	1.61E-25	4.52E-23	susd4
ENSXETG00000021408	43.4509065	-7.1307954	0.74570539	-9.5624833	1.15E-21	1.74E-19	dnah5
ENSXETG00000038478	469.183351	-7.126195	0.56139502	-12.693727	6.41E-37	2.02E-33	

ENSXETG00000003692	13.4903488	-7.1203804	1.06852091	-6.6637727	2.67E-11	8.43E-10	man1c1
ENSXETG00000039800	32.8440531	-7.1161508	0.92087843	-7.7275681	1.10E-14	5.59E-13	
ENSXETG00000030265	21.9063585	-7.1160976	0.93823584	-7.584551	3.34E-14	1.57E-12	mchr1.2
ENSXETG00000027748	22.2479566	-7.1060096	0.77161414	-9.2092786	3.28E-20	3.75E-18	cyp26c1
ENSXETG00000034502	76.0631074	-7.1004652	0.900396	-7.885936	3.12E-15	1.73E-13	SYNDIG1
ENSXETG00000010566	25.7336619	-7.0822128	0.96499587	-7.339112	2.15E-13	9.28E-12	ndst4
ENSXETG00000017098	15.4254972	-7.0788528	0.97485739	-7.2614239	3.83E-13	1.57E-11	cpne9
ENSXETG00000023224	30.6573135	-7.0751545	1.02318165	-6.9148568	4.68E-12	1.62E-10	gabrg2
ENSXETG00000031786	2214.1942	-7.0640954	0.59427947	-11.886824	1.39E-32	1.22E-29	vsnl1
ENSXETG00000000351	200.533463	-7.0548444	0.61545872	-11.462742	2.03E-30	1.23E-27	epdr1
ENSXETG00000039137	335.165688	-7.053439	0.61654578	-11.440252	2.63E-30	1.54E-27	adcyap1
ENSXETG00000025709	1344.37484	-7.0521693	0.71086088	-9.9206041	3.39E-23	6.51E-21	tac1
ENSXETG00000011917	14.9703205	-7.0468857	1.07636657	-6.5469199	5.87E-11	1.76E-09	gabrb2
ENSXETG00000035719	24.3668353	-7.0462847	0.77617651	-9.0781988	1.10E-19	1.18E-17	OTP
ENSXETG00000016154	21.3911027	-7.0390555	0.74770517	-9.4142127	4.77E-21	6.21E-19	inpp5j
ENSXETG00000032202	34.8915548	-7.0329387	1.13771664	-6.1816259	6.34E-10	1.63E-08	TRHDE
ENSXETG00000023298	12.431335	-7.0021991	1.0643657	-6.578753	4.74E-11	1.44E-09	clvs2
ENSXETG00000039228	12.8333878	-6.996968	0.96786735	-7.2292634	4.86E-13	1.93E-11	GPR101
ENSXETG00000039114	15.2364278	-6.9917336	0.84030555	-8.3204658	8.76E-17	5.97E-15	
ENSXETG00000006011	46.9136375	-6.9863565	0.73407897	-9.517173	1.78E-21	2.50E-19	slc45a1
ENSXETG00000027983	71.8443105	-6.9846844	0.84692114	-8.2471486	1.62E-16	1.05E-14	myt1l
ENSXETG00000020336	26.8754516	-6.9845224	0.99744218	-7.0024334	2.52E-12	9.09E-11	prom1
ENSXETG00000030525	20.2435702	-6.9844631	0.82514626	-8.4645153	2.57E-17	1.94E-15	
ENSXETG00000036446	12.0588156	-6.9824089	0.85931245	-8.1255763	4.45E-16	2.74E-14	ABCD2
ENSXETG00000007649	30.8247243	-6.980254	0.90065988	-7.7501554	9.18E-15	4.76E-13	c11orf87
ENSXETG00000027302	12.3485419	-6.9694697	1.1649318	-5.9827277	2.19E-09	5.14E-08	gabra5
ENSXETG00000016434	46.7270033	-6.9605006	0.76424611	-9.1076689	8.42E-20	9.09E-18	TENM2
ENSXETG00000040550	19.6279023	-6.9538842	0.94938772	-7.3245989	2.40E-13	1.02E-11	rnf182
ENSXETG00000009640	14.7251928	-6.9528636	0.90082465	-7.7183319	1.18E-14	5.95E-13	prrg3
ENSXETG00000011510	128.983167	-6.9488184	1.03874513	-6.6896279	2.24E-11	7.10E-10	pou3f1
ENSXETG00000030030	65.3325369	-6.9410301	0.87042023	-7.9743437	1.53E-15	8.75E-14	KCTD16
ENSXETG00000019539	19.9425937	-6.9405854	0.74229253	-9.3502025	8.75E-21	1.07E-18	cfap52
ENSXETG00000036107	12.3329717	-6.9363727	1.04036677	-6.6672378	2.61E-11	8.25E-10	
ENSXETG00000015467	151.821406	-6.9278276	0.91209443	-7.5955158	3.07E-14	1.46E-12	zic1
ENSXETG00000007532	15.0367109	-6.9210013	0.81059343	-8.5381908	1.36E-17	1.07E-15	dlx2
ENSXETG00000007892	22.8906139	-6.9172114	0.97872059	-7.0676059	1.58E-12	5.82E-11	grm1
ENSXETG00000035498	48.3723794	-6.9108374	0.98710907	-7.0010879	2.54E-12	9.16E-11	
ENSXETG00000005053	13.7762971	-6.9072853	0.98542423	-7.0094534	2.39E-12	8.71E-11	dgkb
ENSXETG00000030377	47.4115152	-6.9021442	0.92734183	-7.4429341	9.85E-14	4.49E-12	

ENSXETG00000010250	82.9943165	-6.9010727	0.88695225	-7.7806587	7.21E-15	3.79E-13	chrnb3
ENSXETG00000018872	12.5998966	-6.9008282	0.83074532	-8.3067916	9.83E-17	6.62E-15	zic5
ENSXETG00000017814	17.2439962	-6.8929399	0.7823004	-8.8111164	1.24E-18	1.12E-16	pou4f1
ENSXETG00000030958	15.3168304	-6.8925333	0.99227964	-6.9461601	3.75E-12	1.33E-10	kcnh5
ENSXETG00000016741	83.8346718	-6.884787	0.87889954	-7.8334175	4.75E-15	2.57E-13	elavl3
ENSXETG00000030389	394.967191	-6.882517	0.73946925	-9.3073741	1.31E-20	1.58E-18	MYH7
ENSXETG00000018304	113.246945	-6.8727558	0.7799592	-8.8116863	1.23E-18	1.12E-16	tlx3
ENSXETG00000001772	22.3480878	-6.865367	0.78915563	-8.6996363	3.33E-18	2.81E-16	gdap1l1
ENSXETG00000002554	11.0268374	-6.864305	1.09089943	-6.2923353	3.13E-10	8.32E-09	rxfp3
ENSXETG00000036821	131.667068	-6.8633618	0.67070638	-10.233035	1.41E-24	3.32E-22	
ENSXETG00000005641	32.4760603	-6.863061	0.95047318	-7.2206782	5.17E-13	2.03E-11	sgcz
ENSXETG00000032843	102.269151	-6.8622086	0.90056806	-7.6198668	2.54E-14	1.23E-12	TENM1
ENSXETG00000040826	12.2898506	-6.853943	0.98687871	-6.9450713	3.78E-12	1.34E-10	
ENSXETG00000022966	12.4998819	-6.8530132	0.96416279	-7.1077346	1.18E-12	4.46E-11	
ENSXETG00000017865	17.2407531	-6.8421921	0.94951817	-7.2059623	5.76E-13	2.25E-11	cpne5
ENSXETG00000018631	14.6453579	-6.8384308	0.76829586	-8.9007779	5.55E-19	5.36E-17	nxph3
ENSXETG00000005443	16.63553	-6.82336	0.98613422	-6.9193015	4.54E-12	1.58E-10	jakmip3
ENSXETG00000006793	51.6173348	-6.8232673	0.83087363	-8.2121601	2.17E-16	1.39E-14	pdzrn4
ENSXETG00000007222	61.1298591	-6.8132116	0.96560965	-7.0558653	1.72E-12	6.32E-11	tex2.1
ENSXETG00000015084	28.0986435	-6.8090068	1.04071934	-6.5425965	6.05E-11	1.81E-09	nexmif
ENSXETG00000038978	88.4393814	-6.8060663	0.9427719	-7.2192078	5.23E-13	2.05E-11	rab3a
ENSXETG00000014068	10.5240734	-6.8042813	0.81307407	-8.3685873	5.83E-17	4.14E-15	neurod1
ENSXETG00000036204	13.261865	-6.8025734	1.07541886	-6.3255105	2.52E-10	6.81E-09	
ENSXETG00000019626	20.0018599	-6.7964067	0.77029424	-8.8231306	1.11E-18	1.03E-16	pah
ENSXETG00000022648	85.4346089	-6.7958724	0.71667881	-9.482452	2.48E-21	3.40E-19	cdh24
ENSXETG00000037469	11.5108755	-6.7943364	1.01264509	-6.7094942	1.95E-11	6.22E-10	ttc9b
ENSXETG00000002245	21.6931285	-6.7838614	0.84128863	-8.0636551	7.40E-16	4.42E-14	frmpd1
ENSXETG00000000355	12.4239554	-6.7805283	1.21308538	-5.5894898	2.28E-08	4.46E-07	cck
ENSXETG00000009175	19.1641769	-6.7730529	0.9794919	-6.9148636	4.68E-12	1.62E-10	astn1
ENSXETG00000003826	13.0638243	-6.770393	1.33698626	-5.0639211	4.11E-07	6.47E-06	wnt8a
ENSXETG00000004451	29.1820304	-6.7677502	0.8725361	-7.7564128	8.74E-15	4.54E-13	khdrbs2
ENSXETG00000036844	67.1185748	-6.7648779	0.88522934	-7.6419495	2.14E-14	1.05E-12	
ENSXETG00000016052	19.0895824	-6.7611964	0.81151086	-8.3316154	7.97E-17	5.51E-15	msx1
ENSXETG00000034752	271.264063	-6.7580614	0.65160924	-10.371341	3.35E-25	8.79E-23	BSN
ENSXETG00000015325	151.578841	-6.7509972	0.80810658	-8.3540926	6.59E-17	4.64E-15	cntn2
ENSXETG00000027648	9736.68413	-6.7415676	0.66975838	-10.065671	7.84E-24	1.62E-21	acbd7
ENSXETG00000041189	14.9511467	-6.7393606	0.90532908	-7.4441004	9.76E-14	4.46E-12	RIMS4
ENSXETG00000022097	11.7592225	-6.7356318	1.17856859	-5.7150953	1.10E-08	2.24E-07	gipc3
ENSXETG00000039327	13.8686323	-6.70267	0.99004361	-6.7700755	1.29E-11	4.18E-10	

ENSXETG00000016085	40.7230868	-6.6866811	0.7459406	-8.9640932	3.13E-19	3.14E-17	grid2ip
ENSXETG00000038849	14.873618	-6.6729843	1.13066585	-5.9018182	3.60E-09	8.12E-08	TMEM229A
ENSXETG00000014693	11.4359692	-6.6705191	0.90311448	-7.386128	1.51E-13	6.67E-12	galr1
ENSXETG00000019260	309.670775	-6.6639398	1.03735482	-6.4239735	1.33E-10	3.76E-09	proca1
ENSXETG00000015457	80.2429092	-6.6452826	0.93845711	-7.0810723	1.43E-12	5.33E-11	slain1
ENSXETG00000038969	10.9140157	-6.643022	1.087922	-6.1061566	1.02E-09	2.54E-08	serp2
ENSXETG00000022081	9.52305658	-6.638006	1.02020189	-6.5065612	7.69E-11	2.27E-09	sema6b

REFERENCES

1. Duellman, W.E. and L. Trueb, *Biology of amphibians*. 1986, New York: McGraw Hill. xvii, 670 p.
2. Li, J.T., et al., *New insights to the molecular phylogenetics and generic assessment in the Rhacophoridae (Amphibia: Anura) based on five nuclear and three mitochondrial genes, with comments on the evolution of reproduction.* Mol Phylogenet Evol, 2009. **53**(2): p. 509-22.
3. Essner, R.L., Jr., et al., *Landing in basal frogs: evidence of saltational patterns in the evolution of anuran locomotion.* Naturwissenschaften, 2010. **97**(10): p. 935-9.
4. Jenkins, F.A. and N.H. Shubin, *An Early Jurassic Jumping Frog the Evolution of the Anuran Pelvis.* Journal of Vertebrate Paleontology, 1995. **15**: p. 38a-38a.
5. Shubin, N.H. and F.A. Jenkins, *An Early Jurassic Jumping Frog.* Nature, 1995. **377**(6544): p. 49-52.
6. Haas, A. and S.J. Richards, *Correlations of cranial morphology, ecology, and evolution in Australian suctorial tadpoles of the genera Litoria and Nyctimystes (Amphibia: Anura: Hylidae: Pelodryadinae).* J Morphol, 1998. **238**(2): p. 109-41.
7. Trueb, L. and J. Hanken, *Skeletal development in Xenopus laevis (Anura: Pipidae).* J Morphol, 1992. **214**(1): p. 1-41.
8. Pugener, L.A. and A.M. Maglia, *Skeletal morphogenesis of the vertebral column of the miniature hylid frog Acris crepitans, with comments on anomalies.* J Morphol, 2009. **270**(1): p. 52-69.
9. Griffiths, I., *The phylogeny of the salientia.* Biol Rev Camb Philos Soc, 1963. **38**(2): p. 241-92.
10. Mookerjee, H.K., *On the Development of the Vertebral Column of Anura.* Philosophical Transactions of the Royal Society of London. Series B, Containing Papers of a Biological Character, 1931. **219**: p. 165-196.

11. Gadow, H., J.F. Gaskell, and H.L. Green, *The evolution of the vertebral column: a contribution to the study of vertebrate phylogeny*. 1933, Cambridge [Eng.]: The University Press. xiv, 355, [1] p.
12. Handrigan, G.R. and R.J. Wassersug, *The anuran Bauplan: a review of the adaptive, developmental, and genetic underpinnings of frog and tadpole morphology.* Biological Reviews, 2007. **82**(1): p. 1-25.
13. Lofberg, J. and A. Collazo, *Hypochord, an enigmatic embryonic structure: study of the axolotl embryo.* J Morphol, 1997. **232**(1): p. 57-66.
14. Cleaver, O., D.W. Seufert, and P.A. Krieg, *Endoderm patterning by the notochord: development of the hypochord in Xenopus.* Development, 2000. **127**(4): p. 869-79.
15. Eriksson, J. and J. Lofberg, *Development of the hypochord and dorsal aorta in the zebrafish embryo (Danio rerio).* J Morphol, 2000. **244**(3): p. 167-76.
16. Cleaver, O. and P.A. Krieg, *VEGF mediates angioblast migration during development of the dorsal aorta in Xenopus.* Development, 1998. **125**(19): p. 3905-14.
17. Cleaver, O., et al., *Neovascularization of the Xenopus embryo.* Dev Dyn, 1997. **210**(1): p. 66-77.
18. Warga, R.M. and C. Nusslein-Volhard, *Origin and development of the zebrafish endoderm.* Development, 1999. **126**(4): p. 827-38.
19. Melby, A.E., R.M. Warga, and C.B. Kimmel, *Specification of cell fates at the dorsal margin of the zebrafish gastrula.* Development, 1996. **122**(7): p. 2225-37.
20. Shook, D.R., C. Majer, and R. Keller, *Pattern and morphogenesis of presumptive superficial mesoderm in two closely related species, Xenopus laevis and Xenopus tropicalis.* Dev Biol, 2004. **270**(1): p. 163-85.
21. Meegaskumbura, M., et al., *Diversification of shrub frogs (Rhacophoridae, Pseudophilautus) in Sri Lanka - Timing and geographic context.* Mol Phylogenet Evol, 2019. **132**: p. 14-24.
22. Meegaskumbura, M., et al., *Sri Lanka: an amphibian hot spot.* Science, 2002. **298**(5592): p. 379.
23. Brown, D.D., *The role of deiodinases in amphibian metamorphosis.* Thyroid, 2005. **15**(8): p. 815-21.
24. Brown, D.D. and L. Cai, *Amphibian metamorphosis.* Dev Biol, 2007. **306**(1): p. 20-33.

25. Mukhi, S., M.E. Horb, and D.D. Brown, *Remodeling of insulin producing beta-cells during Xenopus laevis metamorphosis.* Dev Biol, 2009. **328**(2): p. 384-91.
26. Shi, Y.-B., *Amphibian metamorphosis : from morphology to molecular biology*. 2000, New York: Wiley-Liss. xiv, 288 p.
27. Laudet, V., *The origins and evolution of vertebrate metamorphosis.* Curr Biol, 2011. **21**(18): p. R726-37.
28. Barnes, M.D. and K.E. Alley, *Maturation and recycling of trigeminal motoneurons in anuran larvae.* J Comp Neurol, 1983. **218**(4): p. 406-14.
29. Schreiber, A.M., L. Cai, and D.D. Brown, *Remodeling of the intestine during metamorphosis of Xenopus laevis.* Proc Natl Acad Sci U S A, 2005. **102**(10): p. 3720-5.
30. Weaver, M. and M.A. Krasnow, *Dual origin of tissue-specific progenitor cells in Drosophila tracheal remodeling.* Science, 2008. **321**(5895): p. 1496-9.
31. Buchholtz, E.A., *Modular evolution of the Cetacean vertebral column.* Evol Dev, 2007. **9**(3): p. 278-89.
32. Buchholz, D.R., *Xenopus metamorphosis as a model to study thyroid hormone receptor function during vertebrate developmental transitions.* Mol Cell Endocrinol, 2017. **459**: p. 64-70.
33. Buchholz, D.R., et al., *A dominant-negative thyroid hormone receptor blocks amphibian metamorphosis by retaining corepressors at target genes.* Mol Cell Biol, 2003. **23**(19): p. 6750-8.
34. Buchholz, D.R., et al., *Molecular and developmental analyses of thyroid hormone receptor function in Xenopus laevis, the African clawed frog.* Gen Comp Endocrinol, 2006. **145**(1): p. 1-19.
35. Buchholz, D.R. and Y.B. Shi, *Dual function model revised by thyroid hormone receptor alpha knockout frogs.* Gen Comp Endocrinol, 2018. **265**: p. 214-218.
36. Shi, Y.B. and A. Ishizuya-Oka, *Thyroid hormone regulation of apoptotic tissue remodeling: implications from molecular analysis of amphibian metamorphosis.* Prog Nucleic Acid Res Mol Biol, 2001. **65**: p. 53-100.
37. Shi, Y.B., et al., *Tadpole competence and tissue-specific temporal regulation of amphibian metamorphosis: roles of thyroid hormone and its receptors.* Bioessays, 1996. **18**(5): p. 391-9.

38. Callery, E.M. and R.P. Elinson, *Thyroid hormone-dependent metamorphosis in a direct developing frog.* Proc Natl Acad Sci U S A, 2000. **97**(6): p. 2615-20.
39. Elinson, R.P., B. Remo, and D.D. Brown, *Novel structural elements identified during tail resorption in Xenopus laevis metamorphosis: lessons from tailed frogs.* Dev Biol, 1999. **215**(2): p. 243-52.
40. Maniatis, G.M. and V.M. Ingram, *ERYTHROPOIESIS DURING AMPHIBIAN METAMORPHOSIS : III. Immunochemical Detection of Tadpole and Frog Hemoglobins (Rana catesbeiana) in Single Erythrocytes.* J Cell Biol, 1971. **49**(2): p. 390-404.
41. Furlow, J.D., et al., *A set of novel tadpole specific genes expressed only in the epidermis are down-regulated by thyroid hormone during Xenopus laevis metamorphosis.* Dev Biol, 1997. **182**(2): p. 284-98.
42. Pourquie, O., *Somite formation in the chicken embryo.* Int J Dev Biol, 2018. **62**(1-2-3): p. 57-62.
43. Pillay, L.M., et al., *Somite-Derived Retinoic Acid Regulates Zebrafish Hematopoietic Stem Cell Formation.* PLoS One, 2016. **11**(11): p. e0166040.
44. Saga, Y., *The mechanism of somite formation in mice.* Curr Opin Genet Dev, 2012. **22**(4): p. 331-8.
45. Hester, S.D., et al., *A multi-cell, multi-scale model of vertebrate segmentation and somite formation.* PLoS Comput Biol, 2011. **7**(10): p. e1002155.
46. Sawada, A., et al., *Fgf/MAPK signalling is a crucial positional cue in somite boundary formation.* Development, 2001. **128**(23): p. 4873-80.
47. Kerszberg, M. and L. Wolpert, *A clock and trail model for somite formation, specialization and polarization.* J Theor Biol, 2000. **205**(3): p. 505-10.
48. Hirsinger, E., et al., *Somite formation and patterning.* Int Rev Cytol, 2000. **198**: p. 1-65.
49. Lombardo, A. and J.M. Slack, *Abdominal B-type Hox gene expression in Xenopus laevis.* Mech Dev, 2001. **106**(1-2): p. 191-5.
50. Christen, B., et al., *Regeneration-specific expression pattern of three posterior Hox genes.* Dev Dyn, 2003. **226**(2): p. 349-55.
51. Kielbowna, L., *The formation of somites and early myotomal myogenesis in Xenopus laevis, Bombina variegata and Pelobates fuscus.* J Embryol Exp Morphol, 1981. **64**: p. 295-304.

52. Hamilton, L., *The formation of somites in Xenopus.* J Embryol Exp Morphol, 1969. **22**(2): p. 253-64.
53. Sabillo, A., J. Ramirez, and C.R. Domingo, *Making muscle: Morphogenetic movements and molecular mechanisms of myogenesis in Xenopus laevis.* Semin Cell Dev Biol, 2016. **51**: p. 80-91.
54. Sanchez, R.S. and S.S. Sanchez, *Paraxis is required for somite morphogenesis and differentiation in Xenopus laevis.* Dev Dyn, 2015. **244**(8): p. 973-87.
55. Sanchez, R.S. and S.S. Sanchez, *Characterization of pax1, pax9, and uncx sclerotomal genes during Xenopus laevis embryogenesis.* Dev Dyn, 2013. **242**(5): p. 572-9.
56. Rissi, M., et al., *Zebrafish Radar: a new member of the TGF-beta superfamily defines dorsal regions of the neural plate and the embryonic retina.* Mech Dev, 1995. **49**(3): p. 223-34.
57. Shimeld, S.M. and P.W. Holland, *Vertebrate innovations.* Proc Natl Acad Sci U S A, 2000. **97**(9): p. 4449-52.
58. Erwin, D.H., *Novelty and Innovation in the History of Life.* Curr Biol, 2015. **25**(19): p. R930-40.
59. Erwin, D.H., *A conceptual framework of evolutionary novelty and innovation.* Biol Rev Camb Philos Soc, 2021. **96**(1): p. 1-15.
60. Erwin, D.H., *The topology of evolutionary novelty and innovation in macroevolution.* Philos Trans R Soc Lond B Biol Sci, 2017. **372**(1735).
61. Wagner, G.P. and V.J. Lynch, *Molecular evolution of evolutionary novelties: the vagina and uterus of therian mammals.* J Exp Zool B Mol Dev Evol, 2005. **304**(6): p. 580-92.
62. Wagner, G.P., C. Amemiya, and F. Ruddle, *Hox cluster duplications and the opportunity for evolutionary novelties.* Proc Natl Acad Sci U S A, 2003. **100**(25): p. 14603-6.
63. Wake, D.B. and G. Roth, *Complex organismal functions : integration and evolution in vertebrates : report of the Dahlem Workshop on Complex Organismal Functions--Integration and Evolution in Vertebrates, Berlin 1988, August 28-September 2*. Dahlem workshop reports. 1989, Chichester [England] ; New York: Wiley. xiii, 451 p.
64. Goszczynski, M., *[Role of the germinal layers in formation of the thymus].* Folia Morphol (Warsz), 1953. **4**(4): p. 269-82.

65. Appel, B., et al., *Delta-mediated specification of midline cell fates in zebrafish embryos.* Curr Biol, 1999. **9**(5): p. 247-56.
66. Senevirathne, G., et al., *Ontogeny of the anuran urostyle and the developmental context of evolutionary novelty.* Proc Natl Acad Sci U S A, 2020. **117**(6): p. 3034-3044.
67. Senevirathne, G., et al., *Ontogeny of the anuran urostyle and the developmental context of evolutionary novelty.* Proceedings of the National Academy of Sciences of the United States of America, 2020. **117**(6): p. 3034-3044.
68. Dumont, D.J., et al., *Vascularization of the mouse embryo: a study of flk-1, tek, tie, and vascular endothelial growth factor expression during development.* Dev Dyn, 1995. **203**(1): p. 80-92.
69. Row, R.H., et al., *The zebrafish tailbud contains two independent populations of midline progenitor cells that maintain long-term germ layer plasticity and differentiate in response to local signaling cues.* Development, 2016. **143**(2): p. 244-54.
70. Nieuwkoop, P. and J. Faber, *Normal Table of Xenopus laevis (Daudin) Garland Publishing.* New York, 1994. **252**.
71. Hanken, J. and R. Wassersug, *The visible skeleton.* Functional photography, 1981. **16**(4): p. 22-26.
72. Klymkowsky, M.W. and J. Hanken, *Whole-mount staining of Xenopus and other vertebrates.* Methods in cell biology, 1991. **36**: p. 419-441.
73. Trueb, L., *Bones, frogs, and evolution.* Evolutionary biology of the anurans: contemporary research on major problems, 1973: p. 65-132.
74. Nakai, Y., K. Nakajima, and Y. Yaoita, *Mechanisms of tail resorption during anuran metamorphosis.* Biomolecular concepts, 2017. **8**(3-4): p. 179-183.
75. Denver, R.J., et al., *Thyroid hormone receptor subtype specificity for hormone-dependent neurogenesis in Xenopus laevis.* Developmental biology, 2009. **326**(1): p. 155-168.
76. Harland, R.M., *In situ hybridization: an improved whole-mount method for Xenopus embryos.* Methods Cell Biol., 1991. **36**: p. 685-695.
77. Wake, D., *Aspects of vertebral evolution in the modern Amphibia.* Forma et functio, 1970. **3**(5): p. 33-60.
78. Alarid, E.T., M.T. Preisler-Mashek, and N.M. Solodin, *Thyroid hormone is an inhibitor of estrogen-induced degradation of estrogen receptor-alpha protein: estrogen-dependent*

proteolysis is not essential for receptor transactivation function in the pituitary. Endocrinology, 2003. **144**(8): p. 3469-76.

79. Bassett, J.H. and G.R. Williams, *Role of Thyroid Hormones in Skeletal Development and Bone Maintenance.* Endocr Rev, 2016. **37**(2): p. 135-87.
80. Brown, D.D., et al., *Amphibian metamorphosis: a complex program of gene expression changes controlled by the thyroid hormone.* Recent Prog Horm Res, 1995. **50**: p. 309-15.
81. Hanken, J. and B.K. Hall, *Skull development during anuran metamorphosis. II. Role of thyroid hormone in osteogenesis.* Anatomy and embryology, 1988. **178**(3): p. 219-227.
82. Hanken, J. and C.H. Summers, *Skull development during anuran metamorphosis: III. Role of thyroid hormone in chondrogenesis.* Journal of Experimental Zoology, 1988. **246**(2): p. 156-170.
83. Das, B., et al., *Multiple thyroid hormone-induced muscle growth and death programs during metamorphosis in Xenopus laevis.* Proceedings of the National Academy of Sciences, 2002. **99**(19): p. 12230-12235.
84. Brown, D.D., *The role of thyroid hormone in zebrafish and axolotl development.* Proceedings of the National Academy of Sciences, 1997. **94**(24): p. 13011-13016.
85. Callery, E.M. and R.P. Elinson, *Thyroid hormone-dependent metamorphosis in a direct developing frog.* Proceedings of the National Academy of Sciences, 2000. **97**(6): p. 2615-2620.
86. Marsh-Armstrong, N., L. Cai, and D.D. Brown, *Thyroid hormone controls the development of connections between the spinal cord and limbs during Xenopus laevis metamorphosis.* Proceedings of the National Academy of Sciences, 2004. **101**(1): p. 165-170.
87. Nishikawa, A. and H. Hayashi, *Isoform transition of contractile proteins related to muscle remodeling with an axial gradient during metamorphosis in Xenopus laevis.* Developmental biology, 1994. **165**(1): p. 86-94.
88. Chanoine, C. and S. Hardy, *Xenopus muscle development: from primary to secondary myogenesis.* Developmental dynamics: an official publication of the American Association of Anatomists, 2003. **226**(1): p. 12-23.

89. Shimizu-Nishikawa, K., et al., *Regulation of specific developmental fates of larval-and adult-type muscles during metamorphosis of the frog Xenopus.* Developmental biology, 2002. **251**(1): p. 91-104.
90. Takisawa, A. and Y. Sunaga, *Über die Entwicklung des M. depressor mandibulae bei Anuren im Laufe der Metamorphose.* Okajimas Folia Anatomica Japonica, 1951. **23**(4-5): p. 273-293.
91. Alley, K.E., *Myofiber turnover is used to retrofit frog jaw muscles during metamorphosis.* American journal of anatomy, 1989. **184**(1): p. 1-12.
92. de Jongh, H.J., *Functional morphology of the jaw apparatus of larval and metamorphosing Rana temporaria L*. 1968: Brill Archive.
93. Hanken, J., et al., *Jaw muscle development as evidence for embryonic repatterning in direct-developing frogs.* Proceedings: Biological Sciences, 1997: p. 1349-1354.
94. McDiarmid, R.W. and R. Altig, *Tadpoles: the biology of anuran larvae*. 2000: University of Chicago Press.
95. Nishikawa, K. and R. Wassersug, *Morphology of the caudal spinal cord in Rana (Ranidae) and Xenopus (Pipidae) tadpoles.* Journal of Comparative Neurology, 1988. **269**(2): p. 193-202.
96. Nishikawa, K. and R. Wassersug, *Evolution of spinal nerve number in anuran larvae.* Brain, behavior and evolution, 1989. **33**(1): p. 15-24.
97. Gerber, H.-P., et al., *VEGF couples hypertrophic cartilage remodeling, ossification and angiogenesis during endochondral bone formation.* Nature medicine, 1999. **5**(6): p. 623-628.
98. Yang, L., et al., *Hypertrophic chondrocytes can become osteoblasts and osteocytes in endochondral bone formation.* Proceedings of the National Academy of Sciences, 2014. **111**(33): p. 12097-12102.
99. ZENMYO, M., et al., *Morphological and biochemical evidence for apoptosis in the terminal hypertrophic chondrocytes of the growth plate.* The Journal of pathology, 1996. **180**(4): p. 430-433.
100. Ben-Ami, Y., et al., *Transformation of fetal secondary cartilage into embryonic bone in organ cultures of human mandibular condyles.* Cell and tissue research, 1993. **271**(2): p. 317-322.

101. Durkin, J.F., *Secondary cartilage: A misnomer?* American journal of orthodontics, 1972. **62**(1): p. 15-41.
102. Hall, B.K., *Bones and cartilage: developmental and evolutionary skeletal biology*. 2005: Elsevier.
103. Weiss, A., et al., *Growth and repair of cartilage: organ culture system utilizing chondroprogenitor cells of condylar cartilage in newborn mice.* Journal of bone and mineral research, 1988. **3**(1): p. 93-100.
104. Gosline, W.A., *Functional morphology of the caudal skeleton in teleostean fishes.* Ichthyological Research, 1997. **44**(2): p. 137-141.
105. Bird, N.C. and P.M. Mabee, *Developmental morphology of the axial skeleton of the zebrafish, Danio rerio (Ostariophysi: Cyprinidae).* Developmental dynamics: an official publication of the American Association of Anatomists, 2003. **228**(3): p. 337-357.
106. Hilton, E.J. and G.D. Johnson, *When two equals three: developmental osteology and homology of the caudal skeleton in carangid fishes (Perciformes: Carangidae).* Evolution & development, 2007. **9**(2): p. 178-189.
107. Bensimon-Brito, A., et al., *Vestiges, rudiments and fusion events: the zebrafish caudal fin endoskeleton in an evo-devo perspective.* Evolution & development, 2012. **14**(1): p. 116-127.
108. Schultze, H.P. and G. Arratia, *Reevaluation of the caudal skeleton of some actinopterygian fishes: II. Hiodon, Elops, and Albula.* Journal of Morphology, 1988. **195**(3): p. 257-303.
109. Schultze, H.-P. and G. Arratia, *The composition of the caudal skeleton of teleosts (Actinopterygil: Osteichthyes).* Zoological journal of the Linnean Society, 1989. **97**(3): p. 189-231.
110. Rashid, D.J., et al., *From dinosaurs to birds: a tail of evolution.* EvoDevo, 2014. **5**(1): p. 1-20.
111. Rashid, D.J., et al., *Avian tail ontogeny, pygostyle formation, and interpretation of juvenile Mesozoic specimens.* Scientific reports, 2018. **8**(1): p. 1-12.
112. Maxwell, E.E., *Ossification sequence of the avian order Anseriformes, with comparison to other precocial birds.* Journal of Morphology, 2008. **269**(9): p. 1095-1113.

113. Abitbol, M.M., *Sacral curvature and supine posture.* American journal of physical anthropology, 1989. **80**(3): p. 379-389.
114. Bardeen, C.R., *Studies of the development of the human skeleton.(A). The development of the lumbab, sacbal and coccygeal vertebwe.(B). The cubves and the pbopobtionate regional lengths of the spinal column during the first thbee months of embbyonic developnent.(C). The development of the skeleton of the posterior limb.* American Journal of Anatomy, 1905. **4**(3): p. 265-302.
115. Bar-Maor, J., K. Kesner, and J. Kaftori, *Human tails.* The Journal of bone and joint surgery. British volume, 1980. **62**(4): p. 508-510.
116. Holtzer, H. and S.R. Detwiler, *An experimental analysis of the development of the spinal column. III. Induction of skeletogenous cells.* Journal of Experimental Zoology, 1953. **123**(2): p. 335-369.
117. Strudel, G., * *LINFLUENCE MORPHOGENE DU TUBE NERVEUX SUR LA DIFFERENCIATION DE LA COLONNE VERTEBRALE.* Comptes Rendus des Séances de la Société de Biologie et de ses Filiales, 1953. **147**(1-2): p. 132-133.
118. Ward, L., et al., *The role of the notochord in amniote vertebral column segmentation.* Developmental biology, 2018. **439**(1): p. 3-18.
119. Strudel, G., *L'action morphogène du tube nerveux et de la corde sur la différenciation des vertèbres et des muscles vertébraux chez l'embryon de poulet.* Arch Anat Microsc Morphol Exp, 1955. **44**(3): p. 209-235.
120. Stern, C.D., *Mesoderm induction and development of the embryonic axis in amniotes.* Trends in Genetics, 1992. **8**(5): p. 158-163.
121. Watterson, D., *Problems in the evaluation of psychotherapy.* Bulletin of the Menninger Clinic, 1954. **18**(6): p. 232.
122. Watterson, R.L., *Development of the glycogen body of the chick spinal cord. III. The paired primordia as revealed by glycogen-specific stains.* The Anatomical Record, 1952. **113**(1): p. 29-51.
123. Wassersug, R.J. and D.G. Sperry, *The relationships of locomotion to differential predation on Pseudacris triseriata (Anura: Hylidae).* Ecology, 1977. **58**(4): p. 830-839.
124. Huey, R.B., *Sprint velocity of tadpoles (Bufoboreas) through metamorphosis.* Copeia, 1980. **1980**(3): p. 537-540.

125. Yaoita, Y., *Tail resorption during metamorphosis in Xenopus tadpoles.* Frontiers in endocrinology, 2019. **10**: p. 143.
126. Ascarrunz, E., et al., *Triadobatrachus massinoti, the earliest known lissamphibian (Vertebrata: Tetrapoda) re-examined by μCT scan, and the evolution of trunk length in batrachians.* Contributions to Zoology, 2016. **85**(2): p. 201-234.
127. Evans, S.E. and M. Borsuk-Białynicka, *The early Triassic stem-frog Czatkobatrachus from Poland.* Palaeontologia Polonica, 2009. **65**: p. 79-105.
128. Galis, F. and J.A. Metz, *Evolutionary novelties: the making and breaking of pleiotropic constraints.* Integr Comp Biol, 2007. **47**(3): p. 409-19.
129. Wagner, G.P. and V.J. Lynch, *Evolutionary novelties.* Curr Biol, 2010. **20**(2): p. R48-52.
130. Wagner, G.P., *Evolutionary innovations and novelties: Let us get down to business!* Zoologischer Anzeiger, 2015. **256**: p. 75-81.
131. Shubin, N., C. Tabin, and S. Carroll, *Deep homology and the origins of evolutionary novelty.* Nature, 2009. **457**(7231): p. 818-23.
132. Tarazona, O.A., et al., *The genetic program for cartilage development has deep homology within Bilateria.* Nature, 2016. **533**(7601): p. 86-9.
133. Tschopp, P. and C.J. Tabin, *Deep homology in the age of next-generation sequencing.* Philos Trans R Soc Lond B Biol Sci, 2017. **372**(1713).
134. Branham, A.E. and J.C. List, *Development of the Urostyle during Metamorphosis in 5 Species of Anurans.* Journal of Morphology, 1979. **159**(3): p. 311-329.
135. Kovalenko, E.E. and E.V. Anisimova, *The Structural and Developmental Peculiarities in the Sacral-Urostyle Area of Anura.* Zoologichesky Zhurnal, 1987. **66**(4): p. 557-+.
136. Kovalenko, E.E. and I.G. Danilov, *Diversity of the sacral-urostyle region in the family Bufonidae (Amphibia, Anura). 1. Actual diversity of sacrum in Bufonidae.* Zoologichesky Zhurnal, 2006. **85**(4): p. 500-516.
137. Snell, C.A., *Identifying Ranid urostyle, ilial and anomolous bones from a 15th century London well.* Herpetological Journal, 2015. **25**(4): p. 245-255.
138. Horowitz, M., *Matrix proteins versus cytokines in the regulation of osteoblast function and bone formation.* Calcified Tissue International, 2003. **72**(1): p. 5-7.
139. Karsenty, G., *Transcriptional control of skeletogenesis.* Annual Review of Genomics and Human Genetics, 2008. **9**: p. 183-196.

140. Shen, X.K., et al., *Regulation of the Biological Functions of Osteoblasts and Bone Formation by Zn-Incorporated Coating on Microrough Titanium.* Acs Applied Materials & Interfaces, 2014. **6**(18): p. 16426-16440.
141. Sodek, J. and M.D. McKee, *Molecular and cellular biology of alveolar bone.* Periodontology 2000, 2000. **24**: p. 99-126.
142. Stein, G.S., et al., *Intranuclear organization of RUNX transcriptional regulatory machinery in biological control of skeletogenesis and cancer.* Blood Cells Molecules and Diseases, 2003. **30**(2): p. 170-176.
143. Chen, J., et al., *Spatial transcriptomic analysis of cryosectioned tissue samples with Geo-seq.* Nature Protocols, 2017. **12**(3): p. 566-580.
144. Ordway, G.A., et al., *Gene expression analyses of neurons, astrocytes, and oligodendrocytes isolated by laser capture microdissection from human brain: detrimental effects of laboratory humidity.* J Neurosci Res, 2009. **87**(11): p. 2430-8.
145. Buenrostro, J.D., et al., *ATAC-seq: A Method for Assaying Chromatin Accessibility Genome-Wide.* Curr Protoc Mol Biol, 2015. **109**: p. 21 29 1-21 29 9.
146. Corces, M.R., et al., *An improved ATAC-seq protocol reduces background and enables interrogation of frozen tissues.* Nat Methods, 2017. **14**(10): p. 959-962.
147. Anders, S., P.T. Pyl, and W. Huber, *HTSeq--a Python framework to work with high-throughput sequencing data.* Bioinformatics, 2015. **31**(2): p. 166-9.
148. Langmead, B. and S.L. Salzberg, *Fast gapped-read alignment with Bowtie 2.* Nat Methods, 2012. **9**(4): p. 357-9.
149. Bray, N.L., et al., *Near-optimal probabilistic RNA-seq quantification.* Nat Biotechnol, 2016. **34**(5): p. 525-7.
150. Love, M.I., W. Huber, and S. Anders, *Moderated estimation of fold change and dispersion for RNA-seq data with DESeq2.* Genome Biol, 2014. **15**(12): p. 550.
151. Gaspar, J.M., *NGmerge: merging paired-end reads via novel empirically-derived models of sequencing errors.* BMC Bioinformatics, 2018. **19**(1): p. 536.
152. Zhang, Y., et al., *Model-based analysis of ChIP-Seq (MACS).* Genome Biol, 2008. **9**(9): p. R137.

153. Yamaguchi, T., et al., *In situ DNA-hybridization chain reaction (HCR): a facilitated in situ HCR system for the detection of environmental microorganisms.* Environ Microbiol, 2015. **17**(7): p. 2532-41.
154. Uittenbogaard, M., K.K. Baxter, and A. Chiaramello, *NeuroD6 genomic signature bridging neuronal differentiation to survival via the molecular chaperone network.* J Neurosci Res, 2010. **88**(1): p. 33-54.
155. Rahman, M.M., et al., *PR domaincontaining protein 12 (prdm12) is a downstream target of the transcription factor zic1 during cellular differentiation in the central nervous system: PR domain containing protein is the right form.* Int J Dev Neurosci, 2020. **80**(6): p. 528-537.
156. Mills, M., et al., *Differential expression of the actin-binding proteins, alpha-actinin-2 and -3, in different species: implications for the evolution of functional redundancy.* Hum Mol Genet, 2001. **10**(13): p. 1335-46.
157. Youlten, S.E., et al., *Osteocyte Transcriptome Mapping Identifies a Molecular Landscape Controlling Skeletal Homeostasis and Susceptibility to Skeletal Disease.* bioRxiv, 2020: p. 2020.04.20.051409.
158. Qin, X., et al., *Runx2 is essential for the transdifferentiation of chondrocytes into osteoblasts.* PLoS Genet, 2020. **16**(11): p. e1009169.
159. Chapman, D.L., et al., *Critical role for Tbx6 in mesoderm specification in the mouse embryo.* Mech Dev, 2003. **120**(7): p. 837-47.
160. Radisky, D.C., *Epithelial-mesenchymal transition.* J Cell Sci, 2005. **118**(Pt 19): p. 4325-6.
161. Behr, R., et al., *Epithelial-mesenchymal transition in colonies of rhesus monkey embryonic stem cells: a model for processes involved in gastrulation.* Stem Cells, 2005. **23**(6): p. 805-16.
162. Fernando, R.I., et al., *The T-box transcription factor Brachyury promotes epithelial-mesenchymal transition in human tumor cells.* J Clin Invest, 2010. **120**(2): p. 533-44.
163. Chen, M., et al., *The Roles of Embryonic Transcription Factor BRACHYURY in Tumorigenesis and Progression.* Front Oncol, 2020. **10**: p. 961.
164. Vujovic, S., et al., *Brachyury, a crucial regulator of notochordal development, is a novel biomarker for chordomas.* J Pathol, 2006. **209**(2): p. 157-65.

165. Zhu, J., K.M. Kwan, and S. Mackem, *Putative oncogene Brachyury (T) is essential to specify cell fate but dispensable for notochord progenitor proliferation and EMT.* Proc Natl Acad Sci U S A, 2016. **113**(14): p. 3820-5.
166. Cunliffe, V. and J.C. Smith, *Specification of mesodermal pattern in Xenopus laevis by interactions between Brachyury, noggin and Xwnt-8.* EMBO J, 1994. **13**(2): p. 349-59.
167. Cunliffe, V. and J.C. Smith, *Ectopic mesoderm formation in Xenopus embryos caused by widespread expression of a Brachyury homologue.* Nature, 1992. **358**(6385): p. 427-30.
168. Gentsch, G.E., et al., *Innate Immune Response and Off-Target Mis-splicing Are Common Morpholino-Induced Side Effects in Xenopus.* Dev Cell, 2018. **44**(5): p. 597-610 e10.
169. Ghebranious, N., et al., *A missense T (Brachyury) mutation contributes to vertebral malformations.* J Bone Miner Res, 2008. **23**(10): p. 1576-83.
170. Hayata, T., et al., *Expression of Brachyury-like T-box transcription factor, Xbra3 in Xenopus embryo.* Dev Genes Evol, 1999. **209**(9): p. 560-3.
171. Hotta, K., et al., *Characterization of Brachyury-downstream notochord genes in the Ciona intestinalis embryo.* Dev Biol, 2000. **224**(1): p. 69-80.
172. Messenger, N.J., et al., *Functional specificity of the Xenopus T-domain protein Brachyury is conferred by its ability to interact with Smad1.* Dev Cell, 2005. **8**(4): p. 599-610.
173. Schulte-Merker, S. and J.C. Smith, *Mesoderm formation in response to Brachyury requires FGF signalling.* Curr Biol, 1995. **5**(1): p. 62-7.
174. Wan, Z., et al., *T-box transcription factor brachyury promotes tumor cell invasion and metastasis in non-small cell lung cancer via upregulation of matrix metalloproteinase 12.* Oncol Rep, 2016. **36**(1): p. 306-14.
175. Zhao, L., et al., *Transcriptome profiles of metamorphosis in the ornamented pygmy frog Microhyla fissipes clarify the functions of thyroid hormone receptors in metamorphosis.* Sci Rep, 2016. **6**: p. 27310.
176. Wang, S., et al., *Gene Expression Program Underlying Tail Resorption During Thyroid Hormone-Dependent Metamorphosis of the Ornamented Pygmy Frog Microhyla fissipes.* Front Endocrinol (Lausanne), 2019. **10**: p. 11.
177. Yaoita, Y. and D.D. Brown, *A correlation of thyroid hormone receptor gene expression with amphibian metamorphosis.* Genes Dev, 1990. **4**(11): p. 1917-24.

178. Kanamori, A. and D.D. Brown, *The analysis of complex developmental programmes: amphibian metamorphosis.* Genes Cells, 1996. **1**(5): p. 429-35.
179. Giacomazzi, G., et al., *MicroRNAs promote skeletal muscle differentiation of mesodermal iPSC-derived progenitors.* Nat Commun, 2017. **8**(1): p. 1249.
180. Auxerre-Plantie, E., et al., *Identification of MYOM2 as a candidate gene in hypertrophic cardiomyopathy and Tetralogy of Fallot, and its functional evaluation in the Drosophila heart.* Dis Model Mech, 2020. **13**(12).
181. Hattori, T., et al., *SOX9 is a major negative regulator of cartilage vascularization, bone marrow formation and endochondral ossification.* Development, 2010. **137**(6): p. 901-11.
182. Magrini, E., A. Mantovani, and C. Garlanda, *The Dual Complexity of PTX3 in Health and Disease: A Balancing Act?* Trends Mol Med, 2016. **22**(6): p. 497-510.
183. Velez-delValle, C., et al., *Epithelial cell migration requires the interaction between the vimentin and keratin intermediate filaments.* Sci Rep, 2016. **6**: p. 24389.
184. Gan, Z., et al., *Vimentin Intermediate Filaments Template Microtubule Networks to Enhance Persistence in Cell Polarity and Directed Migration.* Cell Syst, 2016. **3**(5): p. 500-501.
185. Brachvogel, B., et al., *Comparative proteomic analysis of normal and collagen IX null mouse cartilage reveals altered extracellular matrix composition and novel components of the collagen IX interactome.* J Biol Chem, 2013. **288**(19): p. 13481-92.
186. Hessle, L., et al., *The skeletal phenotype of chondroadherin deficient mice.* PLoS One, 2014. **8**(6): p. e63080.
187. Reul, J.M. and F. Holsboer, *On the role of corticotropin-releasing hormone receptors in anxiety and depression.* Dialogues Clin Neurosci, 2002. **4**(1): p. 31-46.
188. Schiaffino, S., et al., *Developmental myosins: expression patterns and functional significance.* Skelet Muscle, 2015. **5**: p. 22.
189. Pickering, C. and J. Kiely, *ACTN3: More than Just a Gene for Speed.* Front Physiol, 2017. **8**: p. 1080.
190. Youlten, S.E., et al., *Osteocyte transcriptome mapping identifies a molecular landscape controlling skeletal homeostasis and susceptibility to skeletal disease.* Nature Communications, 2021. **12**(1): p. 2444.

191. Strauss, B., et al., *Cyclin B1 is essential for mitosis in mouse embryos, and its nuclear export sets the time for mitosis.* J Cell Biol, 2018. **217**(1): p. 179-193.
192. Zhu, Q., et al., *The transcription factor Pou3f1 promotes neural fate commitment via activation of neural lineage genes and inhibition of external signaling pathways.* Elife, 2014. **3**.
193. Gould, R.M., et al., *Myelin sheaths are formed with proteins that originated in vertebrate lineages.* Neuron Glia Biol, 2008. **4**(2): p. 137-52.
194. Widmer, C., et al., *Molecular basis for the action of the collagen-specific chaperone Hsp47/SERPINH1 and its structure-specific client recognition.* Proc Natl Acad Sci U S A, 2012. **109**(33): p. 13243-7.
195. Tigan, A.S., et al., *CDK6-a review of the past and a glimpse into the future: from cell-cycle control to transcriptional regulation.* Oncogene, 2016. **35**(24): p. 3083-91.
196. Bianco, A.C. and R.R. da Conceicao, *The Deiodinase Trio and Thyroid Hormone Signaling.* Methods Mol Biol, 2018. **1801**: p. 67-83.
197. Choi, J.H., et al., *Thrap3 docks on phosphoserine 273 of PPARgamma and controls diabetic gene programming.* Genes Dev, 2014. **28**(21): p. 2361-9.
198. Dong, H., et al., *Regulator of G protein signaling 2 is a key regulator of pancreatic beta-cell mass and function.* Cell Death Dis, 2017. **8**(5): p. e2821.
199. Smith, J.C., et al., *Expression of a Xenopus homolog of Brachyury (T) is an immediate-early response to mesoderm induction.* Cell, 1991. **67**(1): p. 79-87.
200. Yasuoka, Y., C. Shinzato, and N. Satoh, *The Mesoderm-Forming Gene brachyury Regulates Ectoderm-Endoderm Demarcation in the Coral Acropora digitifera.* Curr Biol, 2016. **26**(21): p. 2885-2892.
201. Paraiso, K.D., et al., *Morpholinos Do Not Elicit an Innate Immune Response during Early Xenopus Embryogenesis.* Dev Cell, 2019. **49**(4): p. 643-650 e3.
202. Showell, C., O. Binder, and F.L. Conlon, *T-box genes in early embryogenesis.* Dev Dyn, 2004. **229**(1): p. 201-18.
203. Postma, A.V., et al., *Mutations in the T (brachyury) gene cause a novel syndrome consisting of sacral agenesis, abnormal ossification of the vertebral bodies and a persistent notochordal canal.* J Med Genet, 2014. **51**(2): p. 90-7.

204. Breeland, G., M.A. Sinkler, and R.G. Menezes, *Embryology, Bone Ossification*, in *StatPearls*. 2021: Treasure Island (FL).
205. Mackie, E.J., et al., *Endochondral ossification: how cartilage is converted into bone in the developing skeleton.* Int J Biochem Cell Biol, 2008. **40**(1): p. 46-62.
206. Henderson, S.R., et al., *A molecular map of mesenchymal tumors.* Genome Biol, 2005. **6**(9): p. R76.
207. Tomlinson, R.E., et al., *The Role of Nerves in Skeletal Development, Adaptation, and Aging.* Front Endocrinol (Lausanne), 2020. **11**: p. 646.
208. Mach, D.B., et al., *Origins of skeletal pain: sensory and sympathetic innervation of the mouse femur.* Neuroscience, 2002. **113**(1): p. 155-66.
209. Castaneda-Corral, G., et al., *The majority of myelinated and unmyelinated sensory nerve fibers that innervate bone express the tropomyosin receptor kinase A.* Neuroscience, 2011. **178**: p. 196-207.
210. Williams, G.R., *Thyroid hormone actions in cartilage and bone.* Eur Thyroid J, 2013. **2**(1): p. 3-13.
211. Williams, G.R., H. Robson, and S.M. Shalet, *Thyroid hormone actions on cartilage and bone: interactions with other hormones at the epiphyseal plate and effects on linear growth.* J Endocrinol, 1998. **157**(3): p. 391-403.
212. Endo, T. and T. Kobayashi, *Excess TSH causes abnormal skeletal development in young mice with hypothyroidism via suppressive effects on the growth plate.* Am J Physiol Endocrinol Metab, 2013. **305**(5): p. E660-6.
213. Bagriacik, E.U., et al., *TSH-induced gene expression involves regulation of self-renewal and differentiation-related genes in human bone marrow-derived mesenchymal stem cells.* J Endocrinol, 2012. **212**(2): p. 169-78.
214. Abe, E., et al., *TSH is a negative regulator of skeletal remodeling.* Cell, 2003. **115**(2): p. 151-62.
215. Zhang, W., et al., *Thyroid-stimulating hormone maintains bone mass and strength by suppressing osteoclast differentiation.* J Biomech, 2014. **47**(6): p. 1307-14.
216. Capelo, L.P., et al., *Deiodinase-mediated thyroid hormone inactivation minimizes thyroid hormone signaling in the early development of fetal skeleton.* Bone, 2008. **43**(5): p. 921-30.

217. Lassova, L., et al., *Thyroid hormone treatment of cultured chondrocytes mimics in vivo stimulation of collagen X mRNA by increasing BMP 4 expression.* J Cell Physiol, 2009. **219**(3): p. 595-605.
218. Park, J.Y., et al., *Early Osteological Development of Larvae and Juveniles in Red Spotted Grouper, Epinephelus akaara (Pisces: Serranidae).* Dev Reprod, 2016. **20**(2): p. 87-101.
219. Tague, R.G., *Fusion of coccyx to sacrum in humans: prevalence, correlates, and effect on pelvic size, with obstetrical and evolutionary implications.* Am J Phys Anthropol, 2011. **145**(3): p. 426-37.
220. Kalamchi, L. and C. Valle, *Embryology, Vertebral Column Development*, in *StatPearls*. 2021: Treasure Island (FL).
221. Nakai, Y., K. Nakajima, and Y. Yaoita, *Mechanisms of tail resorption during anuran metamorphosis.* Biomol Concepts, 2017. **8**(3-4): p. 179-183.
222. Ascarrunz, E., et al., *Triadobatrachus massinoti, the earliest known lissamphibian (Vertebrata: Tetrapoda) re-examined by μCT scan, and the evolution of trunk length in batrachians.* Contributions to Zoology, 2016. **85**(2): p. 201-234.
223. Goldstein, J.A., K.V.S. Hoff, and S.D. Hillyard, *The effect of temperature on development and behaviour of relict leopard frog tadpoles.* Conserv Physiol, 2017. **5**(1): p. cow075.
224. Weerathunga, W. and G. Rajapaksa, *The impact of elevated temperature and CO2 on growth, physiological and immune responses of Polypedates cruciger (common hourglass tree frog).* Front Zool, 2020. **17**: p. 3.
225. Lowe, W.H., et al., *Metamorphosis in an Era of Increasing Climate Variability.* Trends Ecol Evol, 2021. **36**(4): p. 360-375.
226. Rose, C.S., *Integrating ecology and developmental biology to explain the timing of frog metamorphosis.* Trends Ecol Evol, 2005. **20**(3): p. 129-35.
227. Kanamori, A. and D.D. Brown, *Cultured cells as a model for amphibian metamorphosis.* Proc Natl Acad Sci U S A, 1993. **90**(13): p. 6013-7.
228. Piekarski, N., J.B. Gross, and J. Hanken, *Evolutionary innovation and conservation in the embryonic derivation of the vertebrate skull.* Nat Commun, 2014. **5**: p. 5661.
229. Gross, J.B., et al., *Use of a ROSA26:GFP transgenic line for long-term Xenopus fate-mapping studies.* J Anat, 2006. **209**(3): p. 401-13.

230. Haeri, M. and B.E. Knox, *Generation of transgenic Xenopus using restriction enzyme-mediated integration.* Methods Mol Biol, 2012. **884**: p. 17-39.
231. Creyghton, M.P., et al., *Histone H3K27ac separates active from poised enhancers and predicts developmental state.* Proc Natl Acad Sci U S A, 2010. **107**(50): p. 21931-6.
232. Arnold, C.D., et al., *Genome-wide quantitative enhancer activity maps identified by STARR-seq.* Science, 2013. **339**(6123): p. 1074-7.
233. Di Gregorio, A., *T-Box Genes and Developmental Gene Regulatory Networks in Ascidians.* Curr Top Dev Biol, 2017. **122**: p. 55-91.
234. Morley, R.H., et al., *A gene regulatory network directed by zebrafish No tail accounts for its roles in mesoderm formation.* Proc Natl Acad Sci U S A, 2009. **106**(10): p. 3829-34.
235. Ablain, J., et al., *A CRISPR/Cas9 vector system for tissue-specific gene disruption in zebrafish.* Dev Cell, 2015. **32**(6): p. 756-64.
236. Love, N.R., et al., *pTransgenesis: a cross-species, modular transgenesis resource.* Development, 2011. **138**(24): p. 5451-8.